BOND STRENGTH OF EPOXY-COATED REINFORCEMENT TO CONCRETE

by

Oan Chul Choi

David Darwin

Steven L. McCabe

A Report on Research Sponsored by

THE NATIONAL SCIENCE FOUNDATION

Research Grant No. CES-8616228

UNIVERSITY OF KANSAS

LAWRENCE, KANSAS

July 1990

50272-101

REPORT DOCUMENTATION PAGE	1. REPORT NO.	2.	3. Recipient's Accession No.

4. Title and Subtitle
Bond Strength of Epoxy-Coated Reinforcement to Concrete

5. Report Date
July 1990

6.

7. Author(s)
Oan Chul Choi, David Darwin and Steve L. McCabe

8. Performing Organization Rept. No.
SM Report No. 25

9. Performing Organization Name and Address
Structural Engineering and Materials Laboratory
University of Kansas Center for Research, Inc.
2291 Irving Hill Drive, West Campus
Lawrence, Kansas 66045

10. Project/Task/Work Unit No.

11. Contract(C) or Grant(G) No.
(C)
(G) NFS CES-8616228

12. Sponsoring Organization Name and Address
National Science Foundation
Washington, D.C. 20550

13. Type of Report & Period Covered

14.

15. Supplementary Notes

16. Abstract (Limit: 200 words)

Beam-end specimens were used to determine the effects of coating thickness (3 to 17 mils), bar size (No. 5 - No. 11), bar position (top-cast and bottom-cast), deformation pattern (3 patterns), and cover (1, 2 and 3 bar diameters) on the bond strength between deformed reinforcement and concrete. The reduction of bond strength by epoxy coating is a function of deformation pattern, bar size, and coating thickness. The bond strength of small bars is more sensitive to coating thickness than the bond strength of larger bars. Large bars are affected more by the presence of epoxy coating than small bars. Bars with relatively larger rib bearing areas are affected less by the coating than bars with smaller bearing areas. Epoxy-coated top-cast bars are affected less by the coating than bottom-cast bars. Designs based on these observations will be less conservative than those based on the development length provisions in the 1989 ACI Building Code.

Nonlinear finite element analysis was conducted to study the role played by epoxy coatings. The model includes representations for deformed steel bar, concrete, and the interfacial material. The interface is represented by special link elements. The longitudinal splitting crack is modeled using a nonlinear fracture mechanics scheme. The interfacial properties, mainly friction, govern bond performance. The finite element studies reveal close agreement between observed laboratory behavior and the computer results.

17. Document Analysis a. Descriptors
beam-end specimen, bond (concrete to reinforcement), coatings, cohesion, deformed reinforcement, epoxy-coated reinforcement, fictitious crack model, fracture mechanics, friction, interface, Mohr-Coulomb surface, nonlinear finite element analysis, reinforcing steels, splitting crack, structural engineering

b. Identifiers/Open-Ended Terms

c. COSATI Field/Group

18. Availability Statement
Release Unlimited

19. Security Class (This Report)
Unclassified

21. No. of Pages
217

20. Security Class (This Page)
Unclassified

22. Price

ABSTRACT

The effects of coating thickness, deformation pattern, bar size, concrete cover, and casting position on the reduction in bond strength between reinforcing bars and concrete caused by epoxy coatings are described. Tests include beam-end specimens containing No. 5, No. 6, No. 8, and No. 11 bars with average coating thicknesses ranging from 3 to 17 mils. Three deformation patterns are evaluated. Specimens with covers of 1, 2 and 3 bar diameters are studied. Both top-cast and bottom-cast bars are tested. Epoxy coatings are found to significantly reduce bond strength, but the extent of the reduction is less than used to establish the development length modification factors in the 1989 ACI Building Code and 1989 AASHTO Bridge Specifications. Coating thickness has little effect on the amount of bond strength for No. 6 bars and larger. However, the thicker the coating, the greater the reduction in bond strength for No. 5 bars. In general, the reduction in bond strength caused by an epoxy coating increases with bar size. The magnitude of reduction depends on the deformation pattern: bars with relatively larger rib-bearing areas are affected less by the coating than bars with smaller bearing areas. Concrete cover increases the bond strength of both uncoated and coated reinforcement, but the reduction in bond strength caused by an epoxy coating is independent of cover. Epoxy-coated bars are relatively insensitive to top-bar effect.

Nonlinear finite element analysis is conducted to study the role played by epoxy coatings on the failure of test specimens. The

finite element model includes representations for the deformed steel bar, the concrete, and the interfacial material. The interface is represented by special link elements that can be adjusted to match the specified stiffness and surface properties of the interfacial material. The longitudinal splitting crack is modeled using a non-linear fracture mechanics scheme, Hillerborg's fictitious crack model. The finite element studies reveal close agreement between observed laboratory behavior and the computed results. The interfacial properties, mainly friction, govern the bond performance. Epoxy coatings reduce the bond strength. Bond strengths of coated and uncoated bars increase nearly linearly with additional cover and lead length, but the relative bond strength of coated bars is independent of cover and lead length. Modeling of the bar-concrete interface using the Mohr-Coulomb surface, coupled with the fictitious crack model, correctly predicts the overall effects of the surface properties on bond performance.

ACKNOWLEDGEMENTS

This report is based on a thesis submitted by Oan Chul Choi to the Department of Civil Engineering of the University of Kansas in partial fulfillment of the requirements for the Ph.D. degree.

The research was supported by the National Science Foundation under NSF Grant CES-8616228. Reinforcing steel was supplied by Chaparrel Steel Company, North Star Steel Company, Sheffield Steel Corporation, and Structural Metals, Inc. The epoxy coating, 3M Scotchkote 213, was applied by ABC Coating Company, Inc. and Simcote, Inc.

Numerical computations were performed on the Harris 800 computer system operated by the Computer Aided Engineering Laboratory and an Apollo DN3500 workstation operated by the Graphics and Computer Applications Laboratory in the Department of Civil Engineering at the University of Kansas. Finite element analysis was carried out using the POLO-FINITE General Purpose Finite Element Program.

TABLE OF CONTENTS

TABLE OF CONTENTS (continued)

LIST OF TABLES

LIST OF FIGURES

LIST OF FIGURES (continued)

LIST OF FIGURES (continued)

LIST OF FIGURES (continued)

LIST OF FIGURES (continued)

CHAPTER 1: INTRODUCTION

1.1 General

Corrosion of reinforcing steel is a major concern in a wide range of concrete structures including bridges, parking structures, ports and marine structures, wastewater treatment plants and cooling towers. A major step toward improving the corrosion resistance of reinforcing steel has been the use of fusion-bonded epoxy coatings to isolate the steel bars from the attack of chloride in concrete. The epoxy coatings have proved effective and economical and are finding an increasingly wider application in reinforced concrete construction.

In spite of the widespread use of epoxy-coated steel, relatively little research has been done on the bond between epoxy-coated reinforcing steel and concrete. The limited work that has been done indicates that epoxy-coated bars develop less bond strength than uncoated bars. This observation is important since the bond between concrete and steel is critical for structural safety.

Many factors can affect the bond of deformed bars to concrete. At least one previous study (Treece and Jirsa 1989) concluded that the amount of bond strength reduction caused by an epoxy coating depends primarily on the degree of confinement. The change of the surface properties of reinforcing bars with epoxy coatings leads to a smoother bar surface and alters the interaction between steel and concrete. This alteration may place more emphasis on other factors

of bar configuration such as rib profile, rib height, bearing area, orientation, and spacing.

New provisions to Building Code Requirements for Reinforced Concrete (ACI 318-89) recognize, for the first time, the bond strength reduction by adopting modification factors to increase the development length of epoxy-coated bars. However, the study on which the modification factors are based was relatively small in scope. A single deformation pattern was evaluated, and no specimens were replicated. Considering the high variability exhibited in bond tests, it is not clear if the limited experimental results provide an accurate picture of the effect of epoxy coating.

The widespread use of epoxy-coated reinforcing steel, combined with the limited knowledge, requires additional work to obtain even the basic understanding of bond behavior necessary for accurate design provisions. This study will help provide that basic understanding and will include the effects of the major variables influencing bond strength. The information obtained will help determine the modifications required in the development length provisions of the ACI Building Code (1989).

1.2 Background

Experimental and theoretical work makes it possible to recognize that basically three mechanisms of bond exist (Lutz 1970): adhesion; friction; and mechanical interaction, mainly between the bar ribs and the surrounding mortar. The roughness of the bar sur-

face influences both the adhesion and the friction between the bar and concrete; the geometric properties of the deformed bar cause the mechanical interaction (Lutz, Gergely and Winter 1966). At increasing values of bond stress, adhesion is destroyed as a consequence of slip and wedging of the ribs. After the loss of adhesion, the next mechanisms, friction and mechanical interaction between the ribs and the concrete, occur together.

The change of surface properties caused by epoxy coatings leads to a loss of adhesion and friction and alters the mechanical interaction between the steel and the concrete; all of which lead to a substantial change in the mechanisms of bond.

In view of the substantial change in bond mechanisms, several researchers have been concerned with the bond of epoxy-coated reinforcement to concrete. Mathey and Clifton (1975, 1976, 1979) conducted the first study of the bond of epoxy-coated bars using pullout specimens. From the initial study, they concluded that bars with epoxy coatings of approximately 10 mils (0.010 in.) or less in thickness, have a bond strength that is "essentially the same" as that of uncoated bars.

Johnston and Zia (1982) tested 6 slab specimens and 40 beam-end specimens using No. 6 and No. 11 bars with a single deformation pattern. Based on these tests they recommended that the development length be increased by 15 percent for epoxy-coated reinforcement. They also concluded that the effect of epoxy coatings is independent of bar size.

Treece and Jirsa (1987, 1989) tested 21 beam specimens to determine the bond strength of epoxy-coated and uncoated reinforcing bars with a single deformation pattern. Beam specimens were constructed with either No. 6 or No. 11 bars spliced in the center of the beam. Their results indicate that epoxy-coated bars develop between 54 and 88 percent of the splice strength of uncoated bars, and they concluded that bond reduction is independent of concrete strength, bar size, and coating thickness.

The magnitudes of the strength reductions obtained in the three studies are very different. The total number of tests in each study was small. Johnston and Zia (1982) and Treece and Jirsa (1987, 1989) used but a single deformation pattern in their studies. Thus, the generality of the conclusions in each study must be considered to be limited.

Since epoxy coatings change the surface properties of reinforcing bars, the effect of the deformation pattern on bond strength is a major parameter that should be considered in any study of the bond of epoxy-coated reinforcing steel to concrete. The effect of concrete properties and confinement also should be included to help understand the interaction between concrete and reinforcing bars.

In spite of the limited understanding of the nature of the bond between the two materials, epoxy-coated bars have been used in increasing amounts over the past fifteen years. The results of the present study are combined with supporting evidence from other investigations to obtain a more complete picture of the influence of the major variables. This information will permit improvements to be

made in design rules to preclude brittle bond failures in structures constructed with epoxy-coated bars.

1.3 Previous Work

Bond Strength

There have been many studies of bond strength of uncoated reinforcing bars in concrete. In 1913, Abrams made an extensive study of the bond of plain and deformed bars. Higher bond stresses were achieved with deformed bars than were obtained with plain bars. An improvement in slip resistance with an increase in rib bearing area per unit length of bar was observed.

Several factors influencing bond were examined by Menzel (1939) by means of pullout tests. These factors included the type of bar surface, the embedment length, the type and positions of the ribs, the position of the bar during concrete placement, and the thickness of the concrete cover. The superiority of transverse ribs over longitudinal ribs illustrated the importance of the larger rib bearing area obtained with transverse ribs.

In 1946 and 1949, Clark reported beam tests and pullout tests on different types of deformed bars. Based on these tests, he concluded that the most important parameter for good slip resistance was the ratio of the shearing area of the bar-concrete interface between deformations (measured parallel to the bar axis) to the bearing area of the deformations (measured as the projected area of the ribs), and

recommended values less than 5 or 6 but in any case less than 10. Most bars today do not meet this criterion.

Studies of bond between reinforcing steel and concrete by Lutz, Gergely and Winter (1966), and Lutz (1970) suggest that three components contribute to the bond between the two materials, chemical adhesion, friction, and mechanical interaction. Bond forces, and the associated slip and cracking were examined for bars with different surface properties.

According to Lutz et al. (1966), slip of deformed bars can occur in two ways: (1) the ribs can push concrete away from the bar by wedging action, and (2) the ribs can crush the concrete in front of the ribs. Lutz also observed that the slip is about the same for all ribs with rib face angles greater than 40 degrees (the face angle of the ribs is measured with respect to the bar axis). This means that for rib face angles greater than 40 degrees, the friction between the rib face and concrete is sufficient to prevent relative slip at the rib interface. The consequence is that slip occurs when the concrete in front of the ribs is crushed by the large bearing pressures exerted by these ribs.

S. M. Skorobogatov and A. D. Edwards (1979) used bars with face angles of 48.5 and 57.8 degrees and concluded that the rib face angle does not affect the maximum bond stress because the steep angle is modified by the crushed concrete wedge which effectively reduces the face angle to a smaller value.

Tepfers (1979) suggested that the concrete cover surrounding a bar behaves like a thick ring and the behavior of the ring at the

point of failure may be perfectly elastic, perfectly plastic or partly cracked elastic, depending on the thickness of the concrete. Tepfers concluded that the partly cracked elastic analysis gives cracking loads just on the safe side of the experimental results. The predicted strength was compared to the experimental strength for lap splices in 193 beams. The values agreed for lap lengths and cover thicknesses that are normally used in practice (Tepfers 1982).

The effects of concrete properties and construction procedures on bond strength were studied by Donahey and Darwin (1985) and Brettmann, Darwin and Donahey (1986). The key variables were concrete slump, consolidation practice, bar position, concrete cover, and bar spacing. They observed that for concrete with the same compressive strength, bond strength decreases with increasing concrete slump. They also observed that high density internal vibration provides improved bond compared to low density internal vibration.

Design Relationships

Experimental bond test results have historically been used to derive design relationships. For example, the ultimate bond stress specified in the 1963 ACI Building Code was based on tests at the University of Texas (Ferguson, Thompson and Neils 1962) and the National Bureau of Standards (Mathey and Watstein 1961). The ultimate average bond force per unit length (in pounds per in.) was expressed as

$$U = 35 \sqrt{f'_c} \qquad (1.1)$$

in which f'_c is the concrete compressive strength, in psi.

Orangun, Jirsa and Breen (1977) used a nonlinear regression analysis of the test results of transversely reinforced beams to develop an equation for calculating the strength of lap splices of deformed bars. From the analysis, a best fit equation obtained is

$$u = \left(1.2 + \frac{3c}{d_b} + \frac{50\ d_b}{l_s} + \frac{A_{tr}\ f_{yt}}{500\ sd_b}\right) \sqrt{f'_c} \qquad (1.2)$$

in which u is the bond strength of bars, in psi; c is the minimum concrete cover, and d_b is the bar diameter, l_s is the splice length, all in inches; A_{tr} is the area of the transverse reinforcement, in square inches; f_{yt} is the yield strength of transverse reinforcement, in psi; and s is the spacing of transverse reinforcement, in inches.

A relationship was developed by Jimenez, White and Gergely (1978) using regression analysis applied to 174 development and splice tests. They suggested that the axial force (in kips) at which splitting occurs is

$$T_j = \frac{d_b\ l_d\ c\ \sqrt{f'_c}}{(35.4d_b + 0.573l_d)} \qquad (1.3)$$

in which l_d is the embedment length, in inches.

A prediction equation was presented by Zsutty (1985) for the strength of lapped splices with and without transverse reinforcing bars. The form of the prediction equation showed that bond strength is a function of the square root of development length, cover, and

transverse steel ratio, and the cube root of the concrete strength. The resulting equation is

$$u_A = 140(f'_c)^{1/3} \left(\frac{d_b}{l_d}\right)^{1/2} \left(\frac{c}{d_b} + 2r\right)^{1/2} \quad (1.4)$$

in which u_A is the lapped tension bond stress, in psi and r is the transverse tie steel ratio (area of transverse reinforcement divided by the product of the tie spacing and the beam width), in percent.

Epoxy-coated reinforcement

The first major field application of epoxy-coated reinforcing bars was in a Pennsylvania bridge deck in 1973. In 1976, Mathey and Clifton made the first study of the bond of epoxy-coated reinforcing bars at the National Bureau of Standards (NBS). They used pullout specimens (No. 6 reinforcing bars embedded in 10x10x12 in. prisms) to evaluate the bond strength between epoxy-coated bars and concrete. In the initial study, 23 epoxy-coated reinforcing bars, using 10 epoxies, were tested along with 6 bars coated with polyvinyl chloride, and 5 uncoated bars. Bars with diamond and barrel deformation patterns were used. Concrete strength was limited to the range of 5730 to 6620 psi.

From the study, Mathey and Clifton concluded that bond strength was unsatisfactory for bars with a polyvinyl chloride coating and bars with thick epoxy coatings but satisfactory for bars with epoxy coatings 10 mils or less in thickness. The average value of the

critical bond strength in 19 pullout specimens with bars having epoxy coatings between 1 mil and 11 mils thick was 6 percent less than that for pullout specimens containing uncoated bars. Bond failure occurred in two epoxy-coated bars having a coating thickness of 25 mils, but all of the uncoated bars and the coated bars with an epoxy coating thickness between 1 and 11 mils yielded in the tests. Unfortunately, the applicability of these tests to the bond of reinforcement in actual structures is limited by the fact that these pullout specimens placed the concrete in compression while the bar was in tension. In most structures, both the bar and the concrete surrounding the bar are in tension.

To obtain a more realistic measure of the effects of epoxy coatings on bond, Johnston and Zia (1982) at North Carolina State University (NCSU) tested 6 slab specimens and 40 beam-end specimens using No. 6 and No. 11 bars. The slab specimens were designed to evaluate the effect of the epoxy coating on crack spacing and crack width. The beam-end specimens, using three different embedment lengths for each bar size, were designed to determine critical slip and flexural bond strength values for the reinforcement. The beam tests included 26 static load specimens (12 with uncoated bars, 12 with epoxy-coated bars, and 2 with blast-cleaned bars), and 14 fatigue specimens (6 with uncoated, 6 with epoxy-coated, and 2 with blast-cleaned bars). Concrete strength ranged from 5720 to 7040 psi. Coating thickness varied between 6.7 and 11.1 mils, but was on the order of 8 to 9 mils for most of the tests. Bars with a diamond deformation pattern were used. The bars were confined by stirrups

that satisfied the minimum requirements of ACI 318 (1983). A 10 inch PVC pipe sleeve was provided at the loaded end to avoid local popout of the concrete surface. The concrete cover was 2.3 in. for No. 6 and 2.0 in. for No. 11 bars, which is approximately 3 d_b for No. 6 and 1.5 d_b for No. 11 bars.

Based on the slab tests, Johnston and Zia concluded that at working stresses there are few differences between the performance of epoxy-coated and uncoated bars. The slabs with epoxy-coated bars had a slightly higher deflection and crack width and exhibited a strength about 4 percent below the strength obtained with uncoated bars. However, the static beam-end tests used to evaluate the flexural bond strength revealed that epoxy-coated bars develop about 85 percent of the bond strength of uncoated bars. Some tests were terminated after yielding of the steel but before a splitting failure occurred, and some tests ended when the bar pulled out at a load above the yield load. All specimens that underwent a bond failure, whether before or after yielding, failed by splitting. Based on a few tests which ended in a bond failure prior to yielding, Johnston and Zia recommended that the development length be increased by 15 percent when using epoxy-coated bars.

Most recently, Treece and Jirsa at the University of Texas (1987, 1989) tested beam specimens to study the strength of splices using epoxy-coated reinforcing bars. Twenty-one beam specimens were constructed with either No. 6 or No. 11 bars spliced in the center of the beams. The beam tests consisted of 10 specimens with No. 6 bars (4 uncoated bar specimens and 6 coated bar specimens) and 11

specimens with No. 11 bars (5 uncoated bar specimens and 6 coated bar specimens). Concrete strength ranged from 3860 to 12600 psi. Four of the specimens were bottom-cast and seventeen were top-cast. Bars with a diamond deformation pattern were used and coating thickness varied between 4.5 mils and 14.0 mils. The concrete cover for 18 specimens was less than 1.5 d_b, and the cover for 3 specimens was greater than 3.0 d_b. All but three of the No. 6 bar specimens had cover less than or just equal to the maximum aggregate size.

From the study, Treece and Jirsa found that epoxy coating significantly reduces the splice strength of reinforcing bars in tension. They concluded that the reduction in splice strength is independent of bar size and concrete strength and insensitive to variations in the coating thickness when the coating thickness is between 5 mils and 14 mils. However, the trends in the data provided in their report indicate that coating thickness apparently does have an effect for No. 6 bars (thicker coatings result in a lower strength), but not for No. 11 bars. Their test results indicate that in terms of strength, there is a size factor, i.e., No. 6 bars seem to be affected less by epoxy coating than No. 11 bars. They observed that the width and spacing of cracks was significantly increased for bars with epoxy coating; however, a comparison of load-deflection diagrams showed no loss of member stiffness when epoxy-coated bars were used. In their analysis, Treece and Jirsa considered both the NBS and NCSU tests to have resulted in pullout failures. It was their opinion that a pullout failure occurred because the steel was

well confined by concrete cover and transverse steel, preventing a splitting failure.

A main conclusion of the study by Treese and Jirsa was that the amount of reduction in bond strength caused by epoxy coating depends on the mode of the bond failure, i.e., pullout or splitting. Their reasoning was that if a splitting failure occurs, the bond strength of epoxy-coated bars is only about 65 percent of the bond strength of the uncoated bars. If a pullout failure occurs, the bond strength is about 85 percent of the uncoated bar bond strength. Based on these conclusions, they recommended that the basic development length of an uncoated bar be multiplied by a factor of 1.5 for epoxy-coated bars with a cover of less than 3 d_b or a clear spacing between bars of less than 6 d_b. In all other cases, the development length should be multiplied by a factor of 1.15. The factor of 1.15 is based on the strength of the NCSU specimens (pullout mode assumed). There is some question about this reasoning because the NCSU specimens failed by splitting with a longitudinal crack in the cover of the top face directly above the test bar (Johnston and Zia 1982). In the NCSU study, the cover of the No. 6 bars was approximately 3.0 d_b, but the cover of No. 11 bars was about 1.5 d_b. The one group of the University of Texas specimens that had cover greater than 3.0 d_b failed due to splitting. Thus, it is not clear that bars with 3 d_b cover or bars with transverse reinforcement will fail by pullout.

New provisions in Building Code Requirements for Reinforced Concrete (ACI 318-89) have essentially adopted the design recommen-

dations of Treece and Jirsa. However, the admissibility of using cover as a criteria for different reduction factors is in doubt.

It is generally believed that many variables affect the bond of deformed bars. In addition to parameters such as concrete strength and bar size, the configuration of the bar deformation pattern also may influence the bond strength of epoxy-coated steel. Since only one deformation pattern was used in each of the previous structural studies, no information exists as to the effect of epoxy coatings on bars with different deformation geometries. Clearly, additional work is required to achieve a complete understanding of the bond of epoxy-coated reinforcement to concrete.

Finite Element Studies of Bond

Considerable numerical research has involved the study of bond between reinforcement and concrete. Some of these studies have attempted to simulate bond strength based on bond failure from experimental tests. Other studies developed mathematical models for the behavior of bond for the finite element analyses of reinforced concrete members and structures. However, no general analytical approach exists to incorporate bond and bond slip into a finite element model.

The early finite element studies of reinforced concrete structures (Ngo and Scordelis 1967; Nilson 1968) used spring linkages to represent bond. Each linkage consisted of two springs, one acting parallel to the bar axis and one acting perpendicular to it. Ngo and

Scordelis used linear springs while the spring stiffness of the Nilson's model was based on an experimental bond slip relation.

An elastic finite element analysis (Lutz 1970) was used to examine the stresses and deformations around a reinforcing bar embedded in concrete. The model consisted of a concrete cylinder with an axially embedded bar. Slip resulting from the inclination of the bar ribs and a radial separation of the concrete and steel were considered.

A finite element model (Herrmann 1978) with interface material governed by the Mohr-Coulomb law was used to simulate Nilson's experimental results from concentric tension tests. Possible slippage of the reinforcement relative to concrete was considered in the model. While the predicted behavior fell within the experimental scatter, the trend did not agree completely because no separation between the steel and concrete and no rib representation were assumed.

Ingraffea et al. (1984) used nonlinear fracture mechanics in a finite element model to investigate the behavior of tension-pull specimens. A nonlinear crack propagation algorithm (Saouma 1980) was used to automatically generate singular elements around a crack tip and to minimize the effects of new nodes and elements added to the mesh. As a crack propagated, interface elements allowing opening and sliding of the crack sides were automatically inserted in the crack. In the study, the dominant mode allowing bond-slip was assumed to be radially propagating secondary cracks. The secondary radial cracking interrelated with primary cracking from bending in a reinforced beam

was modeled to analyze bond-slip. A tension softening element was used in the analysis cases of practical problems.

M. Keuser and G. Mehlhorn (1987) investigated the effects of different approaches for finite element models of bond. The influence of the displacement function and bond stress-slip relationship was investigated. It was shown that a realistic analytical model requires consideration of several local influences, including the position of the bar during the casting of concrete, transverse pressure, secondary cracks in the concrete, and the deterioration of bond near primary cracks.

Bond behavior is complex. The complexity of bond, including bond slip, is one of the major difficulties in the finite element analysis of reinforced concrete structures. The presence of the interface between reinforcing bars and concrete is only one of several complicating factors. Slippage of a ribbed reinforcing bar in concrete is a nonlinear inelastic phenomenon. The geometrical complexity of bars -- the configuration of the deformations -- requires a three-dimension model necessary to capture the essence of the problem. Different failure types and failure modes are possible in bond failure. The displacement mode of a splitting crack is the opening mode. The crack surfaces of a local shear failure, known as pullout failure, are characterized by the sliding or shear mode. Thus, understanding the failure mechanisms of concrete, as well as the role of the interface in the bond mechanism is important in any study of bond.

1.4 Object and Scope

The purpose of this research is to determine the effect of epoxy coatings on the bond strength between reinforcement and concrete and to develop recommendations for changes in the development length provisions of design codes.

Bond strength is evaluated based on flexural bond strength. Bond performance is evaluated in terms of both slip and ultimate bond force. The key parameters in the study are deformation pattern (3 patterns), bar size (No. 5, No. 6, No. 8, No. 11), and coating thickness (3 - 17 mils). In addition, the effects of cover (1, 2, 3 bar diameters) and bar position (top and bottom-cast) are evaluated.

A finite element model is developed to study the effects of the major variables to provide a better understanding of bond mechanisms, as affected by the change in surface properties caused by epoxy coatings.

Bond strength is measured using beam-end specimens similar to the specimens used by Brettmann, Darwin and Donahey (1984, 1986) for their study of the effects of superplasticized concrete on bond strength. The test specimens place both the steel and the concrete surrounding the bar in tension, as occurs in practice. These specimens are similar to those used by Johnston and Zia (1982). Test measurements include load, loaded end slip, and unloaded end slip.

For the most part, bottom-cast bars are used for maximum quality control and to limit the effects of finishing operations on bond strength (Donahey and Darwin 1985). Test bars are ASTM A 615

(1986) Grade 60 steel obtained from several suppliers. The epoxy coating was commercially applied fusion-bonded coating meeting the requirements of ASTM A 775-86 (1986).

A nonlinear finite element model is used to better understand the effect of coatings on bond strength. The model incorporates special link elements (Lopez et al. 1989) to represent the steel-concrete interface and "a fictitious crack model" (Hillerborg, Modeer and Petersson 1976) to represent concrete fracture.

This study is designed to both provide practice information, and cast light on basic concepts involving the behavior of epoxy-coated reinforcement.

CHAPTER 2: EXPERIMENTAL PROGRAM

2.1 General

This chapter describes the experimental program used to determine the effects of commercially applied epoxy coating on the bond strength of reinforcing bars. Beam-end specimens were employed to measure the bond strength. Tests were conducted using procedures developed by Donahey and Darwin (1983, 1985) and Brettmann, Darwin and Donahey (1984, 1986).

In addition to ultimate bond force, values of slip at the loaded and unloaded ends of the test bars were recorded to establish criteria for bond failure and to evaluate load-slip behavior. All specimens failed by splitting.

2.2 Variables of Test Program

The effect of epoxy coatings on the bond strength of epoxy coated reinforcing steel to concrete was investigated using a carefully controlled combination of test variables. Specimens were cast in groups providing for three replications for each combination of variables. The following parameters were evaluated:

Bar Surface: Reinforcing bars with three basic surface conditions were tested: mill scale bars, bars as originally produced; blast-cleaned bars, bars from which the mill scale had been removed in preparation for the application of the epoxy coating; and fusion-bonded epoxy-coated bars.

Coating Thickness: Three nominal thicknesses of epoxy coating, 5, 9 and 12 mils (1 mil = 0.001 in.), were used. Average values of actual coating thicknesses ranged from 3 to 17 mils.

Deformation pattern: Reinforcing bars with three deformation patterns, as described in Section 2.4.1, were tested.

Bar Size: Four bar sizes, No. 5, No. 6, No. 8 and No. 11, were tested. No. 5 and No. 8 bars were used for the more detailed studies, such as the combined effects of coating thickness, concrete cover and casting position.

Casting Position: Both top-cast and bottom-cast bars were evaluated. For the top-cast specimens, 15 in. of concrete was cast below the test bars.

Concrete Cover: Specimens with covers of 1, 2 and 3 bar diameters, d_b, were studied. For No. 5 bars, specimens with a 3 in. concrete cover (4.8 bar diameters) also were tested to evaluate the effects of additional confinement.

A total of 394 specimens were tested in the program presented in this report.

2.3 Test Specimens

Most test specimens were 9 in. wide and 24 in. long (Fig. 2.1). For No. 11 bars, the width was increased to 10 in. The amount of concrete above or below the bars was kept at 15 in., depending on whether the bars were bottom or top-cast. The thickness of concrete above the test region was adjusted to provide the desired cover.

Thus, the depth of the specimens equaled 15 in. plus bar diameter and cover thickness.

The bonded lengths of test bars were initially selected based on earlier studies (Donahey and Darwin 1985, Brettmann, Darwin, and Donahey 1986). Basic bonded lengths of $3\frac{1}{2}$ in. for No. 5, $4\frac{1}{2}$ in. for No. 6, 8 in. for No. 8, and 9 in. for No. 11 bars, were used as the standard specimens. In addition to the basic lengths, bars with longer bonded lengths, $8\frac{1}{2}$ in. for No. 5, $10\frac{1}{2}$ in. for No. 6, and 14 in. for No. 8, were tested to help evaluate the effect of epoxy coating as a function of bonded length.

As shown in Fig. 2.1(b), polyvinyl chloride (PVC) pipes were used as bond breakers to accurately limit the bonded length of the test bar to the specified value and to prevent a cone-type pullout failure on the front surface of the specimens. The length of the bond breaker pipes at the loaded end of the test bars, referred to here as the lead length, was $2\frac{3}{8}$ in. for No. 5, $2\frac{3}{4}$ in. for No. 6, $3\frac{3}{4}$ in. for No. 8, and $1\frac{1}{2}$ in. for No. 11 bars. The choice of the lead length and the bonded length will be discussed in Section 3.3.1.

The bond breaker pipes had inside diameters equal to the test bar diameters. The pipes were sealed against mortar seepage using Dow Corning Silicone Sealant, which was carefully applied between the PVC and the test bar. The test section of the bar was cleaned with acetone prior to testing. A steel pipe was butted against the unloaded face of the test bar and was coupled to the bar using another piece of PVC pipe. The steel pipe was used to provide access to the test bar for unloaded end slip measurements.

The test bar extended 22 in. out from the face of the test specimen. The test bars were oriented with the two longitudinal ribs facing the vertical sides of the specimens. Two auxiliary bars (Fig. 2.2), within the specimen and parallel to test bar, were provided to prevent the specimen from failing in flexure. The size of the auxiliary bars varied depending on the size of the test bar. No. 4, No. 5, No. 6 auxiliary bars were used for both No. 5 and No. 6, No. 8, and No. 11 test bars, respectively. A single transverse bar, located approximately 2 in. beyond the end of embedment length, was used to support the test bar. Two lifting bars, placed perpendicular to the test bar and located approximately at the centroid of the mass of the specimen, were added to help move the specimens (Fig. 2.2). Forms were constructed using 3/4-inch B-B plyform and 2 x 4 studs. Forms were coated with brushing lacquer to prevent water from being absorbed into the plywood. All joints were caulked to prevent water leakage.

2.4 Materials

2.4.1 Steel

ASTM A 615 Grade 60 steel bars were used for all tests. The bars of each size and deformation pattern were taken from the same heat. Yield strengths of the reinforcing bars are shown in Table 2.1.

Reinforcing bars with three deformation patterns were tested (Fig. 2.3). The deformation pattern on bars supplied by Structural

Metals, Inc. (designated S) consisted of ribs perpendicular to the axis of the bar. The deformation pattern on bars supplied by Chaparral Steel Company (designated C) consisted of diagonal ribs inclined at an angle of 60 degrees with respect to the axis of the bar. The deformation pattern on bars supplied by North Star Steel Company (designated N) consisted of diagonal ribs inclined at an angle of 70 degrees with the axis of the bar. The dimensions of the bar deformations were measured as discussed in Appendix A and are summarized in Table 2.1.

2.4.2 Concrete

Non air-entrained concrete was supplied by a local ready-mix concrete plant. Type I portland cement and 3/4 in. nominal maximum size coarse aggregate were used. The coarse aggregate was crushed limestone, and the fine aggregate was Kansas River sand.

Both 5000 psi and 6000 psi concretes were used for tests. 6000 psi concrete was used for the majority of specimens. The mix proportions are shown in Table 2.2. Concrete properties are summarized in Table 2.3.

2.4.3 Epoxy

The epoxy coating was commercially applied 3M Scotchkote 213 powder. The powder was deposited electrostatically. Coating thickness is required by ASTM A 775 (1988) to be 5 to 12 mils. Nominal thicknesses of 5, 9 and 12 mils were provided on the S and C-pattern bars. A 9 mil nominal thickness was provided on the N-pattern bars.

The thickness of the coating film was measured using a magnetic pull-off gage (Mikro-test III Thickness Gage). The gage was calibrated by the manufacturer. In addition, calibration was re-tested by measuring thin shims with similar thicknesses of the epoxy-coating film on a smooth steel plate prepared in the laboratory. To obtain more realistic test measurements, initial readings were taken on blast-cleaned bars. The initial correction factor, typically 1.1 mils, was then subtracted from the reading for the test bar to provide the final measured coating thickness.

Readings were taken at six points around the circumference of the bar between each set of deformations within the test bonded length. The means and standard deviations of the measured coating thicknesses are listed in Table 2.4. The actual measured values varied from the mean values. For example, for an S-pattern No. 8 bar, 72 readings were taken, producing a mean of 9.7 mils and a standard deviation of 0.9 mils. Actual values ranged from 7.6 to 12.5 mils. For an N-pattern No. 5 bar, 48 readings within the bonded length, giving a mean of 9.6 mils and a standard deviation of 1.3 mils. The values ranged from 7.5 to 13.2 mils. Distributions for the two bars are shown in Figs. 2.4 and 2.5.

2.5 Placement

The casting procedure was planned to help insure that the concrete was as uniform in quality as possible from specimen to specimen. Concrete was placed in two lifts using a bucket and overhead

crane. The first lift for all specimens was completed before any specimen received a second lift. Lifts were vibrated at six evenly spaced points.

Test cylinders were cast in steel molds and cured in the same manner as the specimens. Forms were stripped after the concrete cylinders had reached a strength of at least 3000 psi.

2.6 Test Apparatus and Procedure

The test apparatus shown in Fig. 2.6 (Brettmann et al. 1984) was used for the bond strength tests. Load was applied by two 60-ton hollow-core jacks powered by an Amsler hydraulic testing machine. Load was transferred through two 1-in. diameter cold-rolled steel load rods instrumented as load cells. Each load rod was equipped with two longitudinal and two transverse 350 ohm Micro-Measurements strain gages.

The test machine was tied to the structural floor using a wide flange beam and two tension rods, which extended through the structural floor. The test specimen was tied down vertically in a similar manner and was attached to a bearing pad at the front of the specimen to restrain the movement of the specimen in the horizontal direction, as shown in Fig. 2.6.

Slip was monitored at both the loaded and unloaded ends of the test bars. Two LVDT's were attached to the loaded end of the test bar, 1.25 in. from the exterior face of the concrete. To monitor unloaded end slip, a single LVDT was mounted on the projecting end of

the steel pipe embedded behind the test bar. All LVDT core rods were spring loaded so that movement of the bar would cause movement of the core.

The two load cells and three LVDT's were connected to a Hewlett-Packard data acquisition system. Bars were loaded at approximately 3.0 kips per minute for No. 5 and No. 6 bars and at 6.0 kips per minute for No. 8 and No. 11 bars. Load and loaded end slip were plotted as the tests progressed. During the first half of each test, the load was monitored at 2 second intervals. As the bar reached ultimate strength, the intervals were reduced to 1 second. A typical test lasted about 10 minutes.

Each group of specimens was tested within a 12 hour period (except for groups 1, 18 and 19 for which tests were completed over a 60 hour period), at ages ranging from 3 to 9 days, when the concrete reached the desired strength. Standard 6 x 12 in. concrete cylinders were tested in compression at the time of the bond tests to determine concrete strength (Table 2.3).

Bond forces at 0.002 in. unloaded end slip and ultimate are listed along with other test variables in Table 2.4. Table 2.4 also includes "modified" bond forces, which account for differences in concrete strength, cover and, for No. 5 bars, coating thickness. The details of obtaining modified bond forces are presented in Chapter 3.

2.7 Evaluation of Specimen Behavior

2.7.1 Specimen Failure

All specimens failed by splitting and exhibited similar behavior throughout the test. On the front surface of the specimens, one crack was observed to run straight up through the cover from the test bar to the top surface. The top surface then cracked parallel to and above the test bar over the bonded section of the bar, and the crack fanned out over the rear PVC bond breaker.

One or two cracks, generally dependent on the location of the bearing pad, ran down from the test bar. The specimens having a relatively small distance between the test bar and the bearing pad, such as 3 in. for No. 6 and larger bars, exhibited two cracks. Each crack formed at approximately 120 degrees from the first crack. These cracks passed down from the test bar to the sides of the specimen at the top of the bearing pad and continued to the rear PVC bond breaker as shown in Fig. 2.7(a).

The specimens having a large distance between the test bar and the bearing pad, such as 5 in. for No. 5 bars, exhibited failure as a single vertical crack as shown in Fig. 2.7(b). The vertical crack passed down from the test bar to the top of the bearing pad of the testing apparatus. This crack was accompanied by a second crack which ran across the face of the specimen at the top of the bearing pad, perpendicular to the first crack. Cracks on the sides of specimen could not be seen on the surface but continued internally to the

rear PVC bond breaker. These internal cracks could be seen after removal of the top concrete cover following the test.

Although two different crack patterns were observed, the concrete around the test bar always split into three parts: two prisms on either side of the bar from the top of the specimen and the remaining specimen below the bar. A typical crack surface can be seen in Fig. 2.8. The two top prisms were forced apart due to the wedging action of the test bar as the bar slipped.

2.7.2 Appearance After Failure

The bars were examined following testing by removing the top concrete cover over the bond region. Uncoated bars showed evidence of good adhesion (Fig. 2.9). Concrete particles were left on the shaft of the test bar and on the sides of the deformations. Wedges of compacted concrete powder were lodged in front of the ribs, adhering to the ribs on the pull side only.

As observed in the earlier tests of epoxy-coated reinforcement (Zia and Johnston 1982; Treece and Jirsa 1989), however, there was virtually no evidence of adhesion between the epoxy-coated bars and the surrounding concrete (Fig. 2.10). No concrete particles were left on the deformations or the shaft of the coated bar in the bonded length. The concrete in contact with the epoxy-coated bars had a smooth and glassy surface. Occasionally, the epoxy on bar showed minor damage from testing.

2.7.3 Load versus Slip

Insight into the bond behavior of uncoated and coated bars can be obtained by evaluating bar performance on the basis of slippage under load. Force as a function of slip, measured at the unloaded end of the bar, provides a measure of the stiffness of the bonded region. If the presence of an epoxy coating does indeed change the bond force, it would be expected that bond-slip behavior would change as well.

Unloaded end slip is used because loaded end slip is highly dependent upon local effects and, because of the close proximity of the applied load, variations in the data can result. Moreover, unloaded end slip is dependent on the bond over the entire bonded length and is generally a smooth function of load, thus providing a reliable measure of the bond stiffness. Load-unloaded end slip curves are plotted for several groups of specimens. Each figure corresponds to a group of specimens containing coated and uncoated bars of the same size and deformation pattern, allowing direct comparison of the behavior of coated and uncoated bars. These plots for the standard specimens (2 d_b cover, bottom-cast, and basic bonded lengths) are presented in Figs. 2.11 - 2.22. Curves for specimens with different covers (1, 2, and 3 bar diameters) and nonstandard lead lengths are presented in Figs. 2.23 and 2.24, respectively.

The curves clearly show the effects of epoxy coating on bond performance. At very low loads, the slope of the curves is very close for all bars. However, the slope quickly drops for coated bars. Overall, uncoated bars obtained a higher bond strength than

coated bars. At any given load, coated bars slip more than uncoated bars and, in most cases, reach the maximum load at greater values of slip than uncoated bars. The increase in slip for coated bars at the maximum load differed for each combination of bar size and deformation pattern. For example, the N-pattern No. 11 uncoated bars had an average unloaded end slip of 0.0035 in. as the maximum load is attained, while the coated bars had an average end slip of 0.0041 in., an increase of 17 percent. For the N-pattern No. 6 bars, the slip at the peak load increased by 55 percent, from 0.0029 in. to 0.0045 in., due to the coating. For the S-pattern No. 11 bars, the slip at peak load increased by 35 percent, from 0.0029 in. to 0.0039 in. Average values of unloaded end slip for the standard specimens at ultimate load, for the different bar sizes (No. 5, No. 6, No. 8, and No. 11) and the three deformation patterns, are listed in Table 2.5. While the values for average slips presented in this table reveal some differences among the various deformation patterns for each bar size, it is not clear that the specific values have significance.

As illustrated in Figs. 2.23 and 2.24, as cover or lead length increase, bond strength increases for both coated and uncoated bars. The slopes of curves depend on the bar surface properties, but not on the cover or lead length. The uncoated bars produce steeper curves than the coated bars.

The effects of coating on bond can be evaluated based on bond forces at a prescribed value of slip, in essence providing a comparison of bond stiffness. Review of the data plotted in Figs. 2.11 through Fig. 2.22 shows that in almost all tests, bond forces reach

ultimate at unloaded end slips in excess of 0.002 in. That is, in all cases, the bars are still effectively bonded to the concrete at unloaded end slips of 0.002 in. Bond forces corresponding to a 0.002 in. unloaded end slip are listed in Table 2.4 for all specimens in this study.

The lower bond stiffness of coated bars can also be observed by comparing average differences in bond force between uncoated and coated bars as a continuous function of slip. The majority of the bond reduction caused by the epoxy coating occurs at low values of slip. For example, Figs. 2.25 and 2.26 show that the average difference in bond force between uncoated and coated bars as a function of slip for No. 5 and No. 11 bars, respectively. In every case, in excess of 75 percent of the strength reduction caused by the coating occurred at an unloaded end slip of 0.001 in., less than one-third of the slip corresponding to ultimate.

The bond reduction of coated bars appears to be due to a substantial loss of adhesion and friction between the bar and the concrete, leaving mechanical interlock between the deformations and the concrete as the primary bond mechanism. However, considerable slip is required to bring the deformations to bear so mechanical interlock can occur. As a bar slips, the deformations force the adjacent concrete outward, causing splitting stresses which finally cause failure. The loss of adhesion and friction caused by the epoxy surface, as observed from the test bar appearance after failure (Section 2.7.2), is likely the main mechanism behind bond reduction

when epoxy coating is applied. This effect is studied in Chapter 4 using nonlinear finite element analysis.

Based on bond-slip behavior, epoxy coatings clearly affect bar performance. However, there are other parameters that also can influence the bond mechanism and the degree of bond strength reduction caused by an epoxy coating. The effects of parameters such as, coating thickness, deformation pattern, bar size, bar position, and cover will be discussed in detail in Chapter 3.

CHAPTER 3: EVALUATION OF EXPERIMENTAL RESULTS

3.1 General

In this chapter, the test results described in Chapter 2 are analyzed to examine the effects of epoxy coatings on concrete-steel bond strength. The effects of the major parameters -- coating thickness, deformation pattern, bar size, concrete cover and bar position -- are evaluated. In addition, tests designed to validate the test specimen itself are discussed.

Statistical analysis is employed to interpret the variations in the test data. The ratio of the bond strength of coated bars to the bond strength of uncoated bars, or relative bond strength C/U, will be used as the chief measure of the effects of epoxy coating.

So as to make comparison based on similar bases, variations in actual cover, coating thickness and concrete strength are corrected in the following manner. To account for actual deviations in concrete cover, bond strengths are adjusted to a nominal concrete cover of 1, 2 or 3 bar diameters. This adjustment is obtained by plotting all bond strengths for bars of a given size versus the actual measured cover. Covers ranging from 1 to 3 d_b are used. It is observed that the best fit lines for different groups of specimens are nearly parallel for bars of the same size, independent of deformation pattern or bar surface condition. Using the technique of dummy variables (Draper and Smith, 1981), parallel best fit lines are obtained based on the assumption that changes in cover cause the same incremental change in bond force for bars of the same size, independent of

deformation pattern or test group. Thus, each group of specimens is represented by a separate line. A typical plot, in this case for No. 11 bars, is shown in Fig. 3.1. Individual specimen strengths are corrected by shifting the measured bond strength parallel to the best fit line to a value corresponding to the nominal cover. The impact of this correction is small. An analysis using No. 5 and No. 6 bar data that was uncorrected for cover altered no conclusions obtained with the cover-corrected data. No cover correction was made for the No. 8 bars in groups 2 through 6, since actual cover was not measured for these specimens. Although the effect of this correction is small, it does reduce some of the scatter in the data and is applied to the majority of the data, where the cover was measured.

For the epoxy-coated No. 5 bars, a similar correction is necessary based on coating thickness (9 mils is taken as the standard), due to the sensitivity of the bond strength of these bars to the thickness of the epoxy. As will be demonstrated, larger bars do not require a coating thickness correction, because the bond strength of No. 6 bars and larger is not sensitive to coating thickness.

In addition to the cover and coating thickness corrections, test results are normalized with respect to a nominal concrete strength of 6,000 psi using the assumption that, within the concrete strength range used, bond strength is proportional to the square root of the compressive strength. Thus, bond strengths are multiplied by $(6000/f'_c)^{1/2}$ to obtain the final modified values. Both the original and modified values of bond force are summarized in Table 2.4.

3.2 Data Variation

In the course of previous studies, bond tests have been found to exhibit a great deal of scatter. A 10 percent difference between the bond strengths of nearly identical specimens is a typical difference observed in bond tests such as those of Johnston and Zia (1982). Often bond tests are run without replication, making it difficult to ascertain whether the results represent high, low or median values or whether differences in results are due to systematic causes or statistical variations.

In the study reported here, variations in bond strength are observed for replications of tests with mill scale, blast-cleaned, and coated bars. The replications provide a basis for statistical evaluation. Typically, the coefficients of variation in bond strength range from 5 to 10 percent.

There are several reasons for the observed scatter. Concrete is not a homogeneous material, having different constituents resulting in some variability of properties from specimen to specimen. For example, Table 3.1 (ACI Committee 224, 1986) illustrates the variation in results for relatively simple types of concrete tension and compression specimens. The coefficients of variation for splitting tensile strength, modulus of rupture, direct tensile strength, and compression cube strength performed on samples of the same material were 5, 6, 7, and 3.5 percent, respectively. Since bond failure is typically a tension failure, variations in bond strength should be expected to follow this trend and should be larger than variations

reported in Table 3.1 because of the greater number of parameters involved in bond strength.

A second reason for the observed scatter is that the interface between concrete and reinforcement is not uniform. There exist various small voids around the interface that become sites for crack initiation and propagation in the concrete and can affect the failure load. Thus, any study of bond performance must account for the natural variability in these voids and the resulting effect on the bond strength.

A third factor that may affect a reported result involves the methods employed in test selection and data reduction. For example, to examine the effects of epoxy coating on bond performance one would typically use the ratio of the bond strength of coated bars to the bond strength of uncoated bars. The computed ratio, however, has the effect of exaggerating the range of scatter. For example, the ultimate bond forces of the three mill scale bars with the N deformation pattern in group 4 were 45220, 50000 and 44580 lb. The mean and standard deviation for these results are 46600 lb and 2418 lb., respectively. The ultimate bond forces of the three coated bars in the same group were 35820, 42030 and 34970 lb., with a mean and standard deviation of 37607 and 3146 lb., respectively. In both cases, the coefficients of variation are less than 10 percent. Using these results, the ratio of the mean coated bond strength to the mean uncoated bond strength, C/U, is 0.807, which represents a measure of the bond reduction caused by the coating. However, had only a single coated and a single uncoated bar been tested, the reported ratio

could have been one of nine possible combinations of the bond strengths. In this case using individual test results, C/U could have ranged from 0.700 to 0.942, representing a 13 percent drop or a 17 percent gain from the original figure.

In the study by Treece and Jirsa (1987, 1989), strength ratios for pairs of coated and uncoated bars ranged from 0.54 to 0.88, resulting in an average ratio of 0.66, which was used for the design recommendations. However, since no replications were made, the individual test results may represent extreme values, leaving the effect of the test parameters uncertain.

Because of the scatter typically found in bond tests, it is difficult to study the effect of any parameter with a small number of tests. Testing several replications of each combination of parameters is a reliable way to increase confidence in the results and reduce the effects of random variations. In this study, at least three replications were used for each specimen configuration.

In addition to replications, statistical analysis is employed to interpret the variations in data so as to separate systematic differences from differences in test results that are random in nature. Hypothesis testing, specifically the two-sample t-test, as discussed in Appendix B, is performed to establish whether the observed differences in test results are caused by the normal variability in bond properties or some systematic cause. Because the data population is larger than those from previous studies, hypothesis testing becomes an effective tool for making this distinction.

The following sections contain the results of the test program. In each section, the effect of a specific parameter on bond is studied and the concepts discussed in this section are applied. In the course of this discussion, statistical evaluation of multiple replication tests is performed to determine the effects of parameters on bond performance. Care is taken to ensure that the observations and conclusions are based on genuine data trends and not data extremes.

3.3 Specimen Configuration and Steel Surface Effects

3.3.1 Choice of Lead Length and Embedment Length

The beam-end specimen was selected for use in this study because both the reinforcement and the surrounding concrete are placed in tension, as they would be in an actual structure. This contrasts with the conventional pullout specimen (ASTM C 234, 1986) in which the concrete is placed in compression. The beam-end specimen, however, must be designed so as to provide a measure of the bond force developed along the bar-concrete interface while preventing a cone-type pullout failure on the front surface of the specimen. The cone-type failure does not occur in a full-span beam because of the presence of continuous concrete all along the steel in the tension zone. The cone-type failure can be prevented in a beam-end test specimen by moving the bond interface to the interior of the specimen and away from the front surface. This is achieved by using a short section of PVC pipe to surround the bar to prevent bond of the steel to the concrete (Fig. 2.1). Thus, there is a length of unbonded bar, known as

the lead length, ahead of the bonded interface that reduces the stress field at the front surface of the specimen and eliminates the possibility of a pullout failure. Thus, a lead length is used in this type of beam-end specimen. Johnston and Zia (1982) used a relatively long lead length of 10 in. in their test specimens.

The length of bar that is directly bonded to the concrete and placed under load during the test is referred to as the bonded length. In this study, bonded lengths were purposely kept sufficiently short to ensure that the test bars remained elastic throughout the tests, since it is generally accepted that bars that yield do not provide reliable data as to the actual strength of the steel to concrete bond. As described in Chapter 2, the standard lead and bonded lengths in this study were: $2\frac{3}{8}$ in. and $3\frac{1}{2}$ in. for No. 5 bars, $2\frac{3}{4}$ in. and $4\frac{1}{2}$ in. for No. 6 bars, $3\frac{3}{4}$ in. and 8 in. for No. 8 bars, and $1\frac{1}{2}$ in. and 9 in. for No. 11 bars, respectively. The sum of the lead length and the bonded length will be referred to as the embedment length in the following discussion.

Under load, all specimens tested in this study were observed to fail by splitting. The splitting generally occurred along the top of the specimen starting directly over the bonded length and the lead length extending to the front surface of the specimen. Because the fracture process may begin in the bonded region and continue through the unbonded lead length region, there is a definite amount of energy required to fracture this concrete and drive the splitting failure to the front of the specimen. Thus, the lead length, while not directly a part of the bond mechanism, does play an important role in the ac-

tual fracture and splitting failure mechanism of the test specimen. However at the outset of the study, the contribution of the lead length to the bond force, as well as the effect of different lead or bonded lengths on the bond strength reduction caused by epoxy-coating, was unclear. Ideally, the ratio of coated bar bond strength to uncoated bar bond strength, C/U, would be independent of both lead length and bonded length.

To investigate the interaction of lead and bonded lengths on the ultimate bond force and C/U, No. 5 bars (groups 7, 8, 11 and 12) with lead lengths ranging from 0 to $3\frac{3}{4}$ in. with a constant bonded length of $3\frac{1}{2}$ in., and No. 5, No. 6 and No. 8 bars (group 16) with nonstandard lead and bonded lengths were tested.

The ultimate bond forces for the uncoated N-pattern No. 5 bars with $3\frac{1}{2}$ in. bonded length are plotted as a function of lead length in Fig. 3.2. For these tests, the ultimate bond force increases linearly with lead length. The bond forces, divided by the lead length plus bonded length, are plotted as a function of embedment length in Fig. 3.3. The bond strengths are nearly constant as embedment length increases from $3\frac{1}{2}$ to $7\frac{1}{4}$ in. It appears that the lead length does contribute to bond strength even though the reinforcement within the lead length region is not directly in contact with the surrounding concrete. The added strength is due to the extra energy required to drive the crack through the increased area of concrete. This observation points to the structural rather than material nature of bond failures. This point will be examined further using an analytical

model. A nonlinear finite element study of this behavior is presented in Chapter 4.

Fig. 3.4 compares the ultimate bond forces to the lead length for both coated and uncoated bars. As for the uncoated bars, the ultimate bond forces of the coated bars increase almost linearly with the lead length. Based on the best fit lines, C/U varies only from 0.936 to 0.934 for lead lengths of zero and $3\frac{3}{4}$ in., respectively. Thus, lead length does not appear to play a role in the relative bond strengths of coated and uncoated bars.

To study how C/U varies with bonded length, group 16 was used to compare the bond forces of coated and uncoated bars constructed with a long bonded length and a short lead length to the strength of specimens with the standard bonded and lead lengths. The nonstandard bonded lengths were $8\frac{1}{2}$ in. for No. 5 bars, $10\frac{1}{2}$ in. for No. 6 bars, and 14 in. for No. 8 bars. A lead length of $\frac{1}{2}$ in. was used for all bars in this group.

Fig. 3.5 compares the ultimate bond forces of N-pattern No. 5, No. 6, No. 8 and S-pattern No. 5 bars, as a function of bonded length plus lead length. The data points for the longer embedment (all from group 16) represent the average of at least 3 test specimens. The data points for the shorter embedment represent the average of the standard specimens of each type (corrected to a $2d_b$ cover and No. 5 bars corrected to a nominal 9 mil coating). As illustrated, the ultimate bond force increases with increasing embedment for No. 5 bars and No. 6 bars, but decreases with increasing embedment for No. 8 bars. This reduction occurs for both coated and uncoated No. 8 bars.

As point out before, Fig. 3.5 illustrates that maximum anchorage capacity does not depend solely on the length of bar in contact with concrete.

Fig. 3.5 also shows that the bond strengths of coated and uncoated bars respond similarly to changes in specimen geometry, resulting in only small changes in C/U. For the N-pattern No. 8 bars, C/U increases from 0.84 for the standard embedment length to 0.88 for the longer embedment length. For the N-pattern No. 6 bars, C/U increases slightly, from 0.99 for the standard embedment length to 1.01 for the longer embedment length. For the N-pattern No. 5 bars, C/U increases from 0.91 for the standard embedment length to 0.98 for the longer embedment length, while for the S-pattern No. 5 bars, C/U decreases from 0.83 to 0.76. When both deformation patterns are considered for No. 5 bars, C/U remains virtually unchanged for the two embedment lengths, with mean values of 0.87 for both standard and longer embedments.

Overall, these results might be used to suggest that C/U tends to increase with embedment length. However, considering the small number of nonstandard specimens tested, none of these variations is statistically significant. Thus, the evidence is just as strong that the effect of epoxy coating is independent of both the bonded length and the lead length. These observations contrast with the conclusion of Cleary and Ramirez (1989) that C/U drops with increasing anchorage length. However, their conclusion was based on an even smaller sampling of test data than considered here.

In summary, lead lengths of the beam-end specimens were designed so as to produce a splitting-type specimen failure while the bars remained elastic. The tests performed using these specimens reveal that bond strength increases as lead length increases for both coated and uncoated bars. This behavior indicates that a splitting failure is not only a failure of bond at the bar-concrete interface, but is also a structural fracture process. Differences in embedment length do not appear to affect the reduction in bond strength caused by epoxy coatings, thus validating the usefulness and generality of the test results obtained with the beam-end specimens used in this study.

3.3.2 Mill Scale and Blast-Cleaned Bars

To provide baseline data of bar performance as a function of bar surface for uncoated bars, the bond strengths of blast-cleaned bars were compared to the bond strengths of bars with a normal mill scale surface. The bars were of identical size and pattern. On the blast-cleaned bars, the mill scale surface was removed by sand blasting, as is done prior to applying an epoxy coating.

The test results for No. 5 and No. 8 bars, typical small and large bars, and all three deformation patterns are presented here. Both top-cast and bottom-cast bars are considered. The average bond strength of blast-cleaned bars is compared to the corresponding average bond strength of mill scale bars in the same group for the same bar size and deformation pattern in Table 3.2. The ratios of

the mean blast-cleaned bond strength to the mean mill scale (uncoated) bond strength, B/U, are also presented.

For the bottom-cast bars, the bond strength of the mill scale No. 5 bars with the S deformation pattern is greater by 5 percent than that of the corresponding blast-cleaned bars. However, for No. 8 bars with the same deformation pattern, the mean bond strength of the mill scale bars is weaker than that of blast-cleaned bars by 1 percent. Upon investigation of the average bond strength of all three deformation patterns, the No. 5 mill scale bars develop more bond strength than the blast-cleaned bars by 1 percent. However, for No. 8 mill scale bars, the bond strength is weaker than the bond strength of blast-cleaned bars by 3 percent.

For the top-cast bars, the results also show that the bond strengths of blast-cleaned bars are not greatly different from those of mill scale bars. Typical bond strength differences between blast-cleaned and mill scale bars are less than 2 percent for top-cast bars in each group. Clearly these variations in bond strength are not large and may well be within the data scatter typically found in bond tests.

Hypothesis testing, as discussed in section 3.2, can be used to determine if the difference in bond strengths between blast-cleaned and mill scale bars is statistically significant. Thus, the null hypothesis will be that the difference in bond strength between the mill scale and blast-cleaned bars is not caused by actual performance differences but rather is due to random data scatter, or more specifically that the mean bond strengths are equal. The two-sample t-

test, as presented in Appendix B, is used in this analysis. A level of significance, α, of 20 percent is used in this case. This value of α provides for a conservative analysis, because if the results confirm the hypothesis at this large error level, at lower, more typical values, the hypothesis also will agree.

The two-sample t-test is first made using bottom-cast No. 8 bars with the S deformation pattern as a case in point. The mean bond strengths for these mill scale and blast-cleaned No. 8 bars are 42361 and 43448 lb., with standard deviations of 2526 and 4344 lb., and sample sizes of 10 and 5, respectively (Table 3.3). The hypothesis test shows that the calculated t value, -0.62, falls between the critical t values, $\pm$ 1.35, which leads to a decision that the null hypothesis cannot be rejected. In other words, the assumption of the null hypothesis, that the mean bond strength of mill scale bars is equal to the mean bond strength of blast-cleaned bars, cannot be rejected with an assumed 0.20 level of significance. Based on the test results, even though there is a difference in bond strength for the bars with these two different surfaces, the difference in the mean bond strengths cannot be attributed to any actual mechanism other than the normal variability in bond properties and the resulting data scatter.

Similarly, hypothesis tests are made for the other bars shown in Table 3.3. As shown in Table 3.3, the null hypothesis cannot be rejected for any bar size, bar position, or deformation pattern, even at a 20 percent level of significance. Furthermore, the calculated t values in all cases fall well between the critical regions, even with

the relatively small standard deviations which are well below 10 percent of the mean values in all but one case.

In conclusion, baseline data for bar performance as a function of bar surface was obtained using mill scale and blast-cleaned bars. The results show no significant difference in bond between these two surfaces. Moreover, the results provide data for the later comparison with epoxy-coated bars.

3.4 Coating Thickness

Fusion bonded epoxy coatings are applied to reinforcing bars to inhibit contact of chlorides with the steel. Because the bars must have a sufficiently thick coating to prevent corrosion, there is a minimum coating thickness required, which is currently expressed as an average thickness. There is an upper limit on the coating thickness because of the relatively low stiffness of epoxy compared to concrete and steel and the possibility of an unacceptable amount of bond reduction with a thicker coating.

The limits on coating thickness, as set by ASTM A 775 (1988), are 5 and 12 mils. These values are based on the study by Clifton and Mathey at NBS (1976) using bars with nominal coating thicknesses ranging from 1 to 25 mils. In that study, bars with coatings between a 1 and 11 mils, on the average, developed 6 percent less capacity than uncoated bars using a pullout specimen. However, one bar with a 25 mil coating developed less than 50 percent of the bond strength of uncoated bars.

Based on these results, and the severe bond reduction obtained with the 25 mil coating, Clifton and Mathey recommended that epoxy coatings greater than 10 mils not be used in practice. However, since no tests were conducted on bars with a coating thickness between 11 and 25 mils, and only a single data point for a 25 mil coating existed, the relationship between coating thickness and bond strength was not definitely identified in the NBS study.

Coating thickness also was examined as a parameter in the study by Treece and Jirsa (1987, 1989). One of the main conclusions of their study was that bond reduction is insensitive to variations in coating thickness. However, close examination of the trends in the data provided in their report indicates that coating thickness does indeed have an effect for small bar sizes. The C/U ratios, 0.62 and 0.76 for bars with a nominal 12 mil coating, are much less than the values of 0.87 and 0.88 for bars with a 5 mil coating in two groups of No. 6 bars. In a group of No. 11 bars, the C/U ratio for a bar with 12 mil coating, 0.65, can be compared to 0.70 for a bar with a 5 mil coating. In the study by Johnston and Zia (1982), because of the relatively small range of coating thicknesses and the small number of specimens, they were not able to reach effective conclusions about the role of coating thickness on bond. Based on the limited evidence, it can be seen that the effect of coating thickness on bond is not well understood. However, the trend shows that bond performance decreases with increasing coating thickness. Also, larger bars appear to be more sensitive to coating but less sensitive to coating thickness than smaller bars.

To investigate the trends of bond strength with coating thickness, bars with a wide range of average thicknesses (3 to 17 mils) were tested. Because coating thickness is the parameter under evaluation, accurate coating thickness values must be obtained to assess bar performance. Since there is the potential for variation in the actual coating thickness around and along a test bar, in addition to measurement variations, readings were taken at several points around the circumference of the bar between each set of deformations within the test bonded length, as discussed in Chapter 2. The means and standard deviations of the measured coating thicknesses for all test bars are listed in Table 2.4.

To study the relation between coating thickness and the coated to uncoated bar bond strength ratio, C/U, the test results for No. 5 (groups 8, 9, 10, 11 and 12), No. 6 (groups 14 and 17) and No. 8 (groups 2, 3, 4, 5, 6 and 15) bars with the N, C and S deformation patterns are employed. The other variables were held constant -- the specimens in these groups contained bottom-cast bars, with 2 d_b cover, and the standard bonded length for each bar size.

The effect of coating thickness is illustrated in Figs. 3.6, 3.7, and 3.8 for No. 8, No. 6, and No. 5 bars, respectively. In these figures, C/U is plotted as a function of the epoxy coating thickness for each deformation pattern. Each data point represents the ratio of the bond strength of an individual epoxy-coated bar to the average bond strength of uncoated bars with the same deformation pattern in the same group of specimens. Using dummy variables, as discussed in Appendix C, the best fit lines for each deformation pat-

tern are obtained based on the assumptions that the effects of coating thickness are the same for the three deformation patterns but that the individual deformation patterns are affected to different degrees by the coating. In other words, the slope of the trend line represents the effects of coating thickness on all deformation patterns, while the different intercepts account for the distinct levels of bond strength reduction obtained for the individual deformation patterns.

The effect of coating thickness on No. 8 bars is demonstrated in Fig. 3.6. The results indicate that coating thickness plays virtually no role in the magnitude of strength reduction caused by the epoxy coating for No. 8 bars. The slope of the lines is -0.002/mil, representing a total decrease in C/U of only 0.012 as the coating thickness increases from 5 to 12 mils. Therefore, bond strength is essentially invariant with coating thickness for No. 8 bars. Similar results for the No. 6 bars are presented in Fig. 3.7. The best fit line is again virtually horizontal, with a slight positive slope of 0.0003/mil. Like the No. 8 bars, the reduction in bond strength caused by the epoxy coating for No. 6 bars is insensitive to coating thickness.

In contrast to these observations, Fig. 3.8 shows that coating thickness does play a significant role for No. 5 bars. The slope of the lines is -0.012/mil; that is, C/U for No. 5 bars drops 0.084 as the coating thickness increases from 5 to 12 mils, and 0.144 as the coating thickness increases from 3 to 15 mils. This observation does not conflict with the earlier observations (Johnston and Zia 1982,

Treece and Jirsa 1987, 1989), since those studies included no bars smaller than No. 6.

Load-slip curves also show the effect of coating thickness. Figs. 2.11-2.13 illustrate typical load-slip curves for No. 5 bars which exhibit a marked sensitivity to coating thickness. Uncoated bars obtained a higher strength than bars with a nominal 5 mil coating, which, in turn, had a greater bond strength than bars with thicker coatings. The initial slope of the load-slip curve decreases as coating thickness increases. However, Figs. 2.14-2.18 show the insensitivity to coating thickness for No. 6 and No. 8 bars.

As discussed earlier in this section, the limits on coating thickness prescribed by ASTM A 775 (1988) are 5 and 12 mils. In this study a wide range of coating thicknesses, from 3 to 17 mils, was examined, resulting in no significant reduction in bond strength for bars larger than No. 5. The insensitivity of the bond strength of bars larger than No. 5 to coating thickness indicates that coatings thicker than 12 mils might be used on larger bars to improve corrosion protection. This improved protection could be obtained with little reduction in bond strength beyond that currently observed. Additional study is necessary, however, before new limits on coating thickness can be established.

The differences in sensitivity to coating thickness demonstrate that there is a significant interaction between bar size and coating thickness that was not observed in previous research. The reasons behind the observed behavior are complex. Bond reduction appears to be dependent on coating thickness relative to the size of the ribs.

As bar size decreases, coating thickness becomes more significant in relation to the height of the ribs. Clearly, as bar size decreases, coating thickness must eventually play a significant role in bond strength reduction.

3.5 Deformation Pattern

One reinforcing bar deformation pattern can be distinguished from another pattern by parameters such as rib orientation, profile, height, spacing and bearing area. For deformed bars, the mechanical interaction between the ribs and the surrounding concrete is a major mechanism of bond. Therefore, rib characteristics play a key role in developing bond. Prior to the advent of epoxy coating, all deformation patterns in conformance with ASTM A 615 (1987) were assumed to be capable of similar performance. However, in this study, the test results reveal that the three deformation patterns studied do not perform identically when coated with epoxy.

A second look at Figs. 3.6-3.8 provides convincing evidence that the effect of the epoxy coating varies considerably with deformation pattern. For the three bar sizes illustrated, the S-pattern is affected the most. For No. 5 and No. 8 bars, the C-pattern is affected the least, while for No. 6 bars, the N-pattern is affected the least. Also, it can be observed that smaller bars are affected, on the average, less than larger bars. Some smaller bars, however, exhibit lower values of C/U than do larger bars of different deformation patterns.

Mean values of C/U based on group, deformation pattern and bar size are summarized in Table 3.4 for bottom-cast bars with a two bar diameter, 2 d_b, cover. For a 9 mil coating, the mean values of C/U for the S, C, N deformation patterns are respectively, 0.83, 0.96 and 0.92 for No. 5 bars, 0.81, 0.91 and 0.99 for No. 6 bars, and 0.71, 0.90 and 0.84 for No. 8 bars.

For the No. 11 bars, because of the narrow range of coating thicknesses (8-12 mils) and the observed insensitivity of bond strength reduction to coating thickness for No. 6 and No. 8 bars, a mean bond strength is used to calculate of the C/U ratio for each deformation pattern. The ratios are found to be 0.85, 0.76 and 0.76 for bars with the S, N and C deformation patterns, respectively. These values are lower than the ratios obtained for No. 5 and No. 6 bars, as was the case for No. 8 bars. However, unlike the small bars, the coated S-pattern No. 11 bars possess the highest relative bond strength.

Hypothesis testing, as discussed in Section 3.2, is used to determine if the observed differences in bond strength are statistically significant. The evaluation is made for both uncoated and coated bars. For example, if the two-sample t-test is applied to uncoated No. 8 bars with the S and N deformation patterns (mean bond strengths for the S and N deformation pattern bars are 42361 and 44536 lb., with standard deviations of 2526 and 3416 lb., and sample sizes of 10 and 6, respectively), the test results show that the null hypothesis, that the mean bond strength for the S-pattern is equal to the mean bond strength for the N-pattern, cannot be rejected at a

0.05 level of significance. Thus, while there is a difference in the bond strength of uncoated bars for the two deformation patterns, the difference appears to be due to random variability, not a systematic cause.

However, if the test is applied to coated No. 8 bars with the S and N deformation pattern [mean bond strengths for the S and N deformation pattern bars are 31300 and 38828 lb., with standard deviations of 2827 and 3588 lb. and sample sizes of 20 and 8, respectively (Table 3.5)], the results show that the null hypothesis is rejected even at the 0.001 level of significance. Thus, it can be stated with 99.9 percent confidence that a significant difference in bond strength exists between these two deformation patterns and the differences in these bond strengths cannot be attributed to chance, but must be attributed to a systematic cause, i.e., the difference in deformation pattern.

Similarly other tests of coated bars are made for other bar sizes, and deformation patterns (Table 3.5). In most of the cases (8 out of 12), the null hypothesis is rejected. The results show that the bond strength reductions due to epoxy coatings strongly depend on deformation pattern.

Because the bond strength reductions depend on both bar size and deformation pattern, a parameter reflecting both bar size and pattern is needed. Earlier studies (Menzel 1939, Clark 1949) have shown that the bearing area of the deformation, measured as the projected area of the deformation, is one important parameter in the bond-slip behavior of uncoated bars.

In this study, it is observed that the bond strength reduction of coated bars with a large bearing area is generally less than the bond strength reduction of bars with a small bearing area. For example, the S-pattern No. 8 bars have the smallest bearing area per unit length of the No. 8 bars and exhibit the highest bond reduction, while the N-pattern bars have the largest bearing area per unit length of No. 8 bars and the lowest reduction.

Bearing areas also are a function of bar size. The bearing areas of large bars are larger than those of smaller bars. To compare the performance of bars of different size, bearing areas per inch of length can be divided by bar diameters or cross-sectional areas.

A parameter, the bearing area ratio, R_b (Table 2.1), equal to the ratio of the rib bearing area per inch of length to the nominal cross-sectional area of the bar, provides a correlation with C/U. The average values of C/U for individual groups of No. 5, No. 6, No. 8, and No. 11 bars are compared with R_b in Fig. 3.9. The comparison shows that C/U decreases significantly as R_b decreases.

Another parameter, known as the related rib area (Rehm 1961, Soretz and Hölzenbein 1979) (really the ratio of the bearing area of the ribs to the shearing area between ribs), R_r (Table 2.1), provides a similar correlation with C/U as shown in Fig. 3.10. R_r is considered to be an important predictor of the bond strength of deformed bars. For both R_b and R_r, the general correlation cuts across bar size, but the relative order of the bars in terms of R_b and R_r is not constant. Based on these comparisons, R_r provides slightly better

correlation with C/U, while comparisons with R_b have the advantage that bars of a given size are more closely grouped than if R_r is used. With additional analysis, it is likely that other parameters will be found to play a role.

Up to this point, the discussion has been based on the C/U values evaluated individually by deformation pattern. Thus, a coated bar may have a low C/U based on uncoated bars of the same deformation pattern, but, in fact, have a higher bond strength than another coated bar that has a high value of C/U because its uncoated bars have a low bond strength. For the balance of the discussion, the values of C/U will be based on the mean strengths of all uncoated bars of the same size.

The ratios of the mean strengths of uncoated bars in each group to the mean strength of all uncoated bars of the same size, U/U, are summarized in Table 3.4 for bottom-cast bars with 2 d_b cover. The mean values of U/U for the S, C, and N-patterns are, respectively, 1.03, 0.99 and 0.98 for No. 5 bars, 1.00, 0.98 and 1.01 for No. 6 bars, 0.98, 0.96 and 1.06 for No. 8 bars and 0.96, 1.00 and 1.04 for No. 11 bars.

Similarly, the mean values of C/U for a 9 mil coating calculated for the S, C, and N-patterns are, respectively, 0.86, 0.95 and 0.88 for No. 5 bars, 0.81, 0.90 and 1.00 for No. 6 bars, 0.73, 0.83 and 0.90 for No. 8 bars and 0.82, 0.75 and 0.79 for No. 11 bars. These values for U/U and C/U are compared with the bearing area ratio and the related rib area in Figs. 3.11 and 3.12, respectively. While there is no clear relationship between R_b or R_r and the relative

strengths of uncoated bars, relationships between both R_b and R_r and the relative strengths of coated bars are evident. It is worth noting that not only is the order of relative strength different for coated and uncoated bars of the same size, but that the range in the mean values of C/U significantly exceeds the range in the mean values of U/U. The wider spread in bond strengths of the coated bars emphasizes the strong dependence of bond strength reduction on deformation pattern.

Load versus slip curves can be used to compare the bond performance of epoxy-coated bars to that of uncoated bars. As discussed in Chapter 2, a comparison based on an unloaded end slip value of 0.002 in. will be employed. For No. 5 bars at 0.002 in. slip, C/U is 0.59, 0.67 and 0.65; for No. 6 bars, C/U is 0.70, 0.61 and 0.70; for No. 8 bars, C/U is 0.69, 0.93 and 0.73; for No. 11 bars, C/U is 0.68, 0.69 and 0.63, for bars with the S, C and N-patterns, respectively. The values of C/U at a 0.002 in. slip are lower than the corresponding C/U at ultimate. The order of relative strength by deformation pattern based on values of slip and ultimate is the same for No. 5 and No. 8 bars, but different for No. 6 and No. 11 bars. The role of deformation pattern on the bond reduction based on forces at a prescribed value of slip is not as clear as it is based on strength.

The reason for the lower values of C/U at 0.002 in. slip is that the majority of the bond reduction due to epoxy coating occurs at small values of slip, as illustrated in Figs. 2.25 and 2.26. At higher values of slip, the coated bars "catch up" somewhat, once the uncoated bars reach ultimate. For example, for No. 5 bars with the N

deformation pattern, the average value of C/U at 0.002 unloaded end slip, 0.65, is smaller than the average value of C/U at ultimate, 0.91. Since ACI 318-89 is based on strength, the C/U values at ultimate are selected for comparison in this study. However, it is clear that epoxy coating does indeed lower the bond performance of the bars causing more slippage under load as well as a decrease in bond strength.

In summary, the bond strength of coated bars depends on deformation pattern and bar size. Statistically significant differences in the bond strengths of coated bars are found for different deformation patterns, while no significant differences are seen in the strengths of uncoated bars. Bars with relatively higher rib bearing areas are affected less by the coating than bars with smaller bearing areas.

3.6 Bar Size

The effect of epoxy coating on bond strength as a function of bar size is shown in Fig. 3.13, which compares the relative bond strengths of coated and uncoated bottom-cast bars with 2 d_b cover by deformation pattern. The relative strengths are expressed in terms of the mean strength of uncoated bars of all three deformation patterns.

As illustrated in Fig. 3.13 and Table 3.4, large bars are affected to a greater degree by the presence of a coating than small bars. The mean values of C/U are 0.90, 0.90, 0.82 and 0.79 for No.

5, No. 6, No. 8 and No. 11 bars, respectively. Clearly, the bond reductions for No. 8 and No. 11 bars are larger than those for No. 5 and No. 6 bars. The C/U values obtained for No. 6 and No. 11 bars, 0.90 and 0.79, contrast sharply with the mean C/U values obtained by Treece and Jirsa (1987, 1989) for splices: 0.74 for No. 6 bars and 0.64 for No. 11 bars.

As discussed in Section 3.5, as the bearing area ratio, increases, the bond reduction of coated bars decreases. The bearing area ratios of smaller bars are, in general, greater than the bearing area ratios of the larger bars. The mean values of the bearing area ratio for No. 5, No. 6, No. 8 and No. 11 bars of the three deformation patterns in this study are 0.459, 0.396, 0.302 and 0.194 in^2/in^3. This difference in relative bearing area may well be the reason for the better bond performance of smaller coated bars.

In summary, the influence of coating on bond strength depends on bar size. Larger bars are affected by the presence of the epoxy coating more than smaller bars. The differences in the bond performance between different bar sizes appear to be caused by the relative size of the bearing area.

3.7 Concrete Cover

Concrete cover is important in normal design since it protects steel from corrosion. Cover also affects the confinement around a bar thus influencing the effectiveness of the bond process. The effects of cover can be seen in the failure mechanisms and the slippage observed.

Bond failure of deformed bars can occur in one of two ways. The ribs can push the surrounding concrete away from the bar by wedging action, resulting in large tensile stresses in the concrete and a splitting failure. Alternatively, the ribs can bear against the concrete, crush it and instigate a pullout failure. Typically, bond test specimens fail by splitting rather than by pullout, indicating that the tension stress field surrounding the bar is of critical importance. The transition between splitting and pullout is not well established (Jirsa, Lutz and Gergely 1979). However, it is clear that as confinement increases, a splitting failure becomes less likely while a pullout failure becomes more likely.

The new development length provisions in ACI 318-89, for the first time, address the effect of cover on development length and employ a 2 d_b cover as the standard. The new provisions recognize the effects of cover on bond of epoxy-coated bars and employ cover as a parameter for adjusting the specified epoxy-coated bar modification factors. The basic development length of an uncoated bar is multiplied by an adjustment factor of 1.5 for bars with a cover less than 3 d_b; in all other cases, the factor is 1.2.

For epoxy-coated bars the ACI Code (1989) employs the philosophy that when the concrete cover is less than 3 d_b, a splitting will occur, resulting in a large reduction in bond. In cases with more cover, a pullout failure will occur, resulting in a smaller bond reduction. This philosophy is based on the splice specimens tested by Treece and Jirsa (1987, 1989) which failed by splitting and the beam-end specimens tested by Johnston and Zia (1982) which were thought by

Treece and Jirsa to have failed in pullout, but which also failed by splitting. As discussed in Chapter 1, the large differences in modification factor cannot be reliably justified based on cover.

In the present study, three different test groups are used to study the effects of cover on the bond performance of coated and uncoated bars. The groups include bars with different deformation patterns (S and N), bar sizes (No. 5 and No. 8), casting positions (top and bottom-cast bars) and covers (1, 2, 3 and 4.8 d_b).

Group 1 consists of twelve top-cast S-pattern No. 8 bars (3 uncoated and 9 coated). Bond strengths of the uncoated and coated bars are plotted versus nominal cover in Fig. 3.14. Best-fit lines are also shown. For the group, the two best-fit lines are almost parallel. Based on the best fit lines, the values of C/U for bars with 1, 2 and 3 d_b cover are 0.81, 0.85 and 0.87, respectively.

Group 13 consists of bottom-cast N-pattern No. 5 bars. The group included one coated and one uncoated bar with 3 in. (4.8 d_b) cover. Like the bars with less cover, both of these bars failed by splitting, not pullout. However, these bars failed at a load above yield. The best-fit lines for coated and uncoated bars that exclude the bars that yielded cross at approximately 3 d_b cover, as illustrated in Fig. 3.15 (a). Based on the best-fit lines, the values of C/U are 0.94, 0.97 and 1.00 for 1, 2 and 3 d_b cover, respectively. The best-fit lines, including the bars that yielded, cross at a cover in excess of 5 d_b, as illustrated in Fig. 3.15(b). The values of C/U are 0.95, 0.97, 0.98, and 0.99 for 1, 2, 3 and 5 d_b cover, respectively.

In group 18, both top and bottom-cast N-pattern No. 8 bars are examined. The best-fit lines for the top-cast bars are virtually parallel, as shown in Fig. 3.16. The values of C/U are 0.83, 0.89 and 0.91 for 1, 2 and 3 d_b cover, respectively. The best-fit lines for the bottom-cast bars diverge slightly, as shown in Fig. 3.17. The values of C/U are 0.85, 0.89 and 0.90 for 1, 2 and 3 d_b cover, respectively. The values of C/U for these comparisons are summarized in Table 3.6.

The effect of cover on bond strength observed in these tests does not match the new provisions of ACI 318. For example, on one hand the coated No. 5 bar specimens with 1 d_b cover (Fig. 3.15) developed about 85 percent of the bond strength of 2 d_b cover specimens, corresponding to an 18 percent increase in development length. This contrasts with the ACI Code which, for 1 d_b or less cover, requires a 100 percent increase in the development length. On the other hand, bars with 3 d_b cover consistently developed a higher bond strength than bars with 2 d_b cover. The beneficial effect of cover above 2 d_b are not reflected in the development length provisions for uncoated bars in ACI 318-89.

It is worthy of note that in these tests, increasing cover did not result in a transition from a splitting to a pullout failure. In all cases, failure occurred by splitting and no pullout failure was observed in any test. Even the No. 5 bars with 3 in. (4.8 d_b) cover in group 13 failed by splitting not pullout. Cover does affect C/U, but the change is gradual and the results do not justify a 20 percent (1.5 to 1.2) change in the development length modification factor at

a cover of 3 d_b, as provided in the new design provisions (1989). As will be described in Section 5.3, modification factors closer to 1.3 than 1.5 appear to be satisfactory in many applications for bars with a 2 d_b cover.

The bond strength of both coated and uncoated bars consistently increases as cover increases. Overall, the strength difference between coated and uncoated bars is approximately constant as cover changes.

The relationship between bond strength and cover illustrated in Figs. 3.14 - 3.17 demonstrates that the bond strength of coated bars can be improved to that of uncoated bars by adding cover. This feature can be observed for group 13 in Fig. 3.15. Coated No. 5 bars with 2.25 d_b cover develop the same bond strength as uncoated bars with 2 d_b cover. In groups 1 and 18, Figs. 3.14 and 3.16, coated No. 8 bars with the S and N patterns with an additional 0.5 d_b cover develop approximately the same bond strength as the corresponding uncoated bars. Therefore, one option for design is to add additional cover to compensate for the effects of the coating. The additional cover required may vary depending on bar size and pattern; however, an additional 0.5 d_b cover appears to be a safe bound for which there should be no required increase in development length.

In summary, the bond strength of both coated and uncoated bars increases as cover increases. The rate of increase is approximately the same for coated and uncoated bars. The absolute magnitude of the reduction in bond strength caused by coatings appears to be independ-

ent of cover. These observations differ from the epoxy-coated bar provisions in ACI 318-89.

3.8 Bar Position

The bond strength of deformed bars is a function of the quality of the concrete surrounding the bars. The quality of the concrete depends in part on the relative position of the bar in the section when casting. Bars cast in the top part of a section are subjected to sedimentation or settlement that take place during concrete placement. Settlement of the components of the mixture results in a weakened region of concrete under the bar caused by air and lightweight particles that are trapped under the bar. Parameters that affect settlement include the depth of plastic concrete cast below the bar, concrete slump, water-cement ratio, concrete temperature and degree of consolidation.

Settlement causes top-cast bars to have poorer bond than bottom-cast bars. Water, being the lightest component, segregates from the rest of mix as the aggregate particles settle within the mass of the fresh concrete. This water segregation or bleeding leads to the formation of voids under the bars. Bleed water also results in a locally higher water-cement ratio and weaker cement paste. The amount of settlement depends on the rate at which the fresh concrete sets and the water-tightness of the formwork. Settlement can result in longitudinal cracks over bars cast near an upper surface (Dakhil, Cady and Carrier 1975; Donahey and Darwin 1983). These longitudinal cracks can act as incipient bond cracks.

In ACI 318-83, the basic development length, ℓ_{db}, is modified by a factor of 1.4 for top reinforcement to account for position of the bar in freshly placed concrete. In ACI 318-89, this factor is reduced to 1.3 to reflect recent research (Jirsa and Breen 1981; Jeanty, Mitchell and Mirza 1988) that indicates a lower factor is more in line with actual behavior.

An upper limit for combined modification factors is specified in the new code when epoxy-coated bars are used as top reinforcement. The product of the factor for top reinforcement and the factor for epoxy-coated reinforcement need not be greater than 1.7. This factor for epoxy-coated top-cast bars is based on the recommendations by Treece and Jirsa (1987, 1989). Their study includes two series of specimens with bottom and top-cast bars. The results indicate little top-bar effect for uncoated bars: the average bond strength of the top-cast bars is about 5 percent less than that of the bottom-cast bars. Moreover, for coated bars, the bond strengths of top-cast bars were higher than those of bottom-cast bars by 5 and 18 percent in the two series. Even though no reduction in bond was observed due to casting positions, a combined factor for top reinforcement and epoxy-coated bars, up to 1.7, is used based on the assumption that there may exist some additional effect of the coating on top-cast bars.

In the study reported here, the effect of casting position on coated and uncoated bars is studied as a function of bar size and deformation pattern. The amount of concrete below the top bars was 15 in. in all cases, while the slump of the concrete ranged from 1.0 in. to 5.75 in. Both 5000 psi and 6000 psi concretes were used for

tests. The test results for No. 5 (groups 7, 9, 10 and 11), No. 6 (group 17) and No. 8 (group 18) bars with different deformation patterns and different covers (1, 2 and 3 d_b) were studied. The effects of increased section depth and slump were not addressed in this study. Research using deep specimens with 36 in. depth and high slump concrete is the subject of a following report.

To compare top-bar effects, the ratios of the average bond strengths of bottom-cast bars to those for top-cast bars are obtained. The ratios can then be compared to the modification factor for top reinforcement found in the ACI Code (1989). As shown in Table 3.7, the ratios (the top-bar effect) for the uncoated No. 5 bars are 1.22, 1.12, and 1.10 for the S, C, and N-patterns, respectively. For the coated No. 5 bars, the top-bar effects are 1.08, 1.12, and 1.22 for the S, C and N-patterns. The concrete slump used in these specimens ranged from $3\frac{1}{2}$ to $4\frac{1}{2}$ in. No. 8 uncoated bars with 2 d_b cover exhibit top-bar effects for the S and N-patterns of 1.18 and 1.23. For the coated No. 8 bars, the respective ratios are 1.13 and 1.14. In these cases, the top-bar effect does not appear to be a function of either deformation pattern or bar size, and the variations in the top-bar effect are well within data scatter typically found in bond tests. Little variation in the top-bar effect can be observed in group 18 where 1, 2 and 3 d_b covers were employed.

Slump is an important factor in concrete settlement. The ratios for bottom bar strength to top bar strength are plotted versus slump for slumps ranging 1 and $5\frac{3}{4}$ in. in Fig. 3.18. The best-fit lines also are drawn for the uncoated and coated bars. As expected,

the decrease in bond strength of uncoated bars depends on slump and becomes significant at slump values above $3\frac{1}{2}$ in. The top-bar effect for uncoated bars changes from 1.0 at a 1 in. slump to 1.3 at a 6 in. slump. The value of top-bar effect at the high slump matches the 1.3 modification factor used in ACI 318-89.

In contrast to the results obtained for uncoated bars, the decrease in bond strength of coated bars does not appear to be very sensitive to increasing slump. For coated bars, increasing slump does increase the top-bar effect, but the change is gradual, as illustrated in Fig. 3.18. Thus the top-bar effect is only 1.15 at a 6 in. slump. This reduction in the top-bar effect can be attributed to the fact that an epoxy coating and weakened concrete at the interface caused by bleeding and settlement have similar effects on bond strength. This observation is important because the value of the top-bar modification factor, 1.3, used in the ACI Building Code (1989) is based on a "worst case", i.e., for uncoated bars cast in high slump concrete.

The combined factors for top reinforcement and epoxy-coated bars, the bond strength ratios of bottom-cast uncoated bars to top-cast coated bars, are listed in Table 3.5. The values of the combined factors, ranging from 1.10 to 1.37, are considerably below the upper limit of 1.7 on the product of the epoxy coating factor and the top-bar factor in ACI 318-89. The relative insensitivity of coated bars to the top-bar effect suggests that either a lower top-bar factor or a limit for the combined factors below 1.7 be applied for epoxy-coated bars.

In summary, bond strengths decrease for both uncoated and coated top-cast bars. The amount of the decrease appears to be dependent on concrete slump. However, the top-bar effect is much less sensitive to slump for coated bars than for uncoated bars. The combined effect of bar position and epoxy coating is significantly below that suggested by the upper limit on the combined development modification factors in the new ACI Code (1989).

3.9 Summary

The experimental results are analyzed to examine the effect of epoxy coatings on concrete-steel bond strength. The evaluation of the results from this research project can be summarized as follows:

1. Epoxy coatings in the range of 3 to 17 mils significantly reduce the bond strength of deformed reinforcing bars to concrete. However, the extent of the reduction is less than that used to establish the development length modification factors in the 1989 ACI Building Code and 1989 AASHTO Bridge Specifications.
2. For coatings between 3 and 17 mils in thickness, differences in coating thickness have little effect on the amount of the bond strength reduction for No. 6 bars and larger. Thicker coatings cause a greater reduction in bond strength than do thinner coatings for No. 5 bars.
3. Tne magnitude of the reduction depends on deformation pattern and bar size. Bars with relatively larger rib bearing

areas are affected less by the coating than bars with smaller bearing areas.

4. In general, the reduction in bond strength caused by epoxy coating increases with bar size.
5. The bond strength of both coated and uncoated bars increases as cover increases. The rate of increase is approximately the same for coated and uncoated bars. The reduction in bond strength caused by epoxy coating is less sensitive to cover than reflected in the new provisions in ACI 318-89.
6. Bond strength decreases for both uncoated and coated top-cast bars, depending on concrete slump. However, the bond strength of coated bars is less sensitive to increasing slump than the bond strength of uncoated bars. The combined factors for top-cast epoxy-coated bars are 1.4 or less, below the value of 1.7 found in ACI 318-89.
7. No significant difference in bond strength between mill scale and blast-cleaned bars is found.
8. Bond strength increases as lead length increases for both coated and uncoated bars. However, differences in embedment length do not affect the reduction in bond strength caused by epoxy coatings.

In the next chapter, finite element analysis is used to study the effects of several parameters on the bond performance of epoxy-coated bars. The analytical results are then compared with the observations in this chapter along with those made in Chapter 2.

CHAPTER 4: FINITE ELEMENT STUDY OF BOND

4.1 Introduction

This chapter describes a finite element study of the effect of interfacial properties on the bond strength of reinforcing steel to concrete. The role played by epoxy coating on the behavior of beam-end specimens is specifically considered. The analytical model used in this study incorporates both nonlinear fracture mechanics and nonlinear bond interface behavior, yet in a relatively simple model.

Beam-end specimens are designed to duplicate the stress field that occurs in actual beams where both the reinforcing steel and the concrete are placed in tension. Specimen failure has been observed to be a splitting-type failure where the concrete around the bar splits due to the wedging action of the test bar when the bar slips. The finite element study is intended to explore the effects of the several parameters on this behavior and to explain the behavior observed during testing.

The experimental results presented in Chapters 2 and 3, show that epoxy coatings reduce bond strength, but that actual strength also depends on cover thickness and lead length. The load-slip curves for coated bars exhibit a lower initial slope than do the curves for uncoated bars.

The finite element model for the beam-end specimen includes representations for the deformed bar, the concrete, the splitting crack plane and the interface between the steel and the concrete. The concrete and steel are modeled using standard linear isoparamet-

ric elements. The interface is represented by special link elements that can be adjusted to match the specified stiffness and surface properties of the interfacial material. The longitudinal splitting crack is modeled using a nonlinear fracture mechanics scheme, Hillerborg's fictitious crack model (Hillerborg et al. 1976).

The goal of the analytical model is to incorporate the important aspects of material behavior in as simple a representation as possible, while duplicating the principal behavior of the test specimen. The model is used to study the key aspect of this research, the bond strength reduction caused by epoxy coating as a function of surface properties of the interfacial material. Since no definitive experimental tests have been performed to evaluate the actual interfacial properties of either coated or uncoated bars, representative values are used. No attempt is made here to exactly duplicate the experimental results from the beam-end tests. The effects of concrete cover and lead length on bond strength and performance are also investigated to explain their roles. The specific aspects of the finite element model including crack and interface representation are discussed next.

4.2 Crack Representation

The cracks observed in the test specimens consistently reveal a splitting failure with a dominant fracture surface or running crack. These failure surfaces can be characterized as being in an opening mode where local displacements are symmetric with two fracture sur-

faces displaced perpendicular to each other in opposite directions (Barsom and Rolfe, 1987). This basic behavior can be represented using a simple and straightforward nonlinear fracture mechanics approach.

Hillerborg et al. (1976) proposed the fictitious crack model for predicting crack propagation in concrete. In a concrete specimen, it is presumed that although the tensile strength is reached, a microcracked zone, the so-called fictitious crack, can transfer tensile stress. As the microcrack opens, the tensile stress capability decreases with increasing crack width. This stress transfer capability is represented as a stress-displacement curve, illustrated in Fig. 4.1 (Petersson 1980). As the crack width reaches w_o, all of the energy that can be absorbed by the concrete is accounted for and the tensile stress becomes zero. The area under this stress-displacement curve represents the energy absorbed per unit area of the crack surface in opening the crack from zero to w_o and can be calculated as:

$$G_c = \int_0^{w_o} \sigma \, dw \tag{4.1}$$

in which G_c is the fracture energy, σ is the tensile stress at the crack, w is the crack width, and w_o is the displacement at which the tensile stress in the concrete becomes zero. This particular representation has been shown to be accurate in representing overall frac-

ture behavior, and its applicability has been firmly established on a theoretical basis (Petersson 1981).

For the current study, the fictitious crack model is employed in the finite element analysis to represent the splitting crack that forms at the specimen center line. The crack is represented using rod elements perpendicular to a defined fracture plane located at the specimen center line. The elements are constrained to allow for the relative movement of nodes on either side of the crack plane perpendicular to the interface without relative movement parallel to the crack plane. The rod elements have two nodes, and each node has one degree of freedom parallel to the elements. The elements have a unit length and a total area equal to the total contact area across the crack plane.

In the initial elastic response prior to the rod elements attaining a tensile stress sufficient to begin cracking, the elements are intentionally modelled as very stiff, using a modulus of elasticity of 400,000 ksi. Upon reaching the tensile stress corresponding to the onset of tensile cracking, the rod elements are then constrained to follow a predefined stress-displacement relationship, such as illustrated in Fig. 4.2. For the current study, the area inside this stress-displacement curve, the fracture energy, is assumed to be 0.57 lb/in, a G_c value corresponding to the compressive strength of the concrete used in this study (Petersson 1981; Leibengood, Darwin and Dodds 1984). The tensile strength is set at 0.4 ksi based on the 6 ksi compressive strength. With these values, the dis-

placement at which the stress in the concrete becomes zero is determined by equating the area under the stress-displacement curve to the fracture energy of the concrete. This stress-displacement relationship is converted to a stress-strain function for the nonlinear material model of the rod elements, as shown in Fig. 4.3.

4.3 Interface Representation

Many finite element analysis problems in structural engineering include interfaces between two or more bodies which may or may not be mechanically joined (Oden and Pires, 1983; Bathe and Chaudhary, 1985). Example problems for material interfaces include soil-structure interaction (Desai and Nagaraj, 1988), a friction-type bolted connection (Urzua et al., 1977), and many classical contact problems in engineering mechanics.

Forces are transferred from one body to another across an interface by normal stresses and tangential or shear stresses. A key aspect of the interfacial model is the slip surface which defines the combination of normal and tangential stresses which results in movement across the interface. The concrete-steel interface, for coated and uncoated bars, can be represented by a Mohr-Coulomb slip surface (Fig. 4.4). This model relates the normal stress, σ_n, to the shear stress, σ_s, across the interface as

$$|\sigma_s| = c - \sigma_n \tan \phi \qquad (4.2)$$

in which c and ϕ are the cohesion and the angle of friction ($\tan \phi = \mu$ = coefficient of friction), respectively.

The behavior of contact problems can be classified into three distinct modes or states, a stick or nonslip state, where both normal and tangential displacements are continuous; a slip state, where normal and shearing stresses are related according to the specified slip surface; and a separation state, where the surfaces move apart (Fig. 4.4). In the stick state, the magnitude of the tangential stress is lower than the limiting value, and there is no relative movement along the surface. While in the slip state, the magnitude of the shear stress has reached the limiting value on the slip surface corresponding to the current normal stress at that point on the surface, and the surface moves along the contact surface. The separation state, no normal contact force between the bodies exists, occurs as a result of tension and results in a gap between the surfaces.

The three behavior states for the interface are defined as follows:

Contact/stick

$$|\sigma_s| \leq c - \sigma_n \tan \phi \tag{4.3}$$

Contact/slip

$$|\sigma_s| > c - \sigma_n \tan \phi \quad \text{and} \quad \sigma_n \leq \varepsilon \tag{4.4}$$

Separation

$$|\sigma_s| > c - \sigma_n \tan \phi \quad \text{and} \quad \sigma_n > \varepsilon \tag{4.5}$$

The parameter ε is a small tensile stress used to insure that Eq. 4.5 is selected only when tension exists at the interface. A value of 0.01 ksi is used in this study.

The constitutive matrix of the interface element is defined for each of the three possible material states. In the current study, it is assumed that there is no volume change due to shearing strains, because of the relatively smooth crack surface between the concrete and the steel. Thus, the tangential and normal components of deformation are uncoupled making them straightforward to model. The stiffness matrices corresponding to the three states of contact/stick, contact/slip, and separation are represented as

Contact/stick

$$K_{stick} = \begin{bmatrix} k_n & 0 \\ 0 & k_s \end{bmatrix} \tag{4.6}$$

Contact/slip

$$K_{slip} = \begin{bmatrix} k_n & 0 \\ 0 & \mu k_n \end{bmatrix} + \begin{bmatrix} \alpha k_n & 0 \\ 0 & \alpha k_s \end{bmatrix} \tag{4.7}$$

Separation

$$K_{sep} = \begin{bmatrix} \alpha k_n & 0 \\ 0 & \alpha k_s \end{bmatrix} \tag{4.8}$$

The parameter α maintains numerical stability by providing a small separation stiffness and a non-singular slip stiffness. The value of 0.015 is used for α.

The interface between concrete and steel is represented using a two-dimensional interface link element (Fig. 4.5) placed at the contact surface across which slip occurs. These link elements have no physical length, but each element is assumed to act over a specified segment of the interface boundary denoted as the contact length and behaves as if it has a unit length and a unit width. The elements have one degree of freedom tangent to the interface and one degree of freedom normal to the interface. Three nodes are needed to define the position and orientation of the elements. Nodes 1 and 2 (Fig. 4.5) are attached, respectively, to either side of the interface. Node 3 is a coordinate point that is used to define the orientation of the element. The coordinates of nodes 1 and 2 can be coincident, such as may be obtained with a zero thickness coating, or can be separated to represent a finite interfacial dimension.

The elastic properties of the interface can be adjusted to represent either a zero thickness interface, as in the case of no coating, or a epoxy coating of specified thickness. In this study, a zero thickness is used for both uncoated and coated interfaces. In

all cases before slippage, relative movement is resisted by the interface link element, and the relative movement is minimized using a large value of stiffness of the link element. Therefore, in this study, the normal stiffness and tangential or shear stiffness are defined as 400,000 ksi to preclude such slippage prior to reaching the failure surface.

During loading when slip occurs, the cohesion is set equal to zero, collapsing the surface (or sliding it to the left), and the stresses in the interfacial element are corrected to the new slip surface, as illustrated in Fig. 4.6. Thus, the initial slip surface represents adhesion plus friction between the surfaces of concrete and steel, while the newly defined slip surface represents frictional contact only, simulating the situation in concrete when the bar breaks free and the adhesion is destroyed. For this study, the cohesion and coefficient of friction are 0.25 ksi and 0.3, respectively, for uncoated steel. The slip surface values are set to one-tenth of these values, 0.025 ksi and 0.03, respectively, for epoxy-coated surfaces.

4.4 Finite Element Model

The finite element model represents the beam-end specimens in this study through three substructures. These consist of an exterior concrete substructure, a refined interior concrete substructure and a reinforcing bar substructure, together with the representation for the crack plane and the interface between the reinforcing bar and the

concrete. The exterior concrete substructure, representing the overall specimen, is used to simulate the splitting of concrete, while the interior concrete substructure is associated with the reinforcing bar through the interface elements to simulate slippage at the bar-concrete interface. The substructure technique is used to reduce the degrees of freedom and computation time for each substructure. The specific aspects of the finite element modeling are described in this section.

4.4.1 Concrete and Steel Material Models

With the exception of the interface between concrete and steel and the crack plane within the concrete, concrete and steel are represented as linear elastic materials. Concrete is modeled using a modulus of elasticity of 4000 ksi and a Poisson's ratio of 0.2, while steel is represented using a modulus of elasticity of 29000 ksi and a Poisson's ratio of 0.3.

Concrete is represented using either a 4 node two-dimensional isoparametric element or an 8 node three-dimensional isoparametric brick element. Steel is represented using a 4 node two-dimensional isoparametric element. The three-dimensional elements are used to construct the exterior concrete model, while the two-dimensional elements are used to construct the interior concrete and the reinforcing bar model.

The standard linear 8 node brick elements, having no midpoint node, are used to produce a linear shape function. This allows the rod elements at the crack surface to have stress values that are con-

sistent with the stresses in the brick elements on the crack plane of the concrete. Similarly, the standard linear 4 node elements are used to achieve compatibility by assuming that all points on an interface segment, spanned by a single element, are in the same behavior mode (Herrmann 1978).

4.4.2 Beam-End Specimen

The finite element model consists of a single reinforcing bar in contact with the concrete at a distance from the front face of test specimen. Due to symmetry, only one-half of the beam-end specimen is modeled. At the plane of symmetry, the formation of a vertical crack is represented. To further simplify the representation, a square section is used to represent the reinforcing bar, and the deformations are placed only on the side surface and normal to the crack surface.

The finite element representation consists of three substructures (Fig. 4.7): a reinforcing bar substructure, an interior concrete substructure, and an exterior concrete substructure. With rod elements, the exterior concrete substructure is attached to the plane of symmetry, the crack plane. The refined interior concrete substructure is attacned to the reinforcing bar substructure through the interface elements.

The exterior concrete block represents the test specimen, including various cover thicknesses and lead lengths. The depth of the concrete block is 5 in. (below the bar), plus 1 in. for the bar diameter, plus the cover thickness. The length of the block is 9 in.

plus 0.64 in. for the constant bonded length of the bar plus the lead length. The width is 4.5 in., representing one-half of the specimen. The reinforcing bar is simplified using a two-dimensional representation and a limited bar length with one complete deformation, approximating an S-pattern No. 8 bar. The height and the widths at the top and bottom of the deformation are 0.06 in., 0.08 in., and 0.24 in., respectively. The bar length is 0.64 in., just slightly less than the rib spacing on an S-pattern No. 8 bar.

Modeling is carried out in two steps. The first step represents the splitting of the concrete along the crack surface, while the second step represents slippage. In the first step, the exterior concrete block is modeled using the 8 node three-dimensional isoparametric brick elements. Using the substructure technique, the large exterior concrete model is reduced by condensing out the interior nodes. The final model in this step consists of the front and back surfaces and the crack surface connected by rod elements. 443 rod elements are used for the model with 2 d_b cover. In this step, to obtain lateral load-lateral displacement curves, loads are applied only at the nodes where the reinforcing bar substructure is located. The lateral load-displacement curves that are generated with this substructure are used to define a single spring representing the concrete confinement that is used in the second step. This reduces the balance of the problem to two dimensions, greatly simplifying the solution.

In the second step, the reinforcing bar substructure is connected to the interior concrete substructure through interface

elements. The substructures are modeled using the 4 node two-dimensional isoparametric elements and connected by 19 link elements. The nodes on the straight edge of the concrete [Fig. 4.7(b)] are constrained (same lateral displacement on all nodes along the edge), and attached to the single spring whose properties were determined in the first step. The interior concrete block is in contact with the deformed reinforcing bar through the interface elements. In this step, bond slip is simulated by applying loads on the reinforcing bar substructure. Fig. 4.8 illustrates the overall finite element model.

In the first step, condensation is performed twice for the exterior concrete block because of the large numbers of nodes and elements. For example, for the model with 3 d_b cover, the large concrete block contains 2150 nodes and 1220 isoparametric brick elements. This block actually consists of two smaller blocks having 1083 and 1064 nodes, respectively. The interior nodes are condensed out, keeping only the nodes on the front surface and the common inner surface for connection. This substructure, having the front and connection surface, contains only 628 nodes. Another condensation step yields the final exterior concrete substructure with only the front surface, having 481 nodes, on which rod elements simulating the crack plane are connected. This condensation procedure is graphically illustrated in Fig. 4.9. The number of nodes in each condensation step for all cases in this study is summarized in Table 4.1.

The finite element models are generated with the PATRAN-II software system (1989). Nodal renumbering also is performed to mini-

mize the band width and is done with PATRAN-II using the minimum wave front criteria.

4.4.3 Solution Procedure

The solution method uses the incremental iterative Newton-Raphson procedure. There are two nonlinear processes represented in the solution, slippage and cracking. Unbalanced forces that result from slippage at the interface between the reinforcing steel and the concrete or cracks in the crack plane are reapplied in successive iterations until convergence is obtained. Load is applied by imposing displacements. Small increments of displacement (typically, 0.00008 in. and 0.0001 in. in the first and the second steps, respectively) are used to stablize the solution. To limit the computational effort, the initial material properties of the elements are used to form the global stiffness matrix for the initial load application. Global stiffness matrix updates are performed at every other iteration during the first step and during every iteration in the second step. As a convergence criterion, corrective iterations are performed so that the Euclidean norm of the residual nodal loads is less than 0.1 percent of the corresponding norm of the total nodal loads. Convergence behavior is excellent in the first step, with generally five or fewer iterations required for splitting of concrete to meet the convergence criterion. However in the second step, typically 15 iterations are needed to correct the unbalanced forces (resulting from both slip and cracking) to meet the same convergence criterion.

4.5 Numerical Results

In this section, the numerical results for the computed response of the beam-end specimens are presented and the effects of the key parameters are evaluated. The influence of interfacial properties on the bond strength of coated and uncoated bars is examined based on the load-slip behavior. The results for models using different interface materials, covers, and lead lengths are presented and discussed based on the observed behavior of the test specimens.

4.5.1 Splitting of Concrete

This section presents the solution results for the splitting of the concrete (first step). The effects of cover and lead length on the system are also examined.

Fig. 4.10 shows the lateral load-lateral displacement curves for the exterior concrete model with 1, 2 and 3 d_b covers. Similarly, Fig. 4.11 shows the lateral load-displacement curves for models with 1, 2 and 3 in. lead lengths and 2 d_b cover. It can be seen in both of these figures that as cover thickness or lead length increases, the lateral force required for splitting increases and the slope of the descending branch of the load-displacement curves becomes steeper. The load-displacement curves presented in Figs. 4.10 and 4.11 are used to define the single spring used to represent the concrete confinement in the second step (Section 4.4.2).

Crack propagation from the splitting of the concrete is shown in Fig. 4.12 for a model with 2 d_b cover. As expected, cracks start

in the concrete at a position centered on the position of the applied lateral load. Cracks spread through the concrete in all directions from the steel. Cracks rapidly reach the top and front of the specimen. At the peak load, all of the concrete above and in front of the reinforcing bar substructure is cracked, while parts of the concrete below and in back of the steel remain elastic. This crack generally matches the internal crack surface observed in the test specimen, as discussed in Section 2.8.1. Similar patterns of crack propagation are observed for the models with different covers and lead lengths. The following sections describe the solution results in the second step representing the interaction between the concrete and steel that causes the concrete to split.

4.5.2 Load-Slip Response

The performance of the analytical model is examined on the basis of load-slip response. That response, as can be seen in load-slip curves, passes through three stages, corresponding to different material states of the steel-concrete interface.

In the first stage, below one-tenth of the peak load, the interface elements change their material states progressively. Initially, all elements are in a stick state, but elements progress into slip or separation states depending on the location of the element along the deformation of the reinforcing bar. Fig. 4.13 shows typical load-slip curves for coated and uncoated bars at loads less than 1 kip. The progressive loss of tangent stiffness is shown in the figure. Elements change their material states and become softer

as load increases. Fig. 4.14 illustrates the progressive change of the material states along the interface between the concrete and reinforcing bar. Sliding initiates in the front interface elements and advances toward the back. Separation follows in a similar way. Finally, all link elements separate, except for the elements on the compression side of the rib which remain in the slip state.

The interfacial properties control the bond performance from the very beginning. Cohesion is lost early in this stage. Friction along the compression side of the ribs mainly contributes to the bond force.

In the second stage, the material states no longer change as the load is increased further. The elements in a slip state continue to slide and the other elements remain in separation. The complete curves, shown in Fig. 4.15, illustrate the change in nonlinear tangent stiffness up to the failure of the confined concrete.

In this second stage, there are several components to movement along the interface including sliding, relative tangential displacement; offset, relative normal displacement; and the absolute normal displacement due to compression of the concrete. In reality, the value of the offset should be zero. The relative movement normal to the interface can be minimized using a large value of stiffnesses for the link elements, as discussed in Section 4.3. Fig. 4.16 shows the movement of the interface from the initial load to the peak load for the model of an uncoated bar with 2 d_b cover. The offset is 0.00017 in., which is small compared to 0.0037 in. and 0.0050 in., the normal and the sliding movements, respectively.

As the reinforcing bar slides along the concrete surface, slip causes wedging of the surrounding concrete and finally failure. In the last stage, at the peak load and beyond, the models exhibit a typical brittle "bond failure", as illustrated in Fig. 4.15.

As shown in Fig. 4.17, the model with 1 d_b cover possesses a relatively flat load-slip curve. As the concrete cover increases, the bond force drops rapidly, leading to a steep descending branch and brittle failure. Because of numerical instability, the descending branch is not well established for the models with 2 d_b and 3 d_b cover. The negative value of the tangent stiffness of the confining concrete spring (Figs. 4.10 and 4.11) and the sliding of the link element cause the nonlinear solution to oscillate. For future analyses, this problem could be rectified by using a non-negative spring stiffness for constructing the stiffness matrix.

A sudden failure was also observed in the laboratory, as discussed in Section 2.7. The brittle failure may be due not only to the brittle nature of concrete but also to the characteristics of a wedging failure. At the onset of concrete fracture, the resisting capacity to wedging drops. The decrease in resistance causes a sharp increase of the displacement of the wedge. The sharp increase in the lateral displacement at the moment of failure is illustrated in Fig. 4.18.

At this point, it is interesting to examine the factors that govern the ultimate bond force. The maximum slip resistance is attained when the maximum compressive force is exerted on the interface surface. Suppose that two rigid bodies in contact are in equilibrium

and are subjected to a system of forces. To maintain equilibrium, a normal force and a tangential force along the interface must equal the sum of components from the compressive force and the sliding force in the normal and the tangential directions, respectively. If a compressive force acts along the interface with an angle of γ (Fig. 4.19), the sliding force, normal to the compressive force, may be expressed as

$$H = P \frac{(\tan \gamma + \mu)}{(1 - \mu \tan \gamma)} + \frac{Ac}{\cos \gamma (1 - \mu \tan \gamma)} \qquad (4.9)$$

in which H is the sliding force, P is the compressive force, and A is the contact area. The two terms in the right side of the equation represent the contributions of friction and cohesion to the sliding force, respectively. Since c drops to zero once sliding occurs, only the first term on the right side of Eq. 4.9 is of interest.

In all cases in this study, the bond force reaches ultimate, as the lateral force reaches the peak spring force. Clearly the peak spring force of the concrete confinement (P in Eq. 4.9) governs the ultimate bond force. The computed ultimate bond force, for example, 12.98 kips for models of an uncoated bar with 2 d_b cover, can be verified with corresponding value, 12.95 kips, calculated using the first term on the right side of Eq. 4.9, assuming that the peak spring force, 9.55 kips for this case, acts on the model along the inclined surface (γ is 36.9 degrees in this model) as a compressive force. The verification is possible because the model is so simple.

From this discussion, it is observed that concrete confinement is critical for bond performance. As the capacity of the concrete confinement increases, the ultimate bond force increases. As illustrated in Eq. 4.9, the contact area is important only when cohesion is effective. After losing the cohesion, the coefficient of friction, μ, and the angle, γ, are the major parameters. These values have a dual effect on the sliding force. As the value of either μ or γ increases, the numerator in Eq. 4.9 increases and the denominator decreases, which, in turn, results in a dramatic increase in the resistance to sliding. When tan γ becomes equal to μ^{-1} = cot ϕ (ϕ = friction angle), the bond force becomes infinite and sliding does not occur. Since the angle, γ, is not always the rib face angle but in practice may be the angle of the interface formed by crushed concrete in front of the rib, the determination of the actual angle is complicated. Further study, using models of round bars with different deformation configurations is needed to achieve a better understanding.

In summary, the load-slip response of the finite element model is observed through the three different stages. The properties of the slip interface and the confinement provided by the concrete govern the ultimate bond force. The partially closed-form solutions obtained with Eq. 4.9 match the results obtained with the finite element model. The process of changing material states for the interface and the computed behavior are in agreement with the overall load-slip response observed in the laboratory. The following sec-

tions describe the influence of specific parameters on the analytical model for both coated and uncoated bars.

4.5.3 Influence of Interfacial Properties

The interfacial properties defined for the Mohr-Coulomb model include cohesion and friction. The effect of cohesion can be seen before slip occurs and the interface loses cohesion. The effect of friction can be seen while the interface elements are in the slip state.

The influence of cohesion on the bond performance is illustrated in Fig. 4.13 for models representing coated and uncoated bars with 2 d_b cover. At this low load stage, those interface elements that are in the stick state maintain cohesion. However when slip occurs, cohesion is lost. The uncoated bar, c = 0.25 ksi, exhibits higher bond force than the coated bar, c = 0.025 ksi. As cohesion is lost, however, the uncoated bar shows a more marked change in load-slip behavior than the coated bar, because of the greater forces that are released when slip occurs.

After the loss of cohesion, friction along the compression side of the rib governs the overall bond performance, as shown in Fig. 4.15 where the uncoated bar exhibits both higher bond strength and greater load-slip stiffness than the coated bar. (Note that at the scale used in this figure, cohesion has a negligible effect on behavior.)

The reduction in bond strength due to epoxy coating is analytically predicted as 41 percent. This value can be verified using Eq.

4.9. This reduction is larger than the 28 percent observed in the tests for the S-pattern No. 8 bars, suggesting that the relative strength of the coated interface used in this analysis is too low. However, a quantitative agreement with the test results is not a goal in this case.

In general, the two load-slip curves show similar behavior to that observed in the test specimens. The overall effects of the surface properties on bond performance are correctly predicted by the finite element model using the Mohr-Coulomb surface.

4.5.4 Influence of Concrete Cover

The bond force-slip curves in Fig. 4.17 show that as cover increases, bond strength increases for both coated and uncoated bars. For uncoated bars, the ultimate bond forces are 9.89, 12.98 and 16.55 kips for the models with 1, 2 and 3 d_b covers, respectively. For coated bars, the ultimate bond forces are 5.81, 7.63 and 9.75 kips for the models with 1, 2 and 3 d_b covers, respectively. These forces are compared in Fig. 4.20.

As illustated in Figs. 4.17 and 4.20, the bond strength increase with additional cover is nearly linear; the bond strength for 3 d_b cover is slightly greater than would be expected for a truly linear relationship. However, the trend of the analytical results agrees well with the test results discussed in Section 3.7.

Further examination of these results reveals that the relative bond strength, the C/U ratio, is independent of cover. That is the C/U ratio is 0.59 for all three covers. Thus, the absolute differ-

ence in bond strength increases as cover increases. These observations differ somewhat from the observed behavior of the test specimens, discussed in Section 3.7, where C/U was observed to increase somewhat with increased cover, while the absolute magnitude of the reduction in bond strength caused by epoxy coating was found to be nearly independent of cover. Considering the simplicity of the finite element model, however, these differences may not be significant. In any case, these observations suggest that C/U is less sensitive to cover than reflected in provisions of ACI 318-89.

Several similarities are observed between the load-slip curves in Fig. 4.17 and Fig. 2.23 for the test bars with different covers in group 18. As cover increases, bond strength and slip increase for both coated and uncoated bars. At low loads, the slope of the curves depends on the interfacial properties of the bars, but not on the cover, with the uncoated bars producing the steeper curves. Overall, the effect of the bar surface properties is observed in both the analytical and experimental results.

Fig. 4.21 compares the strengths predicted by the finite element analyses to the experimental results for uncoated N-pattern No. 8 bars in group 18. The figure compares the ratios of the ultimate bond forces at different covers to the ultimate bond force for bars with 2 d_b cover. The curve for the finite element results is obtained using a cubic spline function through the data points for 1, 2 and 3 d_b covers. The curve from the finite element analysis fits well within the bounds of the experimental data.

A further comparison can be made using the empirical equations discussed in Chapter 1, the equations developed by Orangun, Jirsa, and Breen (1977) (Eq. 1.2), Jimenez, White and Gergely (1978) (Eq. 1.3), and Zsutty (1985) (Eq. 1.4). For each equation, the ratios of the bond strengths obtained at 1, 2, 3 d_b covers to the value at 2 d_b cover are compared to the analytical and experimental results obtained in this study in Fig. 4.22. The curve generated by Eq. 1.3 (Jimenez et al. 1978) shows a greater sensitivity to cover than exhibited by the test specimens. The other curves, generated by Eq. 1.2 (Orangun et al. 1977) and Eq. 1.4 (Zsutty 1985), closely match both the finite element solution and the test data in this study. It is important to note that the finite element solution agrees well with the empirical equations, although Eqs. 1.2 and 1.4 were based on lap splices and Eq. 1.3 was based on development and splice tests. The close agreement helps confirm that the effect of cover on bond strength is similar for beam-end and splice specimens.

4.5.5 Influence of Lead Length

As discussed in Section 3.3.1, the laboratory tests performed using specimens with different lead lengths reveal that bond strength increases as lead length increases for both coated and uncoated bars, but that the differences in embedment length do not affect the relative bond strength of the bars.

To confirm this behavior, models with 1, 2 and 3 in. lead lengths and 2 d_b cover are analyzed. Bond force-slip curves for coated and uncoated bars with 1, 2 and 3 in. lead lengths are

presented in Fig. 4.23. For uncoated bars, the ultimate bond forces are 10.83, 12.98 and 15.80 kips for the models with 1, 2 and 3 in. lead lengths, respectively. For coated bars, the ultimate bond forces are 6.37, 7.63 and 9.30 kips for the models with 1, 2 and 3 in. lead lengths, respectively. Ultimate bond force is plotted versus embedment length in Fig. 4.24. From these results it can be seen that as embedment length increases, bond strength increases for both coated and uncoated bars.

Once again, as predicted from Eq. 4.9, the relative bond strength, C/U, is independent of lead length. The C/U equals 0.59 for the models with 1, 2 and 3 in. lead lengths. The insensitivity of C/U to lead length agrees with the behavior observed in the laboratory.

There are also similarities between the curves in Fig. 4.23 and the load-slip curves in Fig. 2.24 for the test bars with different lead lengths in group 12. With one notable exception in Fig. 2.24, at low loads, the slopes of the curves depend on the bar surface properties, not on the bond length; the slope of the curves for uncoated bars is steeper than the slope of the curves for coated bars.

Fig. 4.25 compares the ratios of the ultimate bond forces for each value of lead length to the ultimate bond force obtained with a 1 in. lead length for the finite element models and the No. 5 bars in group 12. Although there are significant differences in the geometric properties of the analytical models and the test specimens, such as bar size and bonded length, the overall behavior is strikingly

similar with the curve from the finite element study plotting well within the bounds of the experimental test data.

The close agreement between the laboratory and the analytical results confirms the effect of the lead length on strength, that is that the lead length contributes to bond strength, even though the bar is not contacted with the surrounding concrete through the lead length. The added strength from the lead length is due to the extra energy required to drive the crack through the increased volume of concrete. This observation emphasizes the structural rather than material nature of the bond failure process and helps validate the usefulness and generality of the test results in this study.

4.6 Summary

Finite element analysis is used to study the effects of interfacial properties on the bond strength of reinforcing steel to concrete. The finite element studies, in general, agree closely with the laboratory results. Although the finite element representations are simple, modeling of the bar-concrete interface using the Mohr-Coulomb surface, coupled with the fictitious crack model, correctly predicts the overall effects of the surface properties on bond performance. The similarity in analytical and laboratory behavior helps confirm the modeling process and demonstrates that the parameters thought to affect bond do, in fact, play important roles in controlling bond strength.

CHAPTER 5: SUMMARY, CONCLUSIONS AND DESIGN IMPLICATIONS

5.1 Summary

The purpose of this investigation is to study the effects of epoxy coatings on concrete-steel bond strength. Three hundred ninety-four beam-end specimens were tested. The major variables in this study are bar surface (mill scale, blast-cleaned, and epoxy coated), epoxy coating thickness (3 - 17 mils), deformation pattern (3 patterns), bar size (No. 5, No. 6, No. 8, No. 11), concrete cover (1, 2, and 3 bar diameters), and casting position (top and bottom-cast). The effects of embedment length on the relative bond strength of coated bars are also addressed in this study.

Statistical analysis is employed to interpret the variations in the test data so as to separate systematic differences from random differences in test results. The test results are analyzed to evaluate the effects of the major variables on concrete-steel bond. The test results are also compared with the epoxy-coated bar provisions in the ACI 318-89 (1989) and AASHTO (1989).

Nonlinear finite element analysis is employed to better understand the bond mechanisms as affected by the change in surface properties caused by epoxy coating. The finite element model includes representations for the deformed bar, the concrete, the splitting crack plane and the interfacial material. The model is used to study the bond reduction by epoxy coatings due to the different interfacial properties. In addition, the effects of concrete cover and lead length on bond strength and performance are studied to

examine the interface failure as well as the structural fracture process.

5.2 Observations and Conclusions

The following observations and conclusions are based on the results and analyses of the experimental and finite element studies presented in this report.

5.2.1 Experimental Study

1. Epoxy coatings in the range of 5 to 12 mils reduce the bond strength of deformed reinforcing bars to concrete. The extent of this reduction is less than that used to establish the development length modification factors in the 1989 ACI Building Code and 1989 AASHTO Bridge Specifications.
2. For coatings between 5 and 12 mils in thickness, differences in coating thickness have little effect on the amount of the bond strength reduction for No. 6 bars and larger. Thicker coatings do cause a greater reduction in bond strength than thinner coatings for No. 5 bars.
3. In general, the reduction in bond strength caused by epoxy coating increases with bar size. The mean values of the relative bond strength are 0.90, 0.90, 0.82 and 0.79 for No. 5, No. 6, No. 8 and No. 11 bars, respectively.
4. The magnitude of the reduction depends on deformation pattern. The size of the ribs and their arrangement and

inclination can have a profound effect on performance. Bars with larger rib bearing areas are affected less by the coating than bars with smaller bearing areas. The bearing area parameter is found to be a relatively accurate measure of bar capability.

5. The absolute reduction in bond strength caused by epoxy coating is largely independent of concrete cover. The amount of reduction is nearly constant for 1, 2, and 3 bar diameter covers.
6. Splitting failures are observed for all specimens. For the range of covers studied, increasing cover does not result in a transition from a splitting to a pullout failure for beam end-specimens.
7. Epoxy-coated bars are relatively insensitive to the top-bar effect. The combined factors for top bar and epoxy coated bars in this study are 1.4 or less, below the 1.7 combined factor found in the new ACI Code.
8. No significant difference in bond strength between mill scale and blast-cleaned bars is found.
9. The reduction in bond strength caused by epoxy coating is independent of embedment length. The various embedment lengths tested reveal no effect of bonded length on the amount of reduction.
10. The load-slip stiffness of coated bars is lower than that of uncoated bars. Coated bars slip more than uncoated bars at any load.

11. There is a large amount of scatter in the data, which is the characteristics of bond testing. Statistical work and large numbers of tests are important to establish accurate performance values and to identify systematic variations from random data fluctuations.

5.2.2 Finite Element Study

1. The reduction in the bond strength from epoxy coatings is simulated in the finite element model using different interfacial properties.
2. The interfacial properties govern the bond performance, with friction playing a major role. Adhesion appears not to play a significant role.
3. Bond strengths of coated and uncoated bars increase nearly linearly with additional cover and lead length, but the relative bond strength of coated bars is independent of cover and lead length.
4. The splitting crack in the finite element model generally matches the crack surface observed in the test specimens. The confinement of concrete from splitting is one of the governing factors in the ultimate bond force.
5. The finite element studies reveal close agreement between observed laboratory behavior and the computed results.
6. Modeling of the bar-concrete interface using the Mohr-Coulomb surface, coupled with the fictitious crack model to represent failure of the concrete, correctly predicts the

overall effects of surface properties on bond performance. This straightforward approach to modeling beam-end specimens provides a way to analytically investigate the effects of bar surface properties on the bond process.

5.3 Implications for Design

The results described here have important implications for design. The major observation is that the relative bond strength of epoxy-coated bars is considerably higher than the value of 0.66 used to calculate the 1.5 development length modification factor for bars with less than 3 d_b cover in the 1989 ACI Building Code and 1989 AASHTO Bridge Specifications. The lowest average value of C/U obtained for any bar size or deformation pattern, 0.73 for S-pattern No. 8 bars, translates into a modification factor of 1.37. No. 5, No. 6, and No. 11 bars are affected even less, with modification factors of 1.16, and 1.23, and 1.33, respectively, based on the deformation pattern with the lowest value of C/U. And these values are all based on a cover of 2 d_b.

Thus, a lower penalty is necessary for bars with a 2 d_b cover than recommended by Treece and Jirsa (1987, 1989) and implemented by ACI (1989) and AASHTO (1989) for bars with a cover less than 3 d_b. It appears that development length modification factors can safely be reduced to 1.25 for No. 6 bars and smaller and 1.35 or 1.40 for No. 7 bars and larger (care should be taken in selecting values for No. 14 and No. 18 bars, since no tests have been performed on these bar

sizes). A modification factor of 1.25 for No. 5 bars and smaller is more than needed, based on 9 mil coating, but will help to take into account the lower bond strengths obtained by small bars with thicker coatings.

The results suggest that development length modification factors can be reduced further by (1) altering deformation patterns to improve the bond strength of epoxy-coated bars or (2) standardizing on "strong" deformation patterns on an industry wide basis. Modification factors for each bar size should be based on the deformation pattern with the lowest mean C/U value, rather than the mean value of C/U for all bars of a given size, since deformation is clearly a controllable parameter.

The insensitivity to coating thickness of bars larger than No. 5 indicates that coatings thicker than 12 mils could be used on larger bars to improve corrosion protection. This improved protection could be obtained with little reduction in bond strength beyond that currently observed. Additional study is necessary, however, before new limits on coating thickness can be established.

The results show that no transition from a splitting to a pullout failure is found as concrete cover increases from 2 to 3 d_b. The absolute value of bond reduction is approximately the same for epoxy-coated bar with 1, 2, and 3 d_b cover and the relative strength changes less than 7 percent. This contrasts with the different modification factors, 1.5 for bars with cover less than 3 d_b or clear spacing between bars less than 6 d_b and 1.2 (ACI) or 1.15 (AASHTO) for bars in all other conditions. These results suggest that 2 d_b

cover can be the standard for coated bars, as it is for uncoated bars, with minor modifications made for 1 d_b and 3 d_b covers. The beneficial effects of increased cover may be translated into the use of increased cover rather than increased development length to account for reduced bond strength.

Epoxy-coated bars exhibit less top-bar effect than uncoated bars, 1.15 for uncoated bars in this study compared to 1.3 in ACI 318-89. The highest value of the combined factor in this study, 1.37, is considerably less than the upper limit of 1.7 on the product of epoxy coating factor and the top-bar factor in the ACI (1989) and AASHTO (1989). Therefore, the relative insensitivity of coated bars to top-bar effect suggests that either a lower top-bar factor, 1.15, or a limit on the combined factors of 1.4 or 1.5 be applied for epoxy-coated bars.

5.4 Recommendations for Future Study

Research on the effect of epoxy coating on the bond strength of reinforcing steel is continuing at the University of Kansas. This dissertation includes the results for the initial study. The following is a partial list of questions related to the bond of epoxy-coated reinforcement needed to be studied in subsequent research efforts.

1. What deformation configuration has the best bond performance when bars are coated with epoxy?

2. What are the limits of coating thickness to improve corrosion protection with acceptable reductions in bond strength?
3. At what ratio of cover to bar diameter does a pullout failure occur for splice specimens?
4. How effective is transverse reinforcement for improving the development of epoxy-coated bars?
5. What is the effect of epoxy coating for bars used with high slump concrete?
6. What is the bond performance of epoxy-coated bars in high strength concrete?
7. What is the bond performance of epoxy-coated hooks?
8. Is there an effective way to increase friction and cohesion for epoxy-coated bars?
9. Would grit effectively improve the bond performance of epoxy-coated bars?
10. What are realistic values for the cohesion and the coefficient of friction for both coated and uncoated reinforcing bars and how does the finite element model with these values predict the bond performance?
11. How would an analytical model of round bars, with different deformation configurations, predict the effects of surface properties on bond performance?

BIBLIOGRAPHY

AASHTO Highway Sub-Committee on Bridges and Structures. (1989). Standard Specification for Highway Bridges, 14th Edition, American Association of State Highway and Transportation Officials, Washington, DC.

Abrams, D. A. (1913). "Tests of Bond between Concrete and Steel," Bulletin No. 71, Engineering Experiment Station, University of Illinois, Urbana, IL, 105 pp.

ACI Committee 318. (1963). "Building Code Requirements for Reinforced Concrete (ACI 318-63)," American Concrete Institute, Detroit, MI, June, 144 pp.

ACI Committee 318. (1988). "ACI Workshop on Epoxy-Coated Reinforcement," Concrete International, Vol. 10., No. 12, December, pp. 80-84.

ACI Committee 318. (1989). "Building Code Requirements for Reinforced Concrete (ACI 318-89) and Commentary (ACI 318R-89)," American Concrete Institute, Detroit, MI, 353 pp.

ASTM. (1986). "Standard Test Method for Comparing Concretes on the Basis of the Bond Developed with Reinforcing Steel," (ASTM C234-86) 1989 Annual Book for ASTM Standards, Vol. 04.02, American Society for Testing and Materials, Philadelphia, PA, pp. 150-154.

ASTM. (1987). "Standard Specification for Deformed and Plain Billet-Steel Bars for Concrete Reinforcement," (ASTM A 615-87a) 1989 Annual Book for ASTM Standards, Vol. 1.04, American Society for Testing and Materials, Philadelphia, PA, pp. 381-384.

ASTM. (1988). "Standard Specification for Epoxy-Coated Reinforcing Steel Bars," (ASTM A 775/A775M-88a) 1989 Annual Book for ASTM Standards, Vol. 1.04, American Society for Testing and Materials, Philadelphia, PA, pp. 548-552.

Barsom, John and Rolfe, Stanley. (1987). Fracture and Fatigue Control in Structures, 2nd Edition, Prentice-Hall, pp. 30-38.

Bathe, Klaus-Jurgen and Chaudhary, Anil. (1985). "A Solution Method for Planar and Axisymmetric Contact Problems," International Journal for Numerical Methods in Engineering, Vol. 21, pp. 65-88.

Bazant, Z. P. and Tsubak, T. (1979). "Concrete Reinforcing Net: Optimum Slip-Free Limit Design," Journal of the Structural Division, ASCE, Vol. 105, NO. ST1, February, pp. 327-346.

Bazant, Z. P. and Cedolin, Luigi. (1979). "Blunt Crack Band Propagation in Finite Element Analysis," Journal of the Engineering Mechanics Division, ASCE, Vol. 105, N. EM2, April, pp. 297-315.

Brettmann, Barie B., Darwin, David and Donahey, Rex C. (1984). "Effects of Superplasticizers on Concrete-Steel Bond Strength," SL Report 84-1, University of Kansas Center for Research, Inc., Lawrence, Kansas, April, 32 pp.

Brettmann, Barie B., Darwin, David and Donahey, Rex C. (1986). "Bond of Reinforcement to Superplasticized Concrete," Journal of the American Concrete Institute, Vol. 83, No. 1, January-February, pp. 98-107.

Chadrasekaran, N., Haisler, W. E. and Goforth, R. E. (1987). "A Finite Element Solution Methods for Contact Problems with Friction,"

International Journal for Numerical Methods in Engineering, Vol. 24, pp. 477-495.

Choi, O. C., H. Hadje-Ghaffari, D. Darwin, and S. L. McCabe (1990). "Bond of Epoxy-Coated Reinforcement to Concrete: Bar Parameters," SL Report 90-1, University of Kansas Center for Research, Lawrence, Kansas, January, 43 pp.

Clark, A. P. (1946). "Comparative Bond Efficiency of Deformed Concrete Reinforcing Bars," Journal of the American Concrete Institute, Vol. 43, December, pp. 381-400.

Clark, A. P. (1949). "Bond of Concrete Reinforcing Bars," Journal of the American Concrete Institute, Vol. 46, November, pp. 161-184.

Cleary, Douglas B. and Ramirez, Julio A. (1989). "Bond of Epoxy Coated Reinforcing Steel in Concrete Bridge Decks," Joint Highway Research Project Information Report, JHRP 89-7, Purdue University, 127 pp.

Clifton, James R., Beeghly, Hugh F. and Mathey, Robert G. (1975). "Nonmetallic Coatings for Concrete Reinforcing Bars," Building Science Series, No. 65, National Bureau of Standards, Washington, DC, 1975, 34 pp.

Clifton, James R., Mathey, Robert G. and Anderson, Erik D., "Creep of Coated Reinforcing Bars in Concrete," Journal of the Structural Division, ASCE, Vol. 105, ST10, Oct. 1979, pp. 1935-1947.

Clifton, James R. and Mathey, Robert G., "Bond and Creep Characteristics of Coated Reinforcement Bars in Concrete," Journal of the

American Concrete Institute, Vol. 80, No. 4, July-August 1983, pp. 288-293.

Dakhil, F. H., Cady, P. D., and Carrier, P. E. (1975). "Cracking of Fresh Concrete as Related to Reinforcement," Journal of the American Concrete Institute, Vol. 72, No. 8, August, pp. 421-428.

Desai, C. S. and Nagaraj, B. K. (1988), "Modeling for Cyclic Normal and Shear Behavior of Interfaces," Journal of Engineering Mechanics, ASCE, Vol. 114, No. 7, July, pp. 1198-1217.

Dodds, Robert H. and Lopez, Leonard A. (1980). "Generalized Software System for Non-Linear Analysis," Advances in Engineering Software, Vol. 2, No. 4, Oct., pp. 161-168.

Donahey, Rex C. and Darwin, David. (1983). "Effects of Construction Procedures on Bond in Bridge Decks," Structural Engineering and Engineering Materials, SM Report No. 7, University of Kansas Center for Research, Inc., Lawrence, KS, January, 125 pp.

Donahey, Rex C. and Darwin, David. (1985). "Bond of Top-Cast Bars in Bridge Decks," Journal of the American Concrete Institute, Vol. 82, No. 1, January-February, pp. 57-66.

Draper, N. R. and Smith, H. (1981). Applied Regression Analysis, Second Edition, John Wiley & sons, Inc., pp. 241-249.

Drumm, E. C. and Desai, C. S. (1986). "Determination of Parameters for a Model for the Cyclic Behavior of Interfaces," Earthquake Engineering and Structural Dynamics, Vol. 14, pp. 1-18.

Ferguson, Phil M. and Thompson, J. Neils. (1962). "Development Length of High Strength Reinforcing Bars in Bond," Journal of the American Concrete Institute, Vol. 59, No. 7, July, pp. 887-927.

Ghaboussi, J., Wilson, E. L. and Isenberg, J. (1973). "Finite Element Rock Joints and Interfaces," Journal of the Soil Mechanics and Foundations Division, ASCE, Vol. 99, No. SM10, October, pp. 833-848.

Hadje-Ghaffari, Hossain, Darwin, David and McCabe, Steven L. (1990). "Effects of Epoxy Coating on the Bond of Reinforcing Steel to Concrete," University of Kansas, in progress.

Harnett, Donald L. (1975). Introduction to Statistical Methods, Second Edition, Addison-Wesley Publishing Company, pp. 263-301.

Herrmann, L. R. (1978). "Finite Element Analysis of Contact Problems," Journal of the Engineering Mechanics Division, ASCE, Vol. 104, No. EM5, October, pp. 1043-1057.

Hillerborg, A., Modeer, M. and Petersson, P. E. (1976). "Analysis of Crack Formation and Crack Growth in Concrete by Means of Fracture Mechanics and Finite Elements," Cement and Concrete Research, Vol. 6, No. 6, Nov., pp. 773-782.

IMSL (1987). Problem-Solving Software Systems, Version 1.0, Houston, Texas.

Ingraffea, A. R., Gerstle, W. H., Gergely, P. and Saouma, V. (1984). "Fracture Mechanics of Bond in Reinforced Concrete," Journal of Structural Engineering, ASCE, Vol. 110, No. 4, April, pp. 871-890.

Jimenez, Rafael, Gergely, Peter and White, Richard N. (1978). "Shear Transfer Across Cracks in Reinforced Concrete," Department of Structural Engineering, Cornell University, Ithaca, NY, August, 35 pp.

Jeanty, Paul R., Mitchell, Dennis and Mirza, A. Saeed. (1988). "Investigation of 'Top Bar' Effects in Beams," ACI Structural Journal, Vol. 85, No. 3, May-June, pp. 252-257.

Jirsa, James O., Lutz, LeRoy A. and Gergely, Peter. (1979). "Rationale for Suggested Development, Splice, and Standard Hook Provisions for Deformed Bars in Tension," Concrete International: Design & Construction, Vol. 1., No. 7, July, pp. 47-61.

Jirsa, J. O. and Breen, J. E. (1981). "Influence of Casting Position and Shear on Development and Splice Length-Design Recommendations," Research Report 242-3F, Center for Transportation Research, Bureau of Engineering Research, The University of Texas at Austin, Nov.

Johnston, David W. and Zia, Paul. (1982). "Bond Characteristics of Epoxy Coated Reinforcing Bars," Report No. FHWA-NC-82-002, Federal Highway Administration, Washington, DC, 163 pp.

Keuser, M. and Mehlhorn, G. (1987). "Finite Element Model for Bond Problems," Journal of the Structural Engineering, ASCE, Vol. 113, No. 10, October, pp. 2160-2173.

Leibengood, L., Darwin, D. and Dodds, R. H. (1984). "Finite Element Analysis of Concrete Fracture Specimens," Structural Engineering and Engineering Materials, SM Report No. 11, University of Kansas Center for Research, Inc., Lawrence, KS, May, 120 pp.

Lopez, L. A., Dodds, R. H. Jr., Rehak, D. R. and Schmidt, R. J. (1989). Polo-Finite: A Structural Mechanics System for Linear and Nonlinear Analysis. A technical report by the University of Illinois at Urbana-Champaign.

Lutz, L. A., Gergely, P. and Winter, G. (1966). "The Mechanics of Bond and Slip of Deformed Reinforcing Bars in Concrete," Report No. 324, Department of Structural Engineering, Cornell University, August, 306 pp.

Lutz, L. A. (1970). "Analysis of Stresses in Concrete Near a Reinforcing Bar Due to Bond and Transverse Cracking," Journal of the American Concrete Institute, Vol. 67, Detroit, MI, pp. 778-787.

Mathey, Robert G. and Watstein, David. (1961). "Investigation of Bond in Beam and Pull-out Specimens with High-strength Deformed Bars," Journal of the American Concrete Institute, Vol. 57, No. 2, March, pp. 1071-1098.

Mathey, Robert G. and Clifton, James R. (1976). "Bond of Coated Reinforcing Bars in Concrete," Journal of the Structural Division, ASCE, Vol. 102, ST1, January, pp. 215-229.

Menzel, Carl A. (1939). "Some Factors Influencing Results of Pull-out Bond Tests," Journal of the American Concrete Institute, Vol. 35, June, pp. 517-542.

Mirza, S. A. (1987). "Bond Strength Statistics of Flexural Reinforcement in Concrete Beams," ACI Structural Journal, Vol. 84, No. 5, September-October, pp. 383-391.

Ngo, D. and Scordelis, Alexander C. (1967). "Finite Element Analysis of Reinforced Concrete Beams," Journal of the American Concrete Institute, Vol. 64, No. 3, March, pp. 152-163.

Nilson, A. H. (1968). "Non-linear Analysis of Reinforced Concrete by the Finite Element Method," Journal of the American Concrete Institute, Vol. 65, No. 9, September, pp. 757-766.

Oden, J. T. and Pires, E. B. (1983). "Nonlocal and Nonlinear Friction Laws and Variational Principles for Contact Problems in Elasticity," Journal of Applied Mechanics, Vol. 50, March, pp. 67-76.

Orangun, C. O., Jirsa, J. O. and Breen, J. E. (1977). "A Reevaluation of Test Data on Development Length and Splices," Journal of the American Concrete Institute, Vol. 74, No. 3, March, pp. 114-122.

PATRAN-II Modeling Software. PDA Engineering, 1560 Brookhollow Dr., Santa Ana, Calif. 92705.

Pike, Robert G., Hay, Richard E., Clifton, James R., Beeghly, Hugh F. and Mathey, Robert F. (1973). "Nonmetallic Coatings for Concrete Reinforcing Bars," Public Roads, Vol. 37, No. 5, June, pp. 185-197.

Petersson, P-E. (1980). "Fracture Energy of Concrete: Method of Determination," Cement and Concrete Research, Vol. 10, No. 1, January, pp. 79-89.

Petersson, P-E. (1981). "Crack Growth and Development of Fracture Zones in Plain Concrete and Similar Materials," Report TVBM-1006, Div. of Bldg Materials, University of Lund, Sweden, 174 pp.

Rehm, G. (1957). "The Fundamental Law of Bond," RILEM-Symposium on Bond and Crack Formation in Reinforced Concrete, Vol. II, Stockholm, pp. 491.

Saouma, Victor. (1980). "Automated Nonlinear Finite Element Analysis of Reinforced Concrete: A Fracture Mechanics Approach," Ph.D. Thesis, Cornell University, Ithaca, NY.

Skorobogatov, S. M. and Edwards, A. D. (1979). "The Influence of the Geometry of Deformed Steel Bars on Their Bond Strength in Concrete," Proc., Instn Civ. Engrs, Part 2, 67, June, pp. 327-339.

Soretz, S. and Hölzenbein, H. (1979). "Influence of Rib Dimensions of Reinforcing Bars on Bond and Bendability," Journal of the American Concrete Institute, Vol. 76, No. 1, January, pp. 111-125.

Tepfers, R. (1979). "Cracking of Concrete Cover Along Anchored Deformed Reinforcing Bars," Magazine of Concrete Research, Vol. 31, No. 106, March, pp. 3-12.

Tepfers, R. (1982). "Lapped Tensile Reinforcement Splices," Journal of the Structural Division, ASCE, Vol. 108, No. ST1, January, pp. 283-301.

Timoshenko, S. and Goodier, J. N. (1961). Theory of Elasticity, McGraw-Hill, New York.

Treece, R. A. and Jirsa, J. O. (1987). "Bond Strength of Epoxy-Coated Reinforcing Bars," RMFSEL Report No. 87-1, Phil M. Ferguson Structural Engineering Laboratory, The University of Texas at Austin, January, 85 pp.

Treece, R. A. and Jirsa, J. O. (1989). "Bond Strength of Epoxy-Coated Reinforcing Bars," ACI Materials Journal, Vol. 86, No. 2, March-April, pp. 167-174.

Urzua, J. L., Pecknold, D. A., Lopez, L. A., and Munse, W. H. (1977) "Analysis Procedure for Frictional Contact Problems Using Interface Finite Elements," Civil Engineering Studies Structural Research Series No. 438, University of Illinois at Urbana-Champaign, Urbana, Ill., March, 152 pp.

Yoshikawa, Hiromichi, Wu, Zhishen and Tanabe, Tada-aki. (1989). "Analytical Model for Shear Slip of Cracked Concrete," Journal of Structural Engineering, ASCE, Vol. 115, No. 4, April, pp. 771-788.

Zsutty, T. (1985). "Empirical Study of Bar Development Behavior," Journal of Structural Engineering, ASCE, Vol. 111, No. 1, January, pp. 205-219.

Table 2.1 Average Test Bar Data

Bar size	Def. patt.	Yield str. (ksi)	Def. space (in.)	Def. height+ (in.)	Def. gap (in.)	Def. angle per inch* (deg.)	Bearing area area** (in.)	Related rib ratio***	Bearing area (in.-1)
5	S	70.6	0.423	0.031	0.159	90	0.113	0.057	0.361
5	C	72.3	0.413	0.040	0.140	60	0.143	0.074	0.471
5	N	68.4	0.379	0.041	0.158	70	0.166	0.086	0.545
6	S	63.8	0.502	0.040	0.154	90	0.139	0.060	0.320
6	C	70.9	0.467	0.047	0.122	60	0.188	0.079	0.420
6	N	64.2	0.462	0.051	0.151	70	0.201	0.084	0.448
8	S	67.0	0.674	0.053	0.176	90	0.202	0.064	0.256
8	C	****	0.656	0.062	0.195	60	0.241	0.077	0.305
8	N	63.8	0.602	0.057	0.160	70	0.250	0.080	0.316
11	S	64.6	0.945	0.076	0.217	90	0.313	0.071	0.202
11	C	63.1	0.840	0.074	0.196	60	0.302	0.069	0.196
11	N	64.3	0.914	0.077	0.195	70	0.287	0.065	0.185

\+ Per ASTM A 615 (Ref. Hadje-Ghaffari et al. 1990)

* Bearing areas are measured as described in Appendix A; bar and areas based on nominal dimensions.

** Ratio of the bearing area to the shearing area between ribs

*** Ratio of the bearing area per inch of length to the nominal cross-sectional area

**** Yield strength is greater than 70.0 ksi.

Table 2.2 Concrete Mixture Proportions
(Cubic Yard Batch Weights)

Group	Nominal strength (psi)	W/C ratio	Cement (lb)	Water (lb)	Aggregate Fine+ (lb)	Aggregate Coarse* (lb)
1	5000	0.55	509	280	1537	1575
2	6000	0.41	756	310	1245	1575
3-7	6000	0.45	622	280	1437	1575
8-17	6000	0.45	733	330	1213	1575
18-19	5000	0.55	600	330	1324	1575

+ Kansas River Sand - Lawrence Sand Co., Lawrence, KS, bulk specific gravity = 2.62, absorption = 0.5%, fineness modulus = 3.0.
* Crushed limestone - Hamm's Quarry, Perry, KS, bulk specific gravity = 2.52, absorption = 3.5%, maximum size = 3/4 in., unit weight = 97.2 lb/cubic ft.

Table 2.3 Concrete Properties

Group	Slump (in.)	Concrete temperature (F)	Age at test (days)	Average compressive strength (psi)
1	1	58	4	4150
			5	4450
			6	4750
2	2 1/2	60	3	5700
3	1 1/4	65	5	6090
4	1 1/4	73	4	6130
5	1 1/2	60	4	5920
6	1 1/2	70	5	5870
7	1	68	6	6000
8	3	80	4	5800
9	4	89	6	5650
10	4 1/2	85	7	5990
11	3 1/4	89	6	5970
12	3 1/4	92	7	5940
13	3 1/4	93	9	5840
14	4	88	7	5800
15	4 1/4	74	8	6000
16	3 1/2	72	4	6240
17	5 3/4	78	9	5850
18	4 1/4	57	3	4790
			4	5010
			5	5430
19	3 3/4	68	4	5070
			5	5270

Table 2.4 Bond Forces

Group	Specimen label *	Average coating thick. (mils)	Stand. deviat. of coating thick. (mils)	Cover (in.)	Concr. str. (psi)	Bond force at 0.002 slip (lb)	Ult. bond force (lb)	Modif. bond force (lb)	Lead Length (if non-stand.) (in.)
1	8TS-E 5-8.0	4.9	0.8	1.000	4480	20810	23090	26721	
	8TS-E 9-8.0	8.5	1.3	1.000	4820	20360	21910	24445	
	8TS-E12-8.0	13.8	1.6	1.000	4820	22110	23640	26375	
	8TS-B 0-8.0	0.0		1.000	4420	23210	24180	28172	
	8TS-M 0-8.0	0.0		1.000	4410	25940	27090	31598	
	8TS-E 5-8.0	4.1	0.8	2.000	4750	25630	33680	37853	
	8TS-E 9-8.0	7.9	1.1	2.000	4720	25110	33360	37612	
	8TS-E12-8.0	12.5	1.1	2.000	4710	36000	36000	40631	
	8TS-B 0-8.0	0.0		2.000	4770	32790	39000	43740	
	8TS-M 0-8.0	0.0		2.000	4780	31770	38410	43033	
	8TS-E 5-8.0	3.5	0.7	3.000	4110	26620	43730	52836	
	8TS-E 9-8.0	7.7	1.1	3.000	4080	23910	40000	48507	
	8TS-E12-8.0	11.0	0.5	3.000	4060	41450	41450	50389	
	8TS-B 0-8.0	0.0		3.000	4910	50700	53420	59052	
	8TS-M 0-8.0	0.0		3.000	4910	48360	52170	57670	
2	8BC-E12-8.0	11.0	0.9	1.000	5700	23680	24840	25485	
	8BC-E 9-8.0	9.1	1.2	1.000	5700	24270	25660	26326	
	8BC-E 5-8.0	5.4	1.3	1.000	5700	24050	25000	25649	
	8BC-B 0-8.0	0.0		1.000	5700	29360	33020	33877	
	8BC-M 0-8.0	0.0		1.000	5700	28670	31040	31846	
	8BC-E12-8.0	13.3	1.8	2.000	5700	33600	38300	39294	
	8BC-E 9-8.0	10.0	2.2	2.000	5700	33270	36760	37714	
	8BC-E 5-8.0	5.3	1.3	2.000	5700	34000	35990	36924	
	8BC-B 0-8.0	0.0		2.000	5700	39870	40000	41039	
	8BC-M 0-8.0	0.0		2.000	5700	45770	45990	47184	
3	8BS-E12-8.0	12.8	1.2	2.000	6090	24230	27030	26829	
	8BS-E12-8.0A	13.0	1.2	2.000	6090	27730	32040	31802	
	8BS-E12-8.0B	12.3	1.2	2.000	6090	26820	29110	28894	
	8BS-E 9-8.0	9.7	0.8	2.000	6090	26950	29940	29717	
	8BS-E 9-8.0A	10.2	1.2	2.000	6090	26200	28140	27931	
	8BS-E 9-8.0B	10.2	0.8	2.000	6090	26880	31100	30869	

* Specimen label

#PD-FT- LR

# = bar size : 5, 6, 8, 11
P = cast position : top, bottom
D = deformation pattern : S, C, N
F = bar surface type : mill scale, epoxy coated, blasted cleaned
T = nominal coating thickness : 0, 5, 9, 12 mils
L = bonded length in inches
R = replication I.D. : blank, A, B

Table 2.4 Bond Forces (continued)

Group	Specimen label *	Average coating thick. (mils)	Stand. deviat. of coating thick. (mils)	Cover (in.)	Concr. str. (psi)	Bond force at 0.002 slip (lb)	Ult. bond force (lb)	Modif. bond force (lb)	Lead Length (if non-stand.) (in.)
	8BS-E 5-8.0	5.4	1.1	2.000	6090	27760	28990	28774	
	8BS-E 5-8.0A	6.4	0.8	2.000	6090	28230	28580	28368	
	8BS-E 5-8.0B	6.5	0.8	2.000	6090	30370	32280	32040	
	8BS-B 0-8.0	0.0		2.000	6090	42930	44290	43961	
	8BS-B 0-8.0A	0.0		2.000	6090	43960	45640	45301	
	8BS-B 0-8.0B	0.0		2.000	6090	42190	43920	43594	
	8BS-M 0-8.0	0.0		2.000	6090	37150	43480	43157	
	8BS-M 0-8.0A	0.0		2.000	6090	36140	40960	40656	
	8BS-M 0-8.0B	0.0		2.000	6090	40640	40640	40338	
4	8BN-E 9-8.0	8.6	1.8	2.000	6130	29540	35820	35438	
	8BN-E 9-8.0A	8.5	2.0	2.000	6130	34240	42030	41581	
	8BN-E 9-8.0B	8.8	2.7	2.000	6130	33590	34970	34597	
	8BN-B 0-8.0	0.0		2.000	6130	46600	46630	46132	
	8BN-B 0-8.0A	0.0		2.000	6130	41400	41620	41176	
	8BN-B 0-8.0B	0.0		2.000	6130	41900	41920	41473	
	8BN-M 0-8.0	0.0		2.000	6130	45220	45220	44737	
	8BN-M 0-8.0A	0.0		2.000	6130	47960	50000	49466	
	8BN-M 0-8.0B	0.0		2.000	6130	39630	44580	44104	
5	8BC-E12-8.0	13.8	1.5	2.000	5920	35600	37370	37621	
	8BC-E12-8.0A	13.2	1.2	2.000	5920	30600	30590	30795	
	8BC-E12-8.0B	12.7	1.4	2.000	5920	34100	34560	34792	
	8BC-E 9-8.0	9.5	1.3	2.000	5920	33320	36070	36312	
	8BC-E 9-8.0A	10.0	1.5	2.000	5920	31080	33560	33785	
	8BC-E 9-8.0B	9.4	1.3	2.000	5920	33580	34290	34520	
	8BC-E 5-8.0	5.5	1.5	2.000	5920	33440	33440	33665	
	8BC-E 5-8.0A	4.6	1.4	2.000	5920	32840	35550	35789	
	8BC-E 5-8.0B	3.7	1.2	2.000	5920	32180	35560	35799	
	8BC-B 0-8.0	0.0		2.000	5920	36300	37520	37772	
	8BC-B 0-8.0A	0.0		2.000	5920	43130	46920	47235	
	8BC-B 0-8.0B	0.0		2.000	5920	41000	41150	41427	
	8BC-M 0-8.0	0.0		2.000	5920	33820	34550	34782	
	8BC-M 0-8.0A	0.0		2.000	5920	34320	34740	34973	
	8BC-M 0-8.0B	0.0		2.000	5920	39500	39490	39755	
6	8BS-E 9-8.0	7.9	1.5	2.000	5870	26090	35430	35820	
	8BS-E 9-8.0A	10.8	1.5	2.000	5870	25760	32840	33201	
	8BS-B 0-8.0	0.0		2.000	5870	28060	47530	48053	
	8BS-B 0-8.0A	0.0		2.000	5870	33720	35930	36325	
	8BS-M 0-8.0	0.0		2.000	5870	35050	46500	47012	
	8BS-M 0-8.0A	0.0		2.000	5870	32689	42710	43180	
	8BC-E 9-8.0	10.7	1.7	2.000	5870	31940	33790	34162	
	8BC-E 9-8.0A	9.1	1.6	2.000	5870	32590	36630	37033	
	8BC-B 0-8.0	0.0		2.000	5870	33890	51430	51996	
	8BC-B 0-8.0A	0.0		2.000	5870	42500	42510	42978	
	8BC-M 0-8.0	0.0		2.000	5870	38810	43930	44413	

Table 2.4 Bond Forces (continued)

Group	Specimen label *	Average coating thick. (mils)	Stand. deviat. of coating thick. (mils)	Cover (in.)	Concr. str. (psi)	Bond force at 0.002 slip (lb)	Ult. bond force (lb)	Modif. bond force (lb)	Lead Length (if non-stand.) (in.)
	8BC-M 0-8.0A	0.0		2.000	5870	38880	46820	47335	
	8BN-E 9-8.0	9.2	2.3	2.000	5870	33640	36620	37023	
	8BN-E 9-8.0A	10.4	1.6	2.000	5870	30100	45070	45566	
	8BN-B 0-8.0	0.0		2.000	5870	50810	50810	51369	
	8BN-B 0-8.0A	0.0		2.000	5870	38090	39150	39581	
	8BN-M 0-8.0	0.0		2.000	5870	37470	38000	38418	
	8BN-M 0-8.0A	0.0		2.000	5870	41250	47670	48194	
7	5BN-E 9-3.5	9.5	1.3	1.250	6000	7740	16000	16000	3.75
	5BN-E 9-3.5A	10.1	1.2	1.250	6000	7140	16080	16080	3.75
	5BN-E 9-3.5B	8.9	1.6	1.625	6000	8840	16200	16200	3.75
	5BN-B 0-3.5	0.0		1.313	6000	6490	15730	15730	3.75
	5BN-B 0-3.5A	0.0		1.281	6000	11930	16050	16050	3.75
	5BN-B 0-3.5B	0.0		1.250	6000	10660	16680	16680	3.75
	5BN-M 0-3.5	0.0		1.281	6000	13860	16890	16890	3.75
	5BN-M 0-3.5A	0.0		1.250	6000	12460	15930	15930	3.75
	5BN-M 0-3.5B	0.0		1.563	6000	9230	17100	17100	3.75
	5TN-E 9-3.5	10.3	0.8	1.313	6000	14480	14480	14480	3.75
	5TN-E 9-3.5A	10.0	1.3	1.313	6000	11120	15200	15200	3.75
	5TN-E 9-3.5B	9.0	1.1	1.313	6000	11610	15360	15360	3.75
	5TN-B 0-3.5	0.0		1.344	6000	12370	15620	15620	3.75
	5TN-B 0-3.5B	0.0		1.344	6000	12640	15440	15440	3.75
	5TN-M 0-3.5	0.0		1.313	6000	14480	16330	16330	3.75
	5TN-M 0-3.5B	0.0		1.375	6000	12330	16480	16480	3.75
	5TN-M 0-3.5	0.0		0.750	6000	11730	14580	14580	3.75
	5BN-M 0-3.5	0.0		0.687	6000	11750	12970	12970	3.75
8	5BN-M 0-3.5	0.0		0.656	5800	11840	13860	14096	3.75
	5BN-E 9-3.5	6.1	1.9	0.656	5800	10100	13440	13669	3.75
	5BN-M 0-3.5	0.0		0.656	5800	8680	10180	10354	
	5TN-M 0-3.5	0.0		0.719	5800	9790	10610	10791	
	5BN-E 9-3.5	5.7	1.8	0.687	5800	8910	11780	11981	
	5TN-E 9-3.5	6.5	1.9	0.687	5800	7720	9160	9316	
	5BN-M 0-3.5	0.0		0.625	5800	7540	10270	10445	1.50
	5TN-M 0-3.5	0.0		0.687	5800	8170	8340	8482	1.50
	5BN-E 9-3.5	6.5	1.1	0.656	5800	6810	7850	7984	1.50
	5TN-E 9-3.5	8.3	1.4	0.687	5800	7380	8420	8563	1.50
	5BN-M 0-3.5	0.0		0.687	5800	8410	8500	8645	0.75
	5BN-M 0-3.5	0.0		1.250	5800	14690	18110	18419	3.75
	5BN-E 9-3.5	5.6	1.8	1.281	5800	11460	15860	16131	3.75
	5BN-M 0-3.5	0.0		1.313	5800	10990	14580	14578	
	5TN-M 0-3.5	0.0		1.250	5800	12120	12700	12917	
	5BN-E 9-3.5	7.0	1.3	1.344	5800	9630	14100	13635	
	5TN-E 9-3.5	5.9	1.4	1.281	5800	10310	12700	12456	
	5BN-M 0-3.5	0.0		1.250	5800	10610	10850	11035	1.50

Table 2.4 Bond Forces (continued)

Group	Specimen label *	Average coating thick. (mils)	Stand. deviat. of coating thick. (mils)	Cover (in.)	Concr. str. (psi)	Bond force at 0.002 slip (lb)	Ult. bond force (lb)	Modif. bond force (lb)	Lead Length (if non-stand.) (in.)
	5TN-M 0-3.5	0.0		1.313	5800	10870	10990	11177	1.50
	5BN-E 9-3.5	5.1	0.9	1.250	5800	11180	11180	11371	1.50
	5TN-E 9-3.5	6.0	1.3	1.250	5800	8810	10330	10506	1.50
9	5BS-E 5-3.5	6.9	1.0	1.313	5650	5470	11160	10903	
	5BS-E 5-3.5A	5.5	0.6	1.313	5650	7050	11910	11445	
	5BS-E 5-3.5B	4.4	0.4	1.313	5650	9040	13590	12995	
	5BS-E12-3.5	14.5	1.1	1.313	5650	10520	10520	11495	
	5BS-E12-3.5A	17.1	0.9	1.375	5650	4850	11340	12518	
	5BS-E12-3.5B	11.8	0.9	1.313	5650	4200	10630	11164	
	5BS-B 0-3.5	0.0		1.313	5650	9990	12440	12568	
	5BS-B 0-3.5A	0.0		1.344	5650	10460	13690	13731	
	5BS-B 0-3.5B	0.0		1.313	5650	13710	13890	14062	
	5BS-M 0-3.5	0.0		1.313	5650	11400	14770	14969	
	5BS-M 0-3.5A	0.0		1.313	6310	14870	14870	14249	
	5BS-M 0-3.5B	0.0		1.344	5650	11140	13220	13246	
	5TS-E 5-3.5	5.8	0.6	1.438	5650	6800	12080	11235	
	5TS-E 5-3.5A	6.9	1.1	1.375	5650	5340	11300	10839	
	5TS-E 5-3.5B	5.9	0.6	1.344	5650	5850	10410	9969	
	5TS-E12-3.5	14.3	1.5	1.281	5650	5070	10470	11175	
	5TS-E12-3.5A	15.6	1.7	1.375	5650	5070	10800	11202	
	5TS-E12-3.5B	12.2	0.9	1.375	5650	9820	9820	9849	
	5TS-B 0-3.5	0.0		1.375	5650	8850	11220	10969	
	5TS-B 0-3.5A	0.0		1.438	5650	8850	12520	12012	
	5TS-B 0-3.5B	0.0		1.438	5650	9010	12590	12084	
	5TS-M 0-3.5	0.0		1.281	5650	8080	10770	10950	
	5TS-M 0-3.5A	0.0		1.406	5650	10190	11860	11480	
	5TS-M 0-3.5B	0.0		1.313	5650	8250	12060	12131	
10	5BC-E 9-3.5	9.3	1.4	1.188	5990	8420	12660	12970	
	5BC-E 9-3.5A	10.1	1.7	1.250	5990	6640	12950	13141	
	5BC-E 9-3.5B	8.7	1.2	1.250	5990	7560	12880	12841	
	5BC-E 5-3.5	3.0	0.5	1.313	5990	6360	14700	13473	
	5BC-E 5-3.5A	4.5	0.9	1.250	5990	7190	13370	12640	
	5BC-E 5-3.5B	3.7	0.9	1.313	5990	8220	14110	12997	
	5BC-B 0-3.5	0.0		1.281	5990	13290	13370	13255	
	5BC-B 0-3.5A	0.0		1.250	5990	12410	14560	14572	
	5BC-B 0-3.5B	0.0		1.250	5990	12140	13850	13861	
	5BC-M 0-3.5	0.0		1.281	5990	10790	13660	13545	
	5BC-M 0-3.5A	0.0		1.250	5990	9660	13340	13351	
	5BC-M 0-3.5B	0.0		1.375	5990	12280	14340	13849	
	5TC-E 9-3.5	9.7	1.4	1.313	5990	8640	11460	11243	
	5TC-E 9-3.5A	7.7	1.0	1.406	5990	10290	12070	11207	
	5TC-E 9-3.5B	8.9	1.0	1.375	5990	6810	11980	11386	
	5TC-E 5-3.5	3.4	0.8	1.313	5990	9760	12620	11768	

Table 2.4 Bond Forces (continued)

Group	Specimen label *	Average coating thick. (mils)	Stand. deviat. of coating thick. (mils)	Cover (in.)	Concr. str. (psi)	Bond force at 0.002 slip (lb)	Ult. bond force (lb)	Modif. bond force (lb)	Lead Length (if non-stand.) (in.)
	5TC-E 5-3.5A	4.0	0.9	1.313	5990	9180	12390	11599	
	5TC-E 5-3.5B	3.9	0.8	1.344	5990	8780	11990	11040	
	5TC-B 0-3.5	0.0		1.281	5990	9560	12020	11881	
	5TC-B 0-3.5A	0.0		1.250	5990	8160	12060	12070	
	5TC-B 0-3.5B	0.0		1.313	5990	12090	12090	11803	
	5TC-M 0-3.5	0.0		1.344	5990	12080	12080	11645	
	5TC-M 0-3.5A	0.0		1.313	5990	11980	12210	11923	
	5TC-M 0-3.5B	0.0		1.313	5990	11900	12510	12223	
	5BC-M 0-3.5	0.0		1.875	5990	8860	17330	17344	
	5TC-M 0-3.5	0.0		1.875	5990	14430	14430	14442	
11	5BN-E 9-3.5	9.6	1.2	1.219	5970	5370	12180	12434	
	5BN-E 9-3.5A	10.0	1.8	1.250	5970	10470	11630	11823	
	5BN-E 9-3.5B	9.9	1.8	1.344	5970	5600	11930	11731	
	5BN-B 0-3.5	0.0		1.344	5970	10950	12700	12355	
	5BN-B 0-3.5A	0.0		1.344	5970	12300	12870	12525	
	5BN-B 0-3.5B	0.0		1.250	5970	14220	14220	14255	
	5BN-M 0-3.5	0.0		1.281	5970	11940	12180	12085	
	5BN-M 0-3.5A	0.0		1.250	5970	12710	12800	12832	
	5BN-M 0-3.5B	0.0		1.250	5970	6870	13940	13974	
	5TN-E 9-3.5	9.0	1.3	1.375	5970	29540	11980	11416	
	5TN-E 9-3.5A	9.5	1.2	1.313	5970	34240	9010	8786	
	5TN-E 9-3.5B	10.6	1.5	1.313	5970	33590	8980	8867	
	5TN-B 0-3.5	0.0		1.313	5970	10900	11910	11643	
	5TN-B 0-3.5A	0.0		1.313	5970	11600	11710	11442	
	5TN-B 0-3.5B	0.0		1.219	5970	10700	11060	11236	
	5TN-M 0-3.5	0.0		1.281	5970	11800	11790	11671	
	5TN-M 0-3.5A	0.0		1.250	5970	6000	12080	12110	
	5TN-M 0-3.5B	0.0		1.313	5970	5650	11680	11412	
	5BN-M 0-3.5	0.0		1.281	6090	7000	7050	6997	0.00
	5BN-M 0-3.5A	0.0		1.188	6090	7000	7000	6948	0.00
	5TN-M 0-3.5	0.0		1.313	6090	6700	6770	6719	0.00
	5TN-M 0-3.5A	0.0		1.313	6090	6600	6720	6670	0.00
12	5BN-M 0-3.5	0.0		1.250	5940	15300	15320	15397	
	5BN-M 0-3.5A	0.0		1.250	5940	13500	13830	13899	
	5BN-M 0-3.5B	0.0		1.250	5940	12600	12650	12713	
	5BN-E 9-3.5	9.8	1.1	1.188	5940	9700	12080	12523	
	5BN-E 9-3.5A	10.5	1.3	1.188	5940	9600	12570	13131	
	5BN-E 9-3.5B	9.3	1.1	1.344	5940	8500	11890	11622	
	5BN-M 0-3.5	0.0		1.250	5940	10410	10460	10512	1.50
	5BN-M 0-3.5A	0.0		1.250	5940	11230	11250	11306	1.50
	5BN-E 9-3.5	8.3	1.4	1.250	5940	10690	10690	10743	1.50
	5BN-E 9-3.5A	9.8	1.3	1.125	5940	11350	11350	11407	1.50
	5BN-M 0-3.5	0.0		1.250	5940	9550	9550	9598	1.00
	5BN-M 0-3.5A	0.0		1.313	5940	10240	10730	10784	1.00

Table 2.4 Bond Forces (continued)

Group	Specimen label *	Average coating thick. (mils)	Stand. deviat. of coating thick. (mils)	Cover (in.)	Concr. str. (psi)	Bond force at 0.002 slip (lb)	Ult. bond force (lb)	Modif. bond force (lb)	Lead Length (if non-stand.) (in.)
	5BN-E 9-3.5	9.0	0.9	1.281	5940	8790	9260	9306	1.00
	5BN-E 9-3.5A	9.4	1.3	1.219	5940	8350	10520	10572	1.00
	5BN-M 0-3.5	0.0		1.281	5940	9930	9930	9980	0.50
	5BN-M 0-3.5A	0.0		1.063	5940	8720	8720	8763	0.50
	5BN-M 0-3.5B	0.0		1.188	5940	8720	9290	9336	0.50
	5BN-E 9-3.5	9.2	1.1	1.219	5940	7410	8310	8351	0.50
	5BN-E 9-3.5A	9.6	1.5	1.313	5940	7800	8360	8402	0.50
	5BN-E 9-3.5B	8.8	1.7	1.438	5940	7440	8150	8191	0.50
	5BN-M 0-3.5	0.0		1.281	5940	7980	7980	8020	0.00
	5BN-M 0-3.5A	0.0		1.188	5940	7950	7980	8020	0.00
	5BN-E 9-3.5	9.8	1.4	1.313	5940	6250	6870	6904	0.00
	5BN-E 9-3.5A	8.1	1.1	1.219	5940	6760	7950	7990	0.00
13	5BN-M 0-3.5	0.0		0.625	5844	10400	10420	10558	
	5BN-M 0-3.5A	0.0		0.625	5844	5600	10130	10264	
	5BN-M 0-3.5B	0.0		0.656	5844	10430	11160	11307	
	5BN-E 5-3.5	6.2	1.4	0.625	5844	9960	9960	10092	
	5BN-E 5-3.5A	5.7	1.4	0.625	5844	9970	9970	10102	
	5BN-E 5-3.5B	6.8	1.0	0.656	5844	10520	10520	10659	
	5BN-M 0-3.5	0.0		1.281	5844	9280	12170	12205	
	5BN-M 0-3.5A	0.0		1.250	5844	13560	13660	13841	
	5BN-M 0-3.5B	0.0		1.188	5844	12850	12850	13271	
	5BN-E 5-3.5	7.1	1.4	1.281	5844	13110	13110	12845	
	5BN-E 5-3.5A	6.2	1.4	1.250	5844	10680	12000	11697	
	5BN-E 5-3.5B	6.2	1.6	1.250	5844	10750	11700	11393	
	5BN-M 0-3.5	0.0		1.875	5844	14580	14580	14773	
	5BN-M 0-3.5A	0.0		1.938	5844	14600	14650	14844	
	5BN-M 0-3.5B	0.0		1.875	5844	16090	16090	16303	
	5BN-E 5-3.5	5.8	1.0	1.844	5844	14600	14600	14793	
	5BN-E 5-3.5A	6.4	1.2	1.875	5844	16080	16080	16293	
	5BN-E 5-3.5B	6.2	1.3	1.906	5844	14810	14810	15006	
	5BN-M 0-3.5			3.000	4760	25856	23030	25856	
	5BN-E 5-3.5	5.7	1.0	3.000	4760	22370	22370	25115	
14	6BS-M 0-4.5	0.0		1.469	5800	11470	20130	20660	
	6BS-M 0-4.5A	0.0		1.469	5800	9530	20210	20741	
	6BS-M 0-4.5B	0.0		1.500	5800	16410	16410	16690	
	6BS-E 5-4.5	4.1	0.4	1.563	5800	8290	15630	15524	
	6BS-E 5-4.5A	4.8	0.5	1.500	5800	9330	16140	16415	
	6BS-E 5-4.5B	4.2	0.4	1.500	5800	7140	14560	14808	
	6BS-E12-4.5	11.8	1.8	1.500	5800	7450	15430	15693	
	6BS-E12-4.5A	10.9	1.5	1.563	5800	7640	15250	15137	
	6BS-E12-4.5B	11.6	1.5	1.531	5800	6600	15330	15405	
	6BN-M 0-4.5	0.0		1.500	5800	15820	18000	18307	
	6BN-M 0-4.5A	0.0		1.438	5800	13330	18340	19026	
	6BN-M 0-4.5B	0.0		1.500	5800	7410	20240	20586	

Table 2.4 Bond Forces (continued)

Group	Specimen label *	Average coating thick. (mils)	Stand. deviat. of coating thick. (mils)	Cover (in.)	Concr. str. (psi)	Bond force at 0.002 slip (lb)	Ult. bond force (lb)	Modif. bond force (lb)	Lead Length (if non-stand.) (in.)
	6BN-E 9-4.5	7.2	2.0	1.563	5800	10620	20680	20660	
	6BN-E 9-4.5A	8.8	2.8	1.719	5800	12100	19880	18915	
	6BN-E 9-4.5B	8.0	2.0	1.563	5800	9750	17760	17690	
	6BC-M 0-4.5	0.0		1.500	5800	17720	18850	19172	
	6BC-M 0-4.5A	0.0		1.594	5800	11870	17960	17707	
	6BC-M 0-4.5B	0.0		1.500	5800	17860	19000	19324	
	6BC-E 5-4.5	4.7	0.6	1.563	5800	17720	17290	17212	
	6BC-E 5-4.5A	4.2	1.0	1.594	5800	8440	18460	18216	
	6BC-E 5-4.5B	4.1	0.6	1.563	5800	10660	16970	16887	
	6BC-E12-4.5	9.5	2.3	1.500	5800	18750	18750	19070	
	6BC-E12-4.5A	10.2	2.2	1.500	5800	18930	18930	19253	
	6BC-E12-4.5B	11.4	1.7	1.531	5800	17900	17900	18019	
15	8BS-M 0-8.0	0.0		1.938	6000	27140	41800	42650	
	8BS-M 0-8.0A	0.0		2.000	6000	42650	42700	42700	
	8BS-E 5-8.0	4.1	0.6	2.000	6000	23980	29050	29050	
	8BS-E 5-8.0A	4.7	0.5	2.000	6000	16980	33340	33340	
	8BS-E 5-8.0B	6.8	1.3	1.938	6000	19090	34730	35580	
	8BS-E12-8.0	16.5	2.1	2.000	6000	15260	30500	30500	
	8BS-E12-8.0A	11.7	1.1	2.063	6000	18330	29100	28249	
	8BS-E12-8.0B	14.1	0.9	1.938	6000	18700	32000	32850	
	8TS-E12-8.0	7.0	1.1	2.063	6000	14770	27400	26634	
	8TS-E12-8.0A	12.1	1.9	2.000	6000	11270	30200	30200	
	8BN-M 0-8.0	0.0		2.000	5830	40600	40600	41187	
	8BN-M 0-8.0A	0.0		2.000	5830	42800	42800	43419	
	8BN-M 0-8.0B	0.0		2.000	5830	45140	45140	45793	
	8TN-M 0-8.0	0.0		2.063	5830	38900	38900	38697	
	8TN-M 0-8.0A	0.0		2.063	5830	43020	43020	42876	
	8TN-M 0-8.0B	0.0		2.125	5830	38900	38900	37931	
	8TN-E 5-8.0B	4.2	0.7	2.125	5830	33000	33000	31945	
16	6BN-M 0-10.5	0.0		1.563	6240	25100	25200	24710	0.50
	6BN-M 0-10.5A	0.0		1.469	6240	26460	26500	25985	0.50
	6BN-M 0-10.5B	0.0		1.563	6240	25590	22900	22455	0.50
	6BN-E 9-10.5	7.2	1.8	1.500	6240	25590	26300	25789	0.50
	6BN-E 9-10.5A	8.9	1.9	1.500	6240	23400	23600	23141	0.50
	6BN-E 9-10.5B	9.5	1.8	1.531	6240	25300	25300	24808	0.50
	8BN-M 0-14.0	0.0		2.031	6240	35800	36800	36085	0.50
	8BN-M 0-14.0A	0.0		2.000	6240	36300	38800	38046	0.50
	8BN-M 0-14.0B	0.0		2.031	6240	37700	37800	37065	0.50
	8BN-E 9-14.0	10.3	1.1	2.000	6240	31700	31900	31280	0.50
	8BN-E 9-14.0A	7.7	1.3	2.000	6240	35900	36100	35398	0.50
	8BN-E 9-14.0B	10.0	1.3	2.000	6240	31200	31900	31280	0.50
	5BN-M 0-8.5	0.0		1.250	6240	17950	18400	18042	0.50
	5BN-M 0-8.5A	0.0		1.281	6240	15790	15800	15493	0.50
	5BN-M 0-8.5B	0.0		1.281	6240	19380	19400	19023	0.50
	5BN-E 9-8.5	7.0	1.3	1.156	6240	16630	17600	17258	0.50

Table 2.4 Bond Forces (continued)

Group	Specimen label *	Average coating thick. (mils)	Stand. deviat. of coating thick. (mils)	Cover (in.)	Concr. str. (psi)	Bond force at 0.002 slip (lb)	Ult. bond force (lb)	Modif. bond force (lb)	Lead Length (if non-stand.) (in.)
	5BN-E 9-8.5A	5.6	1.7	1.219	6240	16600	16600	16277	0.50
	5BN-E 9-8.5B	6.5	1.6	1.344	6240	16800	18500	18140	0.50
	5BS-M 0-8.5	0.0		1.344	6240	17950	18200	17846	0.50
	5BS-M 0-8.5A	0.0		1.313	6240	16510	17400	17062	0.50
	5BS-M 0-8.5B	0.0		1.313	6240	15390	17700	17356	0.50
	5BS-E 9-8.5	9.6	0.8	1.281	6240	10430	11200	10982	0.50
	5BS-E 9-8.5A	9.0	0.8	1.250	6240	14650	17000	16669	0.50
	5BS-E 9-8.5B	10.3	0.8	1.250	6240	11880	12100	11865	0.50
17	6BC-M 0-4.5	0.0		1.500	5850	15160	17900	18128	
	6BC-M 0-4.5A	0.0		1.563	5850	13970	19800	19679	
	6BC-M 0-4.5B	0.0		1.438	5850	15950	17870	18470	
	6BC-E 5-4.5	7.1	1.2	1.563	5850	10500	16020	15851	
	6BC-E 5-4.5A	5.9	1.3	1.500	5850	8810	16740	16953	
	6BC-E 5-4.5B	6.5	1.2	1.500	5850	7470	16100	16305	
	6BC-E12-4.5	9.3	1.8	1.500	5850	6690	15890	16092	
	6BC-E12-4.5A	10.5	1.7	1.500	5850	5600	14570	14755	
	6BC-E12-4.5B	10.9	1.8	1.500	5850	8550	16160	16365	
	6BS-M 0-4.5	0.0		1.469	5850	10250	17400	17808	
	6BS-M 0-4.5A	0.0		1.438	5850	14610	18300	18905	
	6BS-M 0-4.5B	0.0		1.500	5850	16230	19200	19444	
	6BS-E 5-4.5	5.7	0.9	1.500	5850	5270	15130	15322	
	6BS-E 5-4.5A	3.8	0.6	1.531	5850	6670	15800	15814	
	6BS-E 5-4.5B	3.6	0.6	1.531	5850	8530	14900	14903	
	6BS-E12-4.5	12.9	1.5	1.469	5850	10480	15900	16288	
	6BS-E12-4.5A	11.5	1.3	1.531	5850	7550	16900	16928	
	6BS-E12-4.5B	11.1	1.5	1.531	5850	7520	13900	13890	
	6TS-M 0-4.5	0.0		1.594	5850	4360	13600	13189	
	6TS-M 0-4.5A	0.0		1.656	5850	14200	14200	13407	
	6TS-M 0-4.5B	0.0		1.625	5850	4590	15900	15323	
	6TS-E12-4.5	13.2	1.7	1.438	5850	2300	14400	14972	
	6TS-E12-4.5A	10.4	1.2	1.656	5850	13700	13700	12901	
18	8BN-M 0-8.0	0.0		0.937	5060	26410	29200	31796	
	8BN-M 0-8.0A	0.0		1.063	5060	26220	29500	32123	
	8BN-M 0-8.0B	0.0		1.063	5060	27750	28660	31208	
	8BN-E12-8.0	13.4	1.5	0.937	5060	22000	23600	25698	
	8BN-E12-8.0A	11.7	1.1	1.063	5060	26910	27190	29608	
	8BN-E12-8.0B	13.5	1.5	0.969	5060	24800	27400	29836	
	8TN-M 0-8.0	0.0		1.063	5060	24180	25200	27441	
	8TN-M 0-8.0A	0.0		1.156	5060	27200	27200	29618	
	8TN-M 0-8.0B	0.0		1.156	5060	26730	27180	29597	
	8TN-E12-8.0	11.1	1.4	1.063	5060	19010	22800	24827	
	8TN-E12-8.0A	12.6	1.1	1.094	5060	18090	21840	23782	
	8TN-E12-8.0B	14.2	0.9	1.063	5060	21300	21300	23194	

Table 2.4 Bond Forces (continued)

Group	Specimen label *	Average coating thick. (mils)	Stand. deviat. of coating thick. (mils)	Cover (in.)	Concr. str. (psi)	Bond force at 0.002 slip (lb)	Ult. bond force (lb)	Modif. bond force (lb)	Lead Length (if non-stand.) (in.)
	8BN-M 0-8.0	0.0		1.875	5060	36240	45600	51357	
	8BN-M 0-8.0A	0.0		1.938	5060	32340	42400	47021	
	8BN-M 0-8.0B	0.0		1.875	5060	35900	41040	46391	
	8BN-E12-8.0	12.2	1.6	1.969	5060	29520	33700	37122	
	8BN-E12-8.0A	9.3	1.1	1.969	5060	27550	35700	39300	
	8BN-E12-8.0B	8.6	0.8	1.938	5060	27550	35950	39997	
	8TN-M 0-8.0	0.0		2.063	5060	27950	32900	35059	
	8TN-M 0-8.0A	0.0		1.938	5060	26920	38600	42798	
	8TN-M 0-8.0B	0.0		2.000	5060	28180	35800	38983	
	8TN-E12-8.0	11.8	0.9	2.000	5060	32630	32630	35531	
	8TN-E12-8.0A	13.7	1.1	2.063	5060	18580	29800	31684	
	8TN-E12-8.0B	12.7	0.9	2.063	5060	21580	31530	33568	
	8BN-M 0-8.0A	0.0		3.188	4790	25600	58400	65361	
	8BN-M 0-8.0B	0.0		3.000	4790	18910	49600	55512	
	8BN-E12-8.0	9.7	1.1	3.031	4790	21900	47100	52714	
	8BN-E12-8.0A	10.3	1.1	2.938	4790	27930	51600	57750	
	8BN-E12-8.0B	12.0	1.1	3.031	4790	21000	50600	56631	
	8TN-M 0-8.0A	0.0		3.063	4790	32599	47110	52725	
	8TN-E12-8.0	12.6	2.2	3.063	4790	10580	42400	47454	
	8TN-E12-8.0A	9.8	1.4	3.063	4790	13100	43300	48461	
	8TN-E12-8.0B	12.4	1.5	3.094	4790	12030	43200	48349	
	8BS-M 0-8.0	0.0		1.969	5440	20380	36920	39199	
	8BS-M 0-8.0A	0.0		2.031	5440	21160	43540	45300	
	8BS-M 0-8.0B	0.0		2.031	5440	24780	37940	39419	
	8BS-E12-8.0	8.1	1.2	2.063	5440	20560	32660	33448	
	8BS-E12-8.0A	9.7	1.3	1.906	5440	23770	29510	32268	
	8BS-E12-8.0B	11.6	1.4	1.906	5440	24710	33510	36468	
	8TS-M 0-8.0	0.0		2.094	5440	19430	32120	32583	
	8TS-M 0-8.0A	0.0		2.156	5440	17870	34270	34075	
	8TS-M 0-8.0B	0.0		2.063	5440	26830	36490	37556	
	8TS-E12-8.0	12.7	1.2	2.094	5440	19920	29010	29317	
	8TS-E12-8.0A	13.5	1.1	2.125	5440	16170	29000	28924	
	8TS-E12-8.0B	12.9	1.4	2.063	5440	14470	29650	30372	
19	11BN-M 0-9.0	0.0		2.813	5070	25710	36000	38666	
	11BN-M 0-9.0A	0.0		2.875	5270	35450	46100	48195	
	11BN-M 0-9.0B	0.0		2.563	5270	32830	36100	40009	
	11BN-E 9-9.0	10.3	2.6	2.750	5270	17420	32000	34144	
	11BN-E 9-9.0A	8.5	2.9	2.750	5070	23000	29600	32200	
	11BN-E 9-9.0B	8.1	1.9	2.750	5270	18360	28200	30089	
	11BN-M 0-9.0	0.0		4.125	5070	23220	48300	52543	
	11BN-M 0-9.0A	0.0		4.125	5270	26500	47500	50683	
	11BN-M 0-9.0B	0.0		4.250	5270	35250	42900	45774	

Table 2.4 Bond Forces (continued)

Group	Specimen label *	Average coating thick. (mils)	Stand. deviat. of coating thick. (mils)	Cover (in.)	Concr. str. (psi)	Bond force at 0.002 slip (lb)	Ult. bond force (lb)	Modif. bond force (lb)	Lead Length (if non-stand.) (in.)
11BN-E	9-9.0	9.6	2.0	4.250	5070	19640	37000	40250	
11BN-E	9-9.0A	9.4	3.0	4.188	5270	19890	44200	47162	
11BN-E	9-9.0B	12.2	2.2	4.188	5270	23580	40900	43640	
11BS-M	0-9.0	0.0		2.688	5270	34560	38600	41683	
11BS-M	0-9.0A	0.0		2.781	5270	35250	36300	38484	
11BS-M	0-9.0B	0.0		2.813	5070	30760	34400	36925	
11BS-E	9-9.0	11.0	0.9	2.750	5270	20800	27600	29449	
11BS-E	9-9.0A	10.9	0.8	2.625	5070	24960	27700	31127	
11BS-E	9-9.0B	12.6	0.9	2.750	5270	22180	36400	38839	
11BC-M	0-9.0	0.0		2.500	5070	33400	37500	42781	
11BC-M	0-9.0A	0.0		2.719	5270	35900	37800	40581	
11BC-M	0-9.0B	0.0		2.688	5270	28800	35100	37948	
11BC-E	9-9.0	12.1	1.1	2.750	5070	22100	29000	31547	
11BC-E	9-9.0A	13.1	0.9	2.750	5270	20200	27700	29556	
11BC-E	9-9.0B	12.4	0.9	2.813	5270	25800	29100	30553	

Table 2.5 Average Unloaded End Slip at Ultimate Bond Force for Bottom-Cast Bars with 2 db Cover

Surface conditions	Bar size	Average slip (in.)		
		S-pattern	C-pattern	N-pattern
Uncoated-mill scale	No. 5	0.0036	0.0037	0.0031
	No. 6	0.0038	0.0034	0.0029
	No. 8	0.0056	0.0022	0.0026
	No.11	0.0029	0.0033	0.0035
Epoxy coated	No. 5	0.0046	0.0056	0.0042
	No. 6	0.0066	0.0057	0.0045
	No. 8	0.0041	0.0024	0.0033
	No.11	0.0039	0.0035	0.0041

Table 3.1 Variability of Concrete Tensile Strength : Typical Results (ACI committee 224, 1986)

Type of test	Mean strength, (psi)	Standard deviation within each batch, (psi)	Coefficient of variation, (%)
Splitting test	405	20	5
Direct tensile test	275	19	7
Modulus of rupture	605	36	6
Compression cube test	5980	207	3.5

Table 3.2 Mill Scale* versus Blast-cleaned Bar

Bar position	Bar size	Def. patt.	Group No.	No. of uncoated* bars	Uncoated* bars bond force (lb)	No. of blast-cleaned bars	Blast-cleaned bars bond force (lb)	B/U
B	5	S	9	3	14155	3	13453	0.95
B	5	C	10	3	13582	3	13891	1.02
B	5	N	11	3	12964	3	13045	1.01
Average of all bottom-cast No. 5** =					13567		13463	0.99
B	8	S	3	3	41384	3	44285	1.07
B	8	S	6	2	45100	2	42192	0.94
Average =					42870		43448	1.01
B	8	C	5	3	36504	3	42144	1.15
B	8	C	6	2	45876	2	47480	1.04
Average =					40253		44278	1.10
B	8	N	4	3	46101	3	42928	0.93
B	8	N	6	2	43304	2	45476	1.05
Average =					44982		43947	0.98
Average of all bottom-cast No. 8** =					2702		43891	1.03
T	5	S	9	3	11520	3	11688	1.01
T	5	C	10	3	11930	3	11918	1.00
T	5	N	11	3	11731	3	11440	0.98
Average of all top-cast No. 5** =					11727		11682	1.00

* Mill scale bars = Uncoated bars

** Each deformation pattern weighted equally

Table 3.3 Two-sample t-Test for Mill Scale versus Blast-cleaned Bars

Bar position	Bar size	Def. patt.	Mean bond force (mill:blast) x1 : x2 (lb)	Standard deviation (mill:blast) s1:s2 (lb)	Sample size (mill:blast) n1:n2	Alpha	Critical t value	Calculated t value	Null hypothesis rejected
B	8	S	42361:43448	2526:4344	10:5	0.20	1.35	-0.62	no
B	8	C	41408:44281	5752:5488	6:5	0.20	1.38	-0.84	no
B	8	N	45462:43947	3689:4816	11:5	0.20	1.35	0.69	no
B	5	S	14154:13454	865:785	3:3	0.20	1.53	1.04	no
B	5	C	13582:13896	251:659	3:3	0.20	1.53	-0.77	no
B	5	N	13358:13045	1043:1051	9:3	0.20	1.38	-0.29	no
T	5	S	11520:11688	591:624	3:3	0.20	1.53	-0.41	no
T	5	C	11930:11918	289:137	3:3	0.20	1.53	0.08	no
T	5	N	11731:11400	207:445	3:3	0.20	1.53	1.43	no

Table 3.4 Mill Scale versus Epoxy Coated Bars
(Bottom-cast and 2 db cover)

Bar size	Def. patt.	Group No.	No. of uncoated bars	Uncoated bars bond force (lb)	No. of coated bars	Coated bars bond force (lb)	C/U+ group	U/U++ all	C/U++ all
5	S	9	3	14154	6	11753	0.83	1.03	0.86
5	C	10	3	13580	6	13009	0.96	0.99	0.95
5	N	11	3	12964	3	11998	0.93	0.95	0.88
5	N	12	3	14003	3	12425	0.89	1.02	0.91
5	N	13	3	13107	3	11977	0.91	0.96	0.87
	Average =			13358		12133	0.91	0.98	0.88
Average of all No. 5 bars* =				13697		12298	0.90	1.00	0.90
6	S	14	3	19363	6	15498	0.80	1.02	0.81
6	S	17	3	18720	6	15525	0.83	0.98	0.82
	Average =			19041		15511	0.81	1.00	0.81
6	C	14	3	18733	6	18112	0.97	0.98	0.95
6	C	17	3	18760	6	16056	0.86	0.99	0.84
	Average =			18746		17084	0.91	0.98	0.90
6	N	14	3	19309	3	19089	0.99	1.01	1.00
Average of all No. 6 bars* =				19032		17228	0.90	1.00	0.90

\+ Numerator and denominator based on group average
++ Numerator based on group average. Denominator based on average for three deformation patterns for each bar size; each deformation pattern weighted equally
* Each deformation pattern weighted equally
** Each bar size weighted equally

Table 3.4 Mill Scale versus Epoxy Coated Bars (Continued)

Bar size	Def. patt.	Group No.	No. of uncoated bars	Uncoated bars bond force (lb)	No. of coated bars	Coated bars bond force (lb)	C/U+ group	U/U++ all	C/U++ all
8	S	3	3	41384	9	29472	0.71	0.96	0.68
8	S	6	2	45104	2	34512	0.77	1.05	0.80
8	S	15	2	42680	6	31600	0.74	0.99	0.73
8	S	18	3	41312	3	34064	0.82	0.96	0.79
	Average =			42365		31303	0.74	0.98	0.73
8	C	2	1	47184	3	37976	0.80	1.10	0.88
8	C	5	3	36504	9	34784	0.95	0.85	0.81
8	C	6	2	45880	2	35600	0.78	1.07	0.83
	Average =			41409		35584	0.90	0.96	0.83
8	N	4	3	46104	3	37208	0.81	1.07	0.86
8	N	6	2	43304	2	41296	0.95	1.01	0.96
8	N	15	3	43464	0	0	0.00	1.01	0.00
8	N	18	3	48256	3	38800	0.80	1.12	0.90
	Average =			45461		38827	0.84	1.06	0.90
Average of all No. 8 bars* =				43078		35238	0.83	1.00	0.82
11	S	19	3	39033	3	33138	0.85	0.96	0.82
11	C	19	3	40437	3	30555	0.76	1.00	0.75
11	N	19	3	42291	3	32148	0.76	1.04	0.79
Average of all No. 11 bars* =				40587		31947	0.79	1.00	0.79
Average of all bars** =							0.86	1.00	0.85

Table 3.5 Two-sample t-Test for Coated Bars between Different Deformation Patterns

Bar size	Def. patt.	Mean bond force x1:x2 (lb)	Standard deviation s1:s2 (lb)	Sample size n1:n2	Alpha	Critical t value	Calculated t value	Null hypothesis rejected
5	S:C	11753:13009	819:282	6:6	0.01	3.17	-3.55	yes
5	S:N	11753:12133	819:612	6:9	0.20	1.35	-1.03	no
5	C:N	13009:12133	282:612	6:9	0.01	3.01	3.25	yes
6	S:C	15511:17082	811:1346	12:12	0.01	2.82	-3.46	yes
6	S:N	15511:19089	811:1493	12:3	0.001	4.22	-4.91	yes
6	C:N	17082:19089	1346:1493	12:3	0.05	2.16	-2.27	yes
8	S:C	31300:35587	2827:2169	20:14	0.001	3.65	-4.77	yes
8	S:N	31300:38828	2827:3588	20:8	0.001	3.71	-5.90	yes
8	C:N	35587:38828	2159:3588	14:8	0.02	2.53	2.66	yes
11	S:C	33138:30555	5007:995	3:3	0.20	1.37	0.88	no
11	S:N	33138:32148	5007:2028	3:3	0.20	1.37	0.32	no
11	C:N	30555:32148	995:2028	3:3	0.20	1.37	-1.22	no

Table 3.6 Bond Strength and C/U for Cover Effect (from Best Fit Lines)

Bar size	Group	Cast position and deform. pattern	Nominal cover 1db uncoated (lb)	1db coated (lb)	1db C/U	2db uncoated (lb)	2db coated (lb)	2db C/U	3db uncoated (lb)	3db coated (lb)	3db C/U
No.5	13	Bottom-cast N-pattern	11025	10364	0.94	12950	12562	0.97	15225	15225	1.00
No.8	1	Top-cast S-pattern	26000	21064	0.81	36800	31280	0.85	47200	41064	0.87
No.8	18	Top-cast N-pattern	24688	20592	0.83	35672	31608	0.89	46648	42624	0.91
No.8	18	Bottom-cast N-pattern	29600	25160	0.85	42000	37384	0.89	54400	48960	0.90

Table 3.7 Bottom-cast versus Top-cast Bars

Bar size	Group	Defor. pattern	Slump (in.)	Cover (db)	Ratio of Bond Strength*		
					Bot.uncoated /top uncoated	Bot.coated /top coated	Bot.uncoated /top coated
No.5	7	N	1	2	1.01	1.06	1.11
No.5	9	S	4	2	1.22	1.08	1.30
No.5	10	C	4 1/2	2	1.12	1.11	1.14
No.5	11	N	3 1/2	2	1.10	1.22	1.30
No.6	17	S	5 3/4	2	1.31	1.12	1.30
No.8	18	S	4 1/4	2	1.18	1.12	1.35
No.8	18	N	4 1/4	1	1.13	1.21	1.33
No.8	18	N	4 1/4	2	1.23	1.14	1.37
No.8	18	N	4 1/4	3	1.16	1.17	1.26

* Each ratio represents the ratio of the mean bond strengths of three bars

Table 4.1 Number of Nodes in Each Codensation Step

Model	Location	Initial structure	After 1st condensation	Combined structure	After 2nd condensation
Standard lead 1 db cover	Upper block	665	191	514	367
	Lower block	1064	323	-	-
Standard lead 2 db cover	Upper block	931	267	590	443
	Lower block	1064	323	-	-
Standard lead 3 db cover	Upper block	1083	305	628	481
	Lower block	1064	323	-	-
Short lead 2 db cover	Upper block	544	241	530	399
	Lower block	952	289	-	-
Long lead 2 db cover	Upper block	980	280	620	465
	Lower block	1120	340	-	-

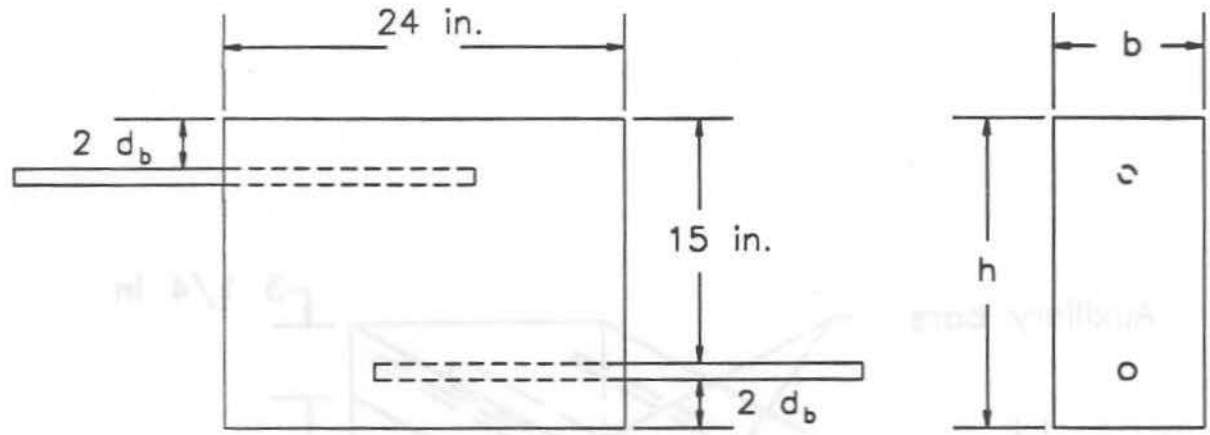

h: 15 in. + bar diameter + cover
b: 9 in. for No.5, No.6 and No.8 bars
10 in. for No.11 bars

(a)

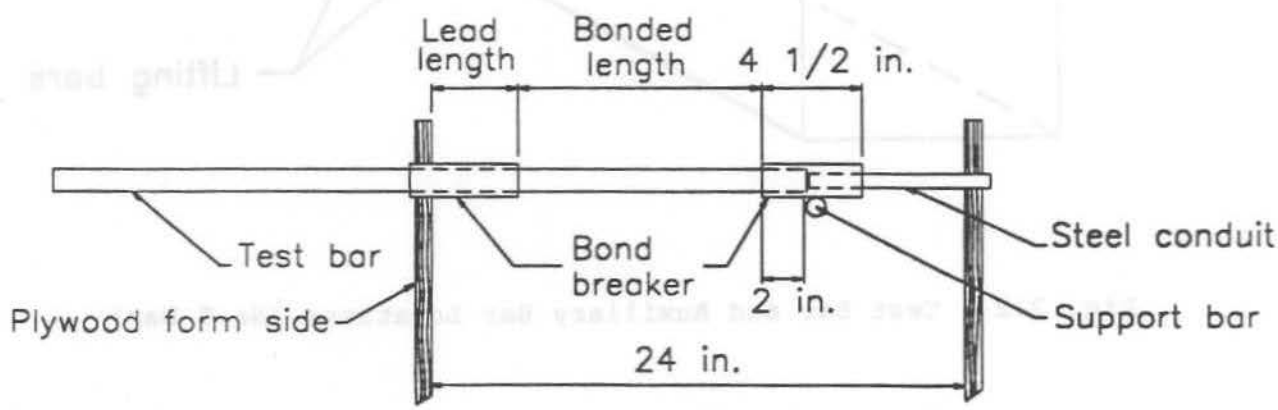

(b)

Fig. 2.1 (a) Specimen Dimensions (b) Test Bar Installation

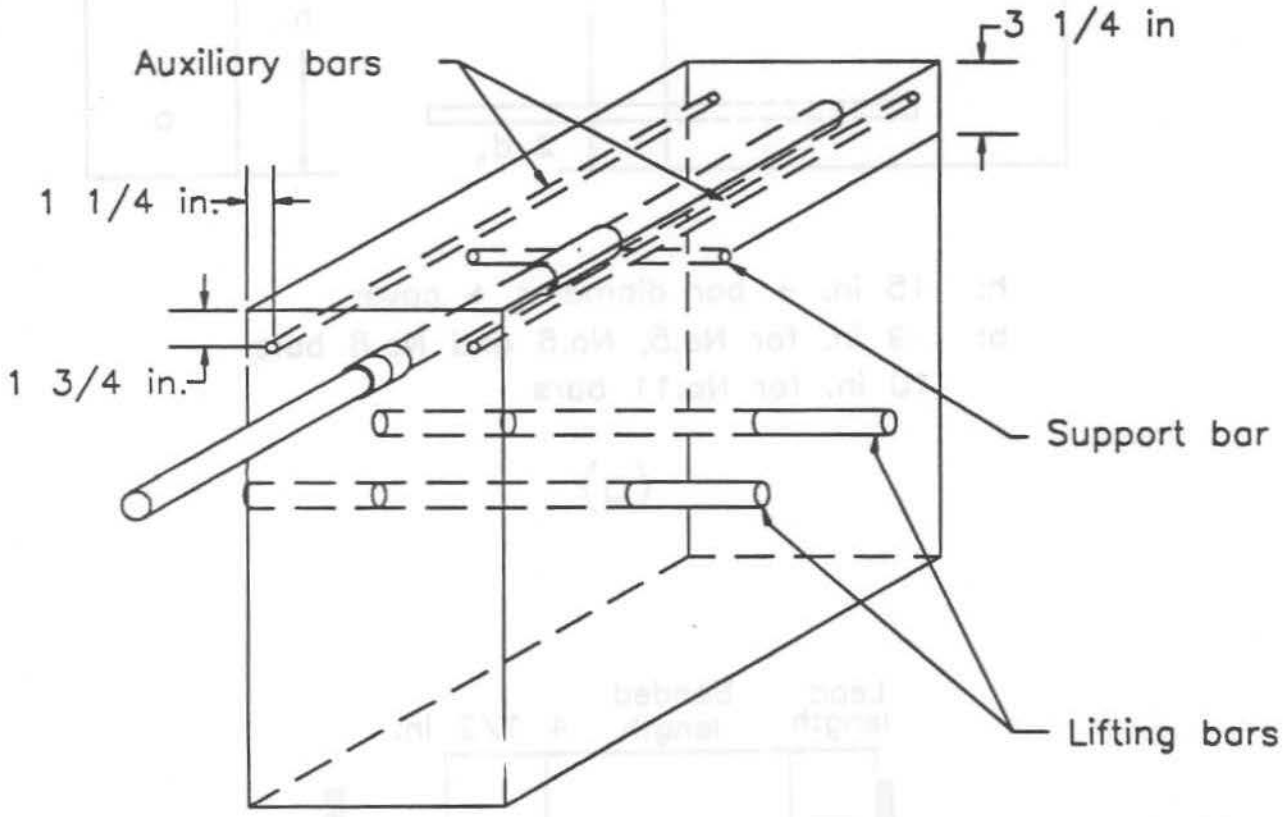

Fig. 2.2 Test Bar and Auxiliary Bar Locations (No.8 Bar)

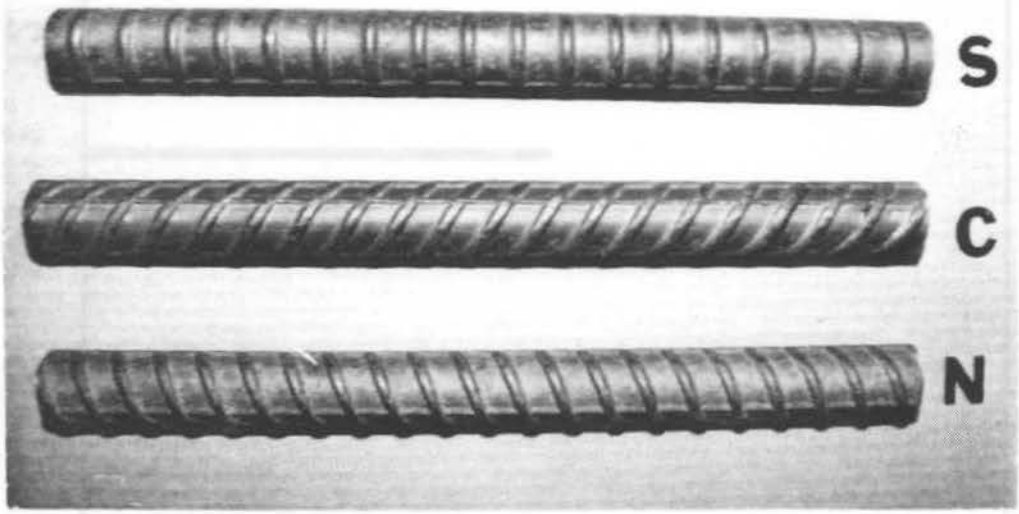

Fig. 2.3 Reinforcing Bar Deformation Patterns

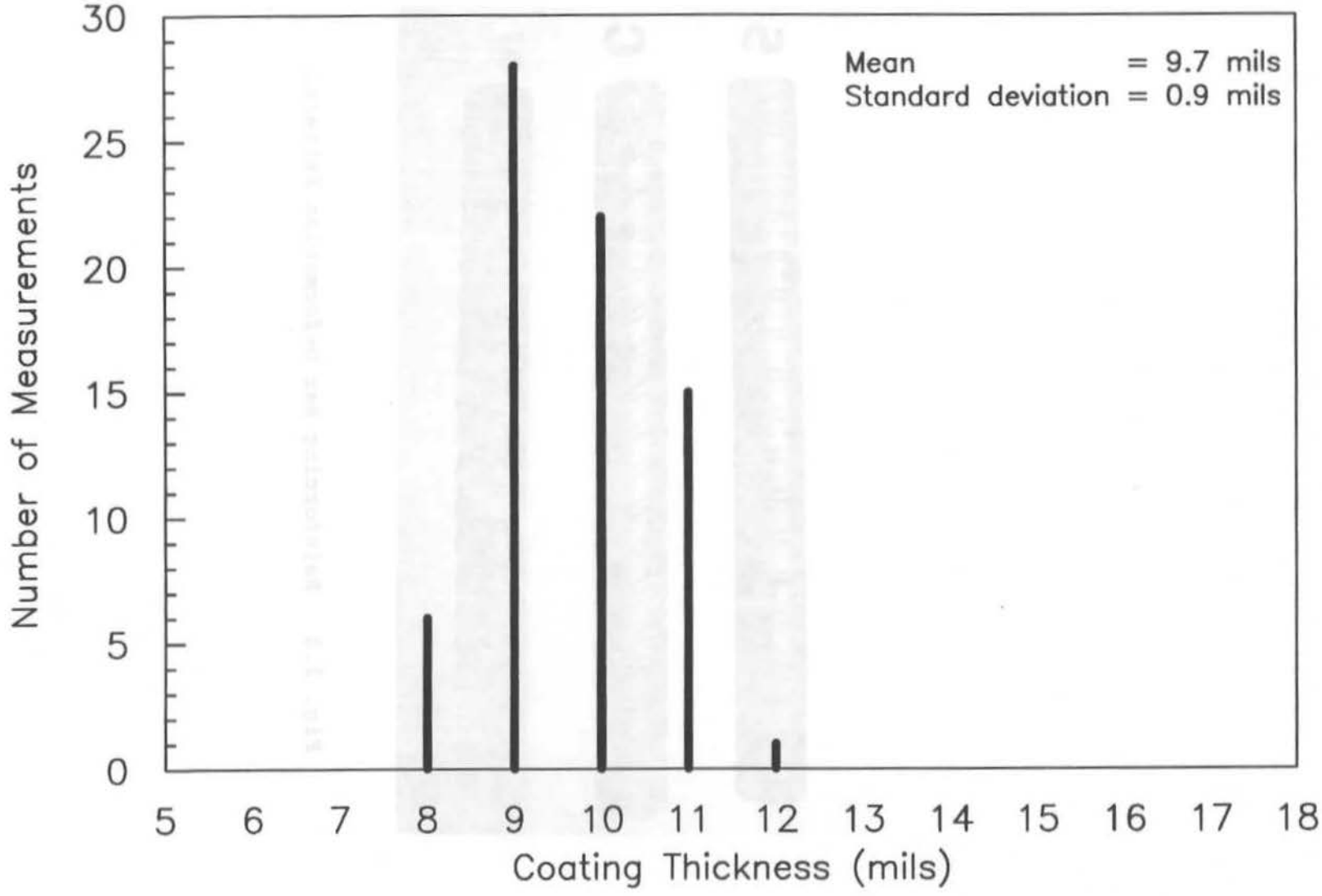

Fig. 2.4 Distribution of Measured Coating Thickness (S-Pattern No.8 Bar)

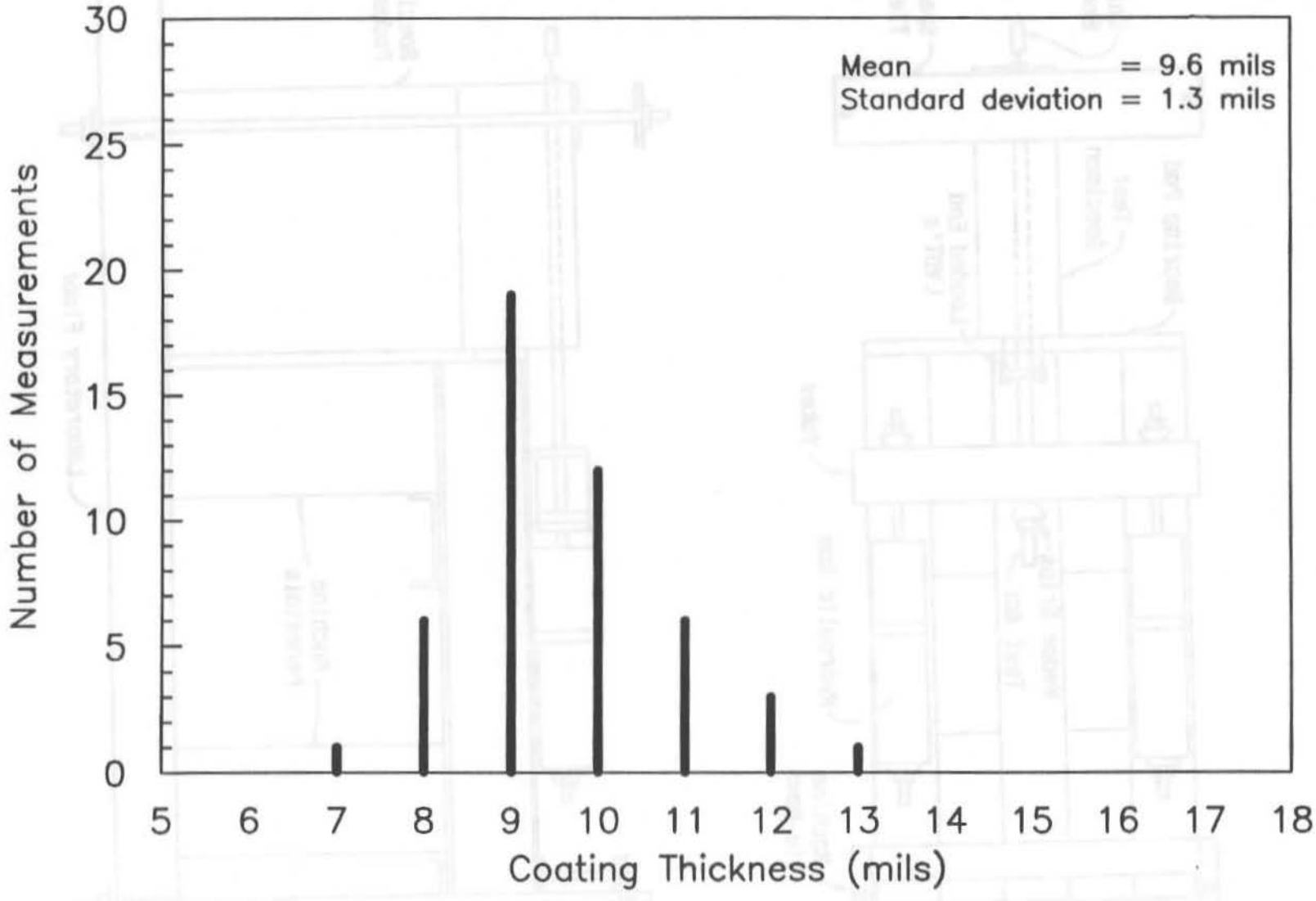

Fig. 2.5 Distribution of Measured Coating Thickness (N-Pattern No.5 Bar)

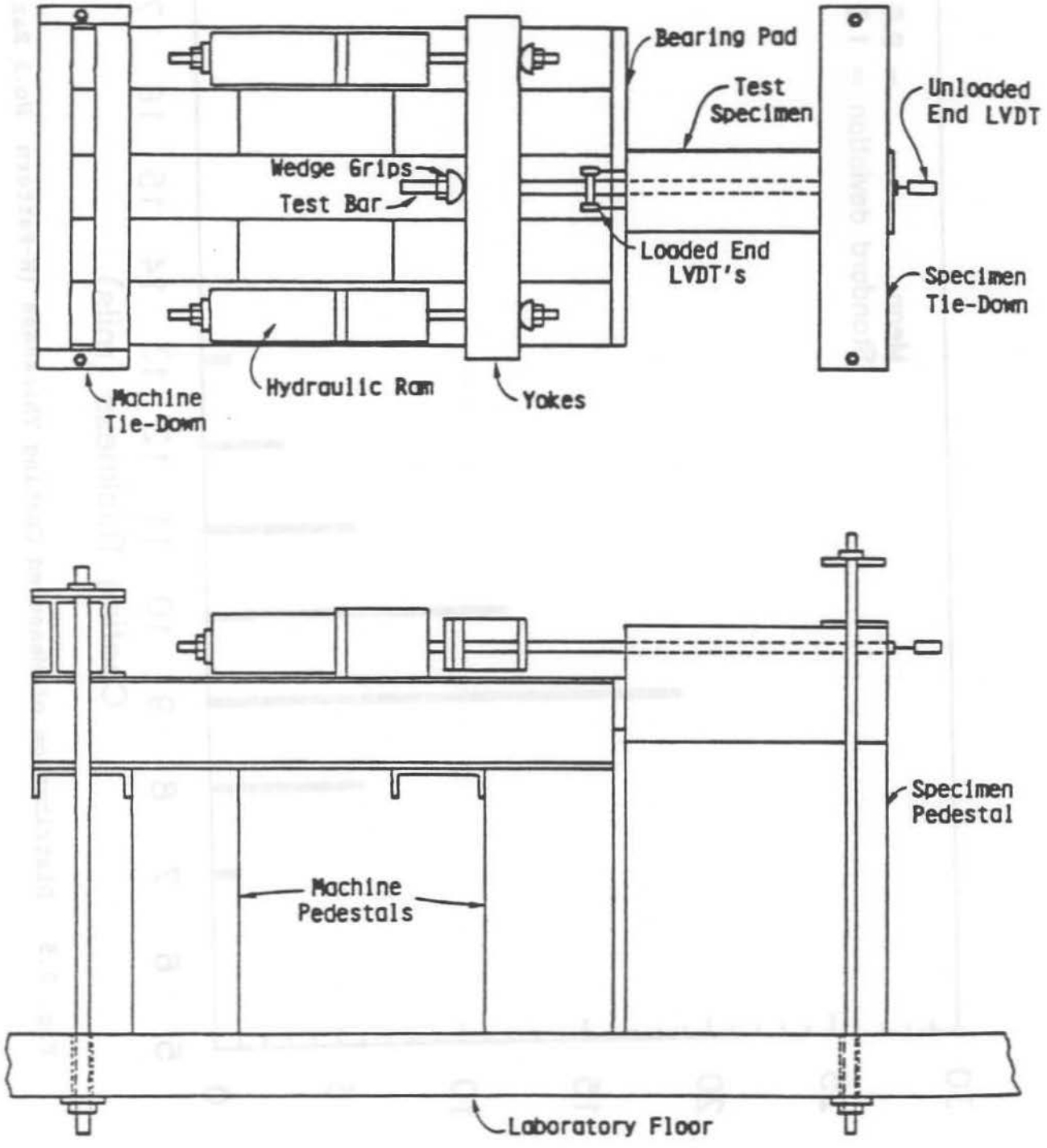

Fig. 2.6 Test Apparatus Schematic (Brettmann et al. 1984)

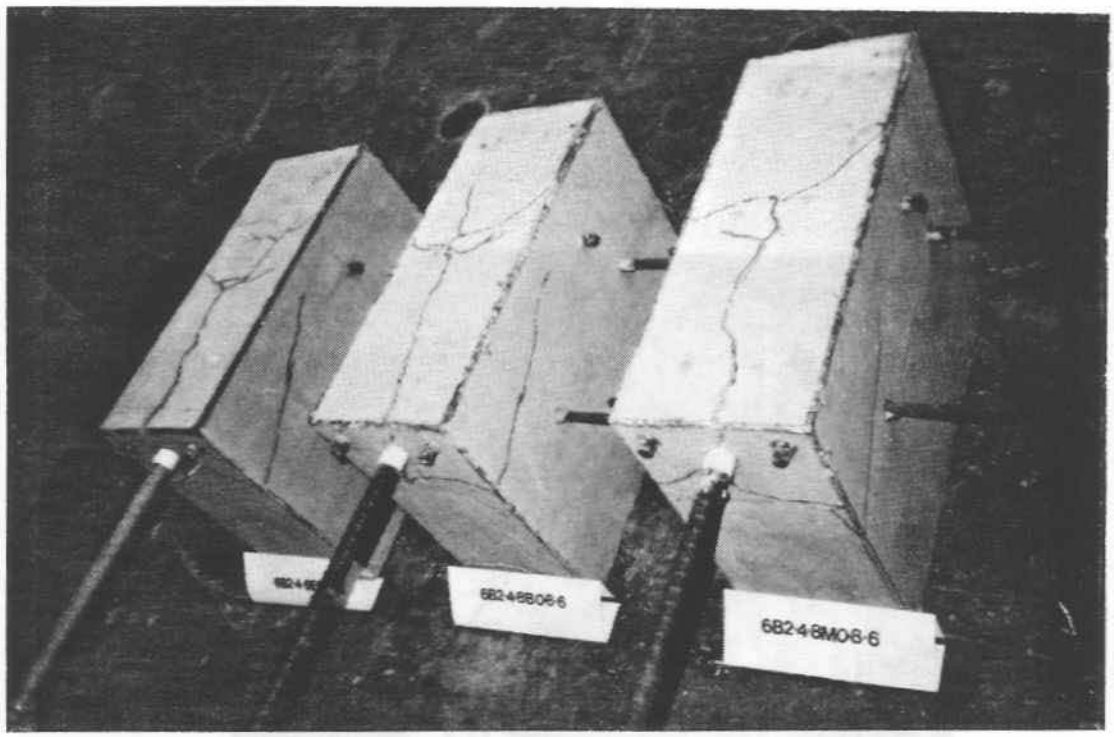

(a)

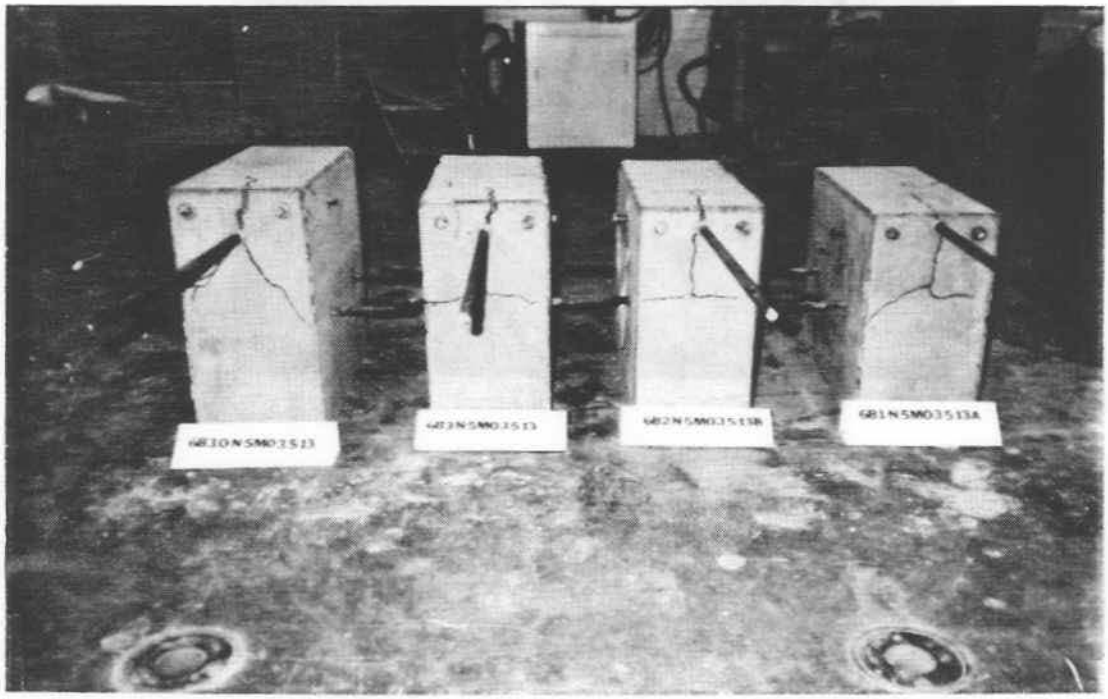

(b)

Fig. 2.7 Cracked Specimens After Failure (a) No.8 Bars (b) No.5 Bars

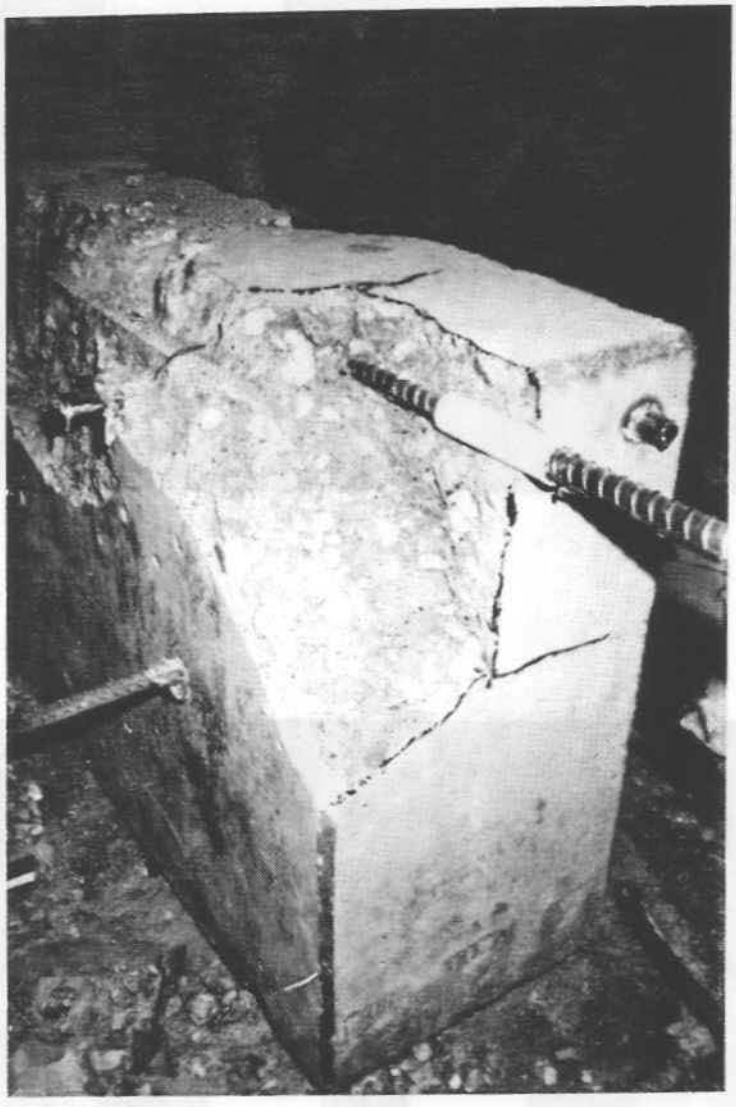

Fig. 2.8 Internal Concrete Crack Surface

Fig. 2.9 Uncoated Bar After Test

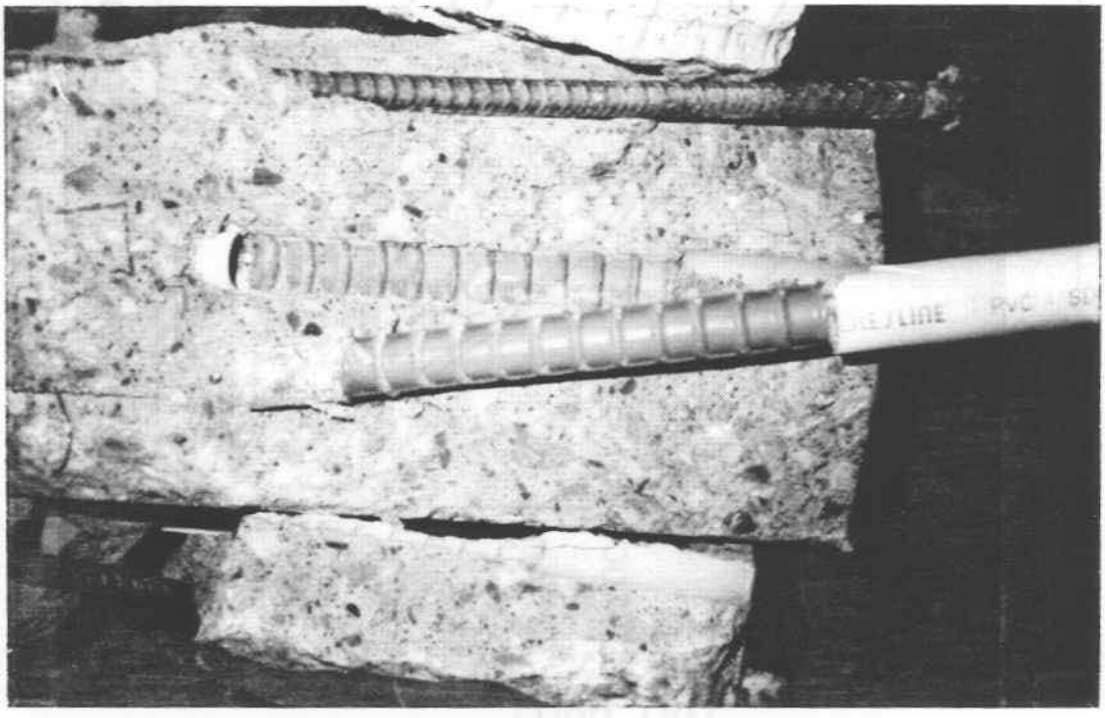

Fig. 2.10 Coated Bar After Test

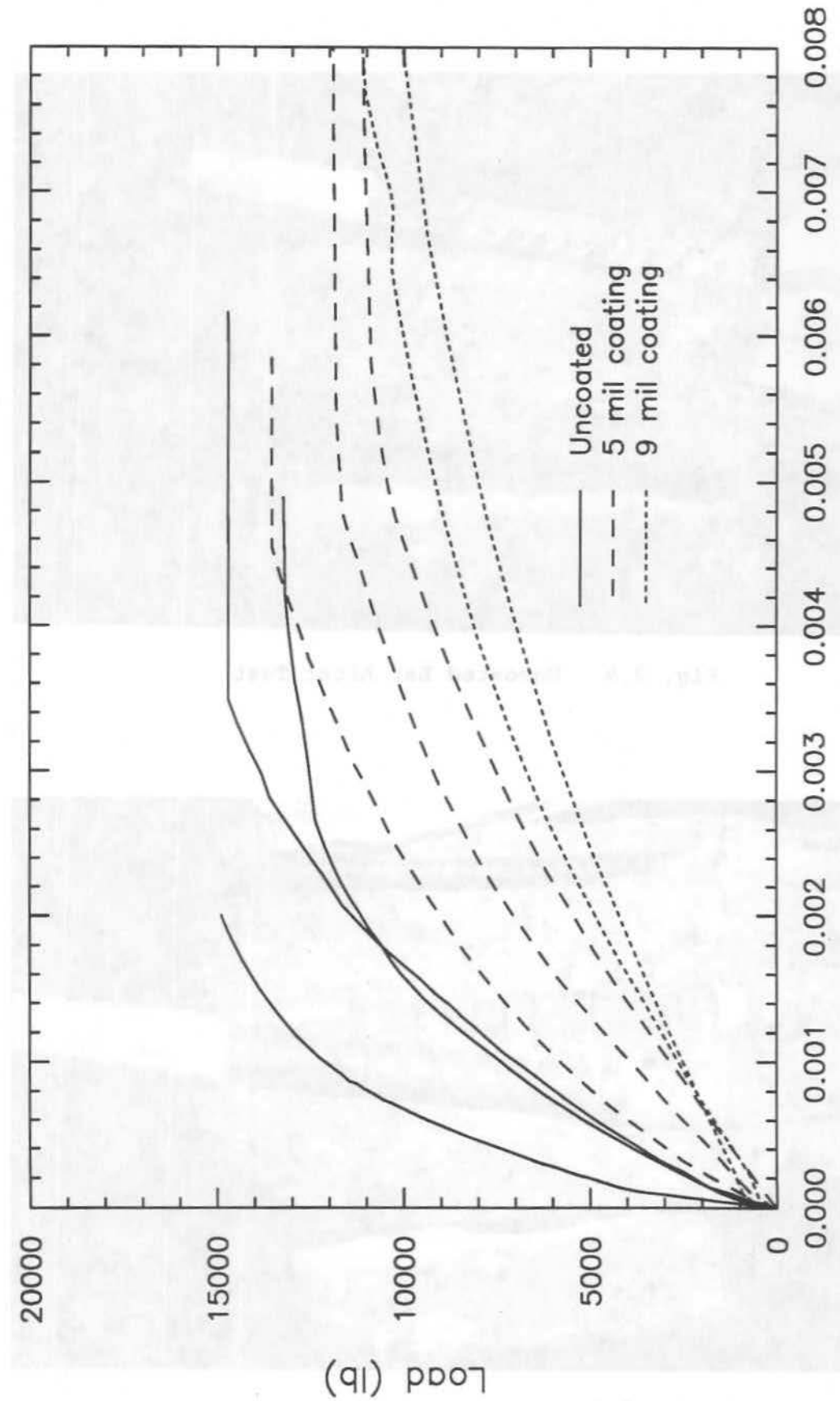

Fig. 2.11 Load-Slip Curves for S-Pattern No.5 Bars

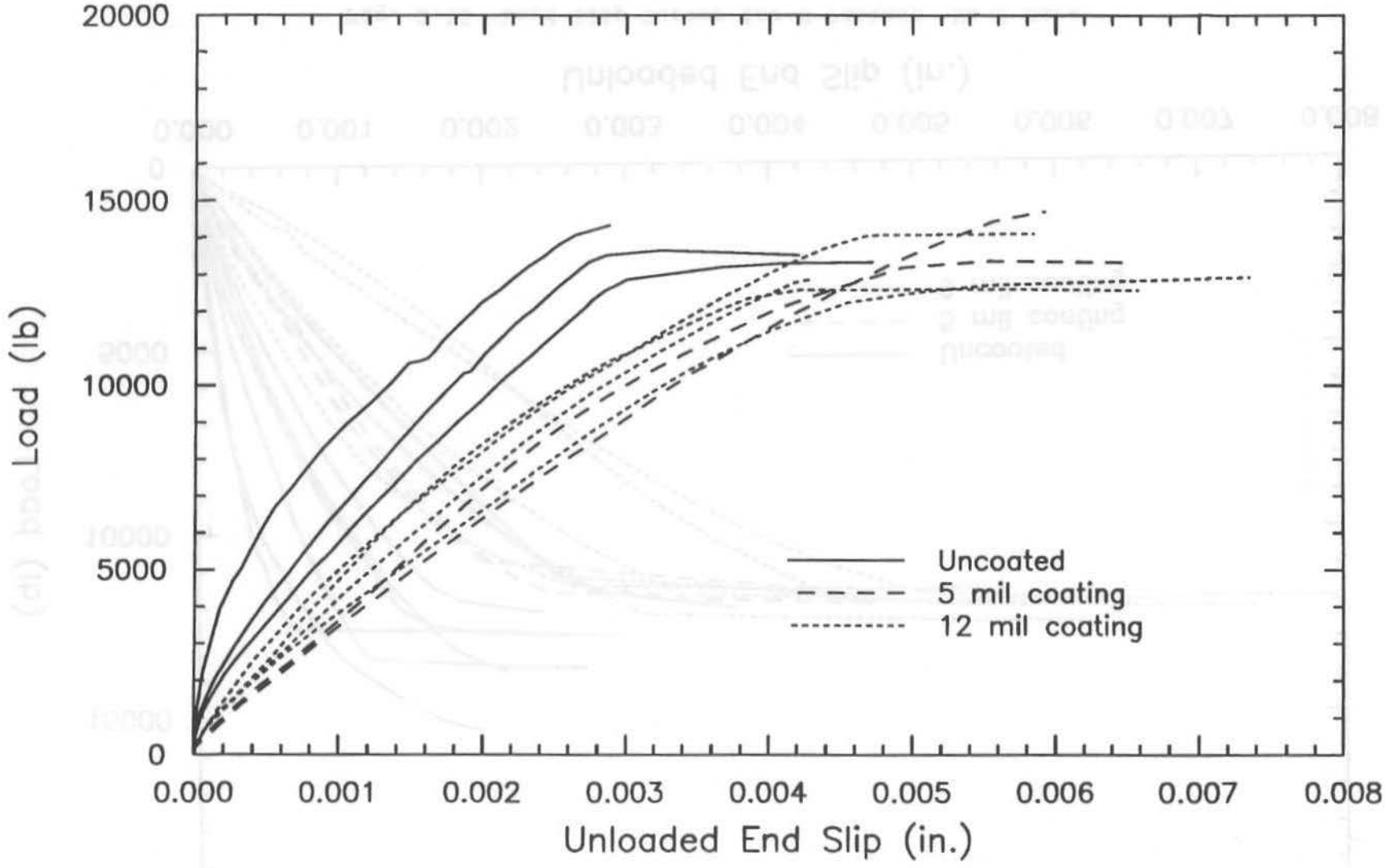

Fig. 2.12 Load-Slip Curves for C-Pattern No.5 Bars

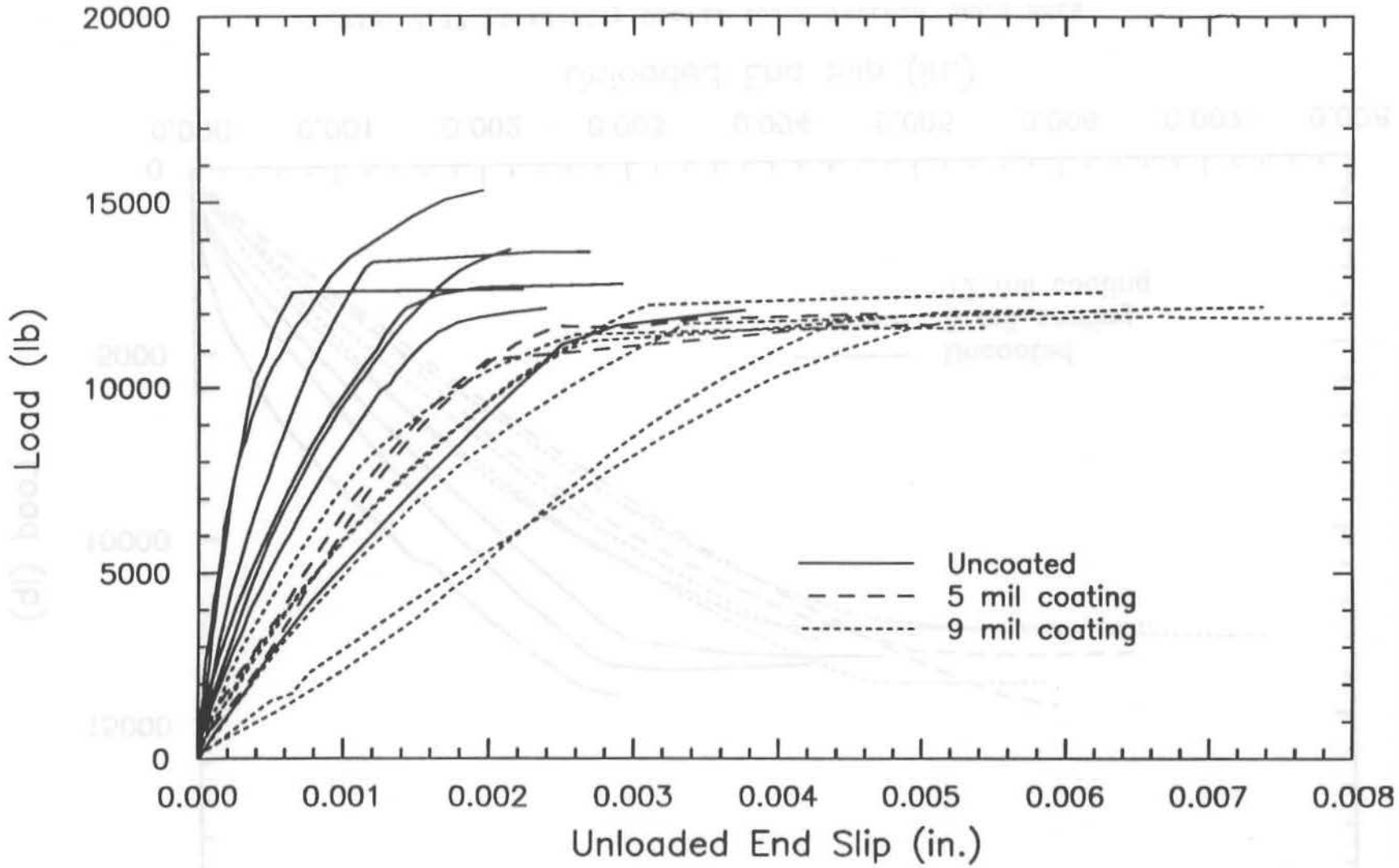

Fig. 2.13 Load-Slip Curves for N-Pattern No.5 Bars

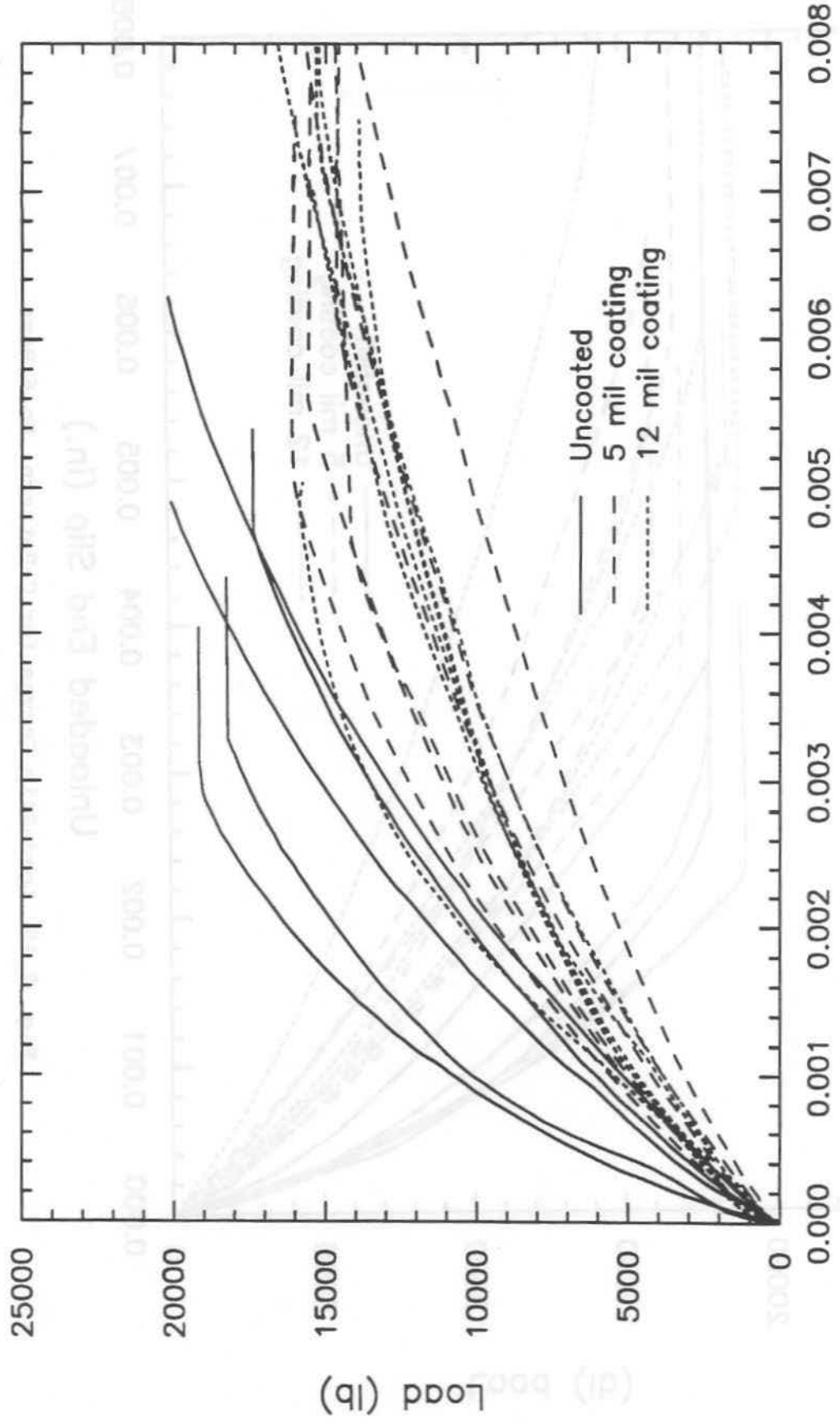

Fig. 2.14 Load-Slip Curves for S-Pattern No.6 Bars

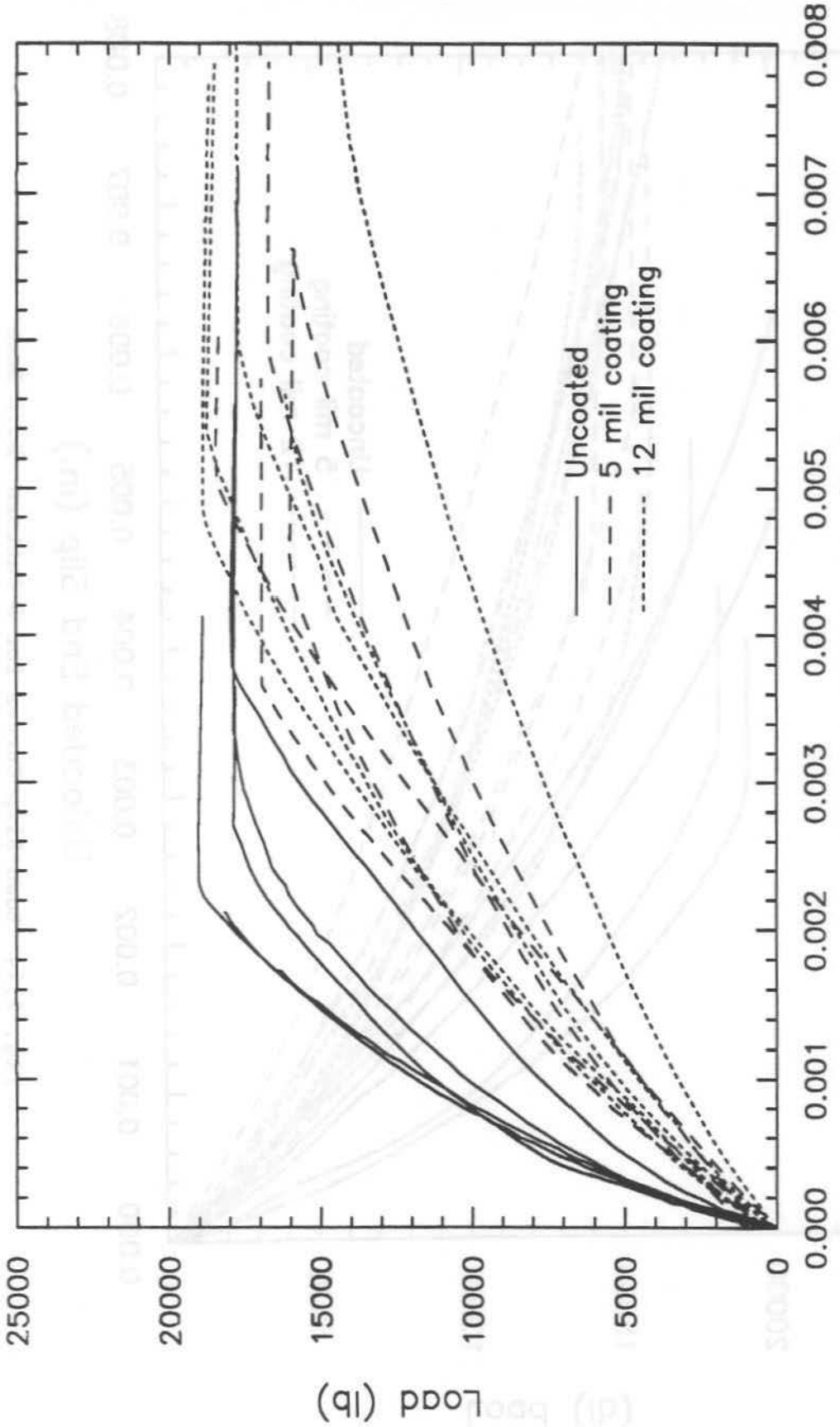

Fig. 2.15 Load-Slip Curves for C-Pattern No.6 Bars

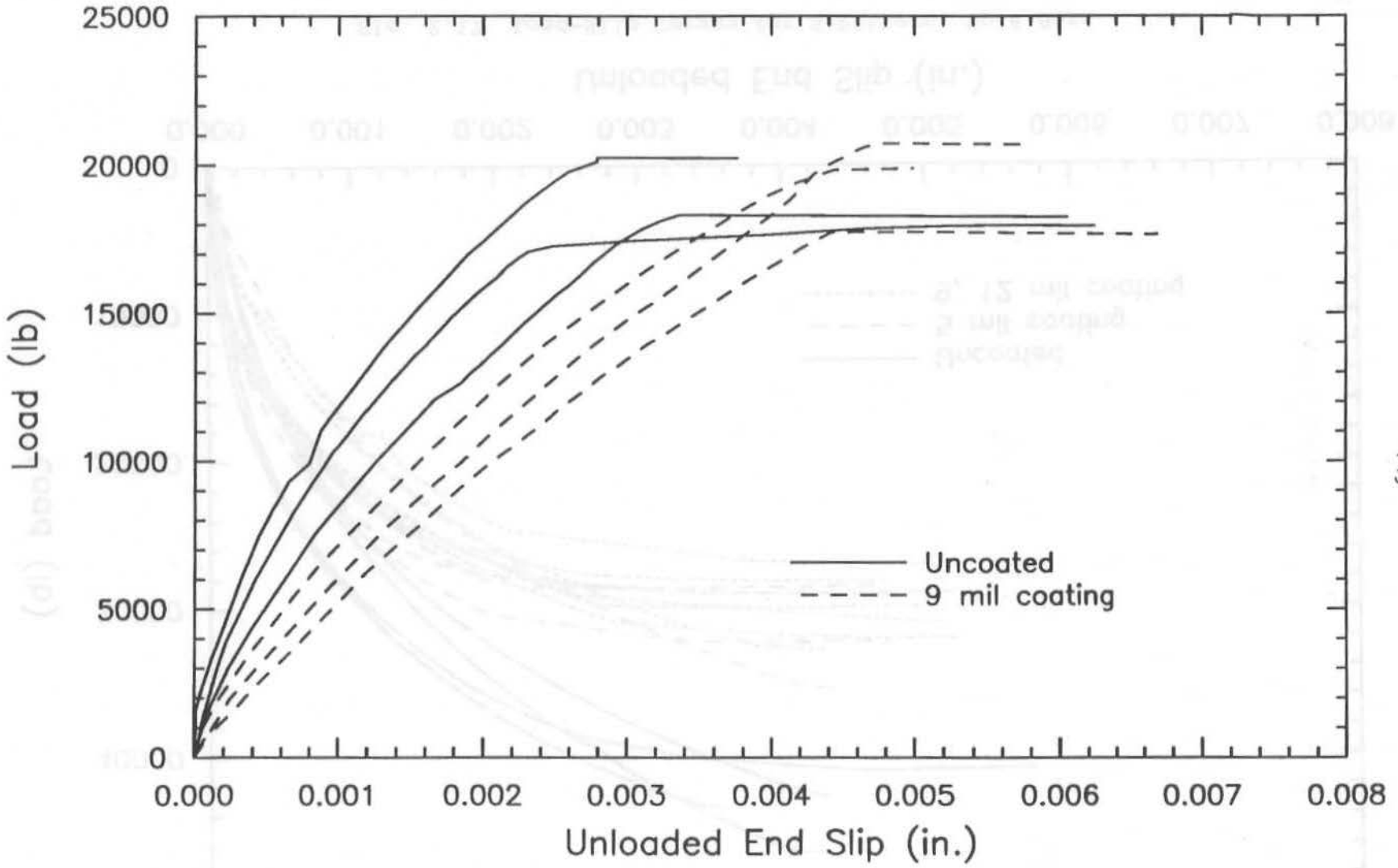

Fig. 2.16 Load-Slip Curves for N-Pattern No.6 Bars

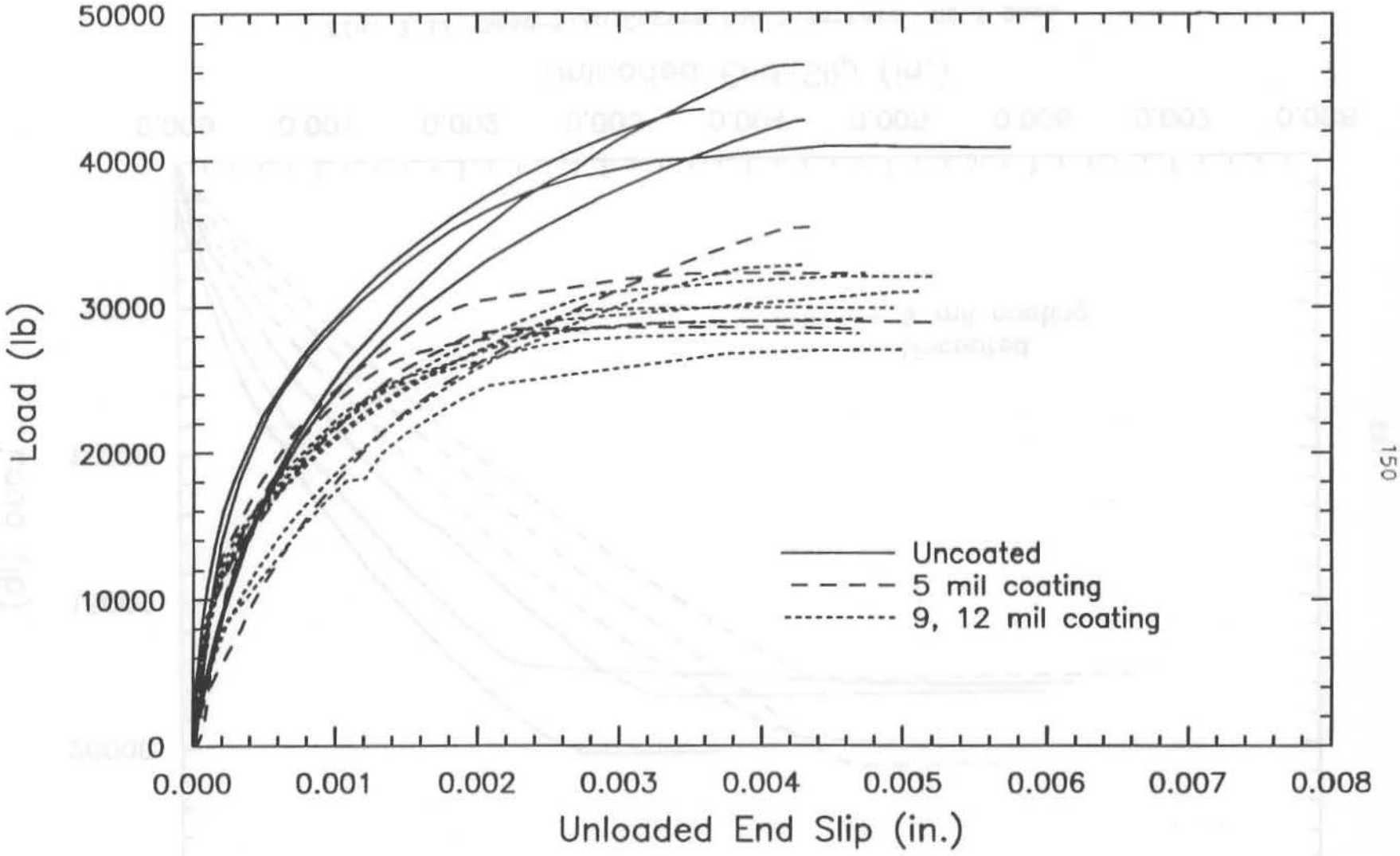

Fig. 2.17 Load-Slip Curves for S-Pattern No.8 Bars

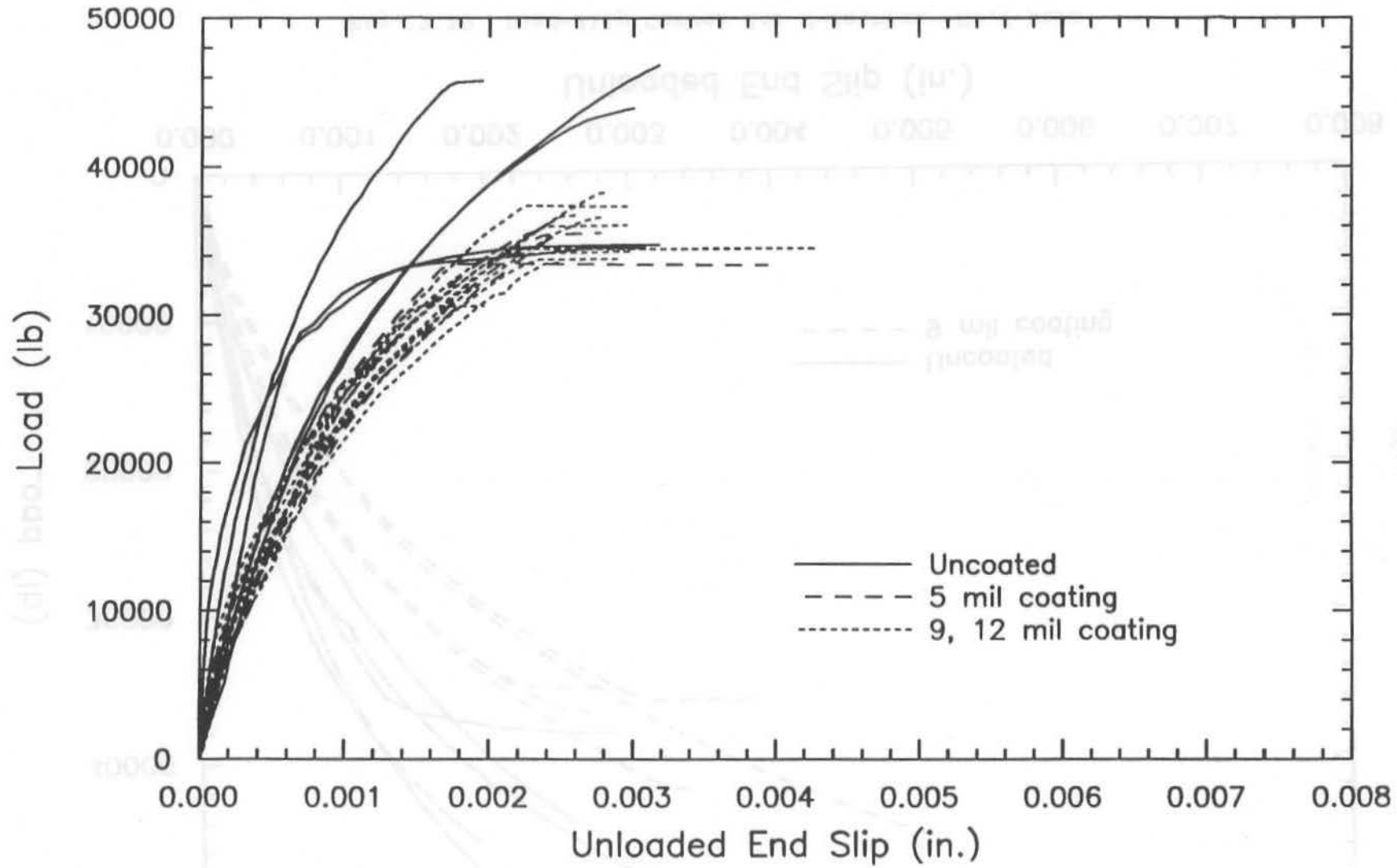

Fig. 2.18 Load-Slip Curves for C-Pattern No.8 Bars

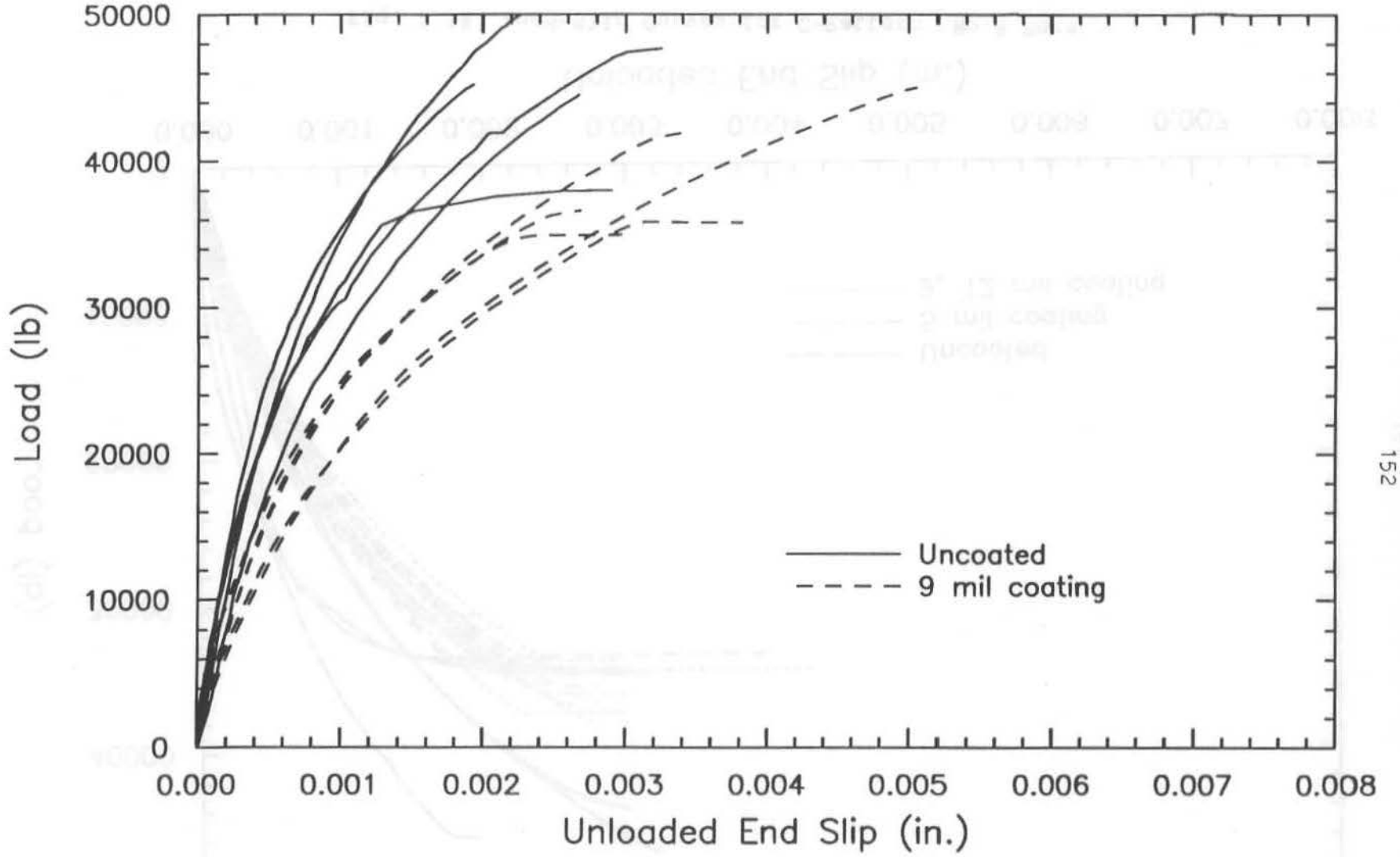

Fig. 2.19 Load-Slip Curves for N-Pattern No.8 Bars

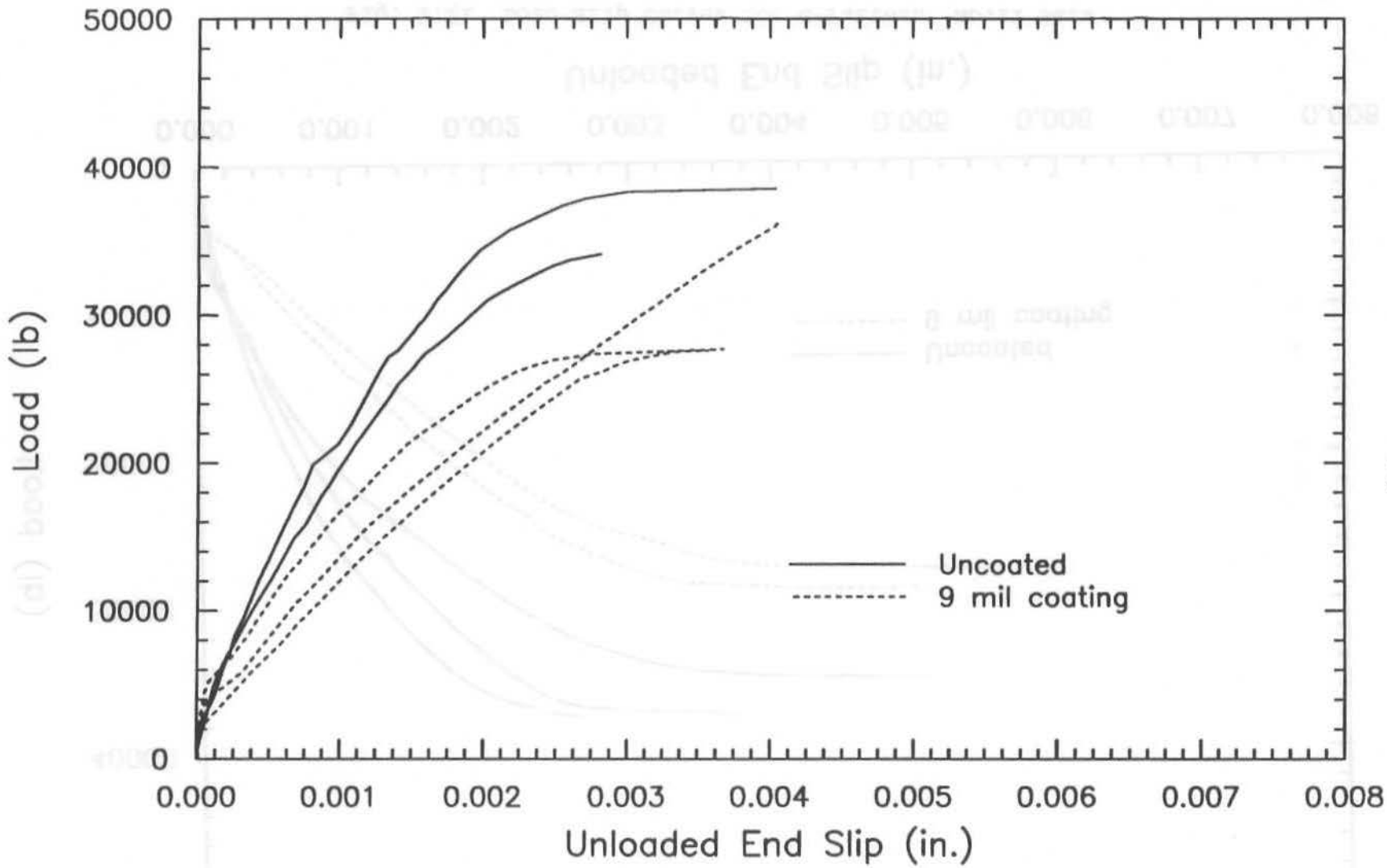

Fig. 2.20 Load-Slip Curves for S-Pattern No.11 Bars

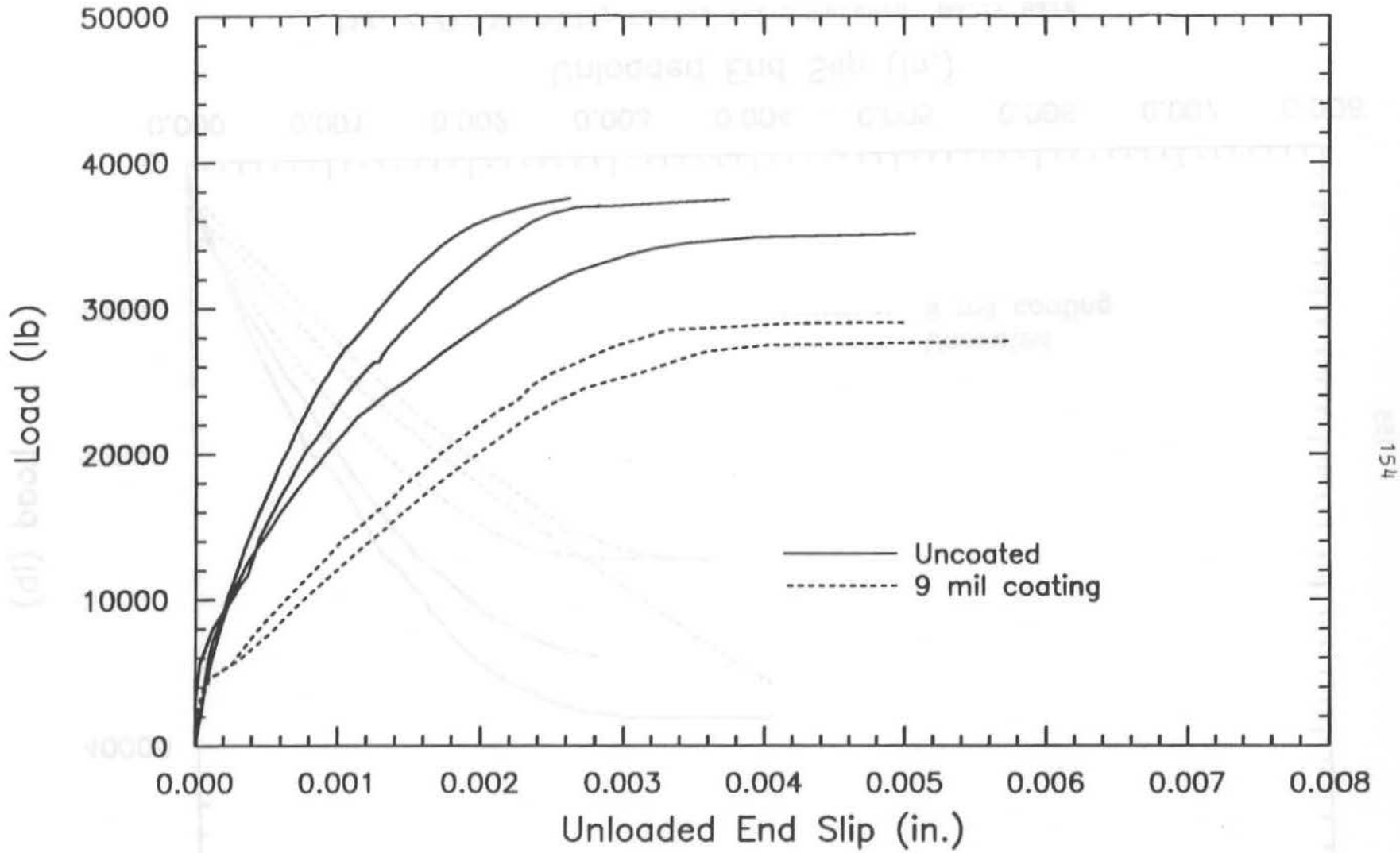

Fig. 2.21 Load-Slip Curves for C-Pattern No.11 Bars

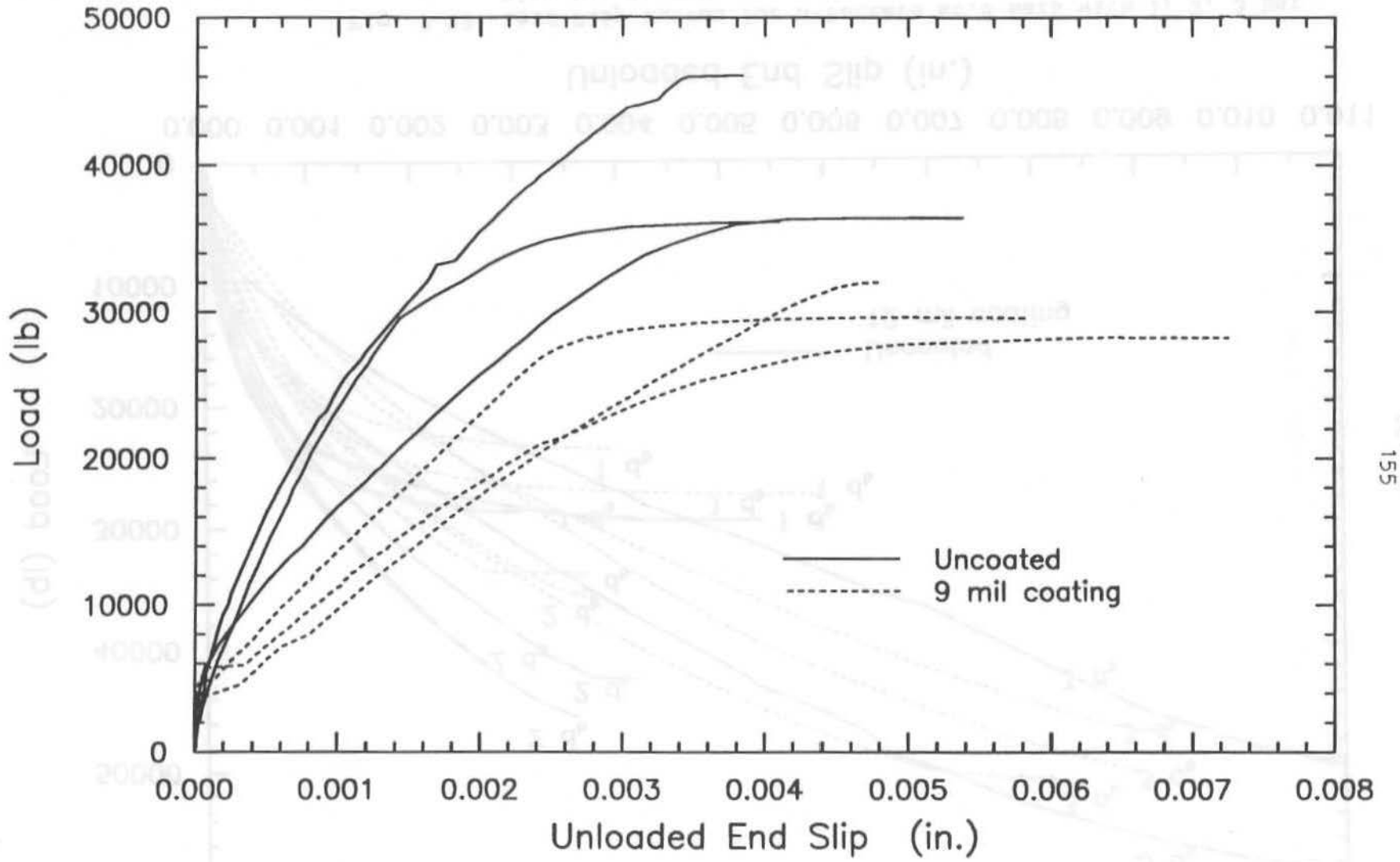

Fig. 2.22 Load-Slip Curves for N-Pattern No.11 Bars

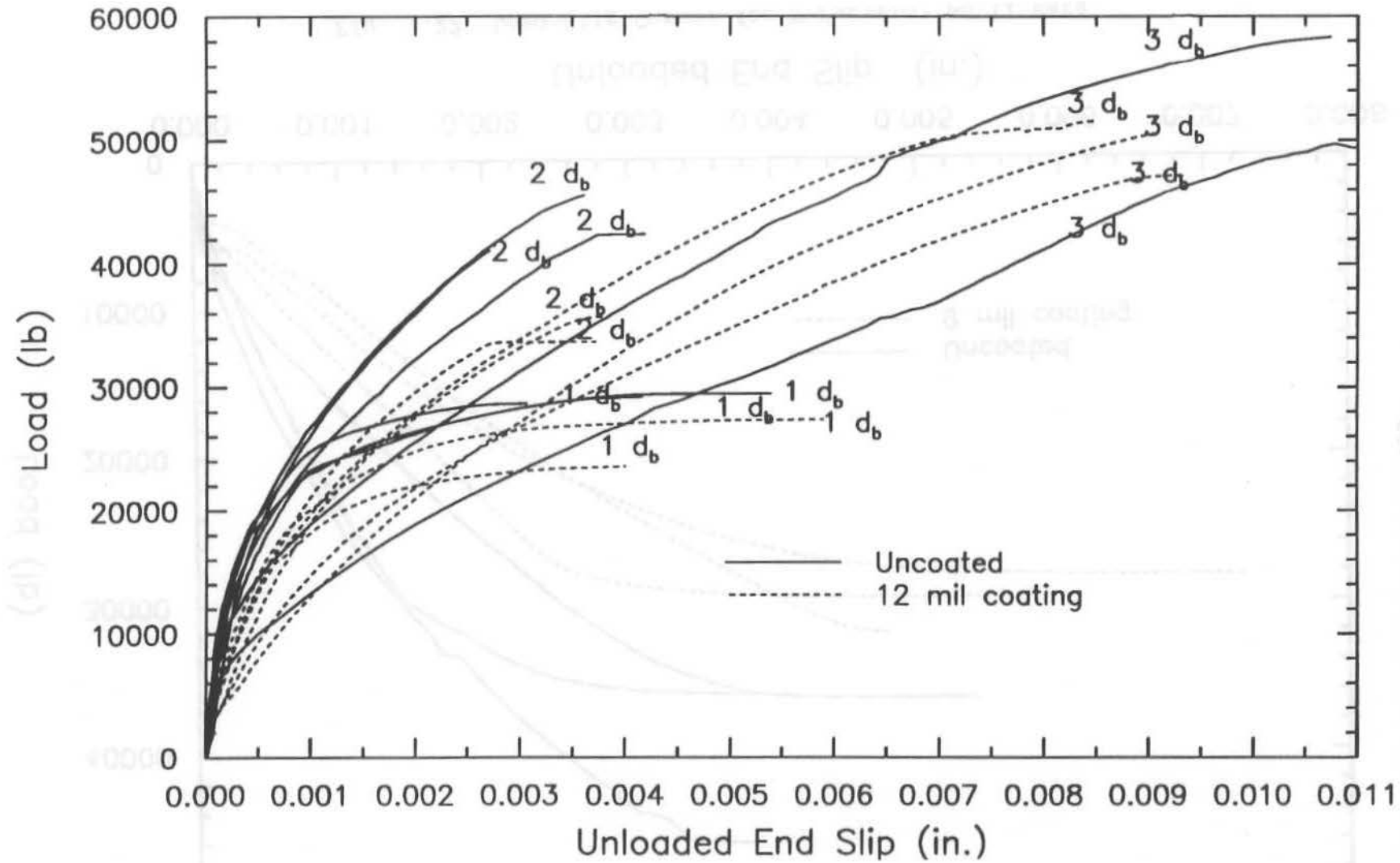

Fig. 2.23 Load-Slip Curves for N-Pattern No.8 Bars with 1, 2, 3 Bar Diameter Covers

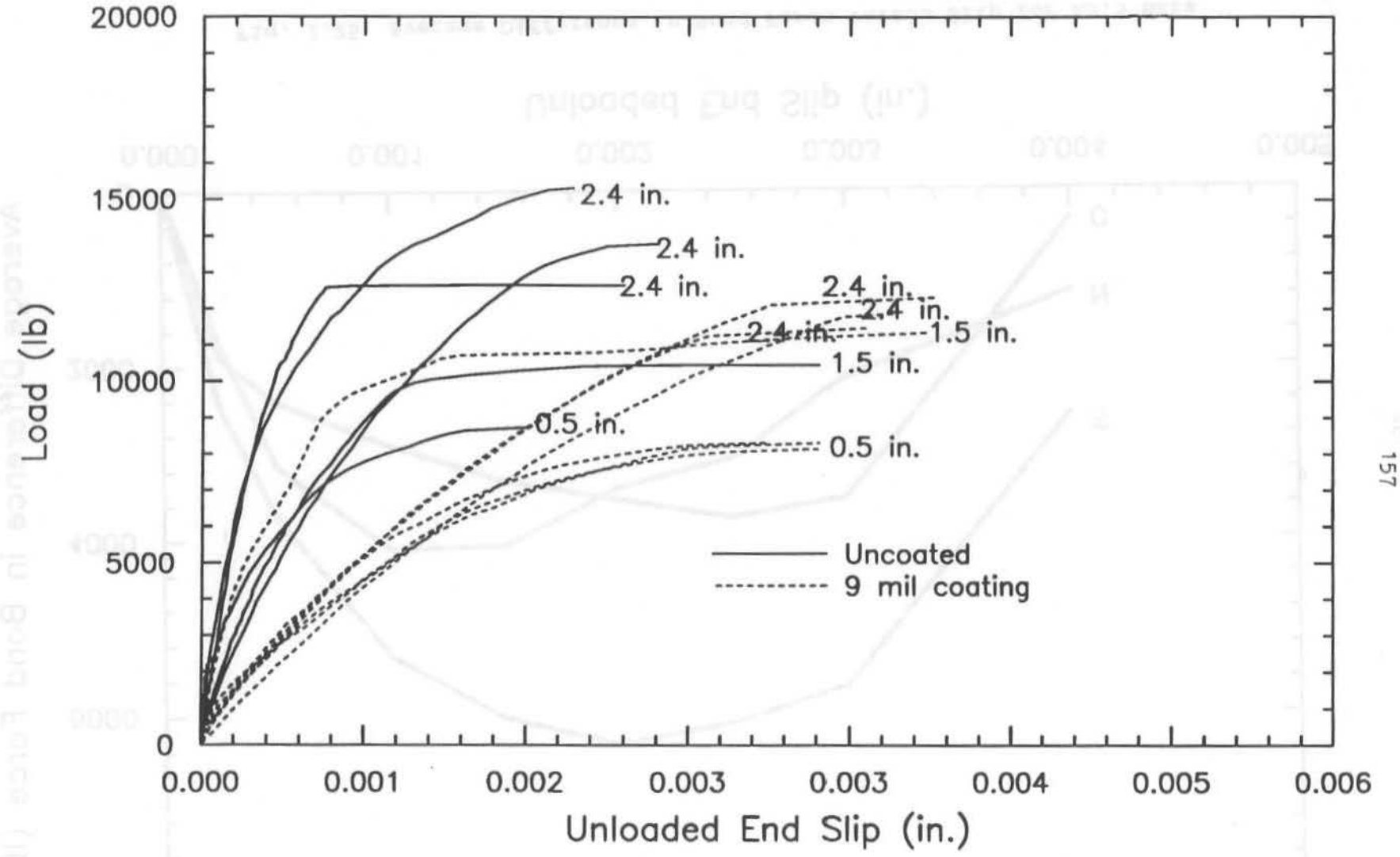

Fig. 2.24 Load-Slip Curves for N-Pattern No.5 Bars with 0.5 in., 1.5 in., and 2.375 in. Lead Lengths

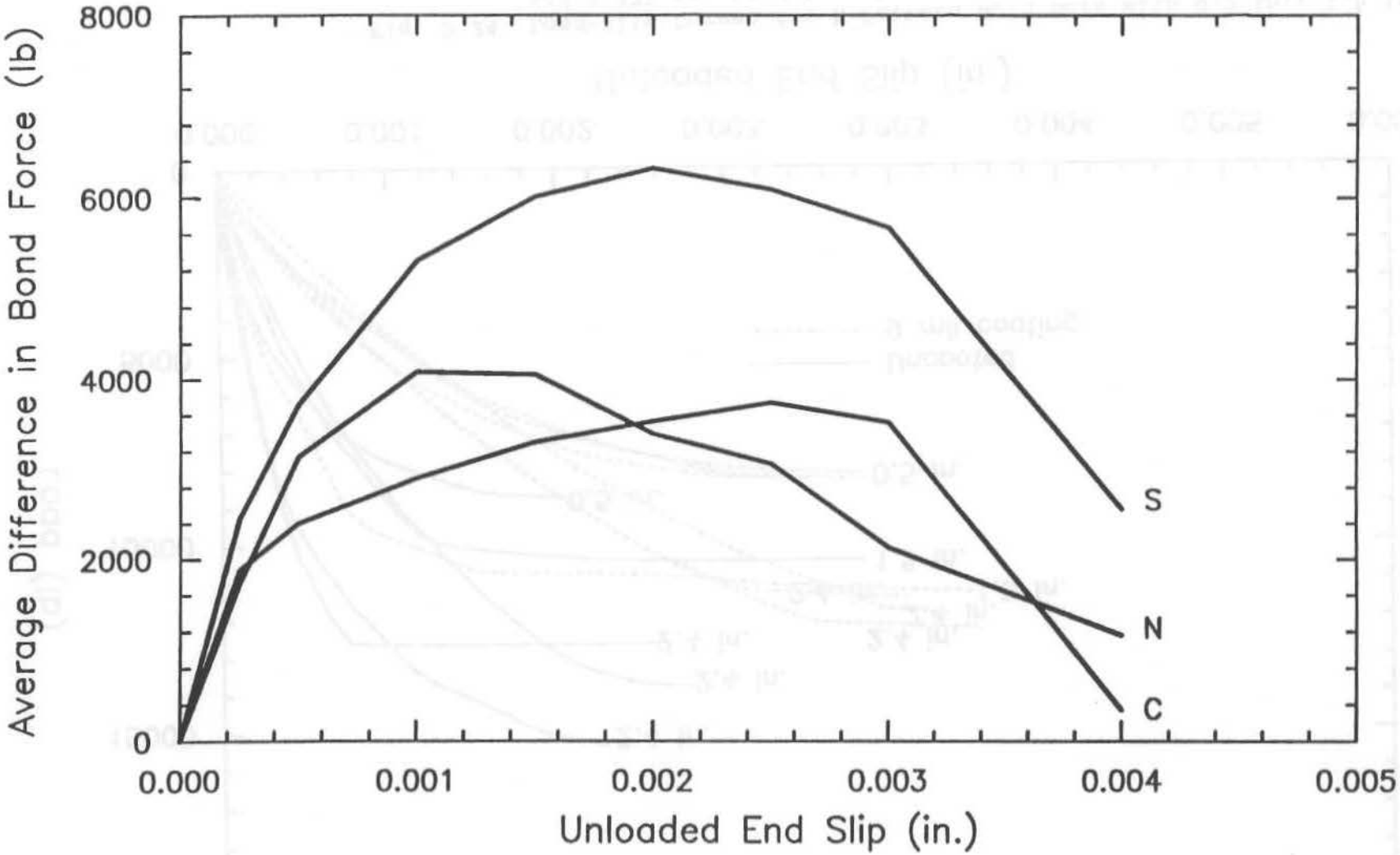

Fig. 2.25 Average Difference in Bond Force versus Slip for No.5 Bars

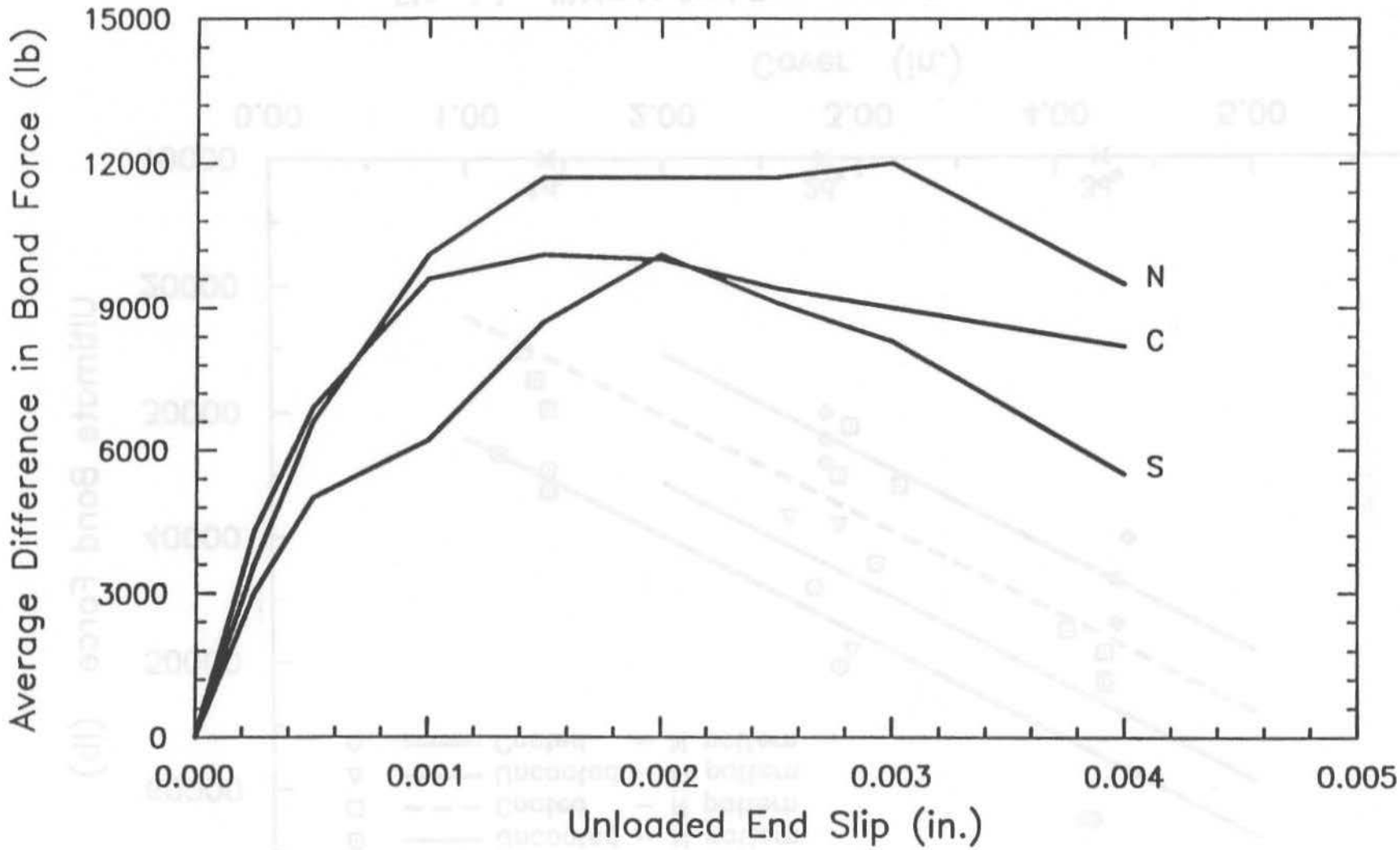

Fig. 2.26 Average Difference in Bond Force versus Slip for No.11 Bars

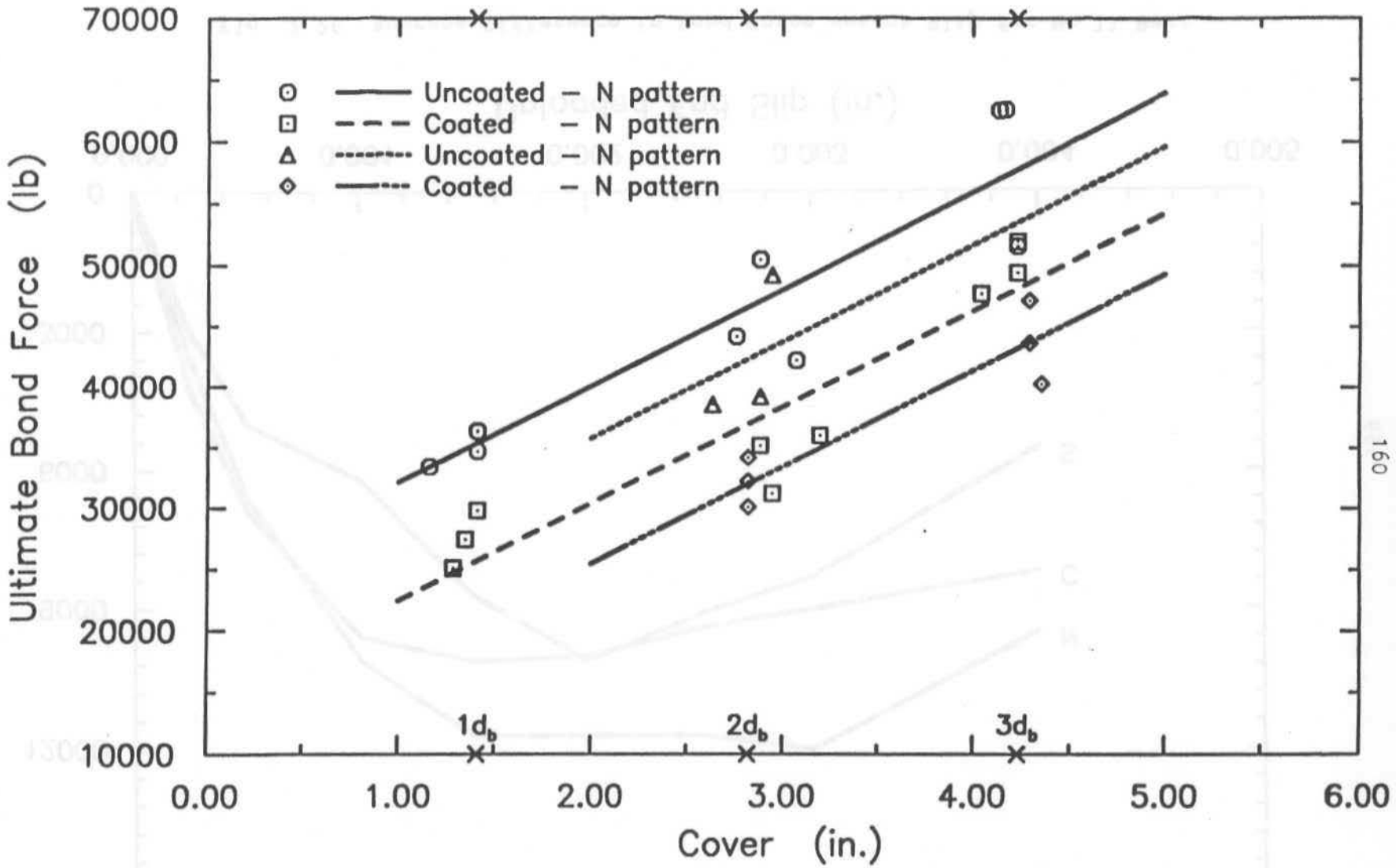

Fig. 3.1 Ultimate Bond Foce versus Cover for No.11 Bars (Hadje-Ghaffari et al. 1990)

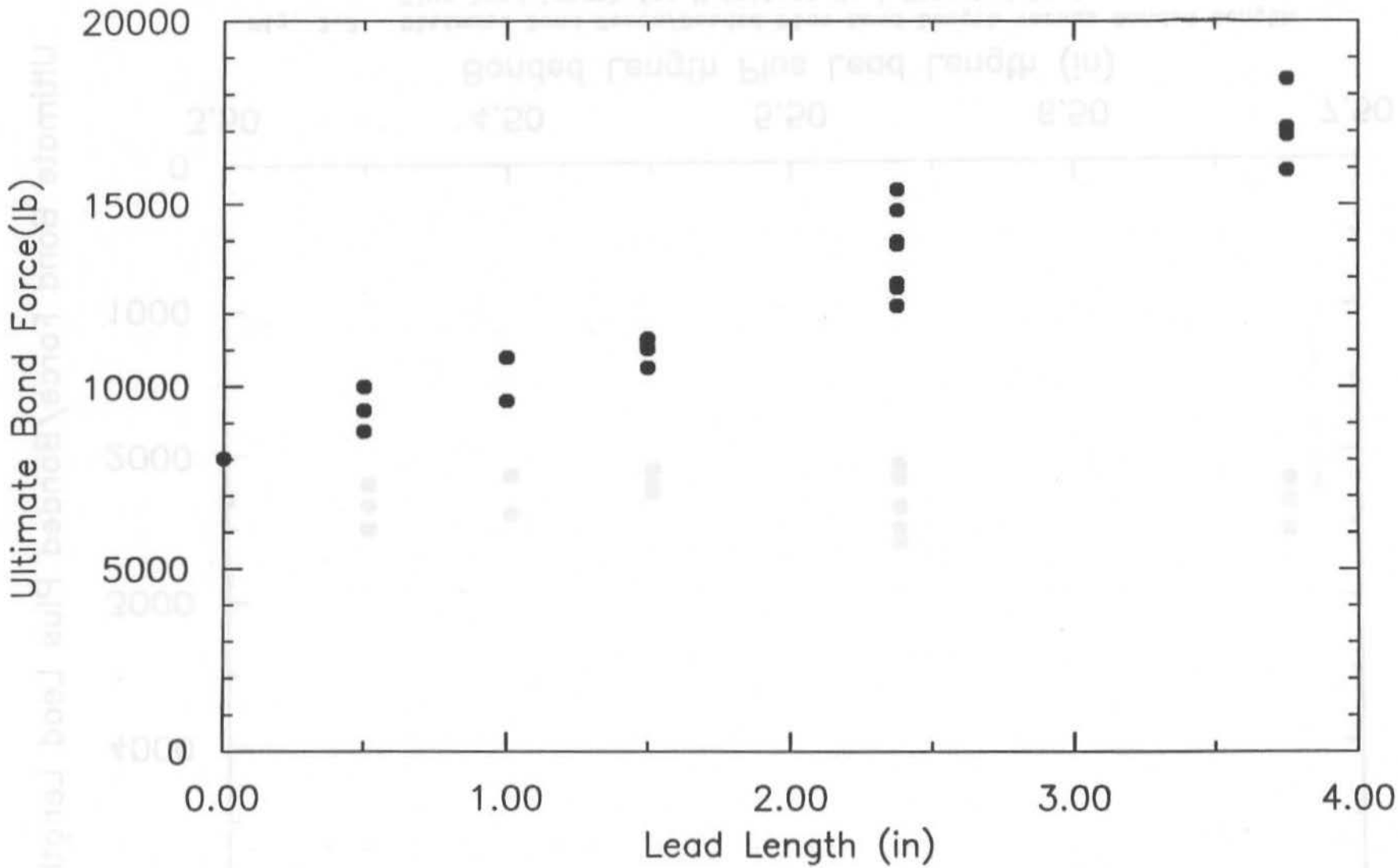

Fig. 3.2 Ultimate Bond Force versus Lead Length for N-Pattern No.5 Uncoated Bars

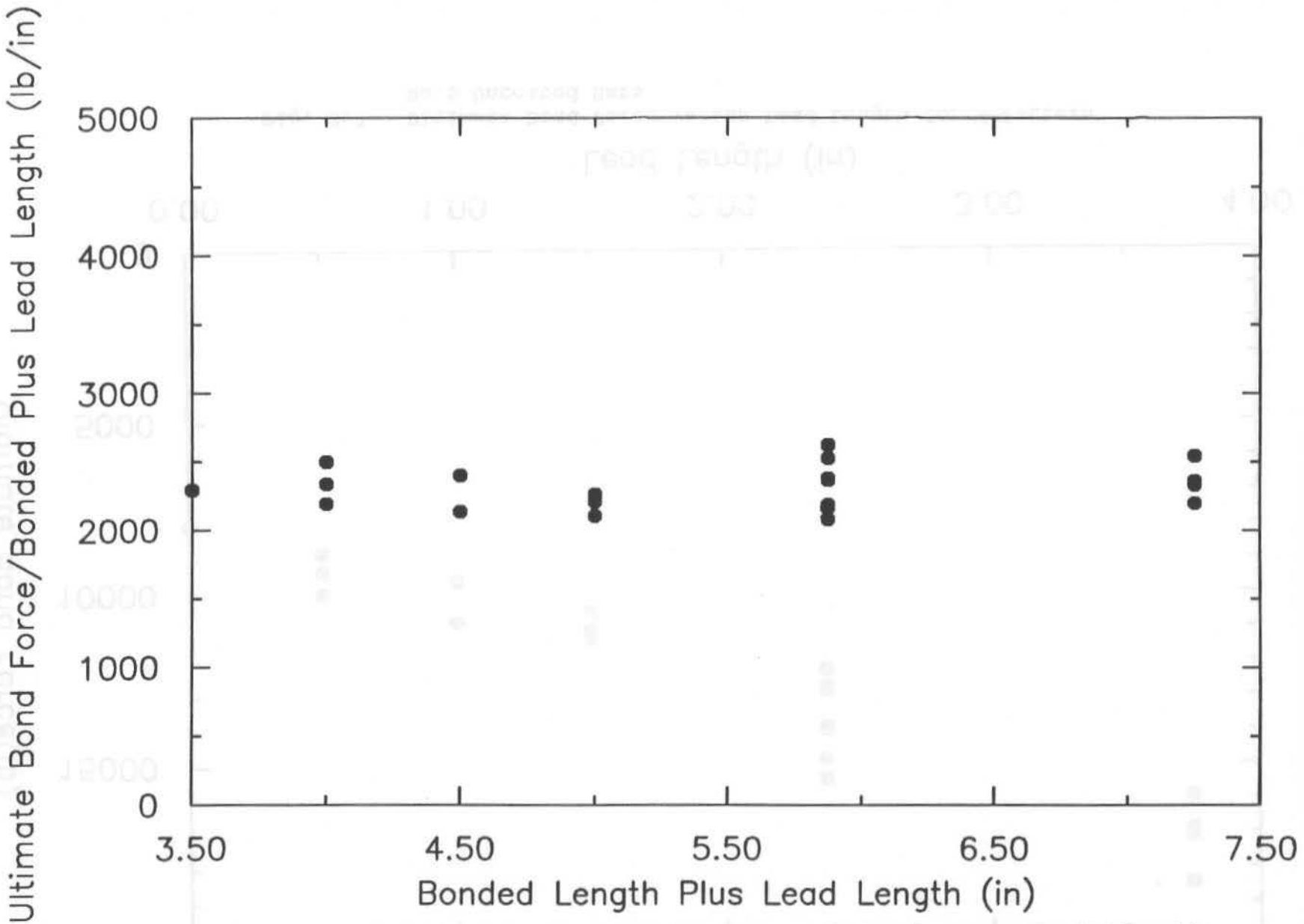

Fig. 3.3 Ultimate Bond Force/Bonded Plus Lead Length versus Bonded Length Plus Lead Length for N-Pattern No.5 Uncoated Bars

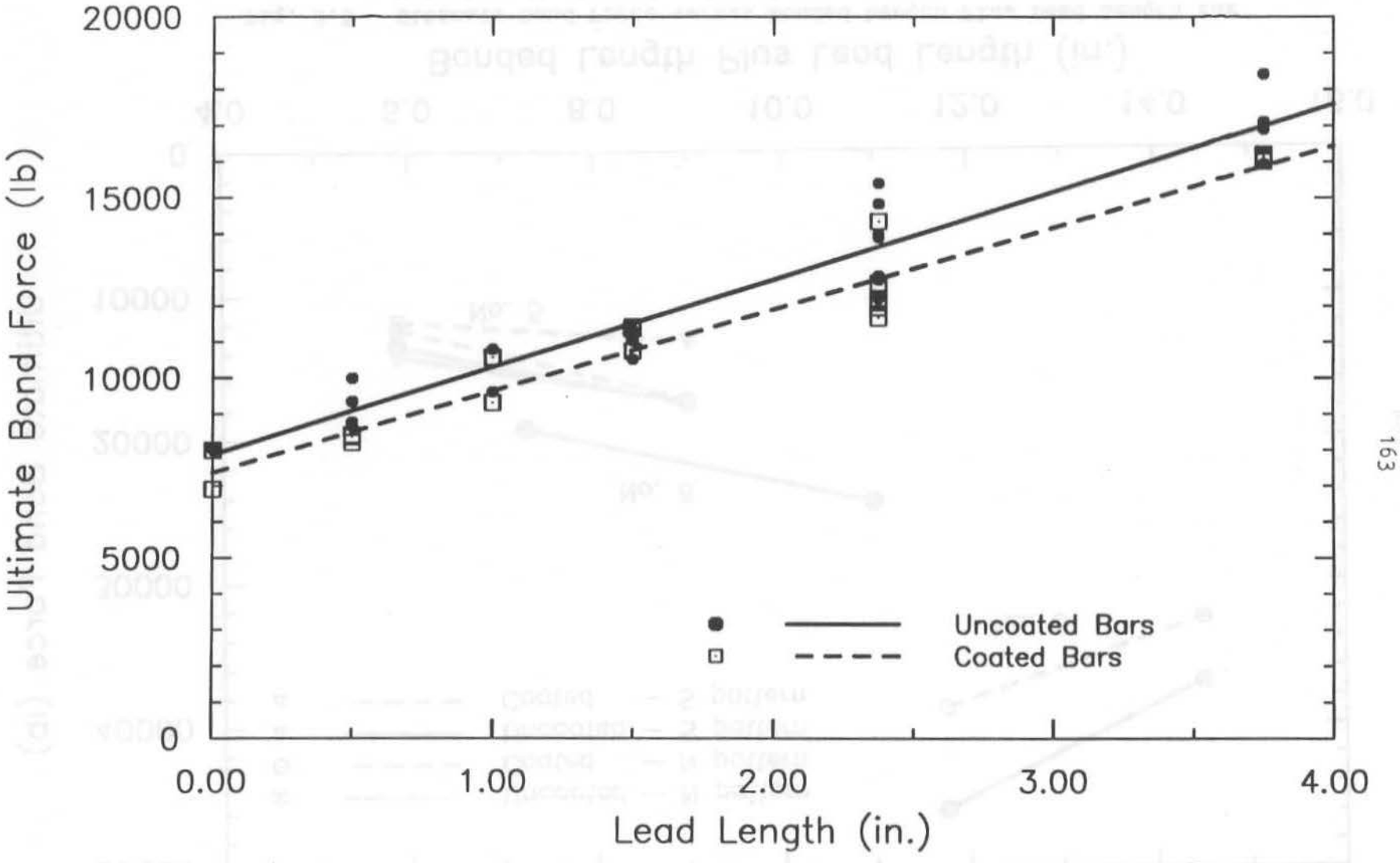

Fig. 3.4 Ultimate Bond Force versus Lead Length for N-Pattern No.5 Uncoated and Coated Bars

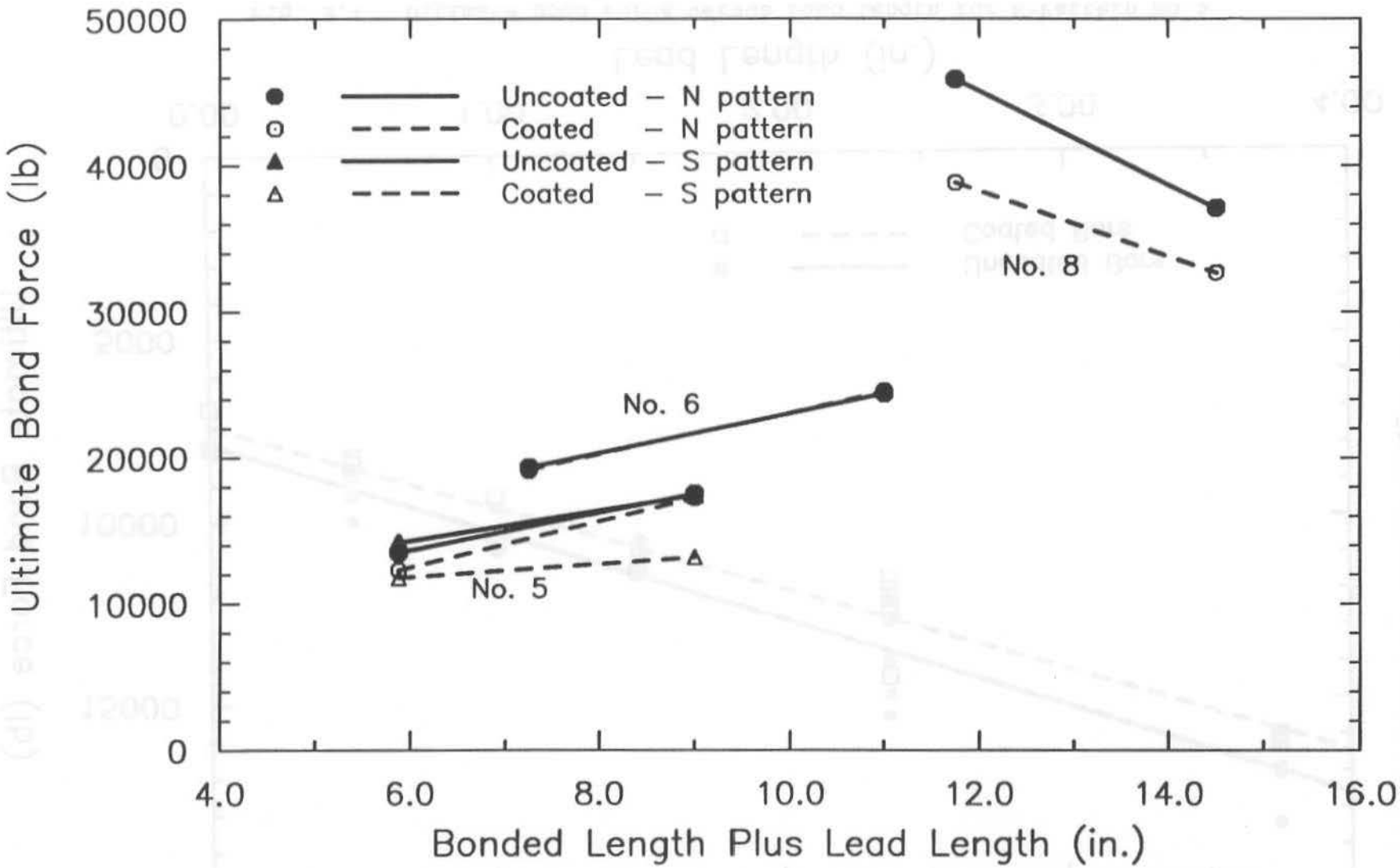

Fig. 3.5 Ultimate Bond Force versus Bonded Length Plus Lead Length for N-Pattern No.5, No.6 and No.8 Bars and S-Pattern No.5 Bars

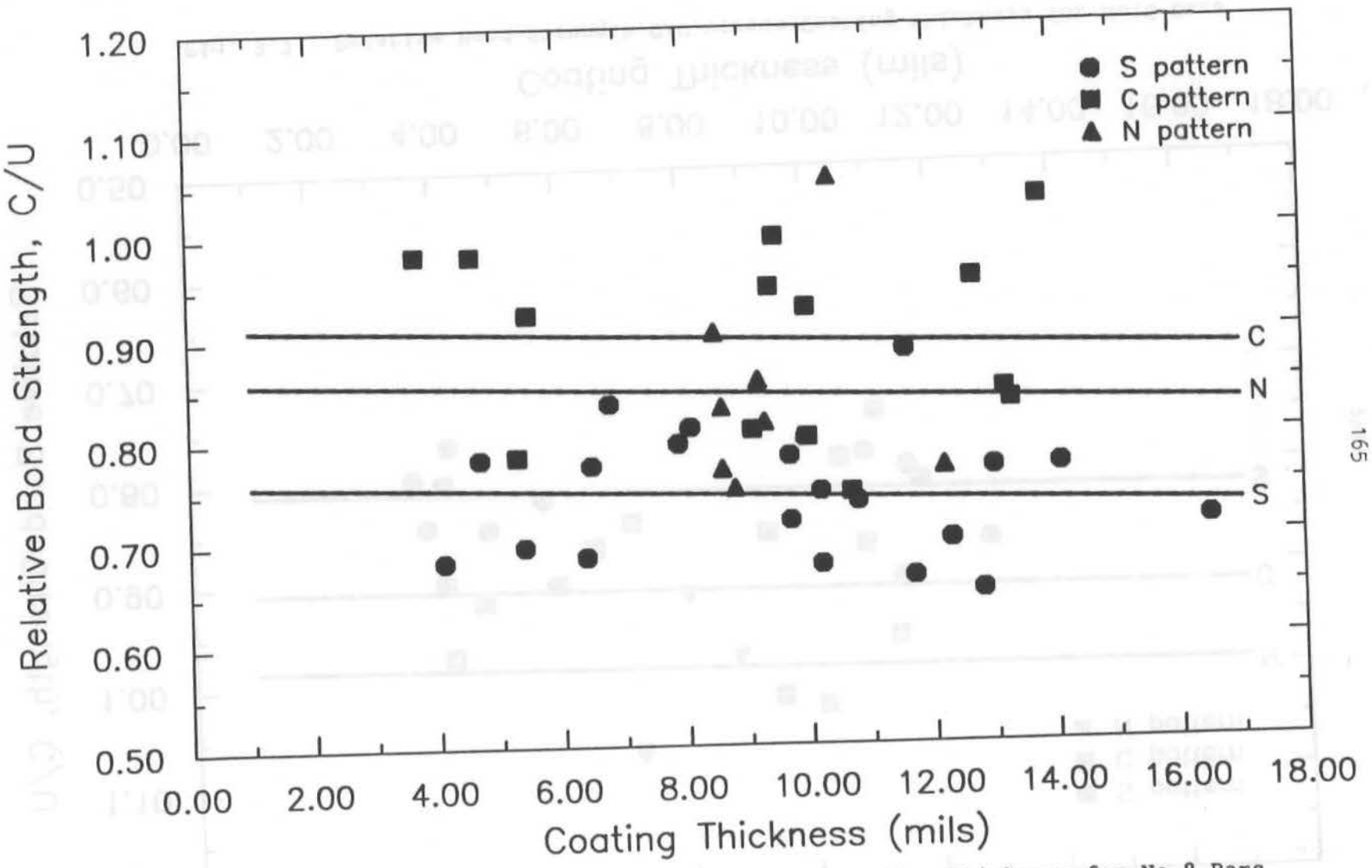

Fig. 3.6 Relative Bond Strength, C/U, versus Coating Thickness for No.8 Bars

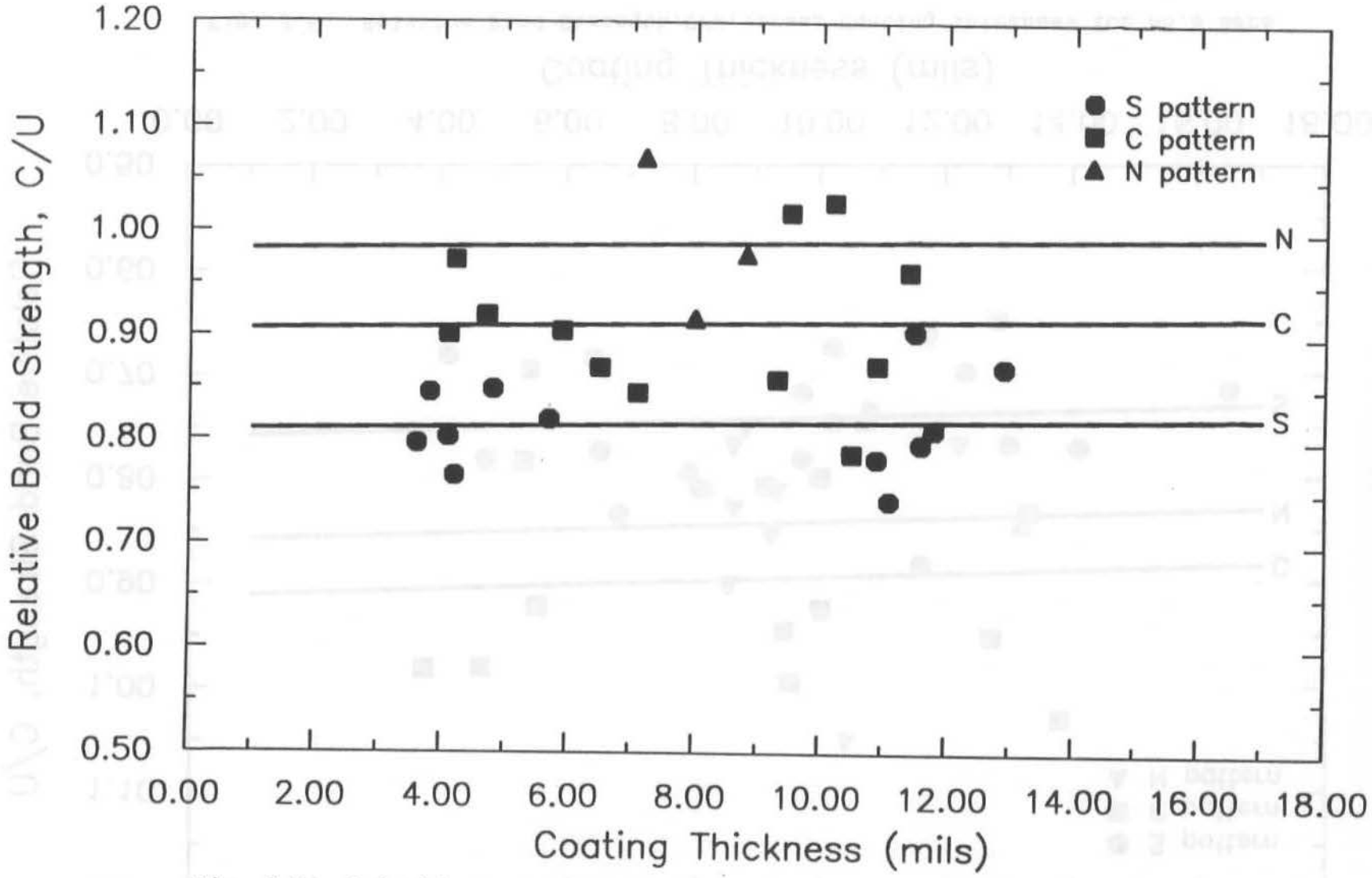

Fig. 3.7 Relative Bond Strength, C/U, versus Coating Thickness for No.6 Bars

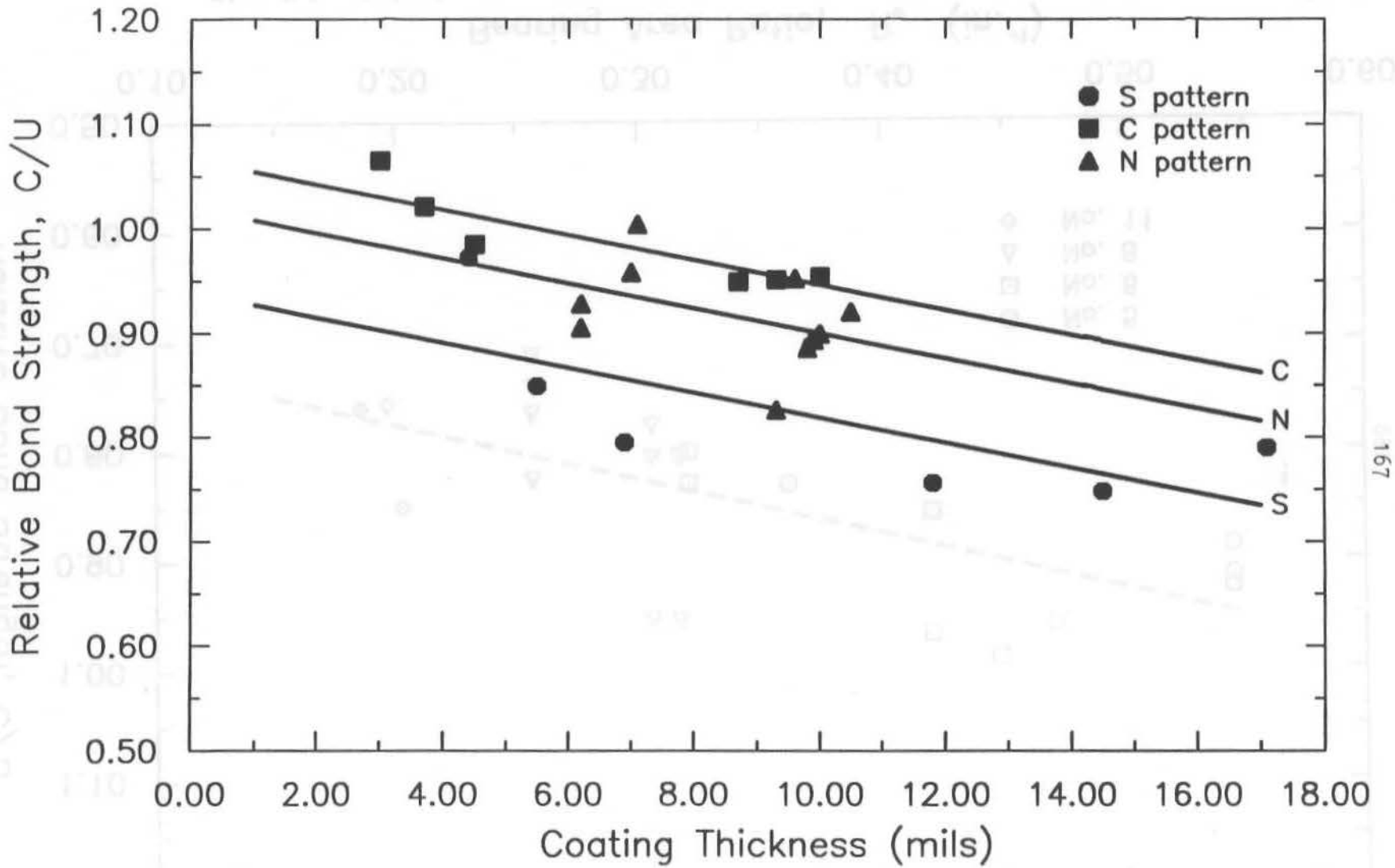

Fig. 3.8 Relative Bond Strength, C/U, versus Coating Thickness for No.5 Bars

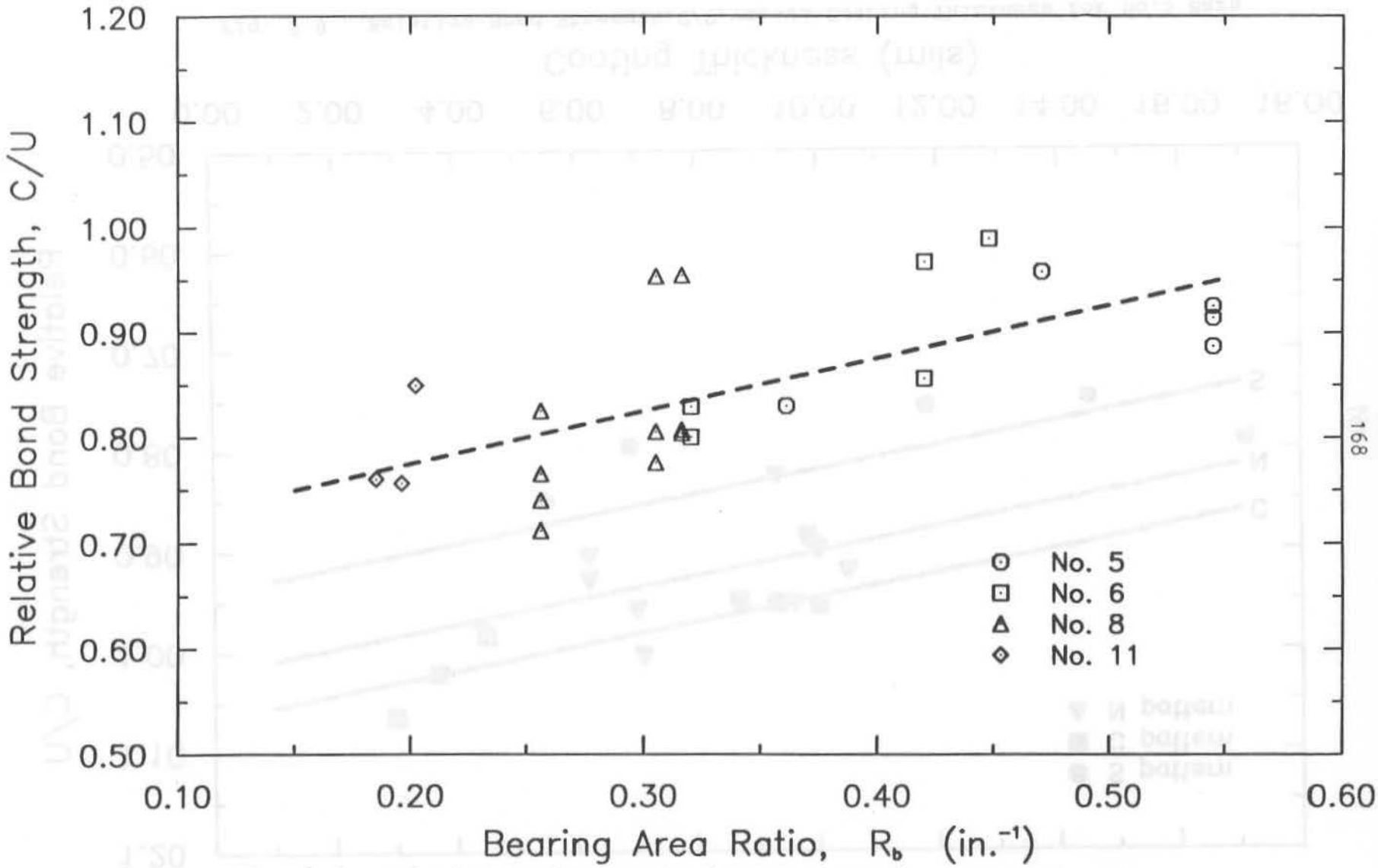

Fig. 3.9 Relative Bond Strength, C/U, versus Bearing Area Ratio, Rb. C and U based on mean bond strength for coated and uncoated bars for each group.

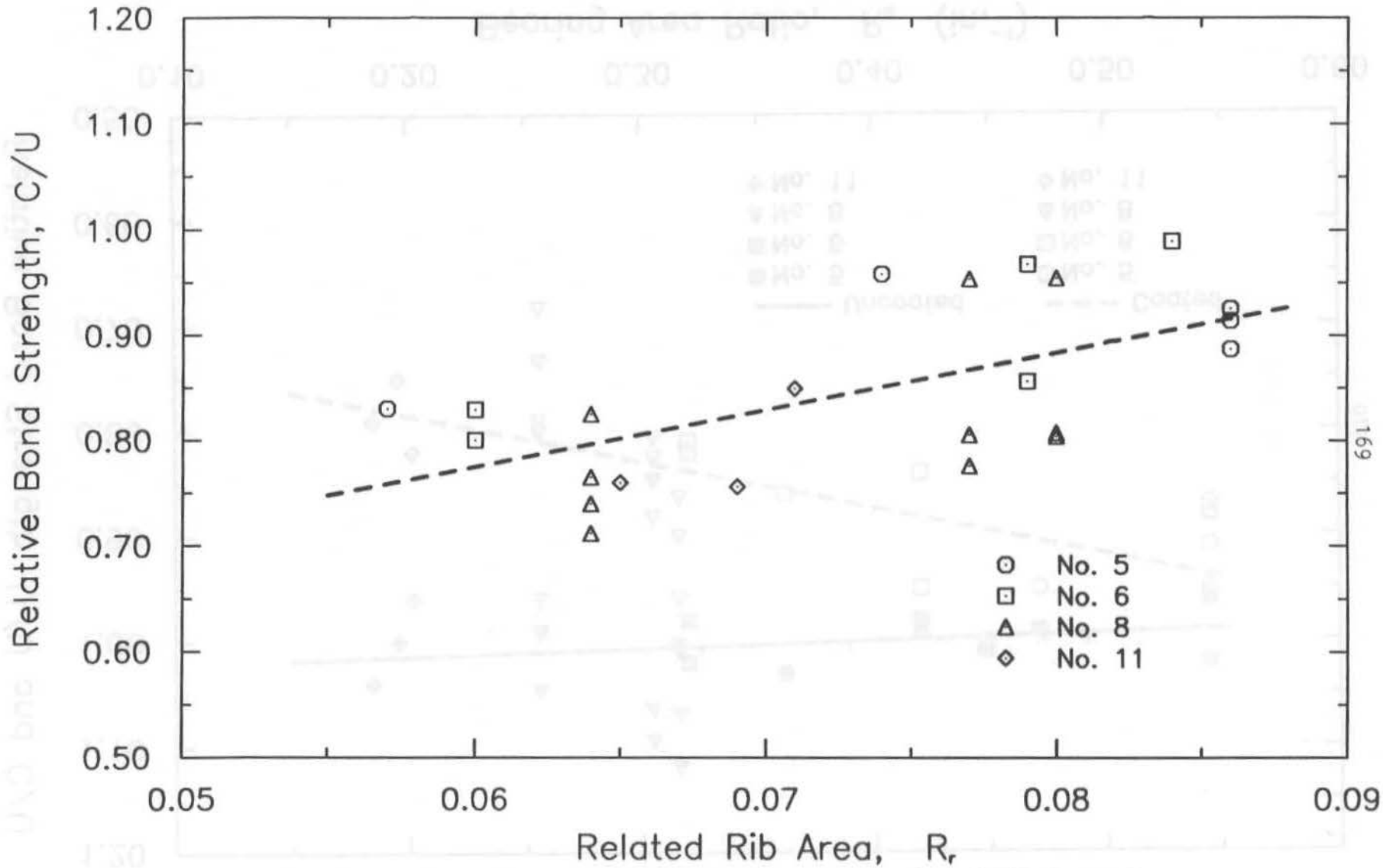

Fig. 3.10 Relative Bond Strength, C/U, versus Related Rib Area, Rr. C and U based on mean bond strength for coated and uncoated bars for each group.

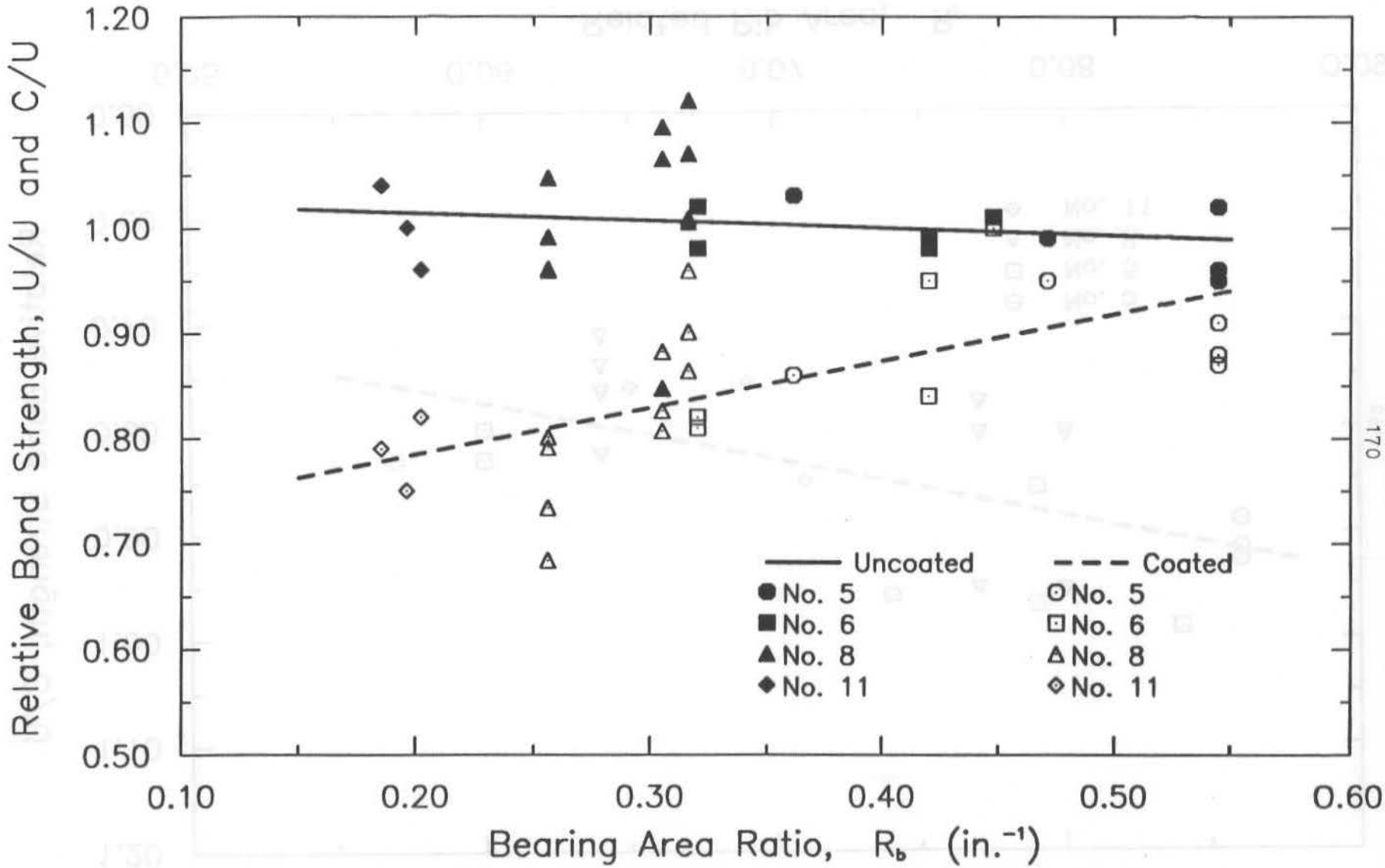

Fig. 3.11 Relative Bond Strength, U/U and C/U, versus Bearing Area Ratio, Rb. Numerator of ratio based on mean bond strength for each group. Denominator based on mean bond strength of all bars of the same size.

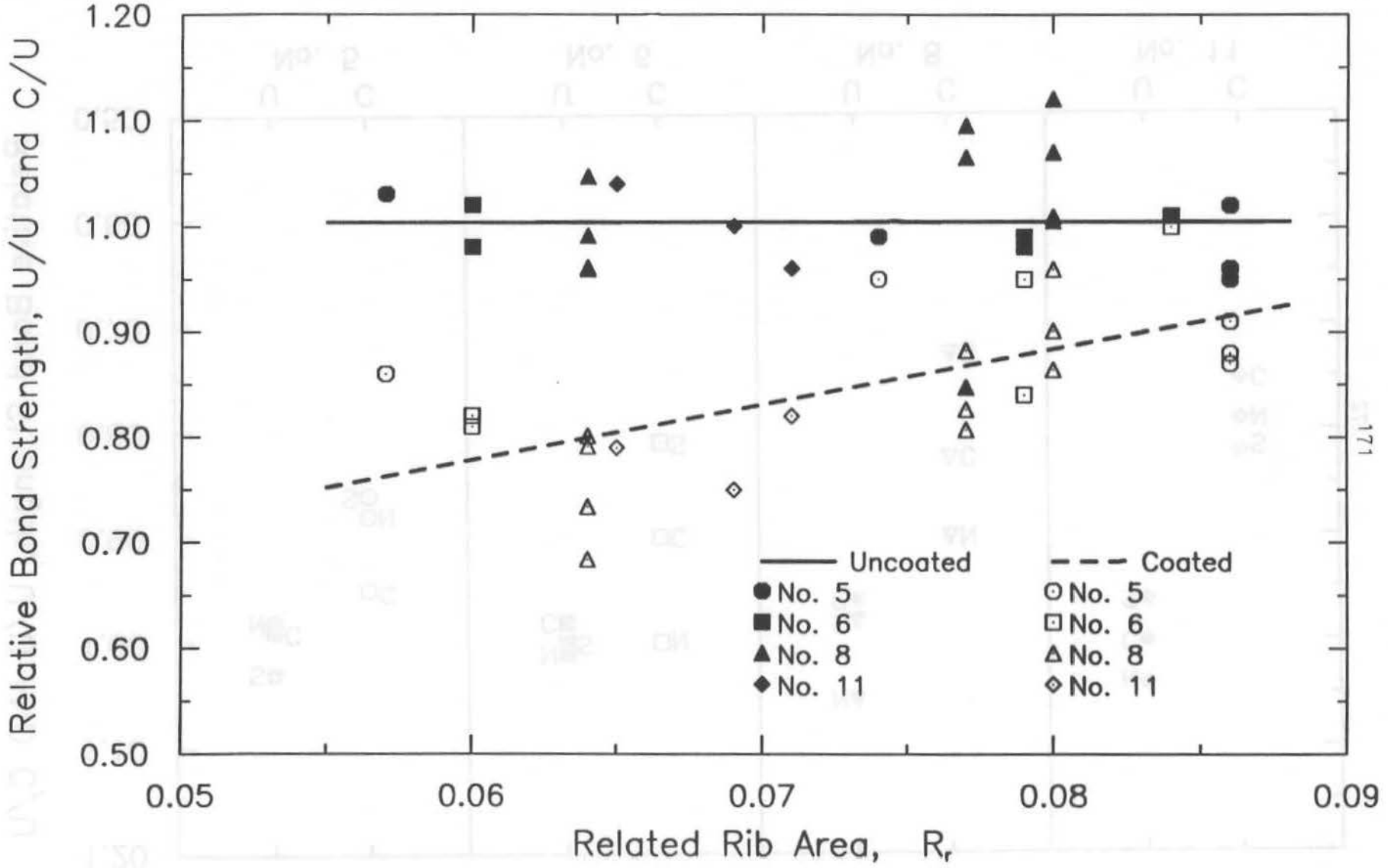

Fig. 3.12 Relative Bond Strength, U/U and C/U, versus Related Rib Area, Rr. Numerator of ratio based on mean bond strength for each group. Denominator based on mean bond strength of all bars of the same size.

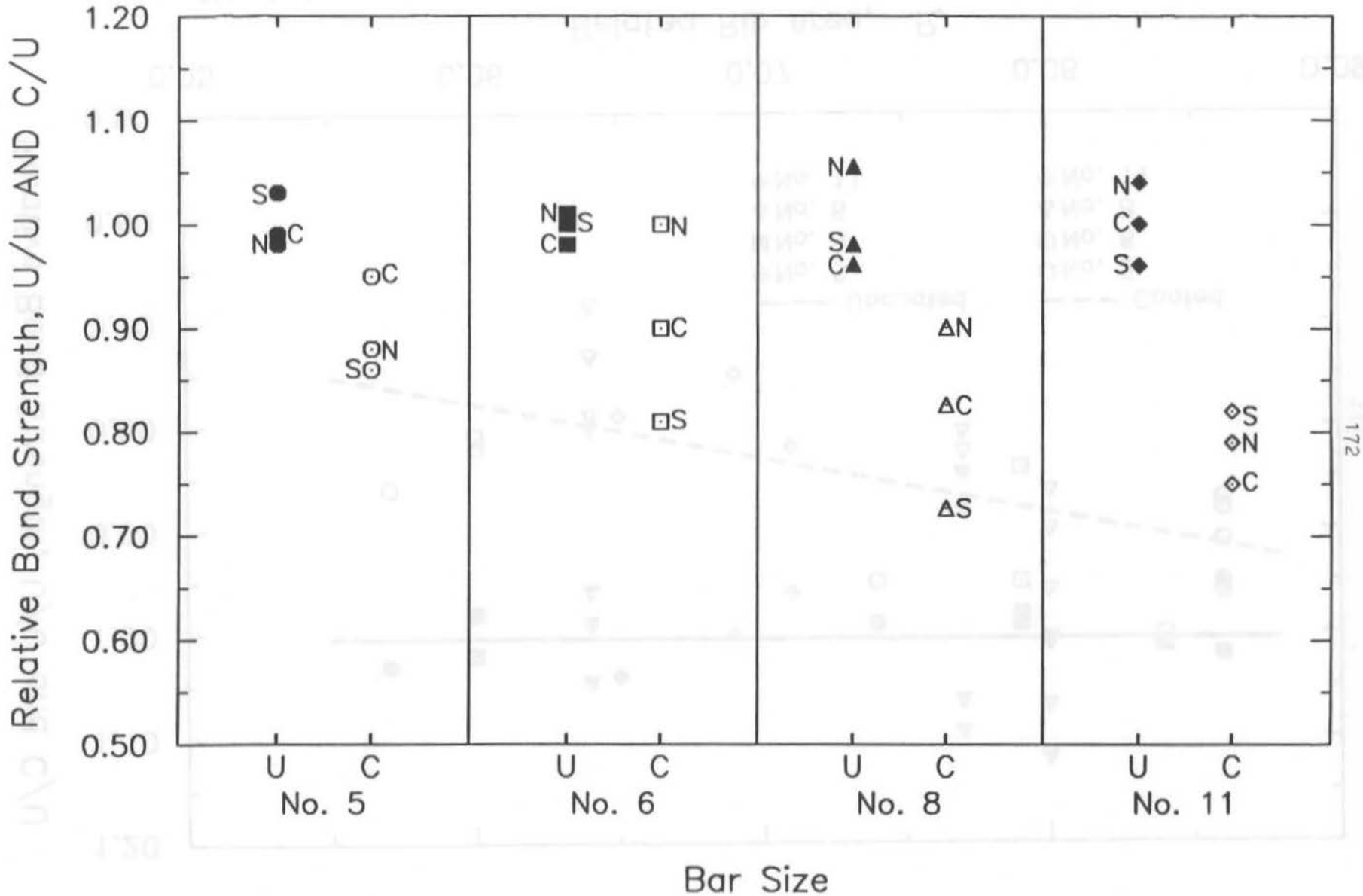

Fig. 3.13 Relative Bond Strengths, U/U and C/U, versus Bar Size

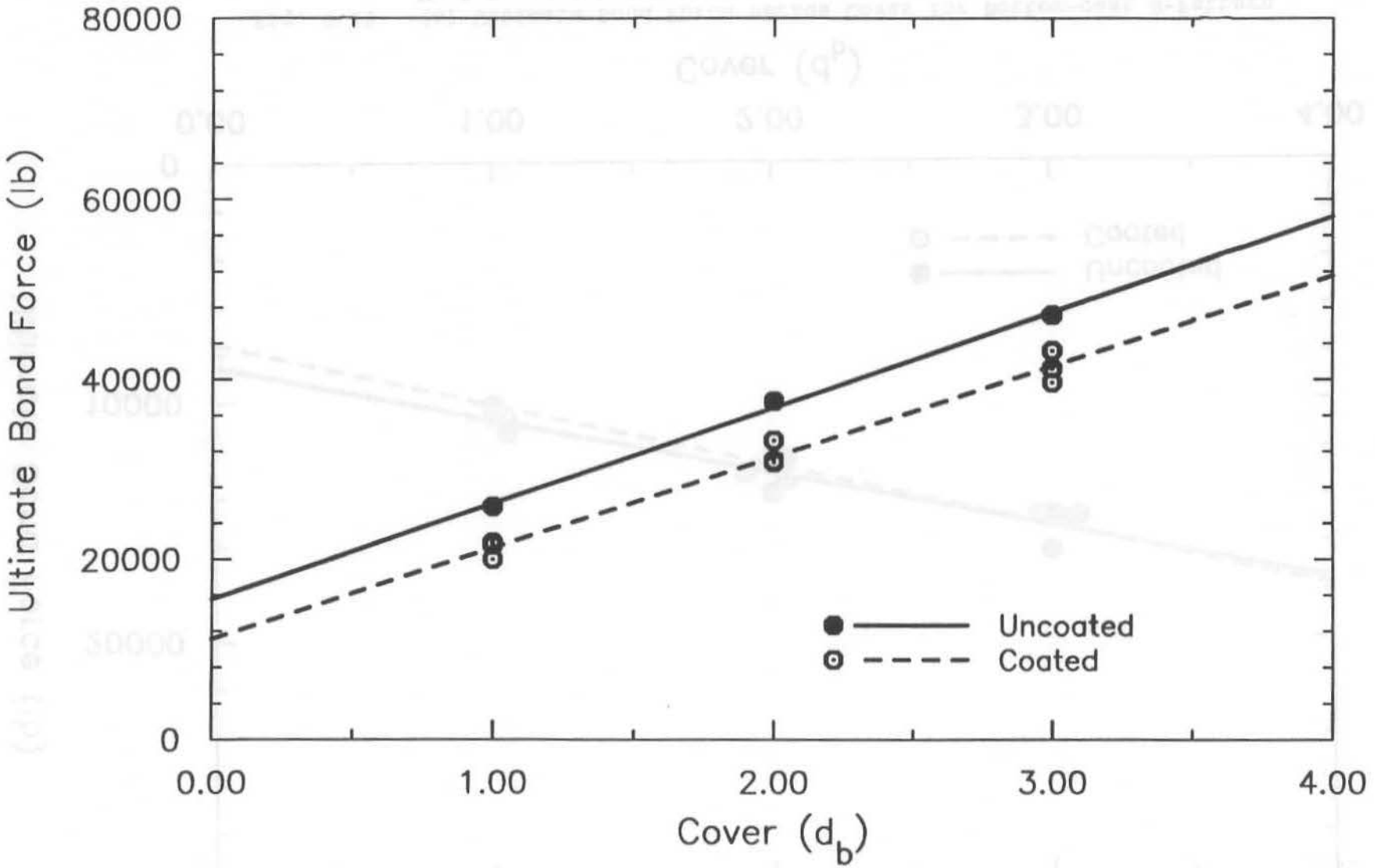

Fig. 3.14 Ultimate Bond Force versus Cover for Top-cast S-Pattern No.8 Bars

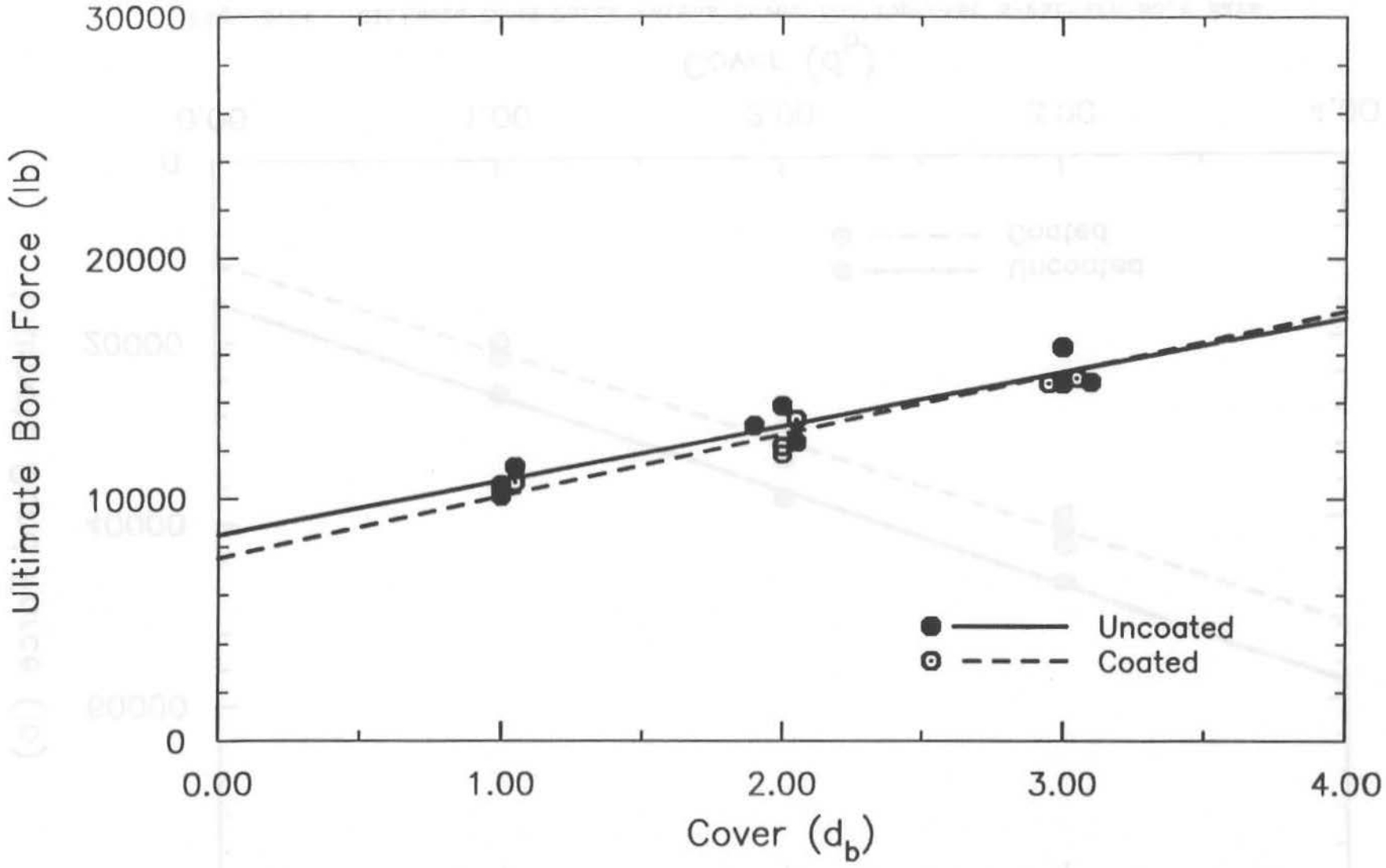

Fig. 3.15 (a) Ultimate Bond Force versus Cover for Bottom-cast N-Pattern No.5 Bars with Covers of 1, 2, 3 Bar Diameter

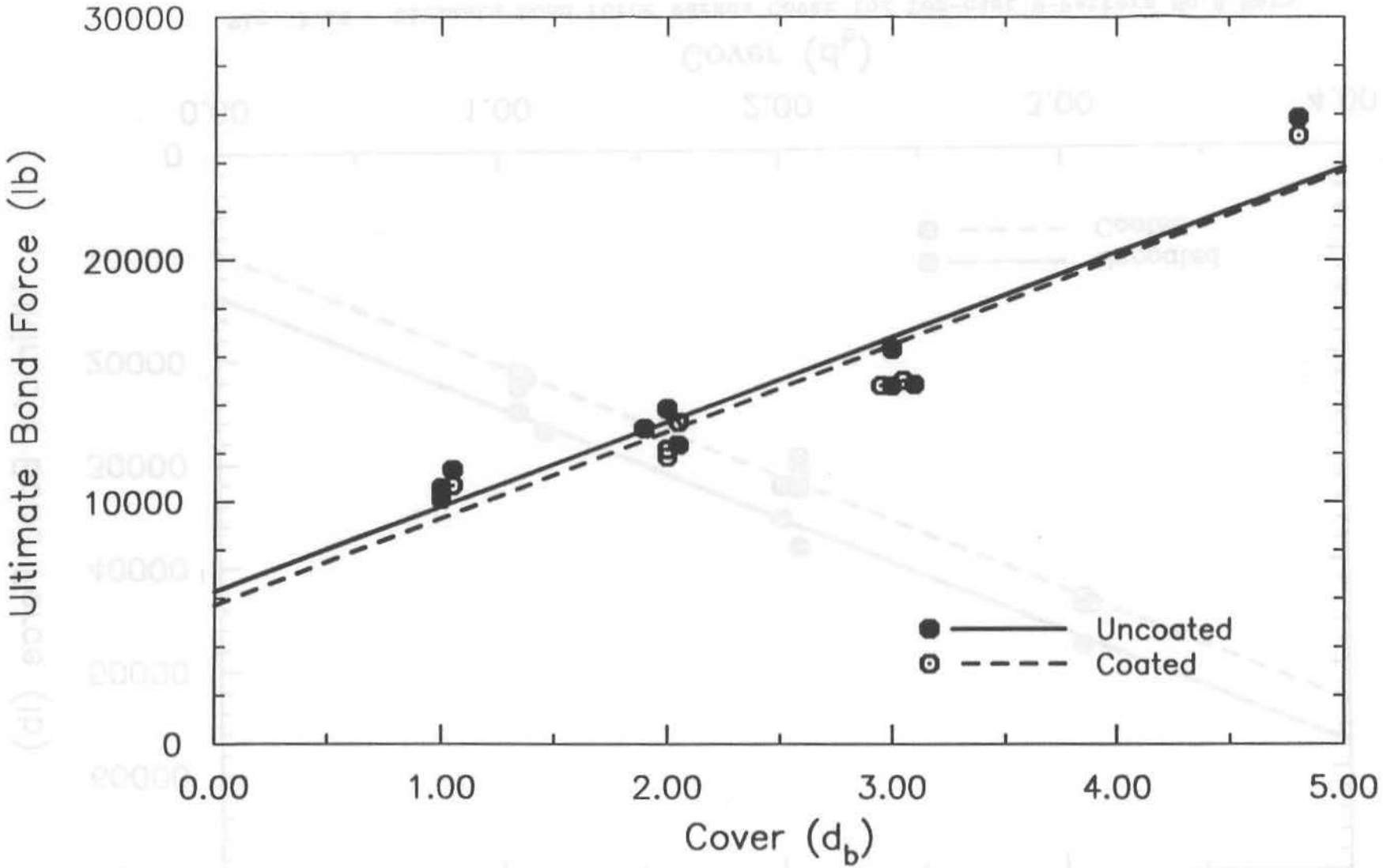

Fig. 3.15 (b) Ultimate Bond Force versus Cover for Bottom-cast N-Pattern No.5 Bars with Covers of 1, 2, 3 and 4.8 Bar Diameter (bars with 4.8 db yielded)

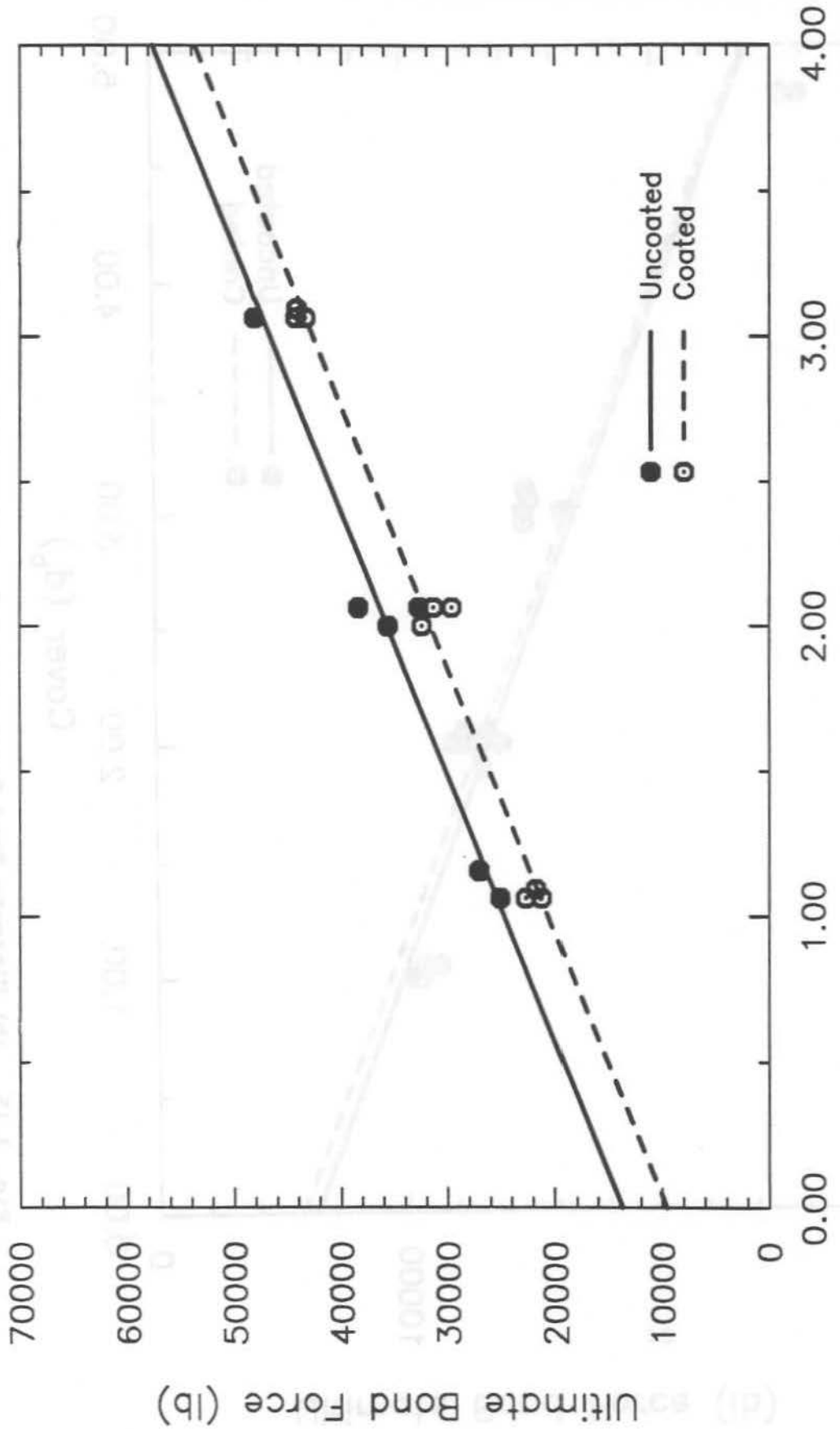

Fig. 3.16 Ultimate Bond Force versus Cover for Top-cast N-Pattern No.8 Bars

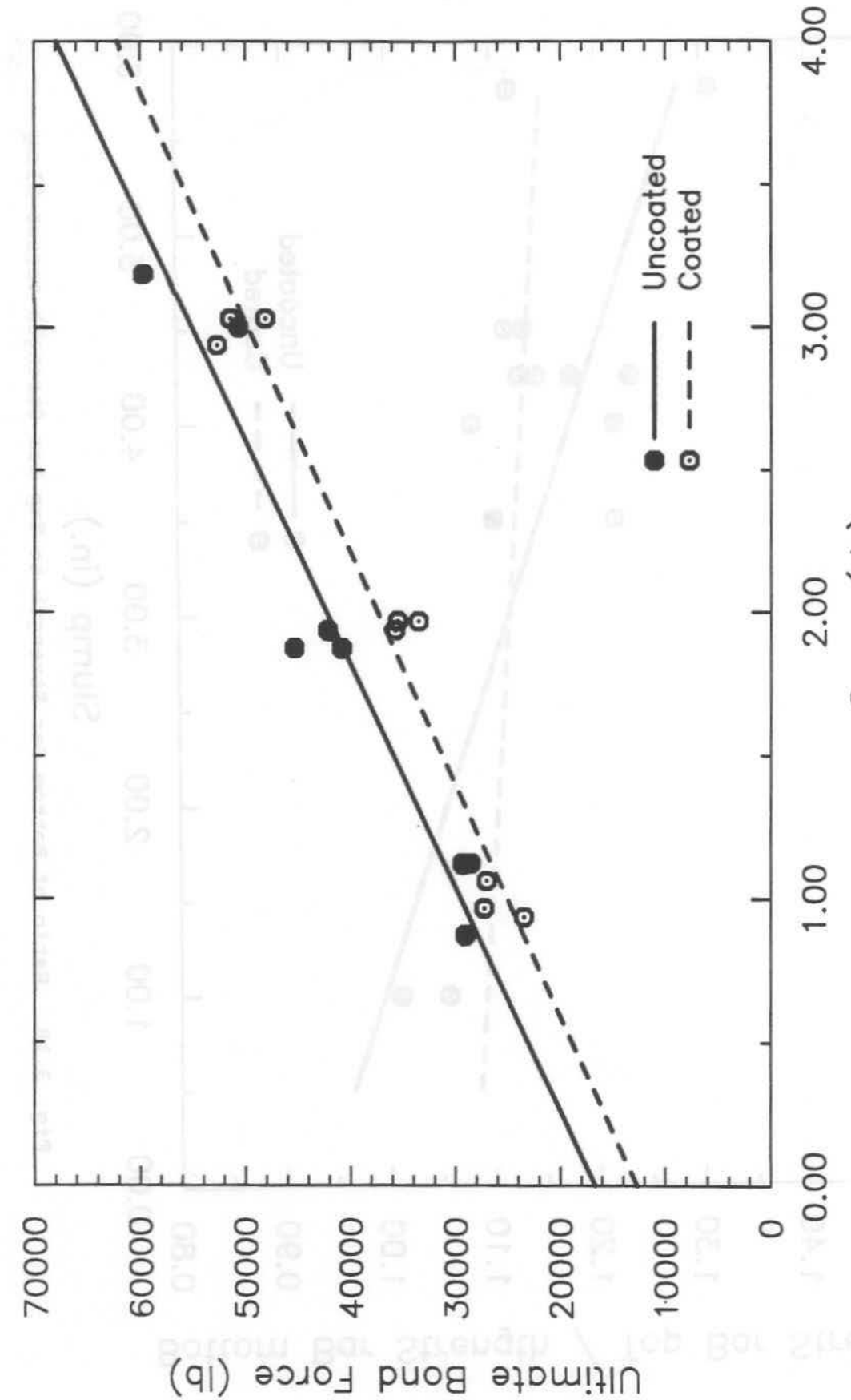

Fig. 3.17 Ultimate Bond Force versus Cover for Bottom-cast N-Pattern No.8 Bars

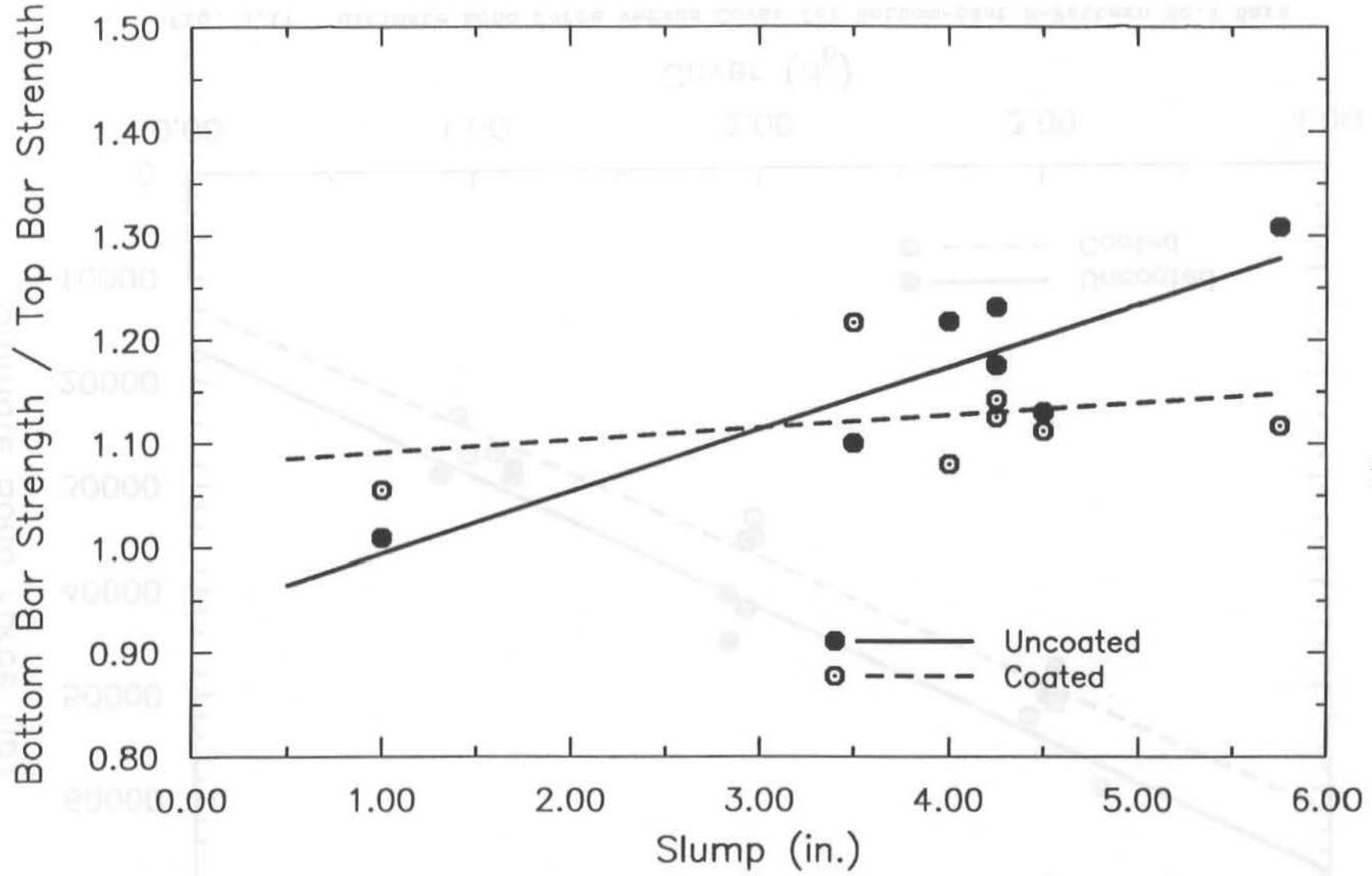

Fig. 3.18 Ratio of Bottom Bar Strength to Top Bar Strength versus Slump

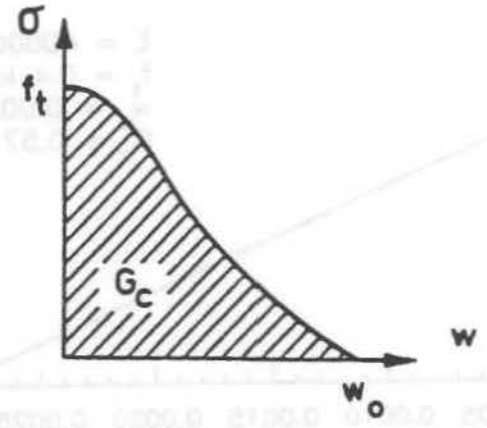

Fig. 4.1 Crack Opening Stress-displacemnent Relationship (Petersson 1979)

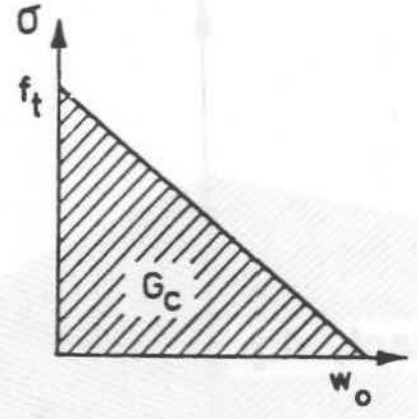

Fig. 4.2 Straight-line Approximation of Crack Opening Stress-displacement Relationship (Petersson 1979)

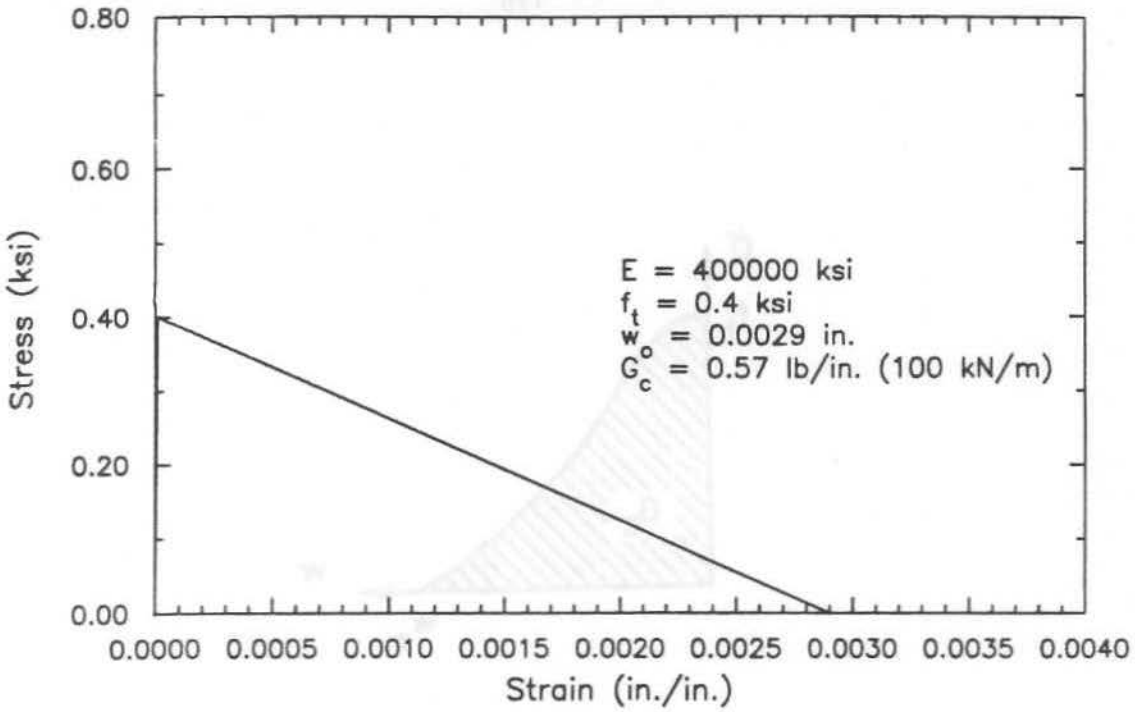

Fig. 4.3 Stress-strain Function for Rod Elements

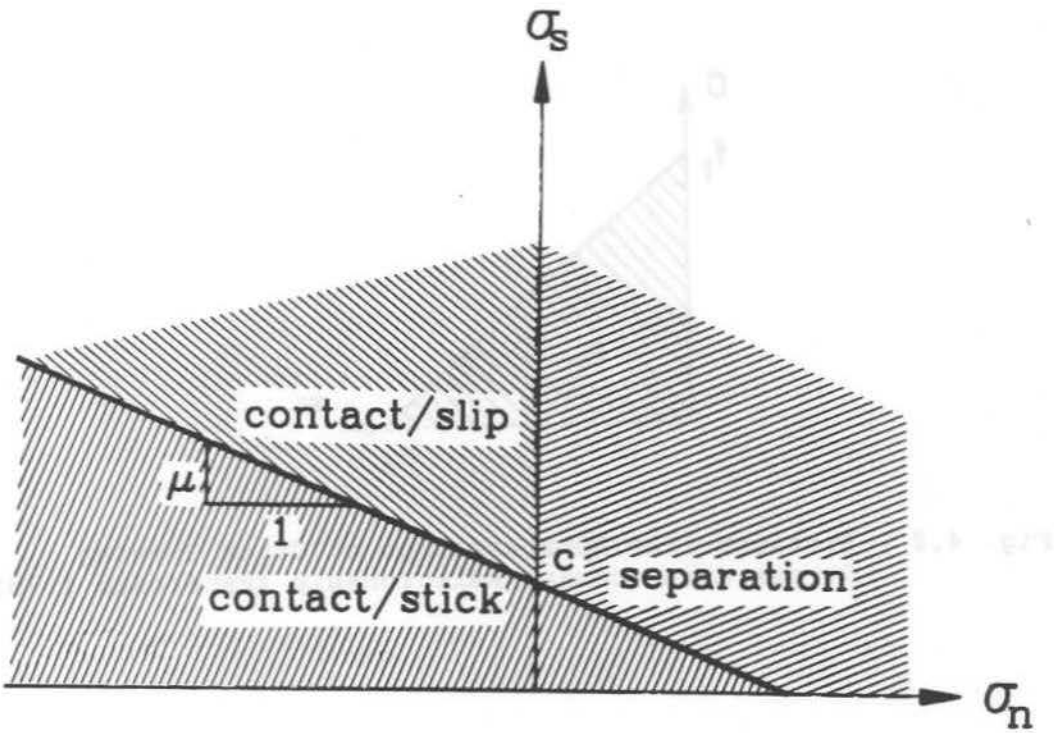

Fig. 4.4 Slip Surface for Two-dimensional Link Element

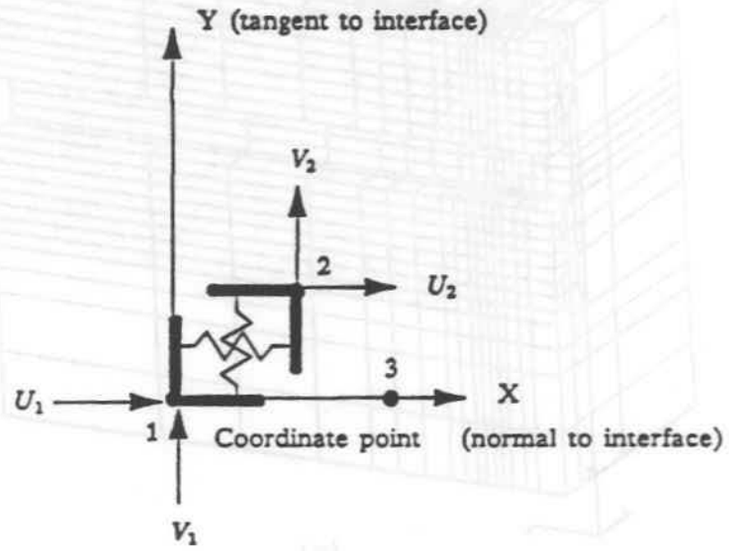

Fig. 4.5 Two-dimensional Link Element (Lopez et al. 1989)

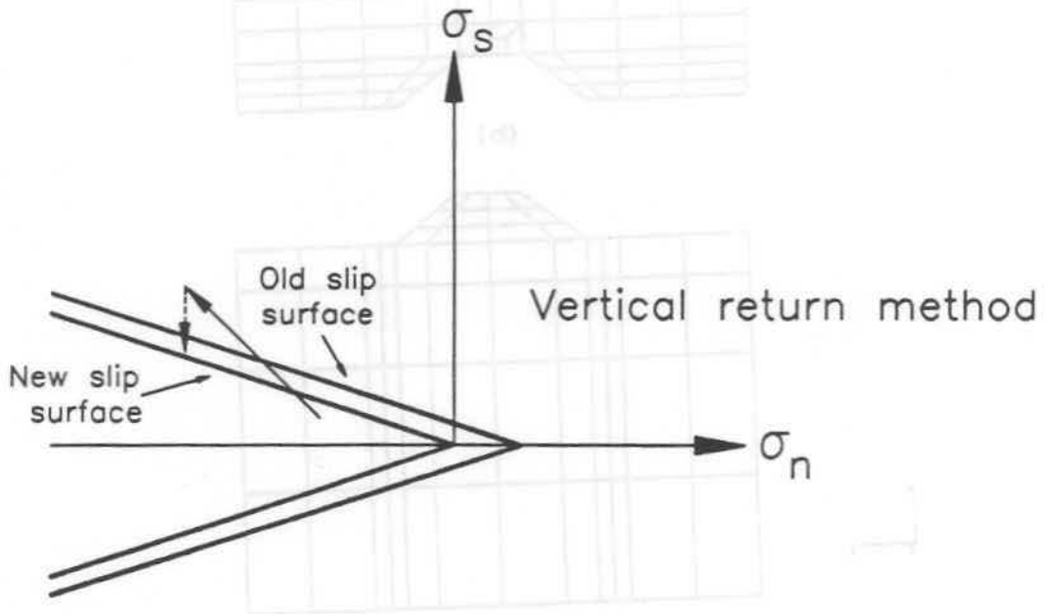

Fig. 4.6 Stress Correction Back to Slip Surface (Lopez et al. 1989)

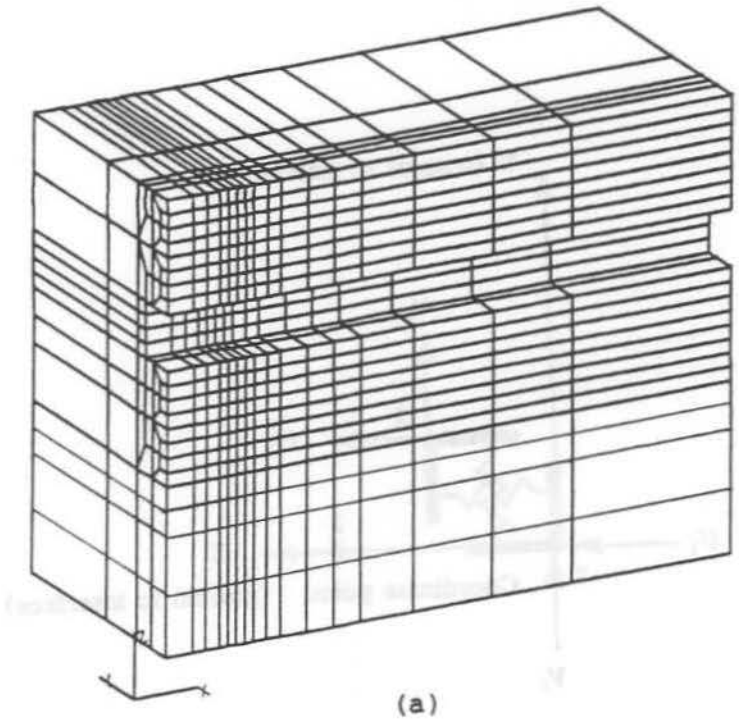

(a)

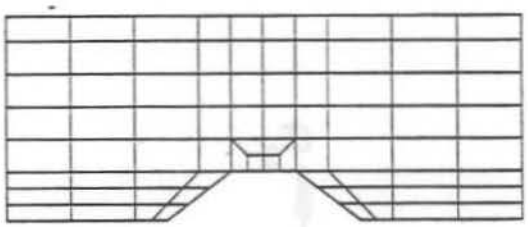

(b)

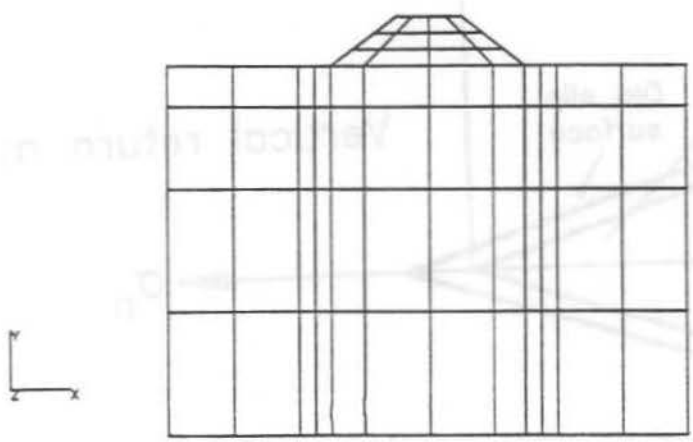

(c)

Fig. 4.7 (a) Exterior Concrete Substructure (b) Interior Concrete Substructure (c) Reinforcing Bar Substructure

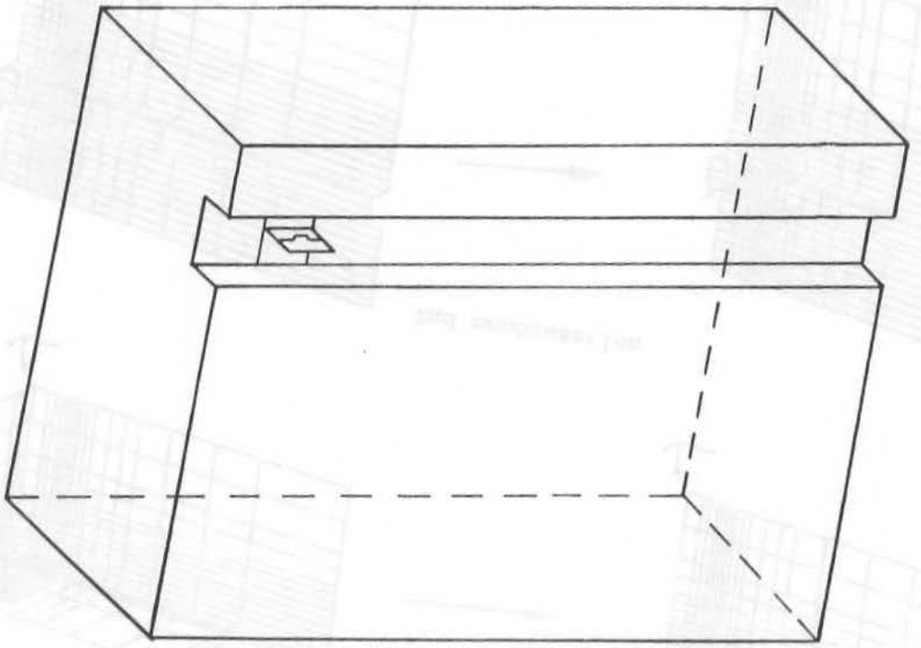

Fig. 4.8 Overall Finite Element Model of the Beam-end Specimen (short lead length)

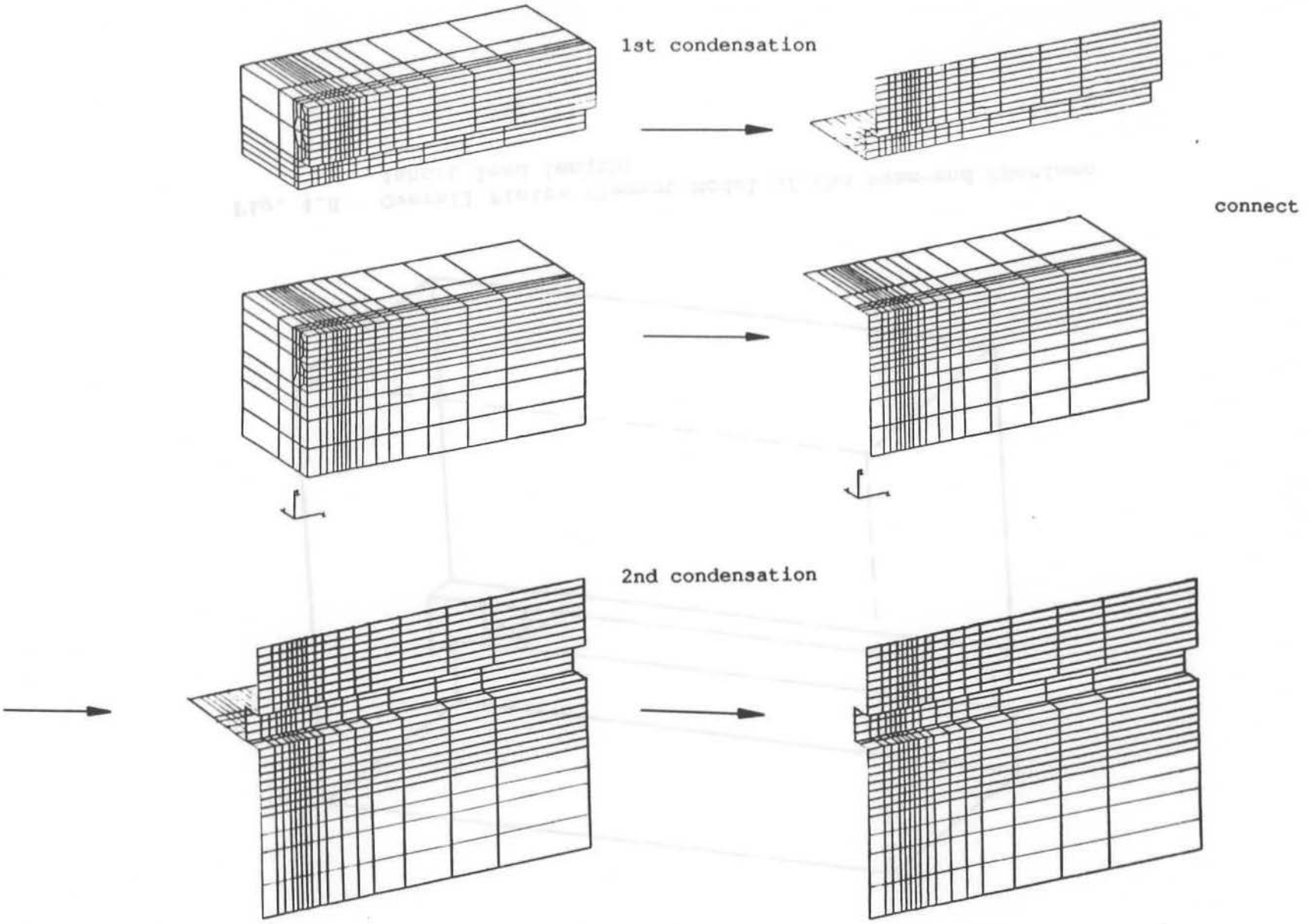

Fig. 4.9 Condensation Procedure for Exterior Concrete Substructure

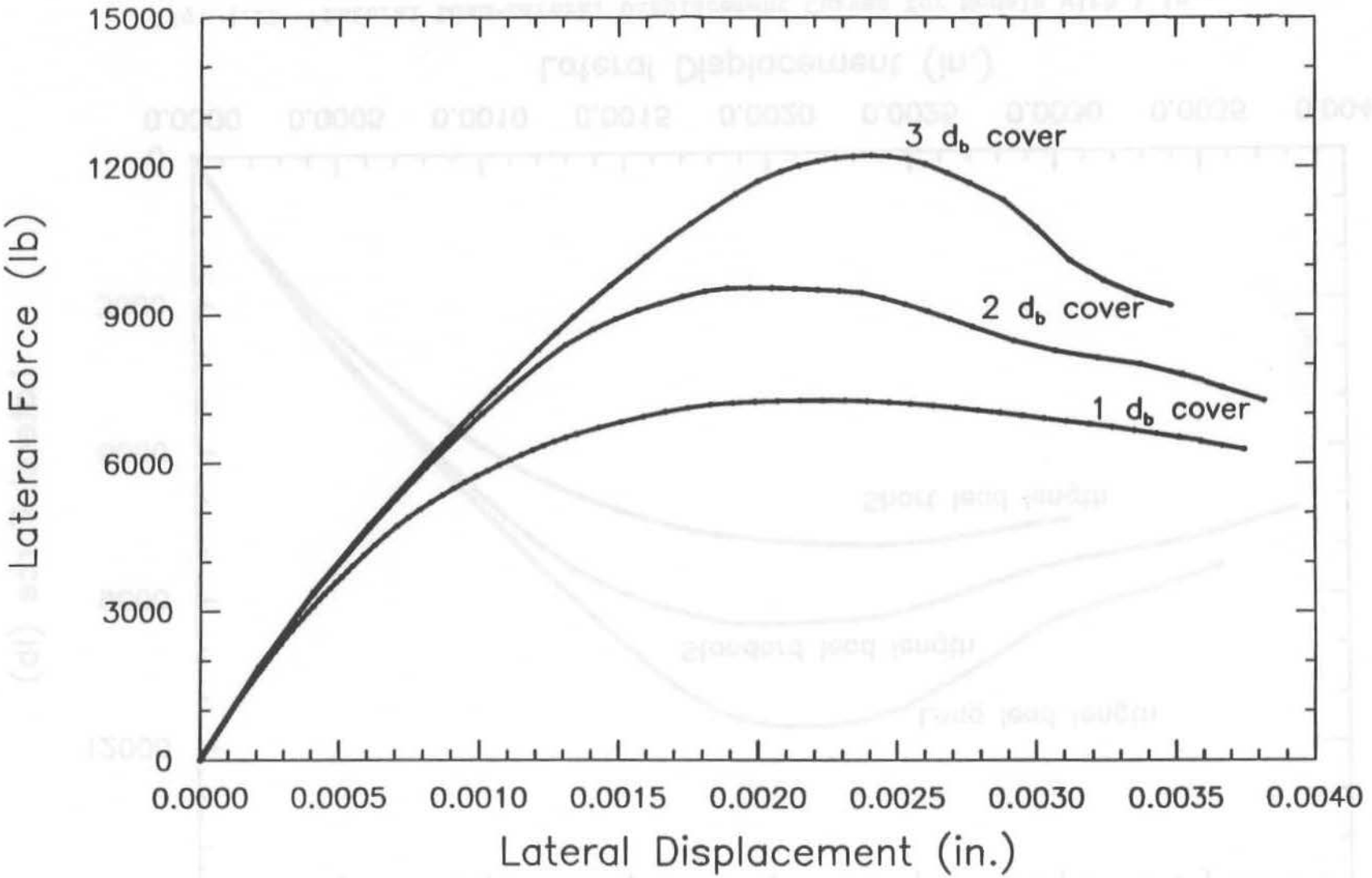

Fig. 4.10 Lateral Load-Lateral Displacement Curves for Models with 1, 2, and 3 Bar Diameter Covers

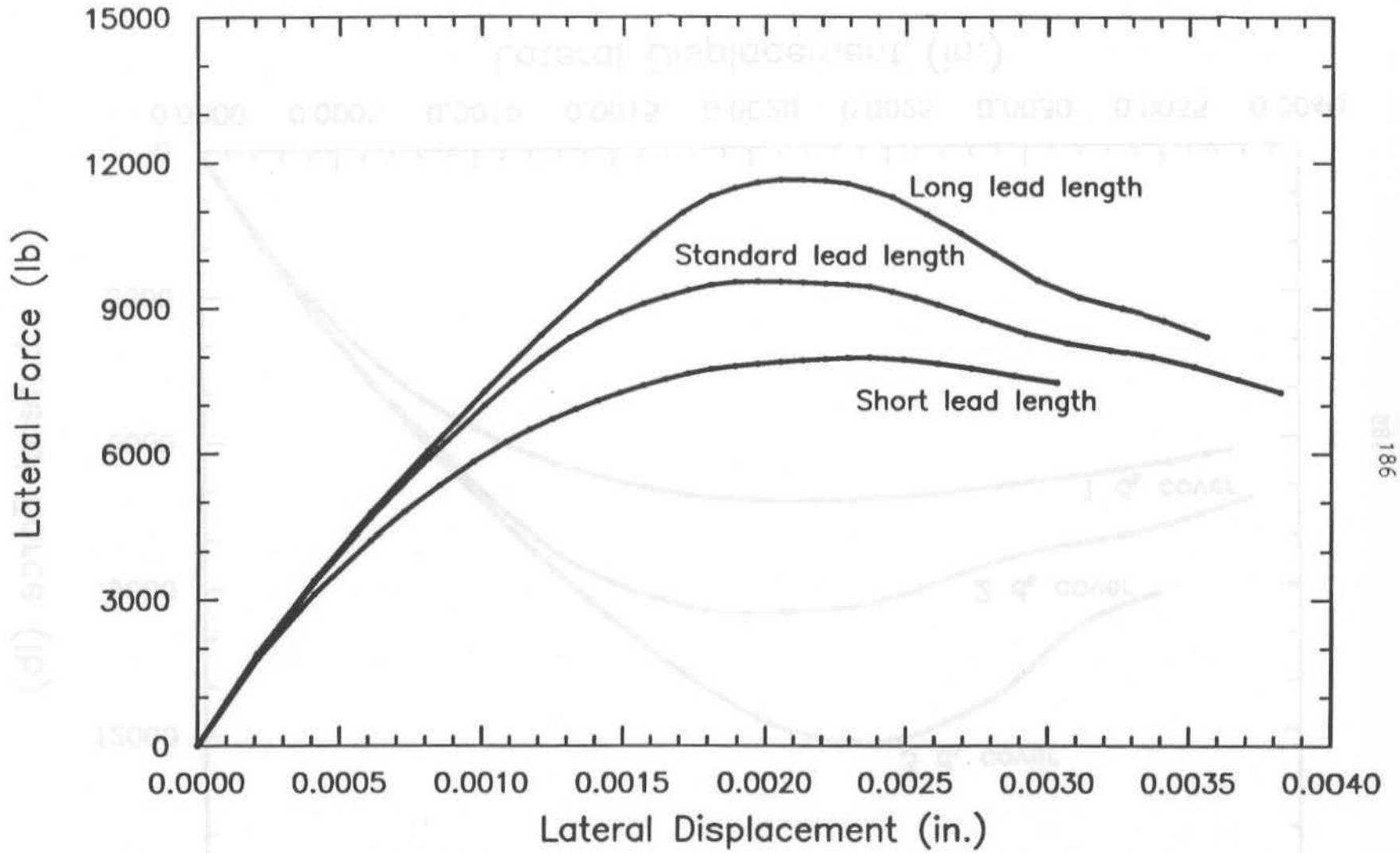

Fig. 4.11 Lateral Load-Lateral Displacement Curves for Models with 1 in., 2 in., and 3 in. Lead Lengths

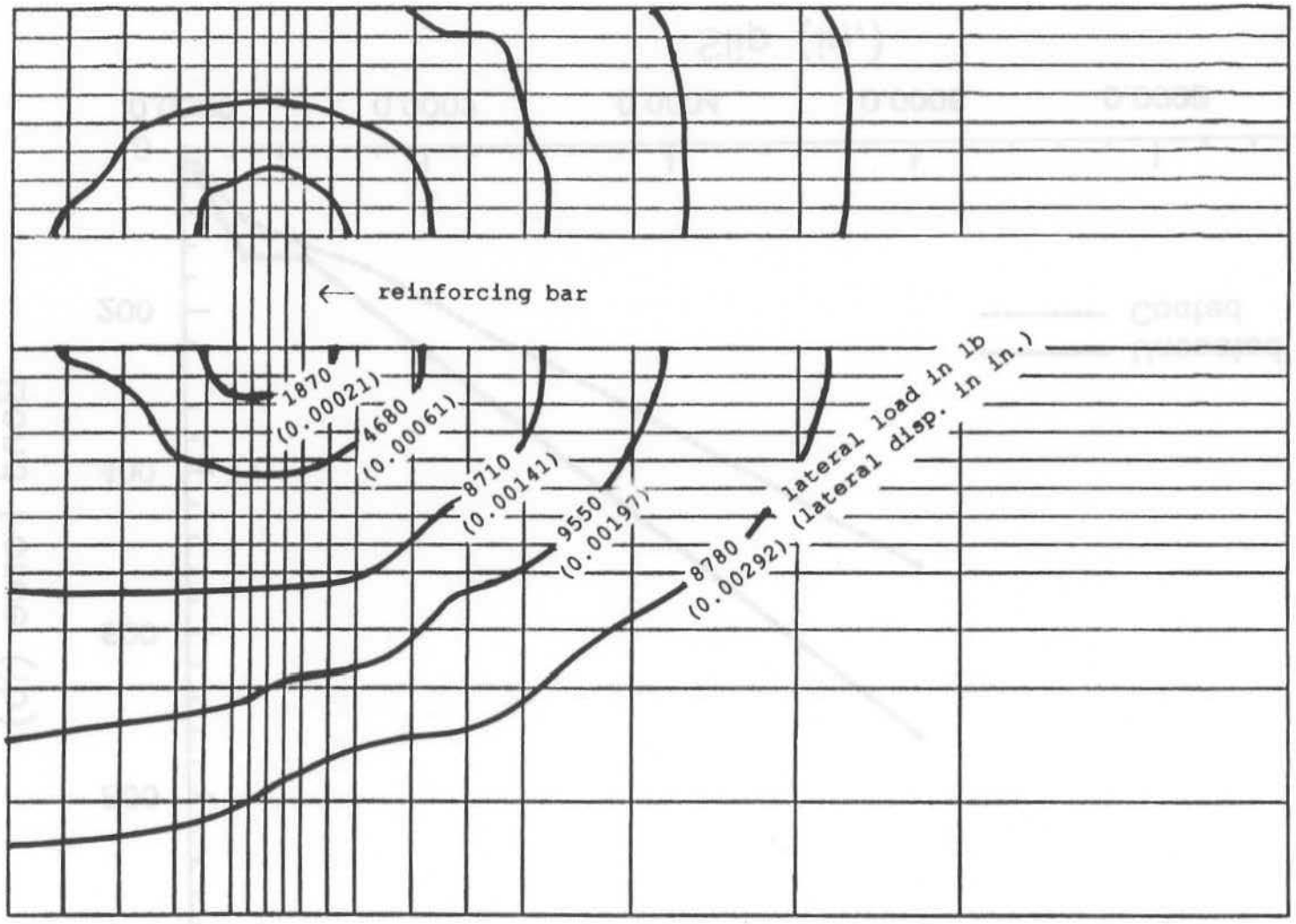

Fig. 4.12 Crack Propagation for Splitting of Concrete
(Model with 2 Bar Diameter Cover)

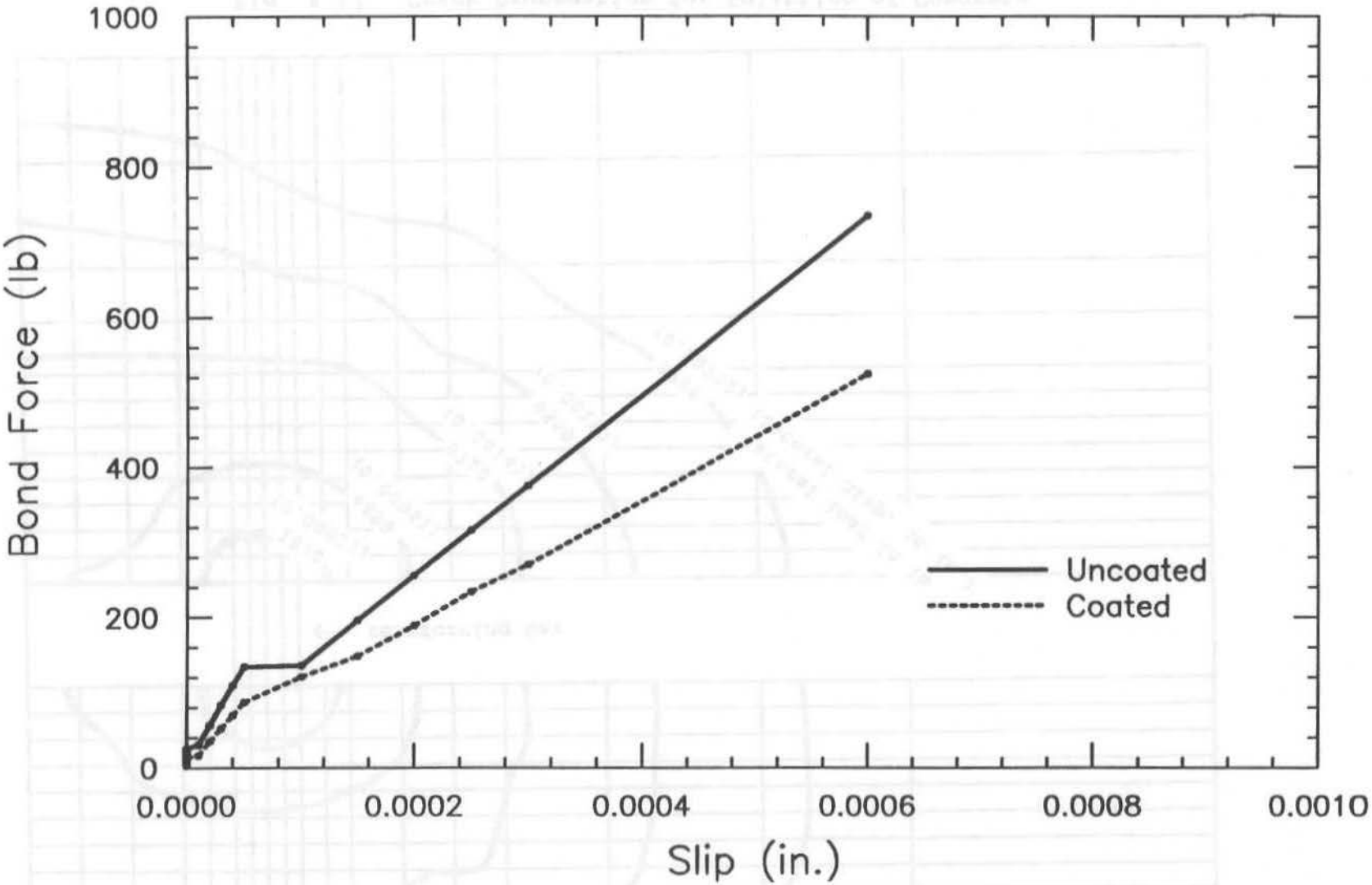

Fig. 4.13 Bond Force-Slip Curves for Model with 2 Bar Diameter Cover (Loads below 1000 lb)

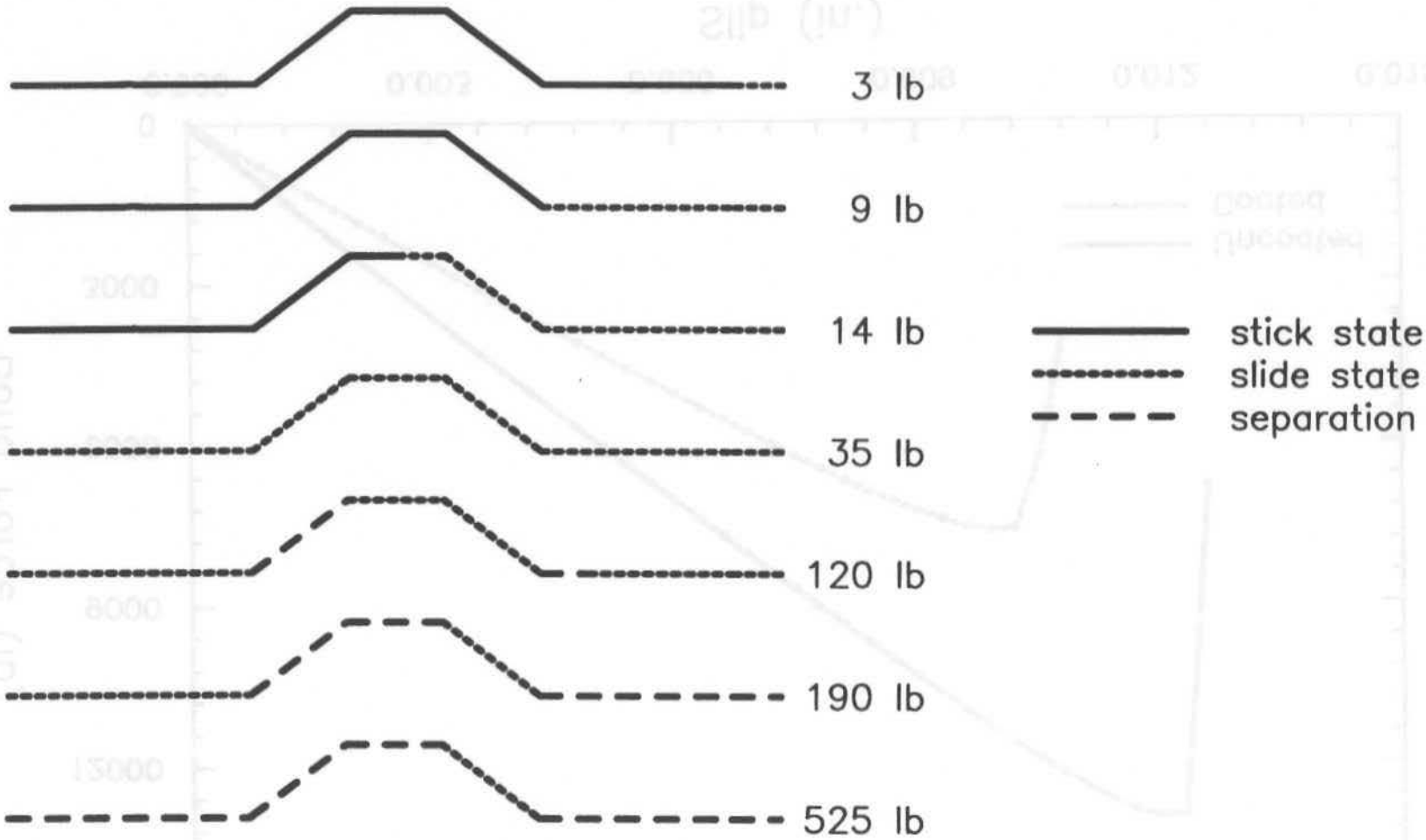

Fig. 4.14 Progressive Change of Material State along Interface
(Model of Uncoated Bar with 2 Bar Diameter Cover)

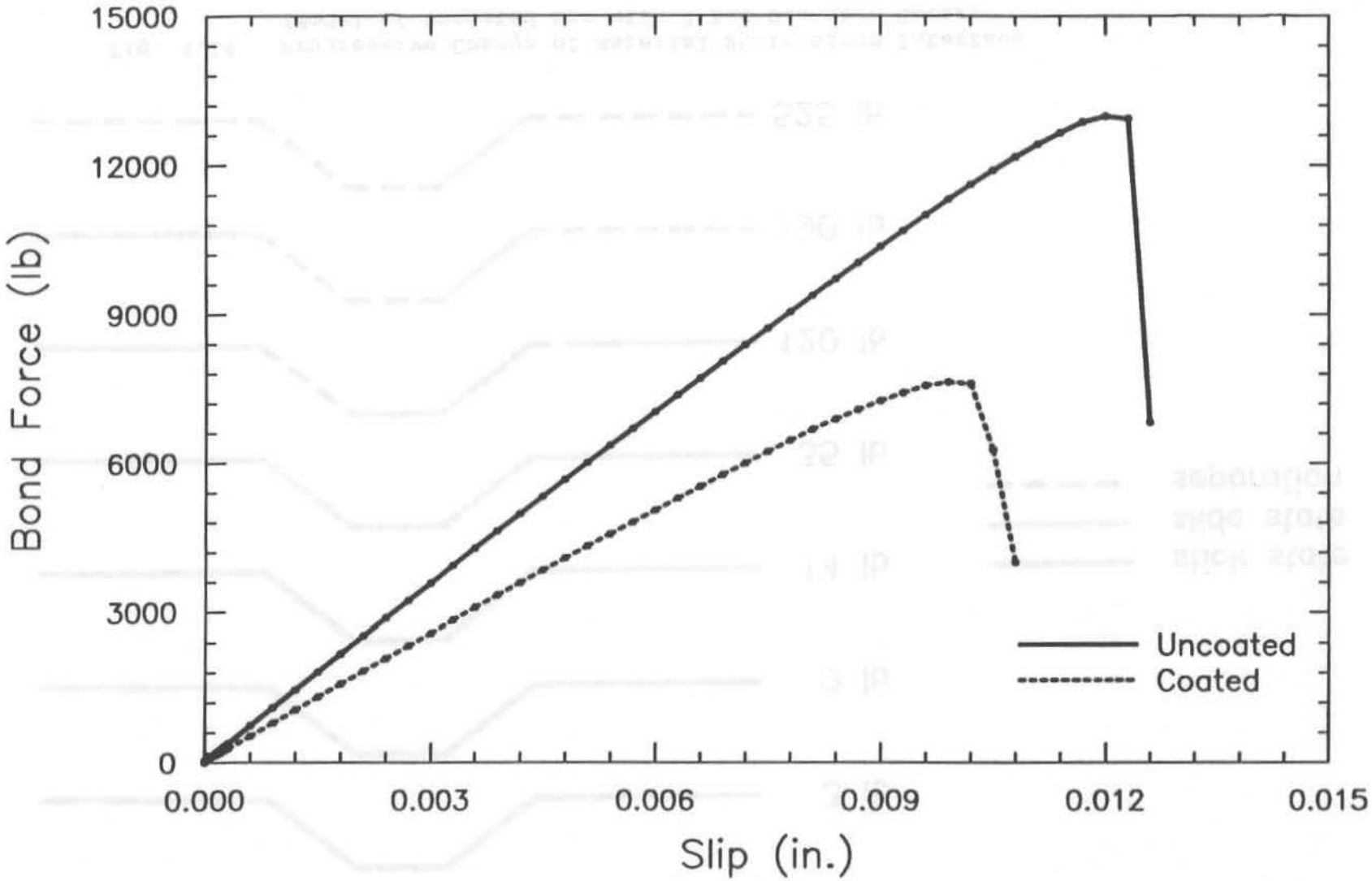

Fig. 4.15 Bond Force-Slip Curves for Model with 2 Bar Diameter Cover

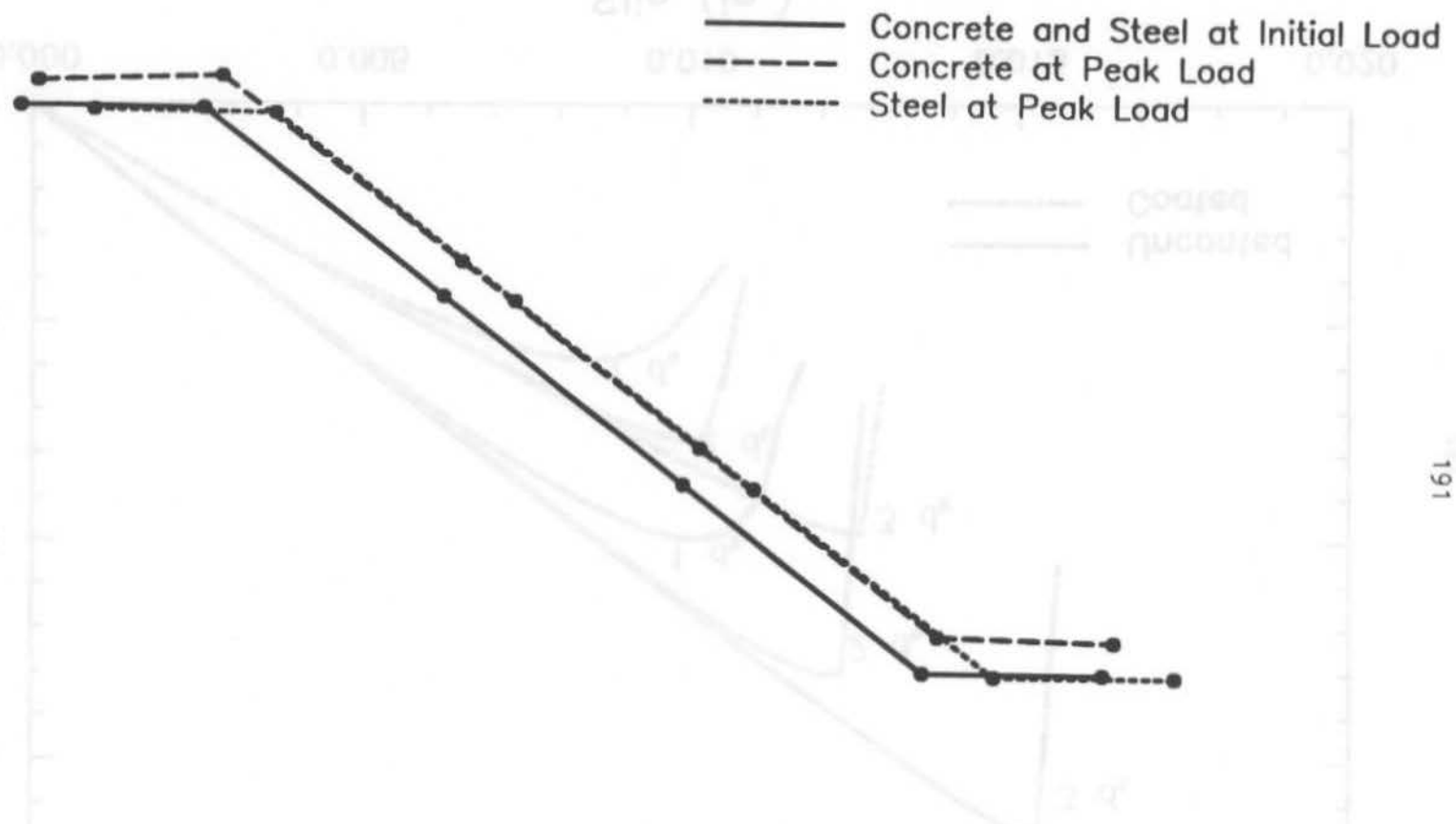

Fig. 4.16 Movement of Interface from Initial to Peak Load
(Model of Uncoated Bar with 2 Bar Diameter Cover)

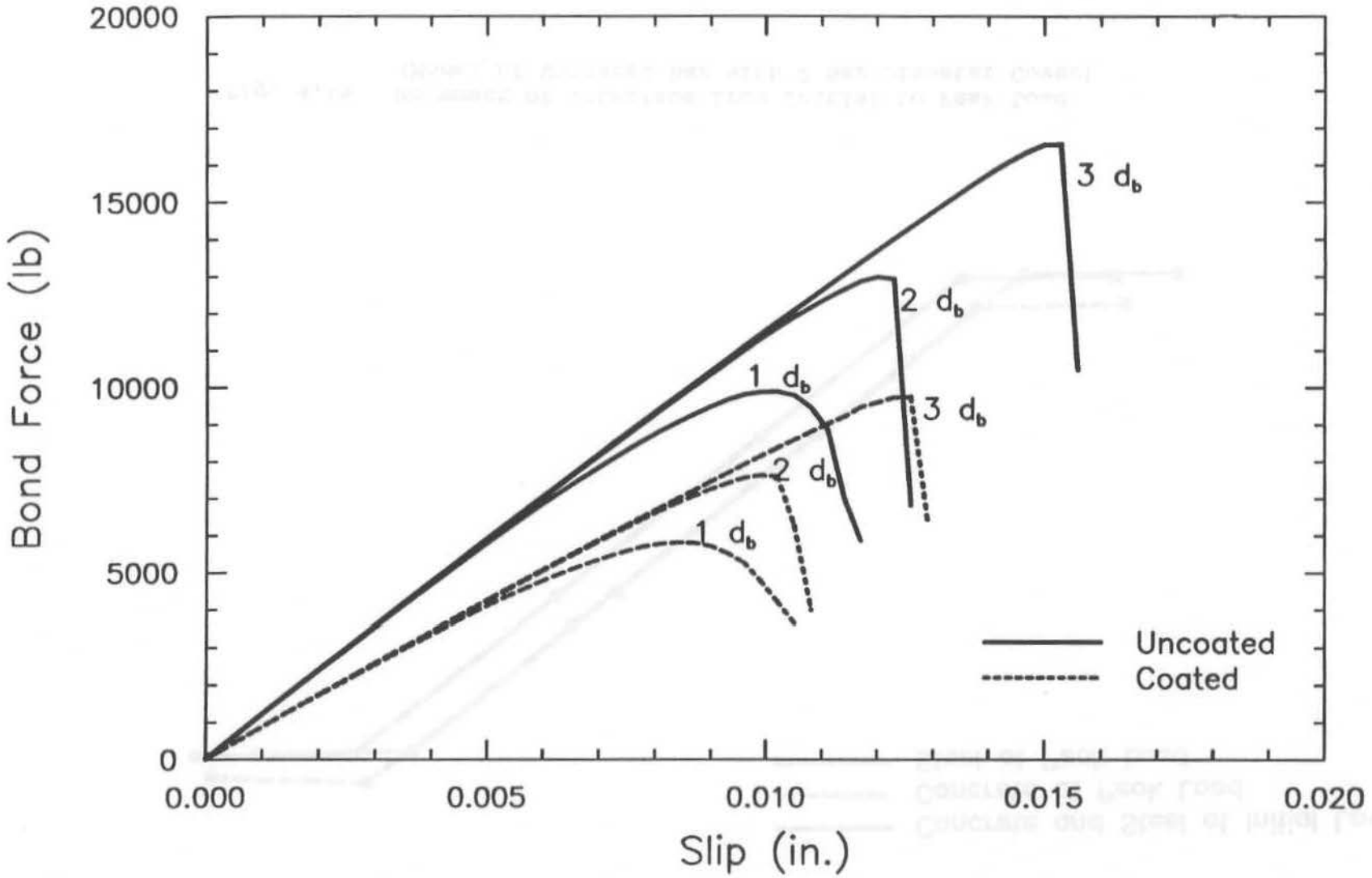

Fig. 4.17 Bond Force-Slip Curves for Models with 1, 2, and 3 Bar Diameter Covers

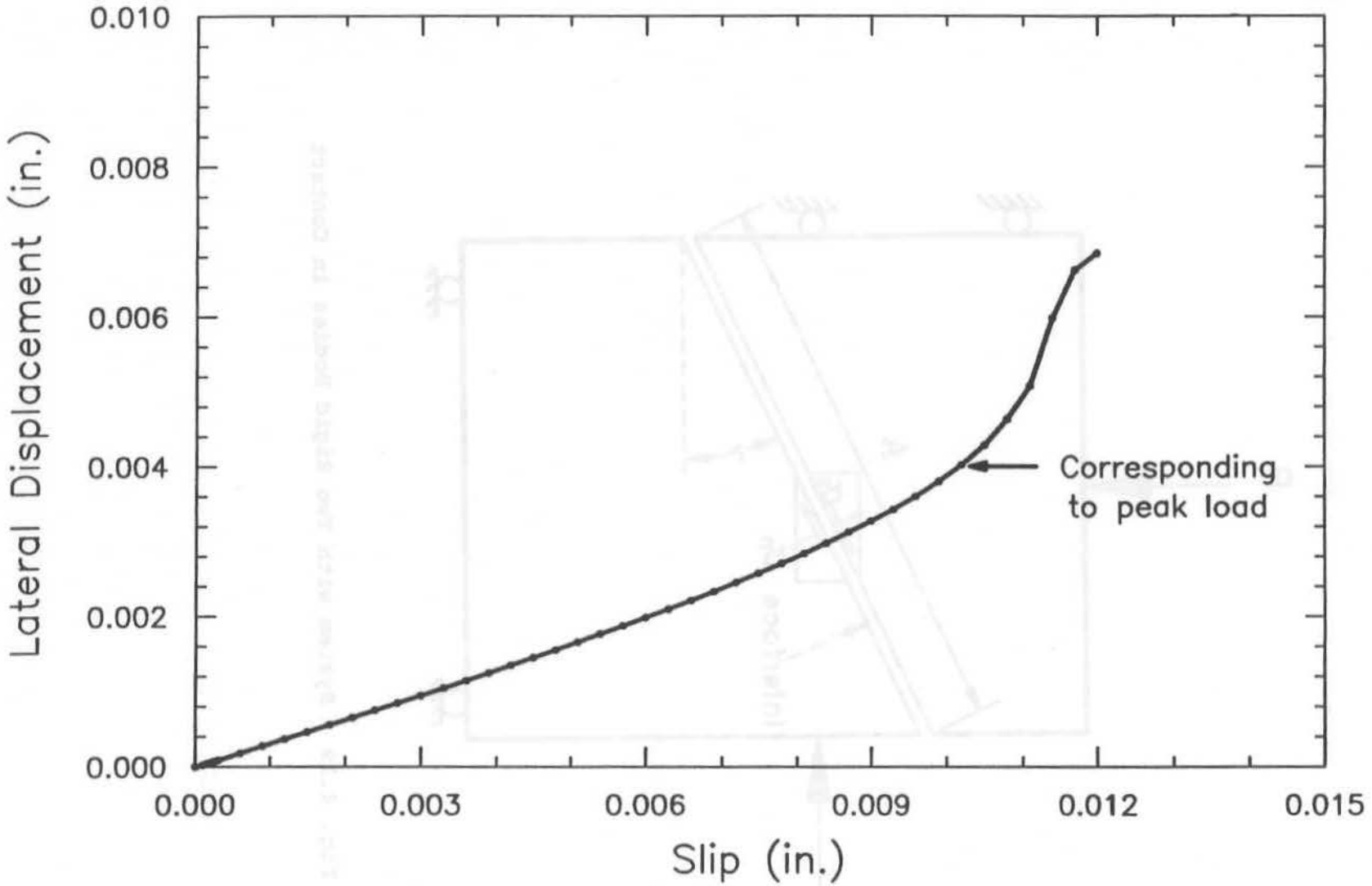

Fig. 4.18 Lateral Displacement-Slip Curve
(Model of Uncoated Bar with 1 Bar Diameter Cover)

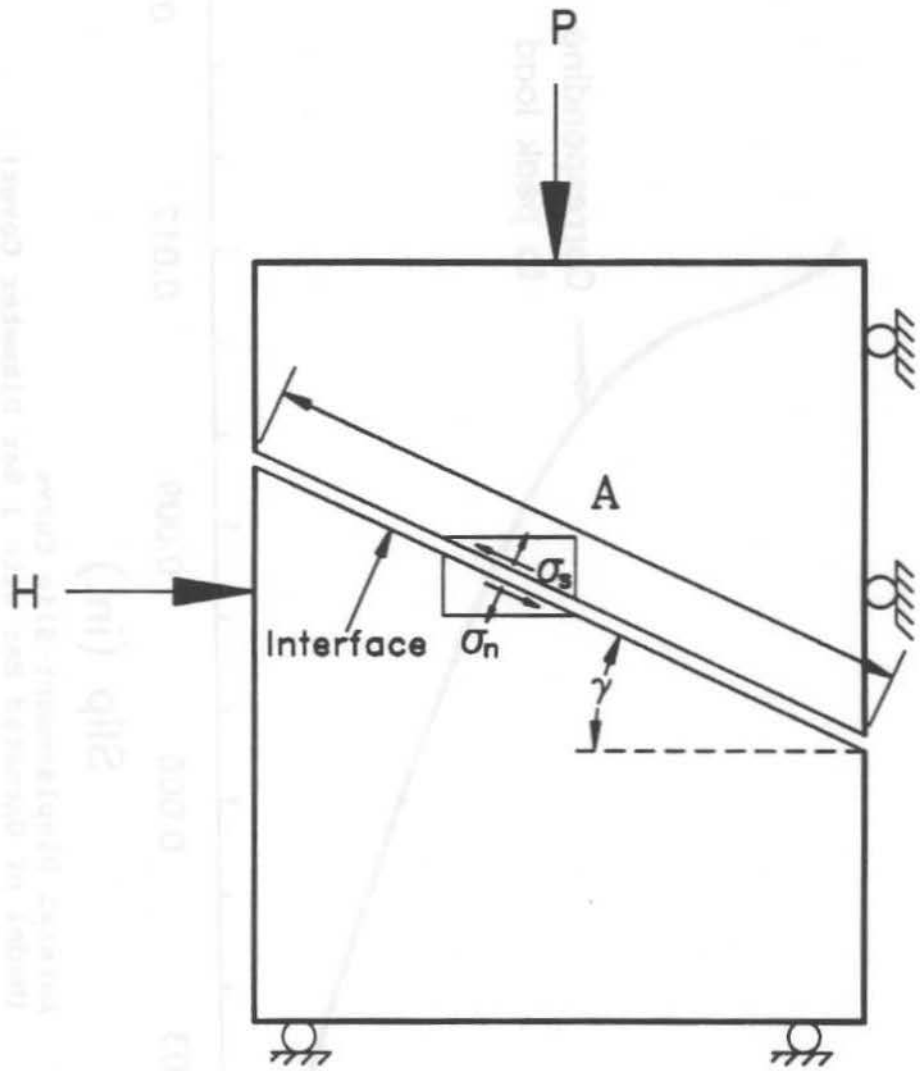

Fig. 4.19 System with Two Rigid Bodies in Contact

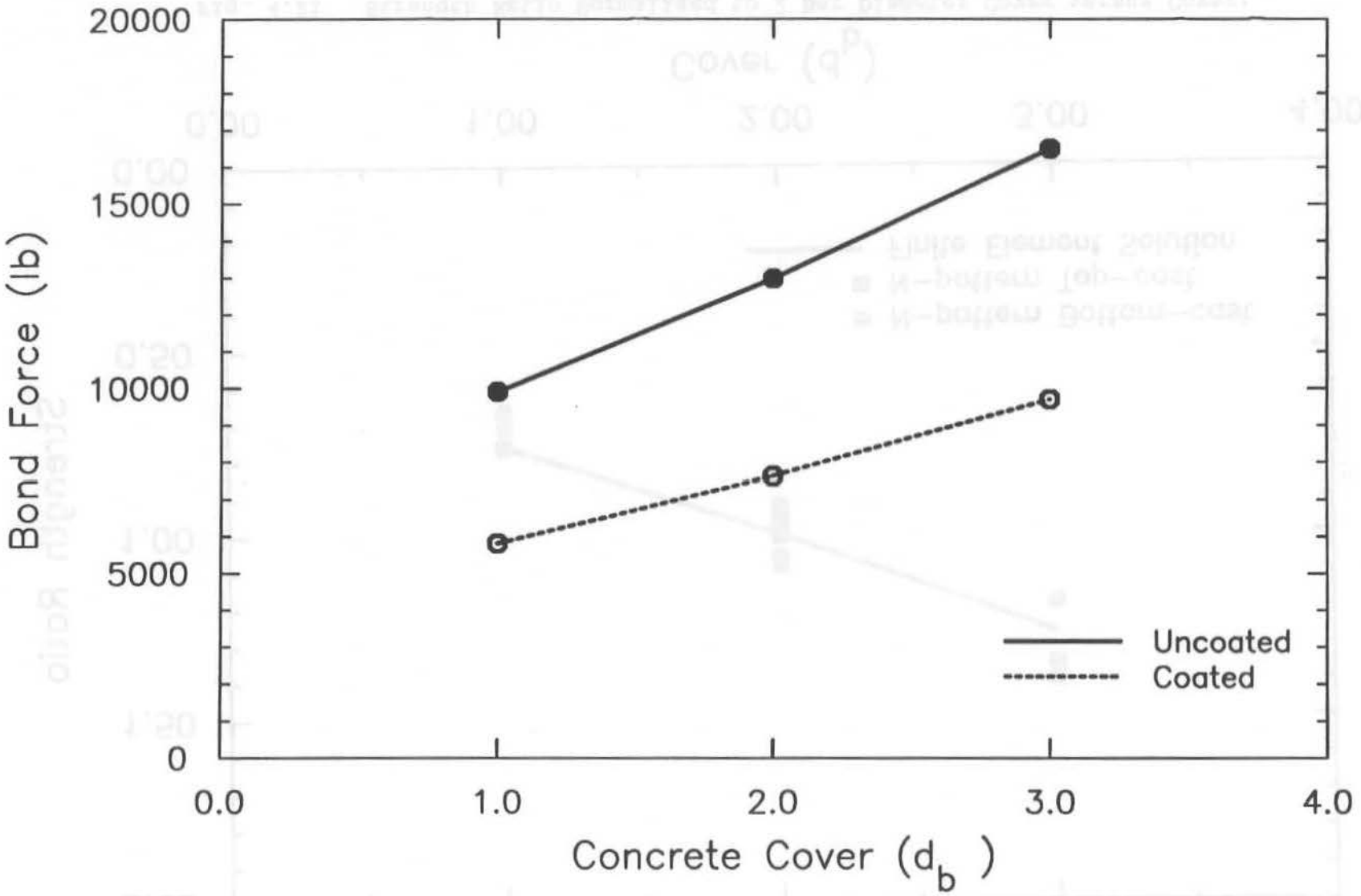

Fig. 4.20 Bond Force versus Cover (Models with 1, 2,and 3 Bar Diameter Covers)

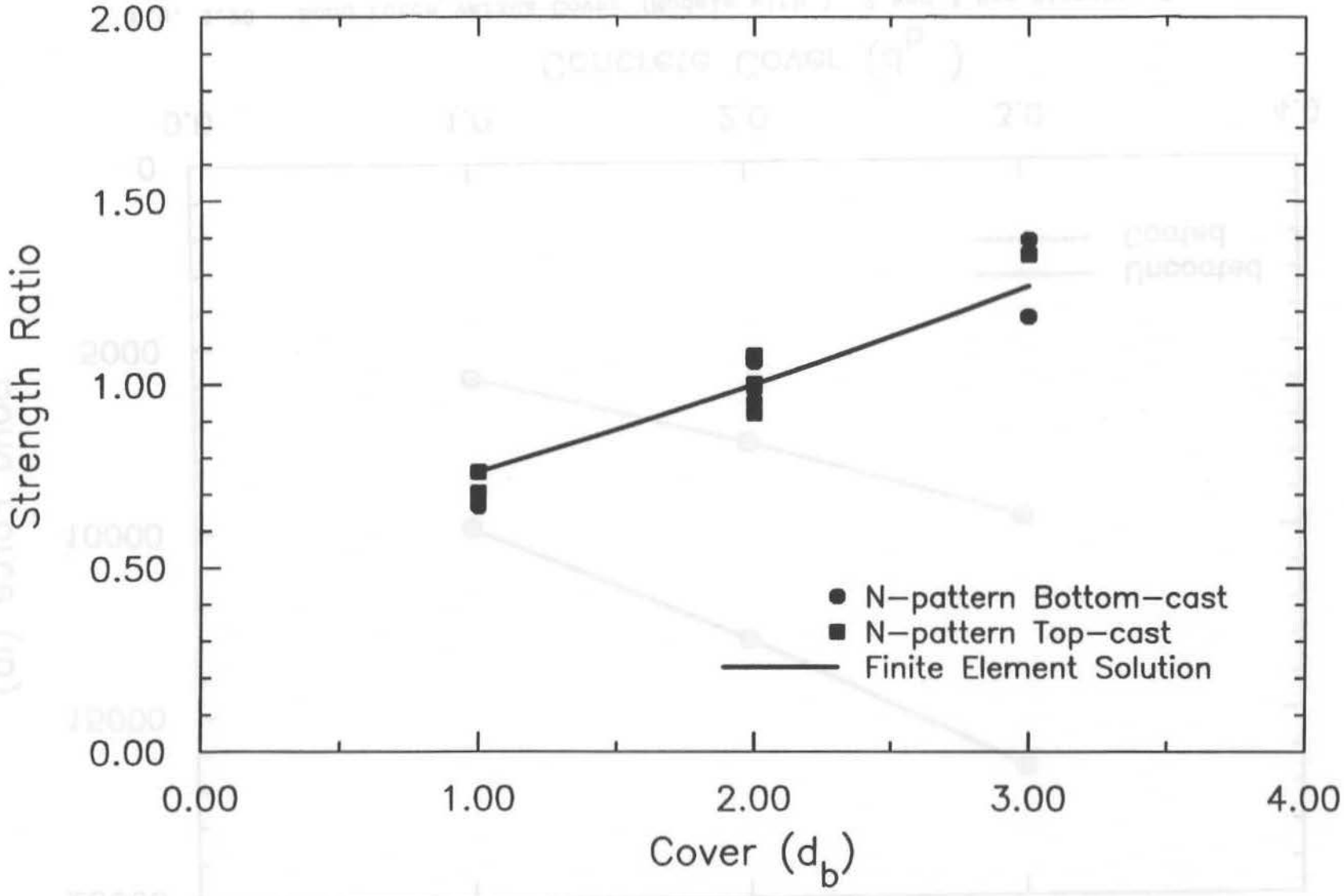

Fig. 4.21 Strength Ratio Normalized to 2 Bar Diameter Cover versus Cover: Finite Element Analyses and Test Results for Uncoated N-pattern No. 8 Bars in Group 18

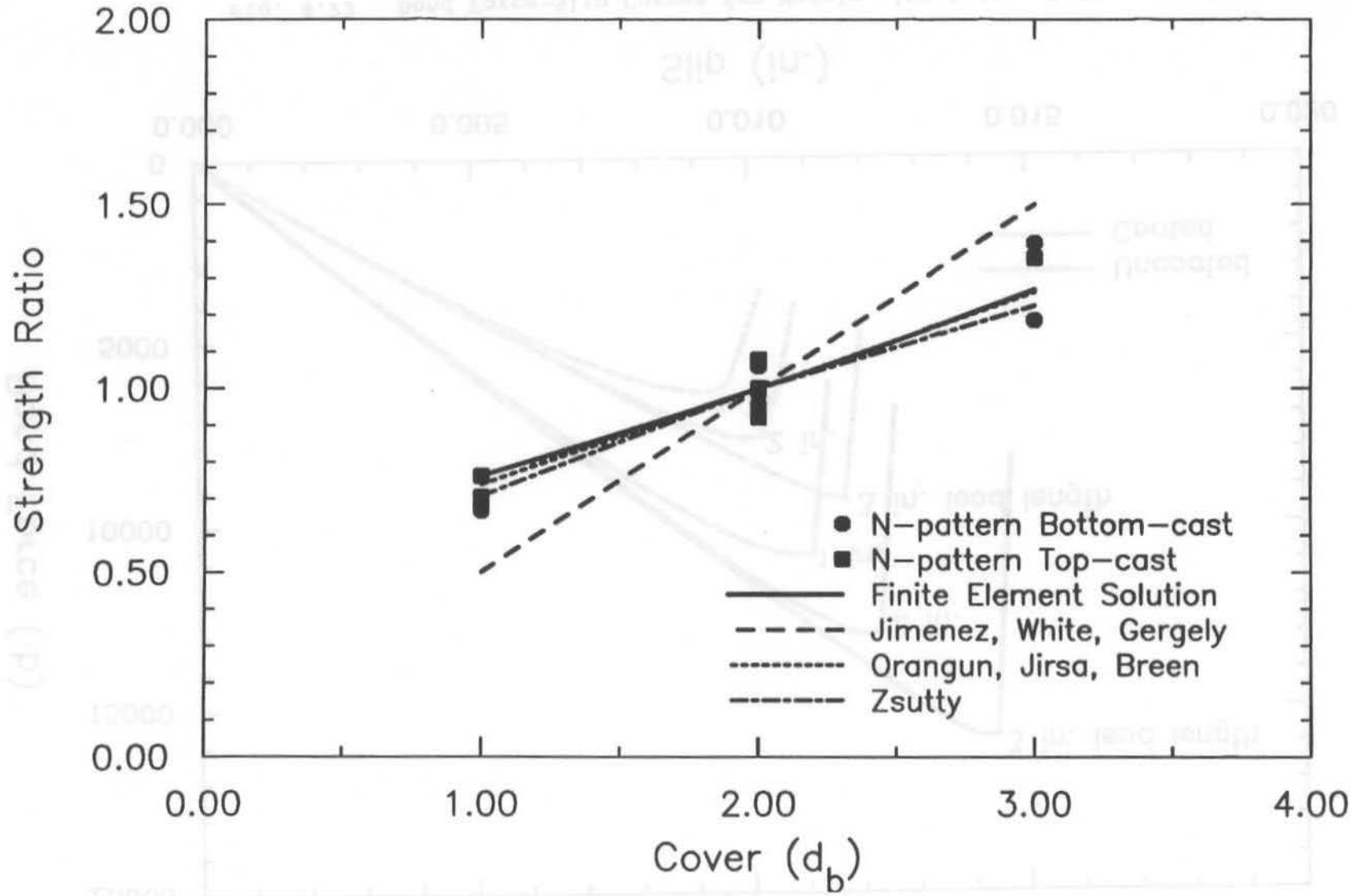

Fig. 4.22 Strength Ratio Normalized to 2 Bar Diameter Cover versus Cover: Finite Element Analyses, Test Results in Group 18 and Empirical Equations

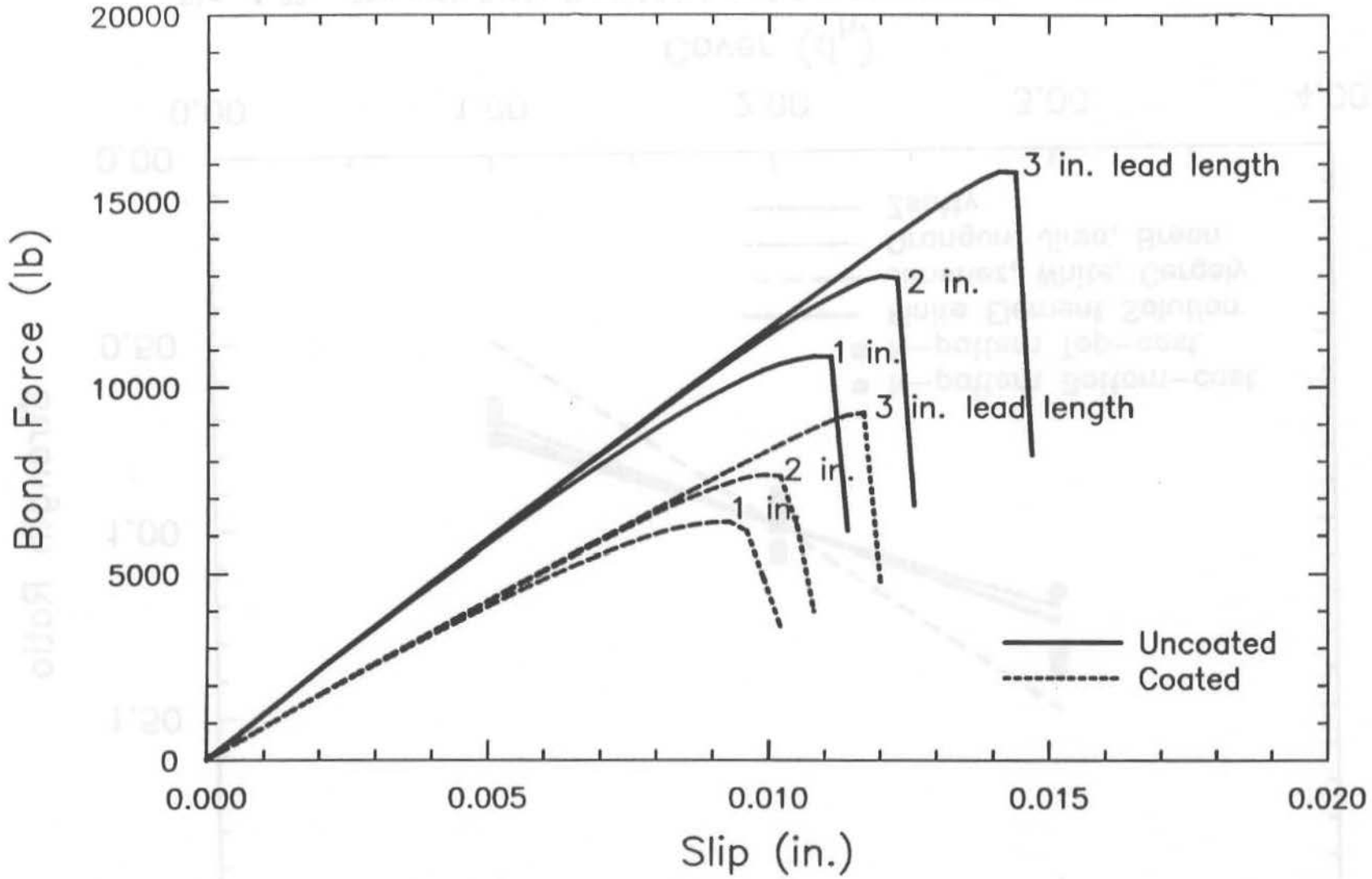

Fig. 4.23 Bond Force-Slip Curves for Models with 1 in., 2 in., and 3 in. Lead Lengths

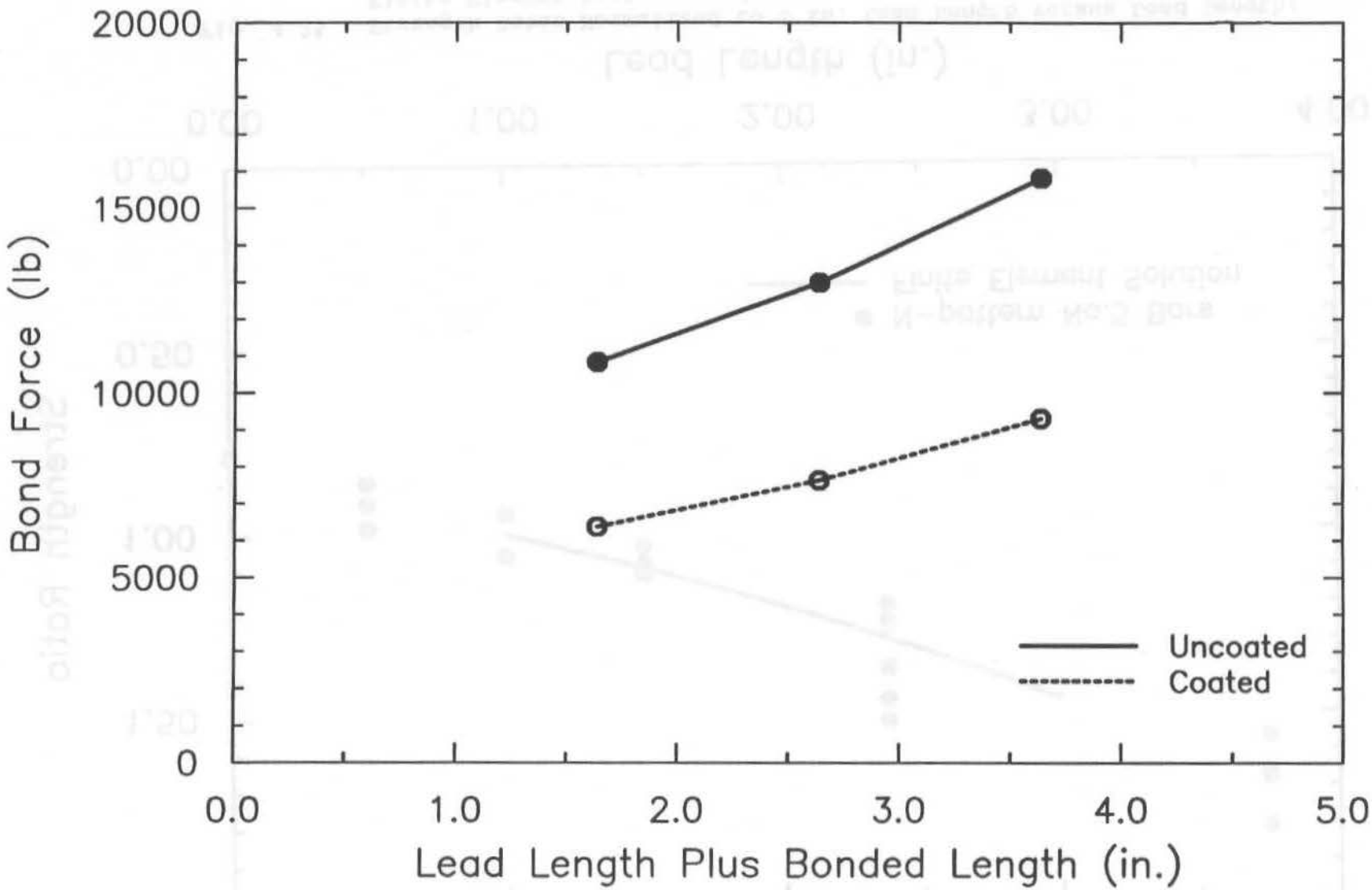

Fig. 4.24 Bond Force versus Lead Length Plus Bonded Length (Models with 1 in., 2 in.,and 3 in. Lead Lengths)

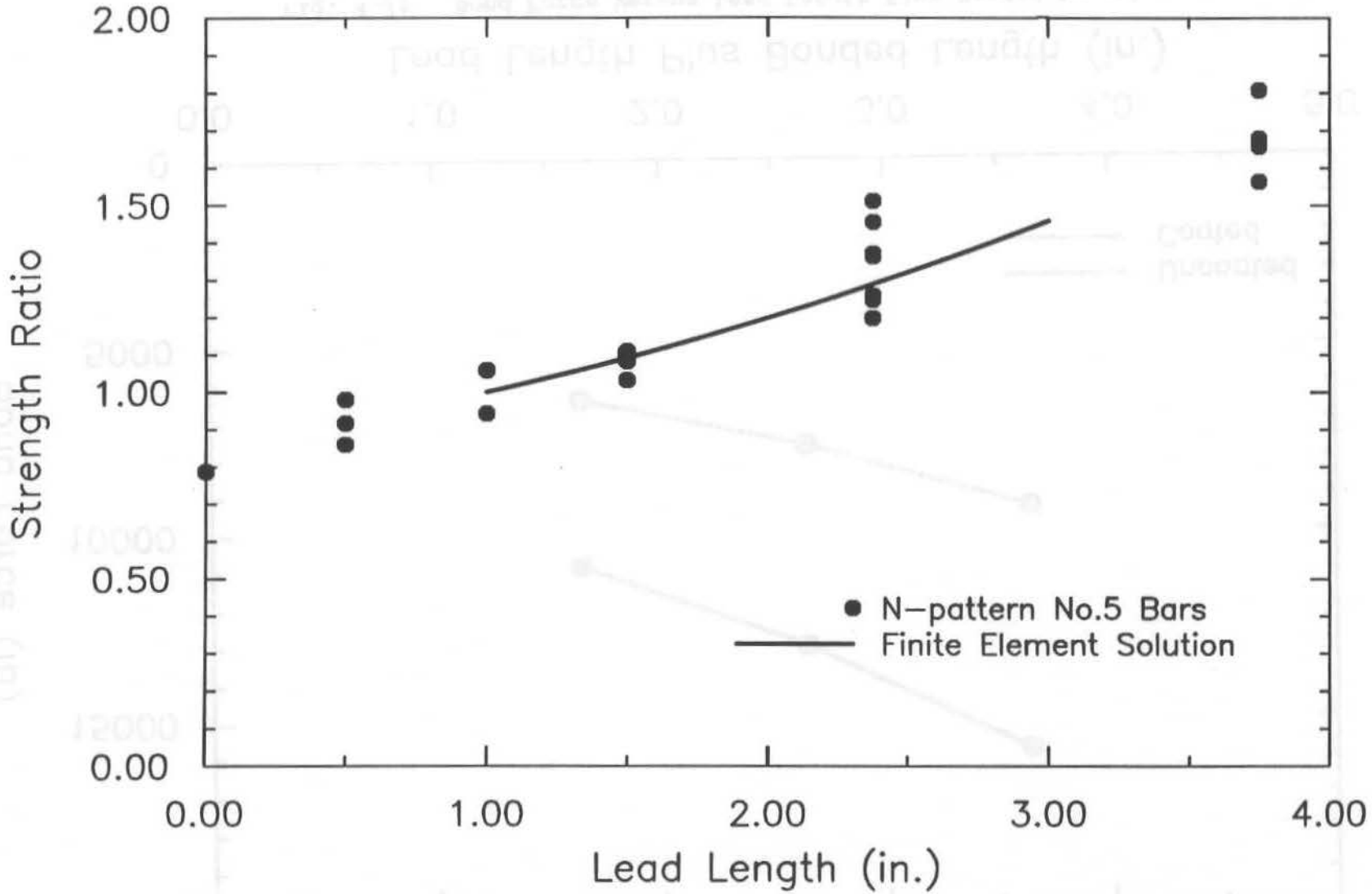

Fig. 4.25 Strength Ratio Normalized to 1 in. Lead Length versus Lead Length: Finite Element Analyses and Test Results for Uncoated N-pattern No. 5 Bars in Group 12

APPENDIX A

BEARING AREA CALCULATION OF REINFORCING STEEL

An important characteristic of reinforcing bars is the bearing area of the deformations per unit length of the bar. There are no methods in ASTM A 615 (1987) for measuring the bearing area. Therefore, the following method was developed for this task.

In this technique, the bearing area is calculated based on closely spaced measurements. As illustrated in Fig. A.1, the deformations are measured at n (typically 20) positions around circumferences. To carry out the measurements, the bars are mounted in a lathe as follows:

1) The bar is placed in the grip assembly of the lathe, which helps to match the center of the lathe and the bar. The wheel of the lathe is divided into n circumferential divisions of equal size, i.e., 20 divisions, 18° apart (Figs. A.1 and A.2).

2) Using a dial gage, the deformations are measured at points as illustrated in Figs. A.3 and A.4. At each division, dial gage readings are obtained with the tip of the dial gage at points A, C_1, D_1, M_1, B_1, B, B_2, M_2, D_2, C_2. The longitudinal dimensions of the ribs E_1, E_2, F, are measured. After each set of measurements, the lathe is rotated to the next division and the process is repeated. Table A.1 illustrates a typical set of data for a single deformation. The widths of the longitudinal ribs (gaps) at

the top and the bottom of the deformation, G_{11}, G_{12}, G_{21}, G_{22} are measured with a caliper (Fig. A.1). The heights of the longitudinal ribs (not shown), d_1 and d_2, are measured with the dial gage. The width of the small longitudinal rib, G_4, is measured with caliper. To determine the height of the small longitudinal rib, d_3, the location of the rib, G_3, is measured with the dial gage. The values of G_{11}, G_{12}, G_{21}, G_{22}, G_3, and G_4 are the average of two values measured at each side of the deformation.

3) After the table is complete, the following steps are used to calculate the bearing area.

R = radius of the wheel of the lathe

X_1 = smaller value of C_1 and D_1

X_2 = smaller value of C_2 and D_2

Y = 0 (Initializing the bearing area of divisions)

Step 1. Repeat from n = 1 to 20

$$W_{1(n)} = R - A + \frac{B_{(n)} + B_{1(n)} + B_{2(n)}}{3} \qquad (A.1)$$

$$W_{2(n)} = R - A + \frac{X_{1(n)} + X_{2(n)}}{2} \qquad (A.2)$$

$$W_{1(n+1)} = R - A + \frac{B_{(n+1)} + B_{1(n+1)} + B_{2(n+1)}}{3} \qquad (A.3)$$

$$W_{2(n+1)} = R - A + \frac{X_{1(n+1)} + X_{2(n+1)}}{2} \qquad (A.4)$$

$$Z_{(n)} = \frac{\pi}{20}\left[\left(\frac{W_{1(n)} + W_{1(n+1)}}{2}\right)^2 - \left(\frac{W_{2(n)} + W_{2(n+1)}}{2}\right)^2\right] \qquad (A.5)$$

$$Y = Y + Z_{(n)}$$

in which W_1 and W_2 are the measured radius of the top and the bottom deformation and Z is the bearing area of each division.

Step 2. Calculate the bearing area.

$$\text{Bearing Area} = \frac{Y - \left[d_1\left(\frac{G_{11} + G_{21}}{2}\right) + d_2\left(\frac{G_{12} + G_{22}}{2}\right) + \frac{d_3\ G_4}{2}\right]}{\text{Spacing of the deformation}} \qquad (A.6)$$

Table A.1 Typical Data for Deformation Measurements

Deformation pattern : N
Surface type : Mill scale
Bar size : No. 5

Measured Points	A	B	B1	B2	C1	C2	D1	D2	M1	M2	E1**	E2**	F**
1	4.269	0.678	0.678	0.670	0.649	0.650	0.650	0.654	0.662	0.664	0.039	0.069	0.043
2	4.269	0.671	0.672	0.664	0.642	0.641	0.641	0.643	0.651	0.654	0.032	0.073	0.044
3	4.269	0.671	0.669	0.668	0.631	0.629	0.630	0.629	0.648	0.657	0.034	0.061	0.039
4	4.269	0.663	0.661	0.660	0.622	0.619	0.621	0.620	0.637	0.636	0.034	0.044	0.057
5	4.269	0.654	0.654	0.651	0.616	0.613	0.615	0.615	0.626	0.624	0.055	0.046	0.047
6	4.269	0.652	0.649	0.651	0.612	0.609	0.611	0.613	0.626	0.627	0.055	0.031	0.032
7	4.269	0.649	0.647	0.649	0.608	0.605	0.612	0.610	0.625	0.628	0.040	0.037	0.051
8	4.269	0.651	0.653	0.651	0.608	0.606	0.608	0.609	0.626	0.626	0.057	0.044	0.050
9	4.269	0.653	0.657	0.649	0.614	0.609	0.614	0.612	0.634	0.625	0.037	0.055	0.063
*10	4.269	0.662	0.659	0.659	0.606	0.604	0.606	0.607	0.624	0.624	0.046	0.050	0.061
11	4.269	0.667	0.668	0.665	0.633	0.631	0.633	0.632	0.647	0.640	0.073	0.056	0.045
12	4.269	0.674	0.671	0.672	0.633	0.633	0.634	0.633	0.650	0.644	0.076	0.052	0.058
13	4.269	0.687	0.685	0.684	0.641	0.639	0.639	0.639	0.658	0.653	0.055	0.044	0.057
14	4.269	0.698	0.696	0.697	0.645	0.649	0.647	0.651	0.669	0.666	0.060	0.036	0.054
15	4.269	0.694	0.690	0.690	0.652	0.655	0.657	0.654	0.664	0.668	0.050	0.064	0.050
16	4.269	0.697	0.695	0.696	0.656	0.659	0.657	0.657	0.671	0.672	0.036	0.065	0.050
+17	4.269	0.707	0.702	0.706	0.657	0.659	0.660	0.661	0.676	0.675	0.044	0.049	0.061
18	4.269	0.703	0.698	0.703	0.658	0.661	0.659	0.663	0.675	0.675	0.047	0.044	0.048
19	4.269	0.695	0.692	0.691	0.658	0.662	0.657	0.662	0.671	0.673	0.044	0.069	0.044
*20	4.269	0.695	0.696	0.693	0.653	0.660	0.659	0.661	0.673	0.673	0.034	0.075	0.050

G11 = 0.088 G12 = 0.089 G3 = 0.687
G21 = 0.165 G22 = 0.150 G4 = 0.092

* Location of longitudinal ribs
\+ Location of small longitudinal rib
** These measurements are used in other calculations

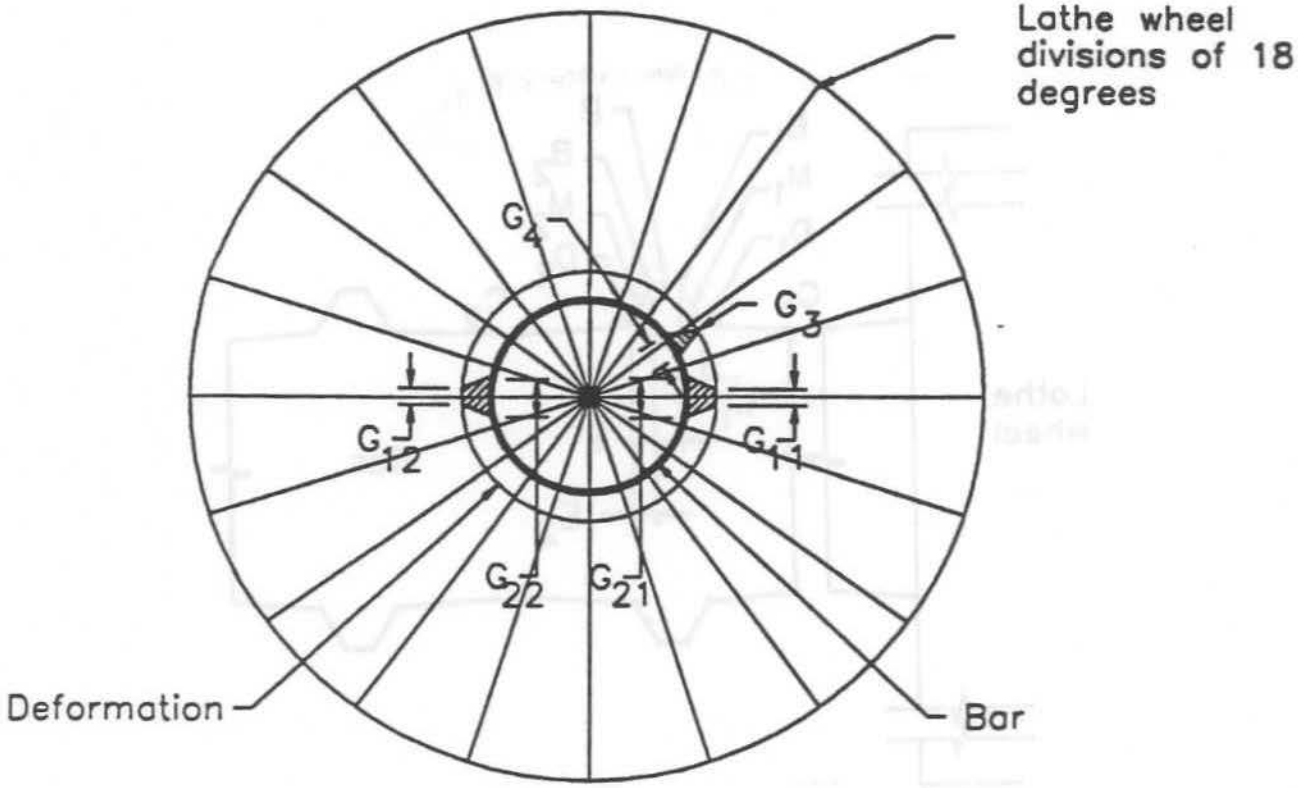

A.1 Equal Division for Deformation Measurement

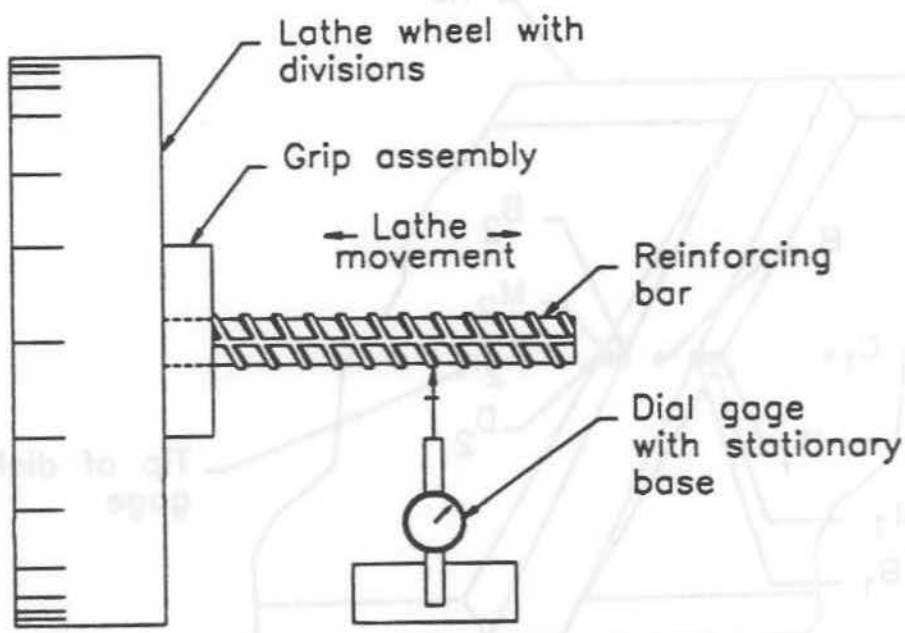

A.2 Instrument Set-Up for Deformation Measurement

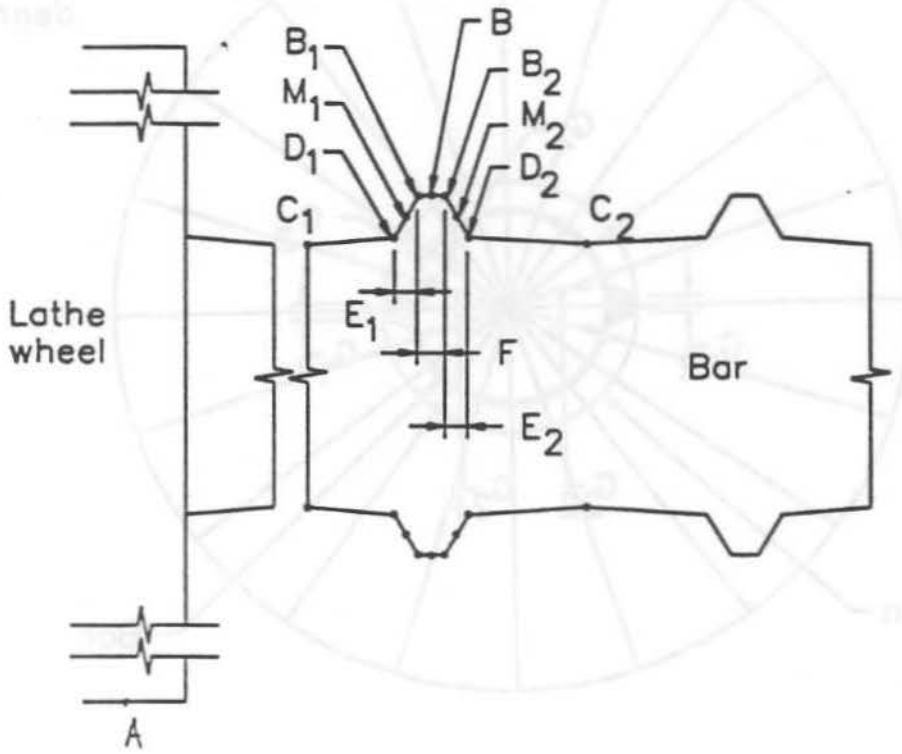

A.3 Measuring Points of Reinforcing Bar

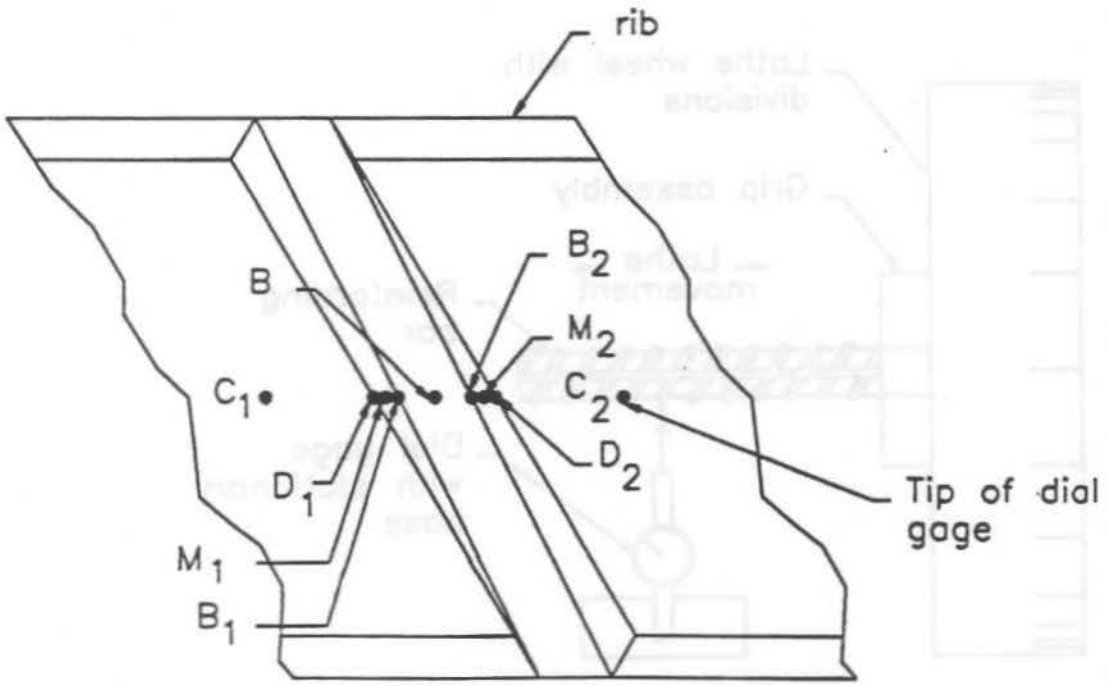

A.4 Detail Measuring Points of Reinforcing Bar

APPENDIX B

HYPOTHESIS TESTING

Bond tests naturally exhibit a great deal of data variation. Therefore, some form of statistical analysis is needed to determine whether observed data variations are statistically significant, that is, the result of actual performance differences, or not significant and the result of random data fluctuation. In this study, hypothesis testing is employed to make this determination. Specifically, the hypothesis that the mean bond strength of one population (μ_1) is equal to the mean bond strength of another population (μ_2) is tested against another hypothesis that these means are not equal. Hypothesis testing is applied to two population means using what is known as the two-sample t-test. In the following, concepts of this statistical method are discussed and examples are given to illustrate the procedures.

In order to apply hypothesis testing, the two hypotheses in a comparison must be conflicting, that is, these hypotheses must be constructed so that if one hypothesis is true, the other is false, and vice versa. The two hypotheses are normally known as the null hypothesis, H_o, and the alternative hypothesis, H_a. The objective of hypothesis testing is to test the null hypothesis H_o, $\mu_1 = \mu_2$, against the alternative hypothesis, H_a, $\mu_1 \neq \mu_2$. From the hypothesis testing, a decision is made whether to accept or to reject the null hypothesis with some level of prescribed error. The mean bond

strength of one population can be equal to the mean bond strength of another population, or these means may not be equal.

The hypothesis tests which we make are based on certain probability assumptions. Specifically, let X_1 be the ultimate bond strength for bars in population No. 1, and X_2 be the ultimate bond strength for bars in population No. 2. Then X_1 and X_2 are random variables which have certain distributions. For the purposes of our tests we assume that X_1 and X_2 are normally distributed with means μ_1 and μ_2 and standard deviations σ_1 and σ_2. We consider the bars which we test to constitute random samples, of sizes n_1 and n_2, respectively, from populations No. 1 and No. 2. Once we have tested the bars in our samples, we can calculate the sample means $\bar{x}_1$ and $\bar{x}_2$ and sample standard deviations s_1 and s_2. Due to random variations, the two sample means $\bar{x}_1$ and $\bar{x}_2$ will in general be different. We want to decide whether the difference between $\bar{x}_1$ and $\bar{x}_2$ is so great as to indicate that $\mu_1 \neq \mu_2$, or whether the difference between $\bar{x}_1$ and $\bar{x}_2$ is small enough that it is consistent with the hypothesis $\mu_1 = \mu_2$.

In the cases which we need to consider, we do not know σ_1 or σ_2. Also, we usually have small sample sizes (n_1 and n_2) each less than 30), so we do not want to assume $\sigma_1 \cong s_1$ and $\sigma_2 \cong s_2$. However, it does seem reasonable to assume, in our cases, that $\sigma_1 = \sigma_2$. Therefore, we make this assumption, i.e., that the population standard deviations are unknown, but equal. Under these assumptions, if the null hypothesis H_o: $\mu_1 = \mu_2$, is true, then the statistic:

$$T = \frac{\bar{x}_1 - \bar{x}_2}{\sqrt{\left(\frac{n_1 - 1}{n_1 + n_2 - 2} s_1^2 + \frac{n_2 - 1}{n_1 + n_2 - 2} s_2^2\right)\left(\frac{1}{n_1} + \frac{1}{n_2}\right)}} \qquad (B.1)$$

has a t-distribution with $n_1 + n_2 - 2$ degrres of freedom (Harnett 1975). It is this statistic T which we use in the two-sample t-test.

Our decision procedure is then as follows. After we have tested the bars in our samples, we calculate $\bar{x}_1$, $\bar{x}_2$, s_1, s_2, and, from these, the observed value of the T-statistic defined above, call it t_{obs}. Due to the fact that T has a t-distribution if H_o is true, we regard extreme values of t_{obs} as evidence that H_o is false, i.e., H_a is true. Specifically, we define a critical region for the test, i.e., a set C of values for T such that if t_{obs} lies in C, then we reject H_o. We take:

$$C = \{t: |t| > t_{\frac{\alpha}{2}, n_1 + n_2 - 2}\}. \qquad (B.2)$$

The number α is called the level of significance of the test; it is the probability that we will reject H_o when in fact H_o is true. Note that if t_{obs} is such that we reject H_o even for small values of α (say $\alpha = .001$), then we have strong evidence that H_o is false. On the other hand, if t_{obs} is such that we accept H_o even for relatively large values of α (say $\alpha = .20$), then we do not have even mildly strong evidence against H_o; in this case, our test results are entirely consistent with the hypothesis $\mu_1 = \mu_2$. Note that in this

second case we have not proved that $\mu_1 = \mu_2$; we can say just that our test results are consistent with this hypothesis.

As an example of this procedure, the significance of an epoxy coating on bond strength is studied for coated and uncoated S-pattern No. 8 bars. The mean ultimate bond forces for coated and uncoated bars in our samples are 31330 and 41464 lb., with sample standard deviations of 2827 and 3384 lb., respectively. The sample sizes for this analysis include 20 coated bars and 10 uncoated bars. It is assumed that the alternative is two-sided (covers situations where μ_1 can be greater than or less than μ_2) and that $\alpha = 0.001$. The critical values in this case from the table of the t-distribution are

$$\pm t_{(\alpha/2,\ n_1 + n_2 - 2)} = \pm t_{(0.0005,\ 28)} = \pm 3.674. \qquad (B.3)$$

in which n_1 and n_2 are sample sizes. These critical values can be compared with the calculated value of t. Using Eq. B.1, and $\bar{x}_1 = 31330$, $\bar{x}_2 = 41464$, $s_1^2 = 2827^2$, and $s_2^2 = 3384^2$, the calculated t value is obtained as -9.44. The calculated t value does fall in the critical region; thus the null hypothesis, that the mean bond strength of coated and uncoated No. 8 bars with the S deformation pattern are equal, can be rejected with 0.001 level of significance. The test results show that the difference in these two sample mean bond strengths may not be attributed to chance, but a significant difference in bond strength must exist between coated and uncoated bars with the same bar size and deformation pattern.

As another example, the two-sample t-test is made for the same No. 8 bar size and the same S-pattern to find any significance in the difference in the sample mean bond strengths of mill scale and blast-cleaned bars. The sample mean ultimate bond forces for mill scale and blast-cleaned bars are 41464 and 43448 lb., with sample standard deviations of 3384 and 4344 lb., respectively. The samples for this test include 10 mill scale bars and 5 blast-cleaned bars. It is assumed that the alternative is two-sided. α will be taken to be 0.20, allowing a large chance of error in rejection, H_o, even if it is true. The critical values in this case are

$$\pm t_{(\alpha/2,\ n_1 + n_2 - 2)} = \pm t_{(0.10,\ 13)} = \pm 1.350. \qquad (B.4)$$

The calculated t value, -1.256 from Eq. B.1, falls between the critical values of t; thus the null hypothesis, that the mean bond strengths of mill scale and blast-cleaned bars are equal, cannot be rejected. There are differences in the sample mean bond strengths, between mill scale and blast-cleaned bars in our samples. However, the difference in the sample mean bond strengths can be satisfactorily explained by the normal variability in bond properties.

Because bond tests naturally exhibit a great deal of scatter, it is important to establish whether differences in test results are caused by normal variability in bond properties or by a systematic cause. Hypothesis testing is used to make this distinction. The two-sample t-test, as used in this study, is effective in evaluating

test results, especially the variations in bond strength accompanying changes in bar and specimen parameters.

APPENDIX C
REGRESSION ANALYSIS USING DUMMY VARIABLES

Multiple regression analysis can be employed to determine how the variation of a set of dependent variables is related to the variation of a set of independent variables. In this study, bond strength and the bond strength ratio of coated to uncoated bars, C/U, are the dependent variables while coating thickness, deformation pattern and bar size are independent variables. Coating thickness and bar size are variables with actual numeric values. However, non-numerical variables, such as deformation pattern, can be used as qualitative or indicator variables in a regression equation and produce quantitative effects on the value of dependent variables. Therefore, even though they may not be quantitative in nature, the effects of the indicator variables can be included in regressiona analysis. Indicator variables also are known as dummy or binary variables (Draper and Smith 1981). In the following discussion, the regression analysis procedure using dummy variables is illustrated and an example using test results in this study is provided.

Multiple linear regression is a extension of simple linear regression. The regression model is specified by the following equation:

$$Y = \beta_0 + \beta_1 X_1 + \beta_2 X_2 + \ldots + \beta_k X_k + \varepsilon \qquad (C.1)$$

in which Y = dependent random variable

X_j = the jth independent variable, j = 1, 2, . . ., k

$\beta_0, \beta_1, \beta_2, \ldots, \beta_k$ are (k+1) parameters in the model

ε = random variable

The values of the estimators, $\beta_0, \beta_1, \ldots, \beta_k$ can be obtained by the least squares approach. Least squares analysis is easily performed in matrix form. Thus, the regression model, Eq. (C.1), can be rewritten in matrix notation as:

$$\{Y\} = [X]\{B\} + \{E\} \qquad (C.2)$$

To find the model parameters {B}, the least squares method minimizes the sum of squares of the random variables $\{E\}^T\{E\}$, where $\{E\} = \{Y\} - [X]\{B\}$. To minimize this expression, vector differentiation and setting the first derivative equal to zero yields

$$\{B\} = ([X]^T[X])^{-1}[X]^T\{Y\} \qquad (C.3)$$

To perform this algebraic computation, computer solution is usually employed in large regression analysis problems.

In multiple linear regression using dummy variables, $X_2, \ldots, X_k$ can be dummy variables. In general, if there are m distinguishable groups to be used as independent variables, there will be j = (m-1) dummy variables required. For example, in this study, since there are three different deformation patterns in each bar size group, two dummy variables are required. In this case, the form of the estimating equation for the effect of epoxy coating thickness is

$$Y = \beta_0 + \beta_1 X + \beta_2 Z_1 + \beta_3 Z_2 + \varepsilon \qquad (C.4)$$

in which X = coating thickness of a sample unit

Y = random variable strength ratio

Z_1 and Z_2 are binary variables defined as:

$(Z_1, Z_2) = (1, 0)$ for the S-pattern

$(Z_1, Z_2) = (0, 1)$ for the C-pattern

$(Z_1, Z_2) = (0, 0)$ for the N-pattern

With the given data and the defined dummy variable, a best fit equation can be obtained by least squares, as in multiple linear regression analysis. In this study, data from the basic specimens of No. 5, No. 6, and No. 8 bars with the N, C and S deformation patterns from this study can be used to illustrate this procedure. In this example, the mean normalized bond strength of the uncoated bars for each deformation is obtained. Then the ratio of bond strength of each coated bar to the mean bond strength of the uncoated bars, the C/U ratio for each bar, is calculated.

A table corresponding to the input variable for the multiple linear regression equation is constructed for No. 8 bars, as shown in Table C.1. The data in the table include independent variable X (coating thickness) and dependent variable Y (C/U ratio) results for thirty-six coated No. 8 bars. Seventeen of the coated bars are from the S-pattern, fourteen from the C-pattern and five from the N-pattern.

From the data in the table, the best fit equation can be obtained using multiple linear regression analysis [IMSL RLMUL

subroutine (1987)]. The following expression was obtained for this example concerning No. 8 bars.

$$Y = 0.8826 - 0.0009\ X - 0.1536\ Z_1 - 0.0149\ Z_2 \qquad (C.5)$$

By substituting for the three sets of values for (Z_1, Z_2), the three best fit equations are obtained for the three different deformations as follows:

$$\begin{aligned} Y &= 0.729 - 0.0009\ X, \quad \text{for S} \\ Y &= 0.868 - 0.0009\ X, \quad \text{for C} \\ Y &= 0.883 - 0.0009\ X, \quad \text{for N} \end{aligned} \qquad (C.6)$$

The three lines have identical slopes and are thus all parallel, but have different intercepts.

In the multiple regression analysis, the dummy variable, indicating a qualitative variable such as deformation pattern, can be employed to estimate the value of dependent variable, such as the C/U ratio as a function of one or more quantitative independent variable. This technique, of course, inherently assumes that the response of the incremental response of the dependent variables (slope in Eq. C.5 and C.6) is independent of the dummy variables.

Table C.1 Test Data and Dummy Variables for No.8 Bars

X (mils)	Y	Deformation pattern	Z1	Z2
5.4	0.674	S	1	0
6.4	0.664	S	1	0
6.5	0.750	S	1	0
4.1	0.680	S	1	0
4.7	0.781	S	1	0
6.8	0.813	S	1	0
9.7	0.696	S	1	0
10.2	0.723	S	1	0
7.9	0.839	S	1	0
10.8	0.778	S	1	0
5.3	0.892	C	0	1
5.5	0.813	C	0	1
4.6	0.864	C	0	1
3.7	0.865	C	0	1
10.0	0.911	C	0	1
9.5	0.877	C	0	1
10.0	0.816	C	0	1
9.4	0.834	C	0	1
10.7	0.825	C	0	1
9.1	0.894	C	0	1
13.1	0.949	C	0	1
13.8	0.909	C	0	1
13.2	0.749	C	0	1
12.7	0.840	C	0	1
8.6	0.798	N	0	0
8.5	0.936	N	0	0
8.8	0.779	N	0	0
9.2	0.834	N	0	0
10.4	1.026	N	0	0